Centre for Ore Deposit and Exploration Studies

Proterozoic sediment-hosted base metal deposits

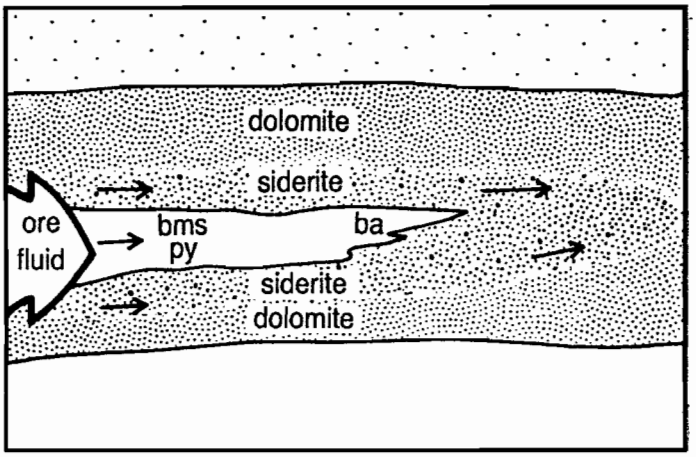

AMIRA/ARC Project P384
Report No.3

University of Tasmania
October 1993

Centre for Ore Deposit and Exploration Studies

Proterozoic sediment-hosted base metal deposits

AMIRA/ARC Project P384
Report No.3

University of Tasmania
October 1993

Contents

Introduction

PROJECT OBJECTIVES: P384

1. To determine the primary geological, geochemical and structural controls on the location and timing of base metal deposits in sedimentary basins.
2. To understand the chemical and hydrological evolution of metalliferous brines in selected Proterozoic sedimentary basins of Australia.
3. To develop basin metallogenic models and specific ore deposit models that may be used in the exploration for large-tonnage base-metal ore deposits.

RESEARCH FRAMEWORK

This research project involves a multi-disciplinary approach using regional geological, geophysical and structural studies, brine chemical modelling and geochemical and isotopic halo studies to provide a foundation on which to build a network of exploration criteria and ore deposit models for major sediment-hosted base metal deposits.

The project consists of three research modules as outlined below:

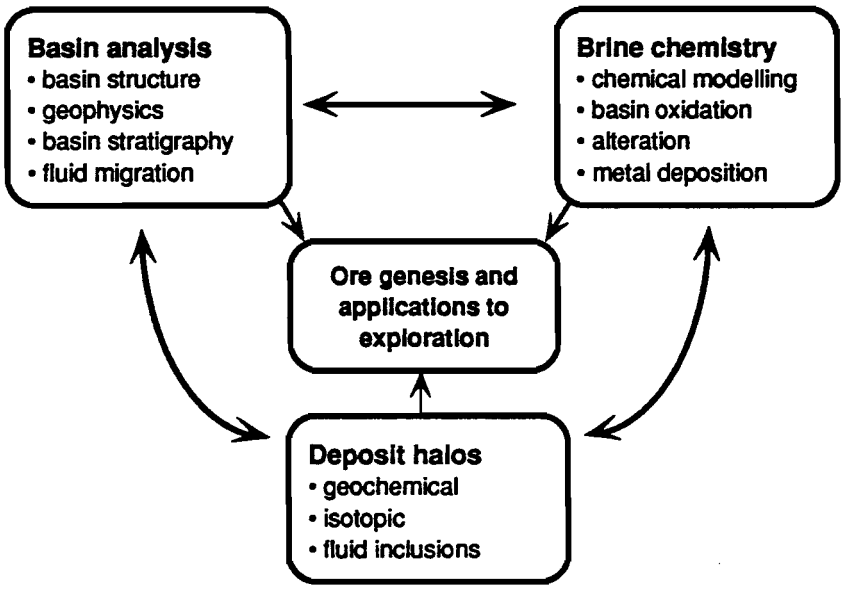

THIS REPORT

This is the third major report on the project and outlines results to date on the Deposit Halos module. A comprehensive account of deposit halo mineralogy and geochemistry is presented for Lady Loretta and HYC. The results have major implications regarding mineral exploration and ore genesis for giant stratiform Pb-Zn deposits.

A further report (No.4), covering work on the Basin Analysis and Brine Chemistry modules, will be distributed to sponsors at the November 29/30 meeting.

It is now 18 months since the commencement of this project and research progress in all aspects of the work has been very pleasing. Acknowledgment for our progress to date is due to the excellent work by the CODES research team and the close cooperation provided by the sponsor companies, AGSO and the NTGS. In particular, for the deposit halos module, we would like to acknowledge Mel Jones and Pancontinental for their support and encouragement on the Lady Loretta study.

Ross Large
Director
CODES

Summary of Research Findings

Geology of the Lady Loretta deposit: review, new developments and implications for ore genesis.

Peter McGoldrick

This reports reviews the regional geology of the Lady Loretta formation and its sedimentary setting. The geology of the host sequence at Lady Loretta mine is described along with some new observations (evaporite pseudomorphs, desiccation cracks and delicate stromatolites) consistent with a very shallow water to emergent setting for the mineralized sequence. Three macroscopic varieties of pyrite types are present in the mine sequence. The most abundant pyrite type is thought to form from decomposing microbial mat in the shallow sub-surface during diagenesis. An external source (?low temperature hydrothermal fluid) for Fe is probably required to form thick Fe sulphide accumulations.

The genesis of the Lady Loretta base metal mineralization is discussed using three genetic models:

(i) an **exhalative-syngenetic model** - base metal sulphides and pyrite precipitate from hydrothermal solutions escaping to the water column and deposit as sedimentary layers during times of (relatively) low sedimentation rates

(ii) **syn-sedimentation - early model** - base metal sulphides post-date diagenetic Fe sulphides and form within the soft sediment a few centimetres or decimetres below the basin floor

(iii) **syn-sedimentation - late model** - base metal sulphides form late in the burial-compaction history of the sediment pile from metalliferous solutions passing through large thicknesses of sediment; thick diagenetic pyrite accumulations are not directly related to the mineralizing event

Sampling and whole rock analyses for the Lady Loretta deposits

Peter McGoldrick

This report documents the sampling program carried out at Lady Loretta in May 1992. Complete analyses for 30 major and trace elements for 104 sediment samples are presented. All samples were analysed at the University of Tasmania, and a summary of the techniques used for geochemical analysis is provided. These analyses provide the basic data for developing the geochemical halo models presented in Large and

McGoldrick, (1993). Appendix 4-I presents an assessment of commercial ICP-ES data for the same group of samples. Appendix 4.II describes the XRF technique used for measuring Tl and compares the XRF data with commercial graphite furnace-AAS analyses.

Primary geochemical halos related to Proterozoic sediment hosted Pb-Zn deposits and applications to exploration

Ross Large and Peter McGoldrick

The purpose of our research in the geochemical halo module of AMIRA Project P384, is to develop a model for geochemical dispersion associated with Australia Proterozoic stratiform Pb-Zn deposits that is applicable to mineral exploration. In this report, primary halos around the Lady Loretta deposit are documented and discussed in detail, based on the sample collection and analysis programme outlined in the previous paper by McGoldrick (1993). The halo model developed for Lady Loretta has two components: 1) an inner siderite halo with anomalous zinc and lead which surrounds the orebody and extends up to 1km along strike; 2) an outer dolomite halo with anomalous Mn and Tl which surrounds the siderite halo and extends further along the ore horizon. Within the nested halos vectors towards ore have been defined using a metal index, an alteration index and the MnO content of carbonate phases.

In light of the model developed for Lady Loretta, previously published data on geochemical dispersion surrounding the HYC deposit has been re-evaluated, leading to the formulation of a halo model and ore vectors for stratiform Pb-Zn deposits throughout the McArthur Basin. The ultimate outcome of this research is the development of a new approach to lithogeochemistry applied to stratiform Pb-Zn exploration, which is analogous to the use of stratigraphic drilling and the source rock/trap rock approach to oil exploration.

DEPOSIT HALOS

3. Geology of the Lady Loretta deposit: review, new developments, and implications for ore genesis

Peter McGoldrick

SUMMARY

This report briefly reviews the regional geology of the Lady Loretta Formation and discusses possible sedimentary settings for these rocks. The geology of the host sequence at Lady Loretta mine is summarized and some new observations consistent with a very shallow water to emergent setting for the mineralized sequence are presented. Three macroscopic varieties of pyrite types are described. Much of this pyrite is thought to form during diagenesis by the interaction of large amounts of decomposing microbial organic matter and Fe-bearing (?hydrothermal) solutions. Three distinct genetic models for the Lady Loretta deposit are presented and their relative merits discussed.

REGIONAL GEOLOGICAL SETTING

The Lady Loretta deposit is a small example (8.3 Mt at 18.4% Zn, 8.5% Pb and 125 g/t Ag) of the giant stratiform sediment-hosted base metal deposits of northern Australia (Fig. 1, Table 1). It is hosted by the Lady Loretta Formation which is the fifth of nine units that make up the McNamara Group (Caveny, 1975, Hutton et al., 1981). Zircons in tuffaceous sediments from near the top of the McNamara Group (Lawn Hill Formation - Pmh_4) have recently been dated at about 1620 Ma (R. Page, pers. comm., 1993). To the north of the South Nicholson Basin Cover the McNamara Group is correlated with the Fickling Group and to the east and south of the Mount Gordon Fault Zone the lower half of the McNamara Group is correlated with the Mount Isa Group (Fig. 2). A 'Tuff Marker Bed' from the Urquhart Shale near the top of the

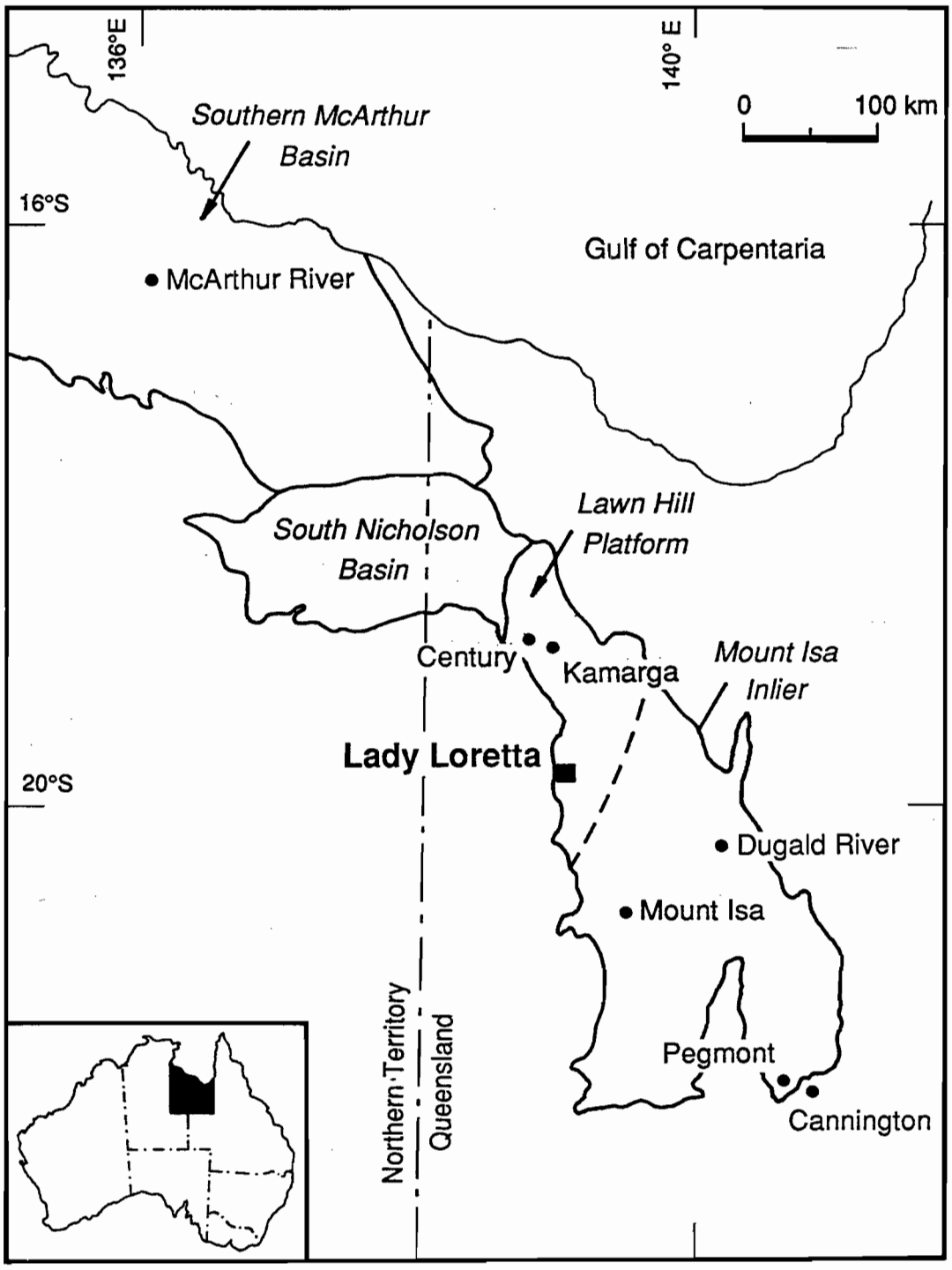

Figure 1 Major geological subdivision of northwest Queensland and eastern Northern Territory with the location of important lead-zinc deposits

Mount Isa Group has been dated at 1653±7 Ma and the Carters Bore Rhyolite which directly underlies the McNamara Group has an age of 1680±3 Ma (Page 1993). Maximum preserved sediment thicknesses are of the order of five kilometres in the Mount Isa Group, ten kilometres in the McNamara Group and about one kilometre in the Fickling Group.

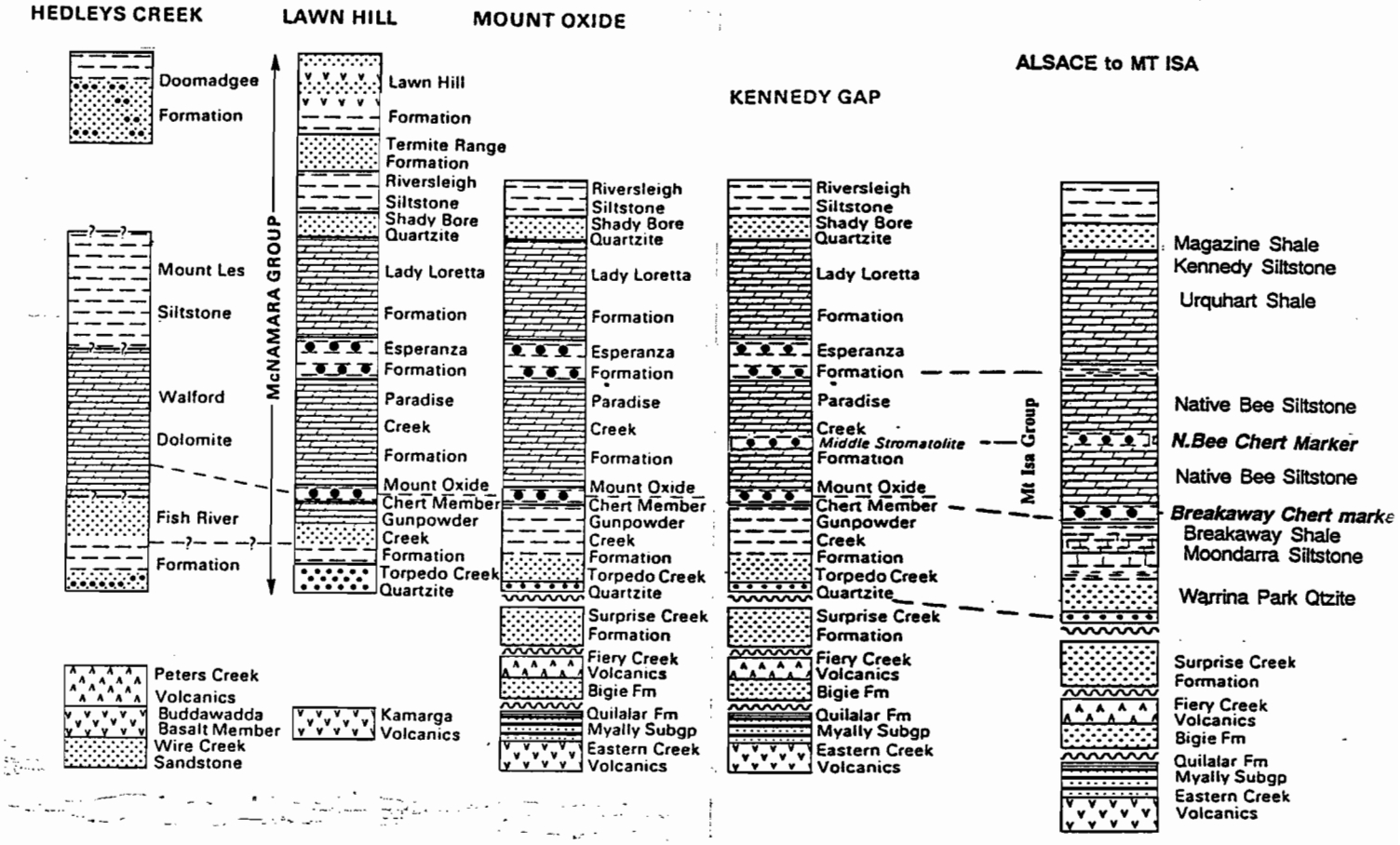

Figure 2 Detailed regional correlations across Mount Isa Inlier and Lawn Hill Platform, names refer to 1:100,000 map sheets (Derrick, 1993 – modified from Hutton and Sweet, 1982)

LADY LORETTA FORMATION

The Lady Loretta Formation has been described in some detail by Hutton et al., (1981), Hutton and Sweet, (1982) and Hutton and Wilson, (1984 and 1985) It comprises mainly dolomite, minor oolitic dolomite, dolomitic siltstone, carbonaceous and pyritic shale, and a basal ferruginous cherty breccia. However, the thickness and relative proportions of lithologies is quite variable. It is more than 2000 m thick in the northern part of the Lawn Hill Platform and (in general) thins to the south and near the Mount Gordon Fault Zone. The 1800 m thick type section is located about 40 km NNW of Lady Loretta mine (10 km northeast of Thorntonia homestead) and 'comprises basal ferruginous and altered, laminated and stromatolitic dolomite, overlain by less altered laminated and intraclast dolomite, stromatolitic

Deposit	Size & grade	Mineralization	Host rocks	Age
HYC	8 ore lenses in abt 70 m; global res. 227 Mt @ 9.2% Zn, 4.1% Pb, current project 104 Mt @ 14.1% Zn, 6.1% Pb and abt 60 g/t Ag	stratiform, f.g. py, sp, minor cpy, marcasite, ars; primary textures well preserved	Barney Creek Fmn - HYC Pyritic Shale; pyritic, organic matter-rich, dolomitic siltstones; crs sedimentary bx interbeds; minor tuffaceous component; low-rank hydrocarbons, up to 7% TOC (Crick et al., 1988)	1631±12 Ma (Page, 1990)
Mount Isa	30 stacked (en echelon) ore lenses in abt 1000 m (most in upper 650 m); pre-production reserve of abt 150 Mt @7% Zn, 6% Pb, 150 g/t Ag; 1990 proven reserve 47 Mt @ 6.6%Zn, 5.4% Pb, 135 g/t Ag	stratiform py, sp, ga, tetrahedrite ± po; ores show locally intense deformation, but some primary textures are preserved	Mount Isa Gp - Urquhart Shale; carbonaceous (graphite - McKirdy & Powell, 1974), pyritic, dolomitic siltstones; important 'tuffaceous' component	1653±7 Ma - 7o/b f/w TMB (Page, 1993)
Hilton / Hilton North	7 stacked ore lenses; approx. 120 Mt @ 10.2% Zn, 5.5% Pb, 100 g/t Ag (Derrick, 1993)	as for Mt Isa, but with higher grade and more Cu-rich fault-related ore	as for Mt Isa	as for Mt Isa
Mount Novit	single lens abt 20 m thick	stratiform/stratabound (massive) crs py, po, mte ±sp, ga	(lower) Mt Isa Gp - Moondarra Siltstone; pellitic schists	probably 1660 to 1650 Ma
Century	2 main ore zones in a 40 m mineralized sequence; 118 Mt @ 10.2% Zn, 1.5% Pb, 36 g/t Ag	stratiform sp, py (5-10%), ga, ±cpy (intimate association with organic matter and authigenic silica); primary textures are preserved	McNamara Gp - Lawn Hill Fmn - unit PMH4; siliclastic, carbonaceous (TOC 1 -5%), shales (mineralized) & siltstones (barren, but sideritic); minor tuffaceous component	abt 1620 Ma (R. Page pers. comm., 1993)
Kamarga	80 m low-grade mineralized sequence; estimated 50 Mt @ abt 3% Zn+Pb, including a zone of abt 10 Mt @ 5 - 10% (Jones, 1986)	stratabound sp, ga, py, as vein-filling, replacement & open space fillings (primary textures)	(lower) McNamara Group - Gunpowder Creek Fmn	around 1650 Ma
Dugald River	40 m thick lode; 38 Mt @ 13.2% Zn, 2.1% Pb, 32 g/t Ag	stratabound py, sp, po, ga, tr. cpy, pyrargyrite, ars, tetrahedrite; mostly recrystallized, but some rare primary textures	Dugald River Slates (Shear Zone) - black, f.g. carbonaceous slates; stratigraphic position is not well constrained (different terrane to Mt Isa Gp rocks, but may be contemporaneous)	
Lady Loretta	single high grade lens with reserve of 8.3 Mt @ 18.4% Zn, 8.5% Pb, 125 g/t Ag; mineralized horizon is abt 50 m thick & is recognisable over several km^2	stratiform py, sp, ga, tetrahedrite, barite, silica , tr. hem; some primary textures preserved	McNamara Gp - Lady Loretta Fmn; carbonaceous, pyritic, dolomitic, sideritic siltstones & shales	abt 1650 Ma (Lady Loretta Fmn is correlated with Urquhart Shale)
Walford Creek	no published reserve; several ore-grade intersections (Cu, Zn, Pb) of a few metres; covers an area of 6 km x 1.5 km in plan	3 stacked lenses of stratiform massive py with sp & ga as a matrix in pyritic beds; primary textures preserved	Fickling Gp - Mt Les Siltstone; dolomitic shale (regionally), highly carbonaceous, dolomitic and pyritic shales & interdigitating talu bxs (locally)	1600 to 1650 Ma

Table 1 Important geological features of northern Australian Proterozoic sediment-hosted Zn-Pb deposits

Metamorphism /deformation	Evaporites	Oxidized sediments	Zoning	Halos	References
essentially unmetamorphosed; basin inversion, but no penetrative deformation	important part of sequences above and below HYC Pyritic Shale are evaporitic	W-Fold Shale (immediate f/w to mineralization) shows extensive patchy reddening; Emu FZ; various units elsewhere in McArthur and Tawallah Gps	small very Cu-rich zone in the north; general (Cu-)Pb-Zn (Williams, 1978; Logan, 1979)	pyrite; Tl regionally; Fe. Mn in carbonates	Logan et al., 1990; Logan et al., 1993; & references therein
(?lower) greenschist facies; D_1 - D_3	pseudomorphs of dolomite after gypsum in Urquhart Sh (McClay & Carlisle, 1978; McGoldrick, 1986); halite casts in siltstone unit above Urquhart Sh; Upper Mt Isa Gp interpreted as a perennial hypersaline lake (Neudert, 1983)	basal Mt Isa Grp; Surprise Creek Fmn (beneath and possibly lateral equivalent to Mt Isa Gp)	(Cu-) Pb - Zn	pyrite; Tl; ?Fe enrichment in carbonates	Forrestal, 1990 & references therein
as for Mt Isa, but locally more structurally complex		as for Mt Isa	upper o/bs most Cu-rich; (Cu-) Pb-Zn moving up-dip	sideritic siltstones reported in Derrick (1993)	Derrick, 1993; Valenta, 1988; Mathias et al., 1973
greenschist/amphibolite transition; D_1 - D_3, but complexity due to faulting		as for Mt Isa		siderite in mineralization (Russell, 1978)	Derrick, 1993; Russell, 1978
sub-greenschist; open folding, faulted ore contacts; stylolitic layering is developed in ore sequence			highest Zn grades transgress the mineralized sequence from SE to NW	py envelope; intense siderite development in siltstones	Waltho & Andrews, 1993; Waltho et al., 1993
sub-greenschist; open folding/doming	host rocks & underlying Paradise Creek Fmn contain(ed) significant amounts of evaporites	Torpedo Creek Quartzite & Surprise Creek Fmn	py- & Cu-rich fault zone ore		Jones, 1986
greenschist - amphibolite transition; D_1 - D_3, re-folded isoclinal folds with mineralized sequence overturned; mineralization has mylonitic contacts	Corella Fmn in stratigraphic footwall is scapolite-rich; Muir (1983) described pseudomorphs after shortite from the mineralized sequence	(?post-D_3 hematitization of Corella Fmn in the stratigraphic footwall	(Cu-) Pb - Zn and S isotopes (Dixon & Davidson, 1993)	K, Li, Rb, Tl, Pb, Se, Ag, & Sr enrichment enhancement in h/w and f/w	Shepherd & Main, 1990; Newberry et al., 1993
greenschist; open - tight synclinal (?D_2) structure locally, more open folding regionally	gypsum moulds from ore horizon; sulphate evaporites important in lower McNamara Group (Paradise Ck Fmn, Gunpowder Creek Fmn)		Pb-Zn core to Zn-Ba flanks of main mineralization	py, siderite, Mn, Tl	Hancock & Purvis, 1990 (& references therein); this report
? sub-greenschist; relatively flat-lying, but bounded by a major regional structure (Fish River Fault)	pseudomorphs after gypsum in Mt Les Siltstone (Sweet et al., 1981)				Webb & Rohrlach, 1992

dolomite and possible tuff, which is in turn overlain by a thin band of green and mauve indurated siltstone and shale. Interbedded laminated and intraclast dolomite overlain by medium-bedded, flaggy, sporadically dolomitic sandstone complete the sequence'. A reference section on the flanks of the Kamarga Dome (100 km N of Lady Loretta mine) comprises 'over 2000 m of laminated medium-bedded dolomite, dolomitic siltstone and sandstone, stromatolitic dolomite, and intraclast dolomite'. In contrast, the Lady Loretta Syncline (Fig. 3) contains a thick sequence (over 1800 m) comprising pyritic, carbonaceous, and dolomitic shales and siltstones, and minor sandstone, quartzite, dolarenite, chert, barite, tuffaceous sediments, and stratiform zinc-lead-silver mineralization.

The Lady Loretta Formation is interpreted to represent a variety of dominantly shallow water depositional environments. Near the type section (NW part of the Mammoth Mines Region

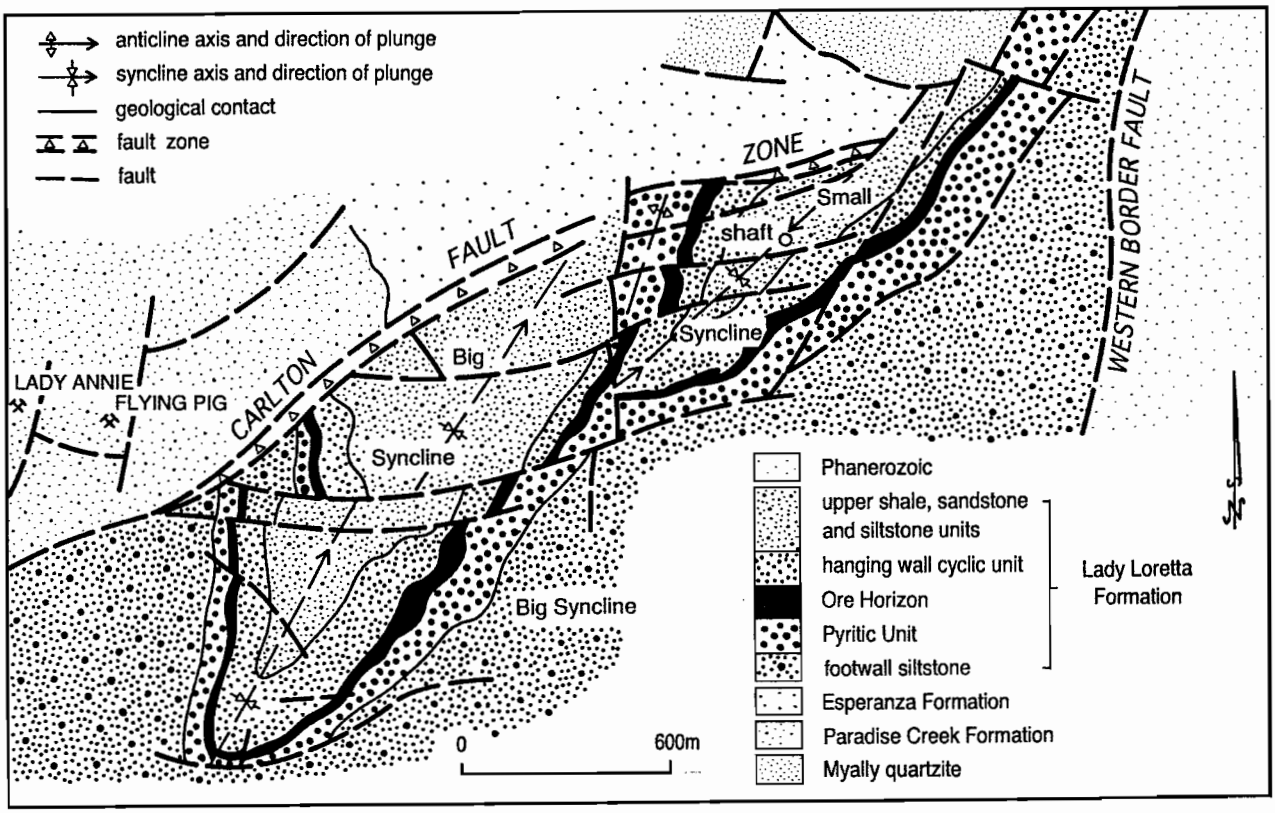

Figure 3 1:25,000 geological plan of the Lady Loretta area, northwest Queensland (from Hancock and Purvis, 1990)

1:100,000 map) a semi-emergent intertidal to supratidal, intermittently high energy and in part hypersaline lagoonal or shallow marine setting is favoured (Hutton and Wilson, 1984). Locally important silty and shaley facies (often in the upper part of the formation) are interpreted as quiet water shallow-marine deposits formed in relatively deeper parts of the basin (Hutton and Wilson, 1985).

The sequence in the Lady Loretta Syncline was thought to represent an isolated sedimentary (sub-)basin bounded to the north by the Carlton Fault (Hutton and Wilson, 1985).

Discussion

Despite the interpretations presented above it is clear that the gross sedimentary setting of the Lady Loretta Formation (and for that matter the entire McNamara Group) is not well understood. In the absence of diagnostic fossils it is very difficult to distinguish between a near-shore shallow marine shelf and a continental lacustrine setting. The distinction is important because the composition of the basin waters is a fundamental control of evaporatively concentrated water chemistry (Eugster and Jones, 1979), and subsequent diagenetic reactions in the sediment pile (and ultimately, the chemical reactions between the basin fill and transient mineralizing fluids).

Evaporation of seawater (which is Ca, Mg and SO42- -rich and weakly alkaline) has little effect on pH and will always cause gypsum (and/or anhydrite) and ultimately halite to precipitate. The occurrence of pseudomorphs, casts and moulds of gypsum, anhydrite and halite in parts of the McNamara Group (Plate 1 a and b) is consistent with a restricted marine setting for these sediments, but does not preclude a saline lacustrine environment. Evaporation of lake water can also produce sulphate evaporites, but may also form more exotic evaporite minerals and water chemistries. For instance, bicarbonate-rich (HCO_3>>Ca+Mg) waters will evaporate to form alkaline (CO_2-rich) brines and alkaline evaporite minerals (e.g., trona - $NaHCO_3.Na_2CO_3.2H_2O$, shortite - $2CaCO_3.Na_2CO_3$).

Alkaline evaporitic settings are also associated with the formation of fine grained siliceous chemical sediments (e.g., Magadi-type cherts; Eugster, 1969), partly in response to the enhanced solubility of silica in alkaline solutions. No unequivocal pseudomorphs of alkaline evaporite minerals or Magadi-type cherts are known from the McNamara Group or its equivalents. However, it is possible to speculate that early diagenetic chert bands and nodules, and K and Na enriched 'tuffs', which are quite common, mark intervals of alkaline diagenesis and a lacustrine setting for (some) of these rocks.

LADY LORETTA SYNCLINE

In the vicinity of the Lady Loretta deposit the Lady Loretta Formation comprises mainly grey to black (carbonaceous) dolomitic and argillaceous siltstones and mudstone/shale, with locally important 'chemical sediment' component ('Ore Horizon' and 'Pyritic Unit', Hancock and Purvis, 1990). Sandier units are common higher in the sequence (Figs 4 and 5).

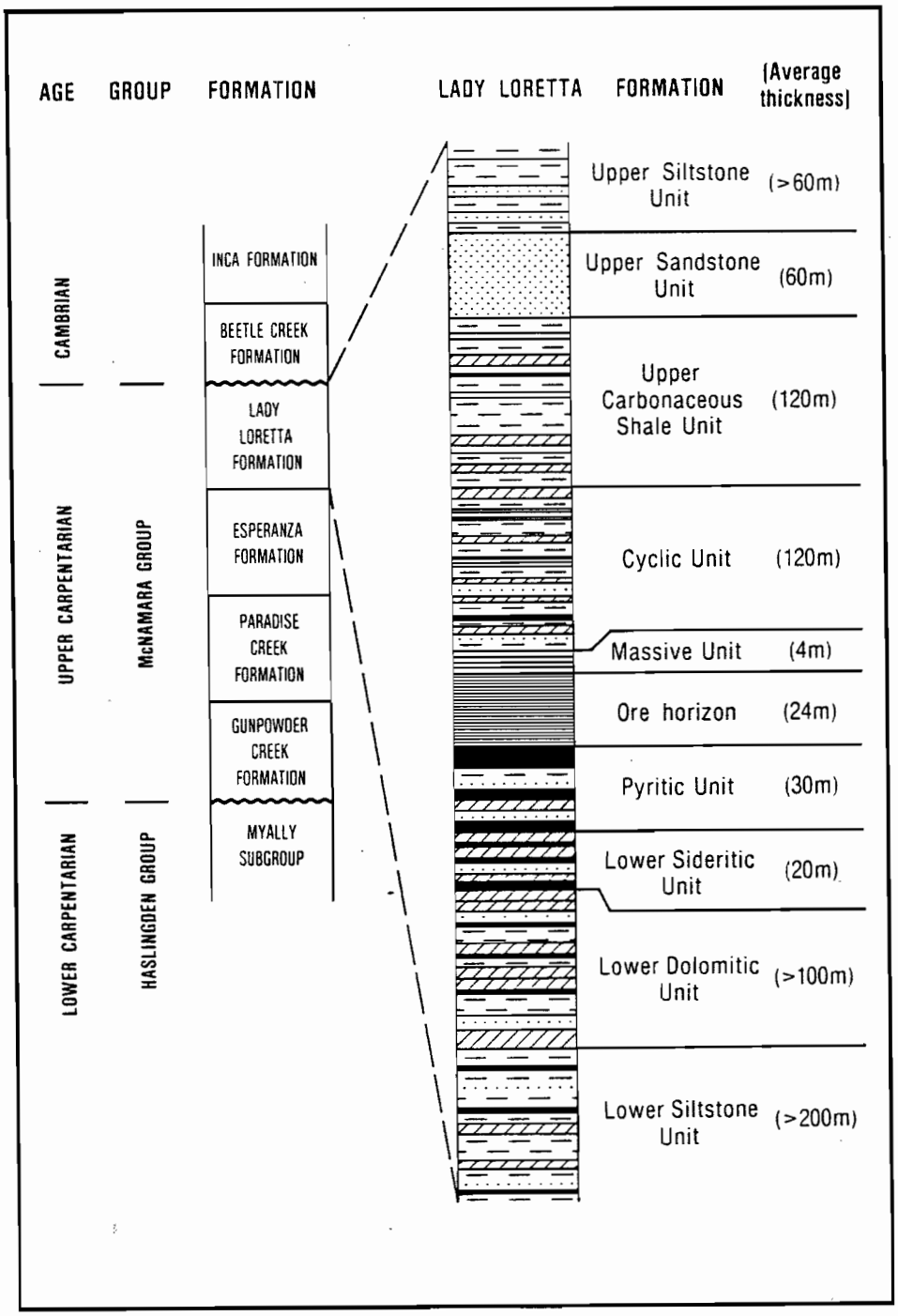

Figure 4 Stratigraphic column for the Lady Loretta Formation, Lady Loretta area (from Hancock and Purvis, 1990)

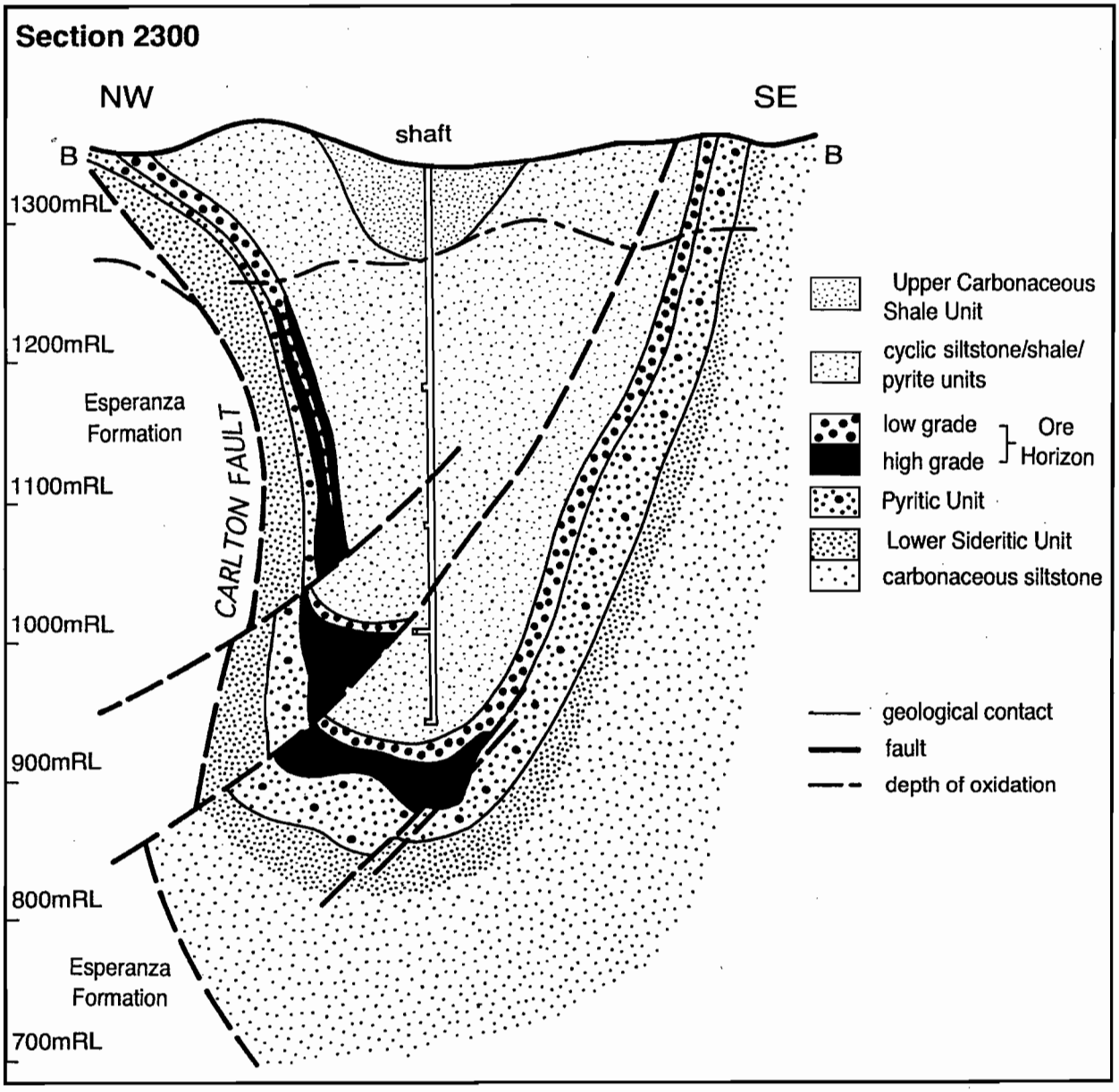

Figure 5 Geological cross section for the central part of the Small Syncline, 2360 m N mine grid (modified from Hancock and Purvis, 1990)

Silstone/shale facies

The major mineralogy of thirty five siltstone and shale/mudstone samples from Lady Loretta were determined by semi-quantitative XRD, and the results are summarized on Figure 6. The non-sulfide component of the sediments in the Lady Loretta Syncline comprise quartz, white mica, carbonate (dolomite or siderite), some K-feldspar and carbonaceous matter.

Siltstones and fine sandstones dominate for at least 300 m into the footwall of the mineralization. These become progressively more dolomitic and contain more fine grained bedded pyrite as the orebody is approached. Siderite is the dominant carbonate mineral within about 50 m of the orebody. Centimetre to decimetre scale grey siltstone beds are interlayered with thinner submillimetre laminated dark grey to black carbonaceous siltstones.

For more than 200 m into the hanging wall of the deposit siltstones and shales occur as cycles ranging from several metres to a few centimetres in thickness, often separated by pyritic bands (see below). The 'Massive Unit' immediately above the mineralization is a very thick (2 to 15 m) example of a single siltstone/shale cycle. Individual cycles are often graded beds with planar laminated (or more rarely cross-bedded) silt or fine sand bases that pass upwards into massive mudstone or shale (Plate 1 c). The coarser lithologies may show well developed fluid-escape structures (e.g., flames, disturbed laminations ('ball and pillow' texture) – Plate 1 d).

Discussion

Although Carr (1981) used chemical and mineralogical evidence to argue against the idea, these textural and sedimentological observations suggest the hanging wall sediments are a series of small turbidite deposits (Neudert, 1987), with E, D and sometimes C units of the Bouma Sequence all present. Hence, individual siltstone/shale cycles in the hanging wall represent geologically 'instantaneous' events.

The footwall siltstones do not have the obvious cyclic character of the hanging wall, but were probably also current deposits. Carbonaceous laminations in these siltstones represent buried microbial mat or organic matter incorporated as clastic material in the currents responsible for depositing the silt (Schieber, 1986).

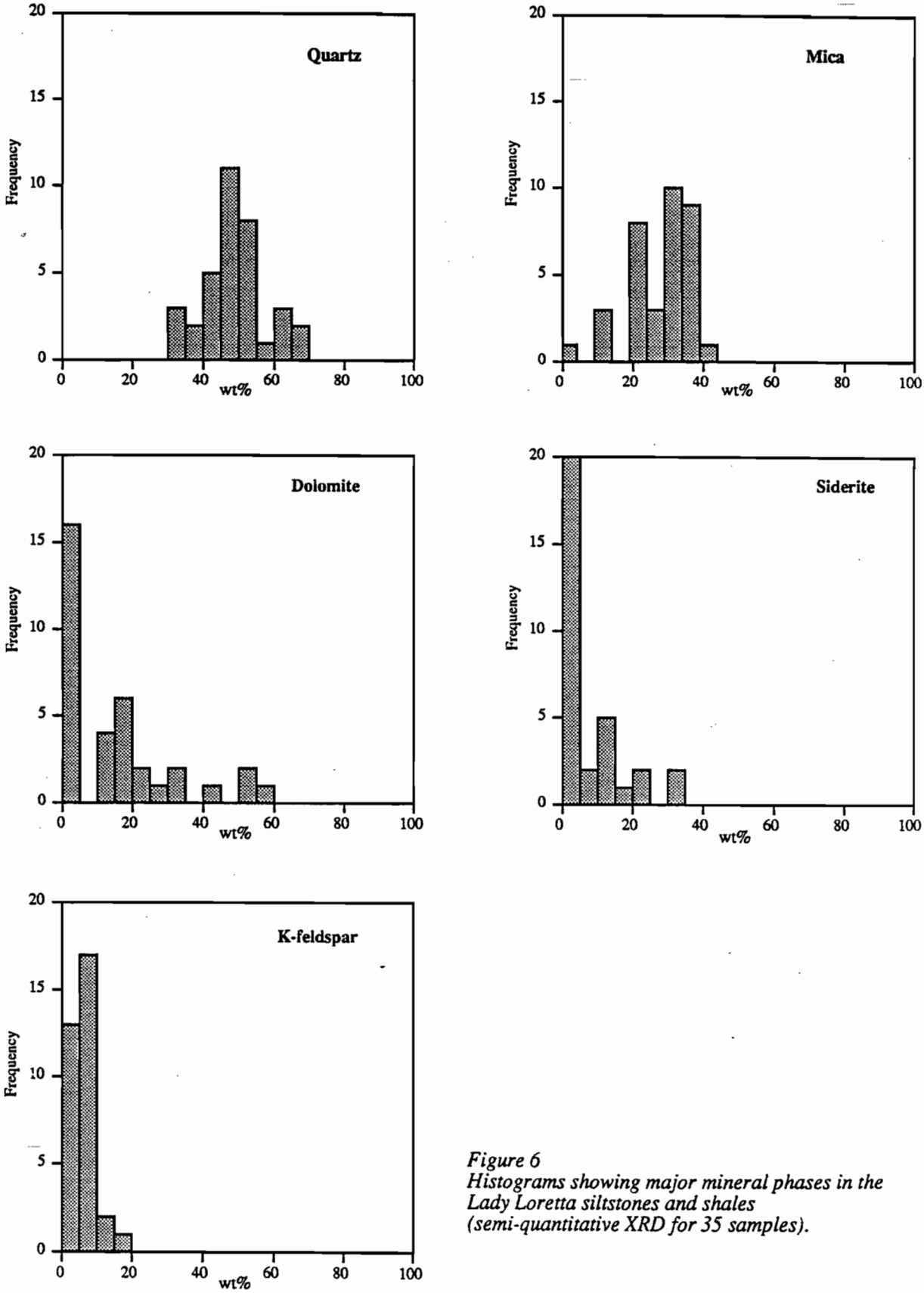

Figure 6
Histograms showing major mineral phases in the Lady Loretta siltstones and shales (semi-quantitative XRD for 35 samples).

Chemical sediments

Pyritic facies

The amount of laminated pyrite interbeds in the siltstones and shales increases in proximity to the Ore Horizon on both sides (Fig. 7; Carr, 1984). At hand specimen scale three types of pyrite can be distinguished (Fig. 8 and Plate 1 d,e, f):

i) Layered/laminated discrete beds ranging from less than a centimetre to several metres thick; this is by far the most common variety. Beds of this pyrite have flat bases and well defined internal, bedding parallel, millimetre and sub-millimetre layering. Where this layering is not well defined the pyrite can have a 'fluffy' appearance. A well developed millimetre spaced penetrative cleavage at a high angle to the layering is present in some areas. The tops can be flat or jagged. This pyrite commonly separates the top of one siltstone/shale cycle from the base of the overlying siltstone.

ii) Pyrite in the siltstone and fine sandstone units. This pyrite type occurs as flecks and disseminations in silty and sandy units immediately overlying bedded pyrite.

iii) Pyrite intimately associated with papery carbonaceous tops to mudstone/shale units.

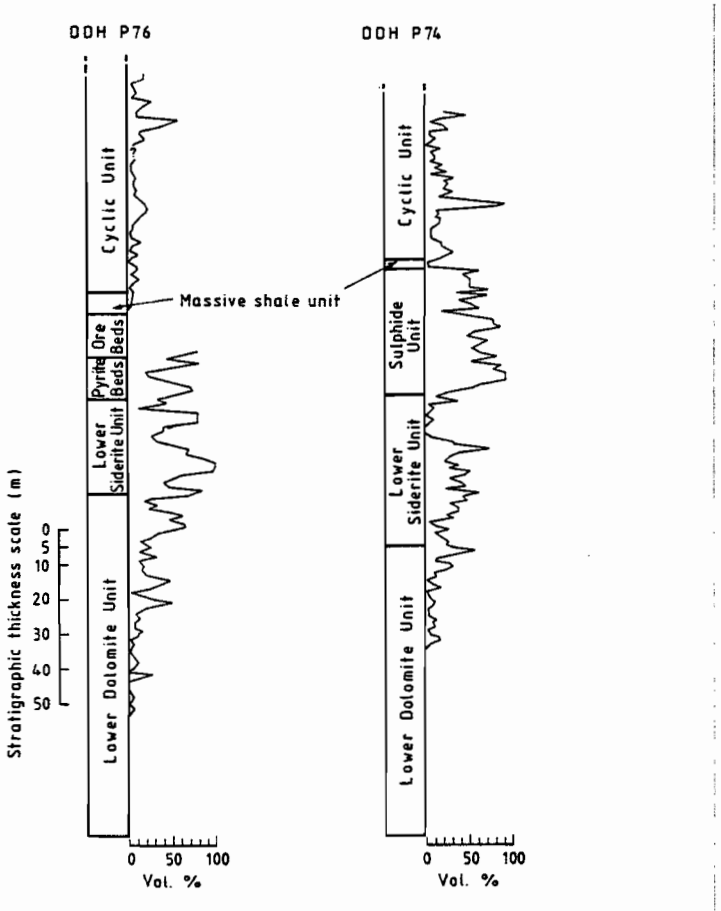

Figure 7 The proportion of pyrite-rich beds through two surface dimond drill holes 500 m apart in the Small Syncline (from Carr, 1984)

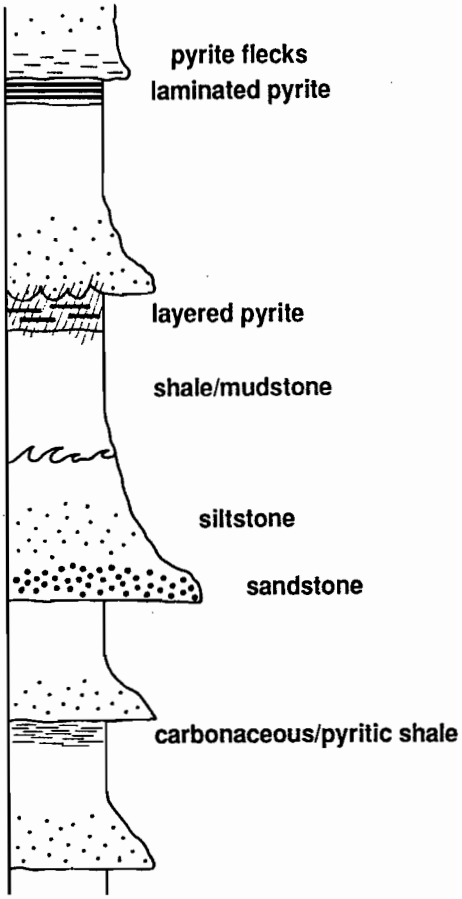

Figure 8 Schematic illustration of the three different pyite types in the Lady Loretta mine sequence rocks

The two latter pyrite occurrences are relatively uncommon and comprise much less than ten percent of the pyrite observed in core.

Pyrite in the Ore Horizon and in the massive Pyritic Unit in the footwall was not easy to categorise due to the poor condition of much of the core, but it often has a laminated or layered appearance which is retained in pyrite within high grade base metal sulphide (Plate 2 b). Granular, more massive pyrite with discordant contacts with base metal sulphide is also present in the OH and PU.

At a microscopic scale all of the pyrite at Lady Loretta comprises aggregates of very fine grained spheroids (Plate. 2 a). True framboids (raspberry-shaped clusters of micron sized pyrite crystals) are also present (Carr , 1981). Etching reveals most fine grained pyrite to be composite grains having a core of pyrite surrounded by a rim of carbonaceous material and overgrown by a second, more easily etched, pyrite type.

•Discussion

The commonest pyrite type (laminated and fluffy pyrite) seems to have accumulated during times of little or no terrigenous clastic input. Because of the intimate association of pyrite with carbonaceous matter Carr (1981) linked formation of thicker pyrite bands to accumulation and breakdown of algal remains. Furthermore, the internal layering and textures in some of the pyrite (Plate 1 e) resembles cryptalgal or microbial structures (Schieber, 1989). It is concluded that much of the bedded pyrite at Lady Loretta formed from the breakdown of thick algal or microbial mat that flourished at times of low terrigenous sediment input into the basin. Anaerobic

breakdown of this material produced reduced S which reacted with Fe in basin or sediment pore waters to fix Fe sulphides. The large quantities of pyrite at Lady Loretta most probably requires an exogenous Fe source.

The pyrite in the base of siltstones is material from the underlying bed which has been ripped up by the current responsible for the overlying turbidite. Carbonaceous papery shales are pelagic deposits where minor pyrite has formed *in situ* (diagenetically), or, possibly, precipitated and settled from an anoxic water column.

Base metal sulphide facies

The Lady Loretta orebody comprises a sulphide lens up to 50 metres thick (in the 'keel' of the Small Syncline). The ore is commonly banded (pyrite and base metal sulphides – Plate 1 g), but a variety of minor ore types and textures are present (Plate 2 b). Highest grades (> 30 wt% Zn equivalent) are in massive ore immediately overlying the 'Pyritic Unit' (Fig. 5). Lower grade parts of the 'Ore Horizon' contain more sediment interbeds. These include siltstone, chert (sometimes with cryptalgal textures – Plate 2 e, f), sedimentary breccias, and at least one potassic, tuffaceous marker bed near the top of the 'Ore Horizon'. The 'Ore Horizon' is barite (±sphalerite) -rich, and galena-poor in upper parts of the west limb of the fold, and in the northern part of the east limb.

Microscopically the base metal sulphide ores comprise fine grained anhedral to subhedral galena and sphalerite aggregates that are interlayered with and surround fine grained euhedral to subhedral laminated pyrite (Plate 2 c). Detrital and chalcedonic quartz and siderite are the most abundant gangue minerals in high grade sulphide ore (Carr, 1981).

On the surface in the Big Syncline the 'Ore Horizon' is marked by a resistant ferrruginous, baritic chert and ferruginous sediments. Mud cracks decorated with (?)gypsum moulds are also present (Plate 2 g). In core in the Big Syncline the 'Ore Horizon' comprises strongly pyritic and hematitic sediments and barite. Ore grade mineralization is known from only one drill hole (P68).

Discussion

Water depth

Carr (1981) argued that the footwall dolomitic unit was deposited in 'less than 10 m' water, and that the Ore Horizon setting was slightly deeper, but not 'much deeper than the 10 m or so indicated in the Lower Dolomite Unit and certainly no deeper than 100 to 200 m'. The delicate

stromatolites and desiccation features reported here indicate shallow to emergent conditions in some parts of the Lady Loretta Syncline during deposition of the 'Ore Horizon', and provide support for Carr's minimum water depth estimate. It is not clear if water depth fluctuated causing periodic emergence of the entire basin, or if local relief allowed parts of the sequence to be (more or less) constantly exposed, or if some combination of these mechanisms operated.

Pyrite – base metal sulphide relationships

Textures in the HYC deposit support a paragenesis for the main sulphides of 'early diagenetic pyrite (Py_1) – later pyrite (Py_2) – base metal sulphides' (Eldridge et al., 1993). These relationships are summarized on Figure 9.

The S isotope data from HYC show two important features:
i) a very wide spread and complete overlap of $\partial^{34}S$ values in Py_1 and Py_2 often within a single sample
ii) galena and sphalerite $\partial^{34}S$ values have a more restricted range of values that lie within the range for pyrite, and moreover, within individual samples there is no systematic relationship between galena and sphalerite, and co-existing pyrite.

Based on these observations Eldridge et al., (1993) prefer a model for HYC mineralization in which Py_1 and Py_2

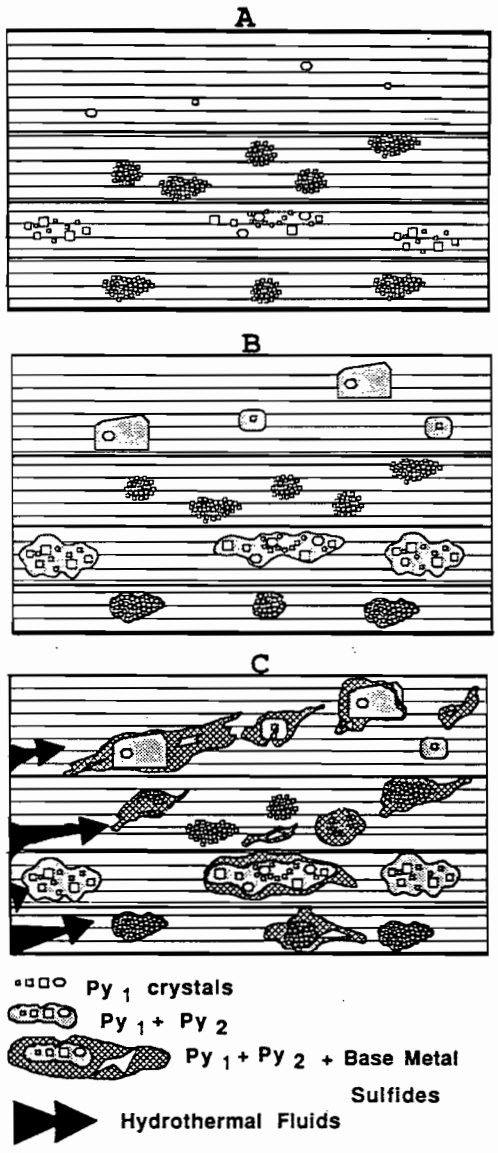

Figure 9 Paragenetic sequence for sulphides at HYC (from Eldridge et al., 1993); A) Py_1 grows in sediment utilizing biogenic H_2S, followed by B) continued biogenic H_2S production, perhaps from a shrinking reservoir of SO_4, and formation of Py_2, terminating with C) introduction of hydrothermal fluids along the bedding depositing sphalerite, galena and some chalcopyrite

formed by bacterial reduction processes in the sediment, and base metal sulphides, marcasite, some carbonate and quartz were precipitated later from hydrothermal fluids moving along the sediment layers. They explained the large quantities of pyrite by invoking a thermal evolution in the hydrothermal system whereby earlier fluids are cooler and Fe-rich and later fluids are warmer and base-metal-rich.

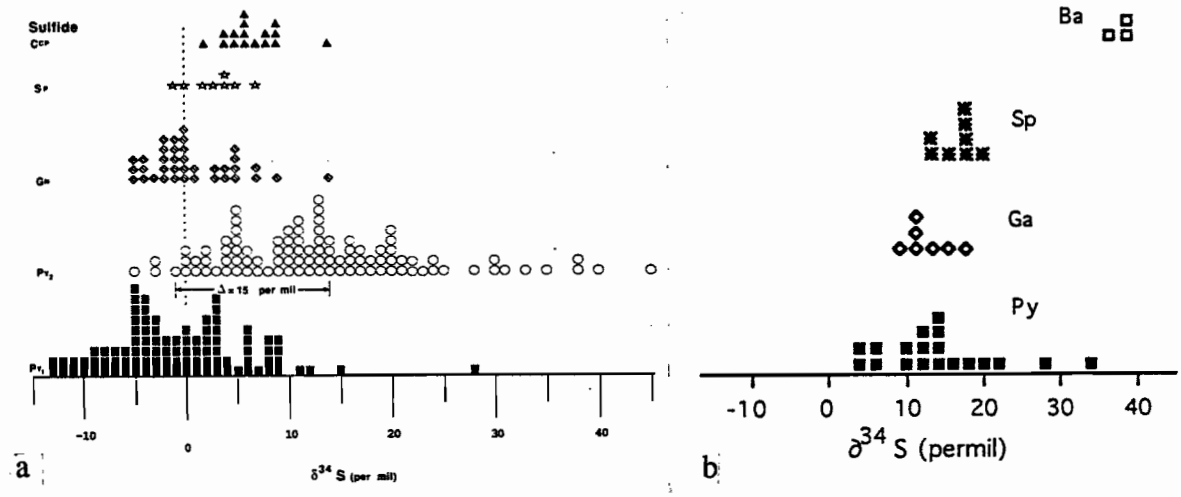

Figure 10 Summary diagrams of isotopic data for a) HYC (SHRIMP analyses from Eldridge et al., 1993 and for b) Lady Loretta (conventional analyses from Carr and Smith, 1977 and Carr et al., 1985)

Although the Lady Loretta deposit is more deformed than HYC and lacks the fine siltstone/sulphide alternations of the HYC ore beds a similar pyrite/base metal sulphide paragenesis is indicated by ore textures (see previous discussion and Plate 2 c). Furthermore, limited conventional S isotope data (Carr and Smith, 1977; Carr et al., 1985) suggest the Lady Loretta ores display the same patterns as HYC (Fig. 10). There is a wide spread in pyrite $\partial^{34}S$ values, with a general trend to heavier S higher in the sequence, and galena and sphalerite have more restricted $\partial^{34}S$ values that show no consistent relationship to co-existing pyrite $\partial^{34}S$ values (Fig. 11).

GENETIC MODELS FOR LADY LORETTA BASE METAL DEPOSIT

Previous descriptions of Lady Loretta have used some variant of an **exhalative-syngenetic model** to explain the base metal mineralization (e.g., Carr, 1981; Derrick, 1993). Both Carr and Derrick invoked a component of biogenic pyrite in the ores, but base metal sulphides, some pyrite and barite all formed from exhaling hydrothermal solutions. Because he recognized difficulties in preventing fluid boiling and loss of metals in the shallow setting of

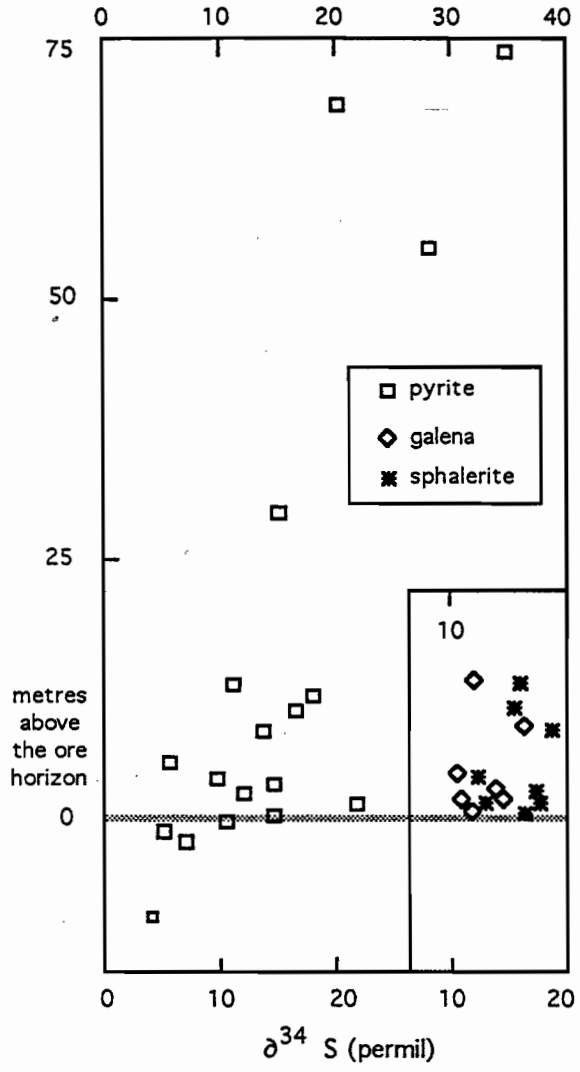

Figure 11 Isotopic composition of S in pyrite, galena and sphalerite in samples collected through the sequence at Lady Loretta. There is a general trend to heavier S in pyrite moving up through the sequence, but no similar trend in the base metal sulphides.

the deposit, Carr (1981) invoked base metal sulphide precipitation deep in a conduit and entrainment of fine sulphide particles in the hydrothermal fluid. When the fluid exhaled the fine particles settled out to form the mineralization. Derrick (1993) did not address the question of boiling and proposed base metal sulphide and pyrite precipitation from dense brine pools ponded in the deepest parts of the Lady Loretta sub-basin, with fluids sourced from syn-sedimentary faults to the north or northeast (Carlton or Western Border Faults).

Derrick suggested syn-sedimentary faults were conduits for mineralizing hydrothermal fluids. Figure 12 schematically depicts a simple exhalative-syngenetic scenario for Lady Loretta.

Although much work remains to be done, because of the pyrite - base metal sulphide textural relationships, and the sulphur isotope data discussed previously, and because of the new understanding of the geometrical relationship between the Lady Loretta orebody and its primary geochemical dispersion halos (see part 5 of this report – Large and McGoldrick, 1993), neither of these exhalative – syngenetic models provides a satisfactorily explanation for Lady Loretta. Alternative models involving formation of mineralization within the unconsolidated sediment pile are considered here as working hypotheses.

These will be discussed using two end-member scenarios:–

'syn-sedimentation – early' model
'syn-sedimentation – late' model

In the **'syn-sedimentation - early' model** (Fig. 13) mineralization forms by increments from hydrothermal fluids

moving through the upper few centimetres or decimetres of sediments. These sediments would have contained substantial amounts of biogenic pyrite, Fe monosulphides, partly decomposed organic matter, and (possibly) reduced gases (e.g., H_2S, CH_4). Base metal sulphide mineralization formed when hydrothermal fluids interacted with this reduced assemblage.

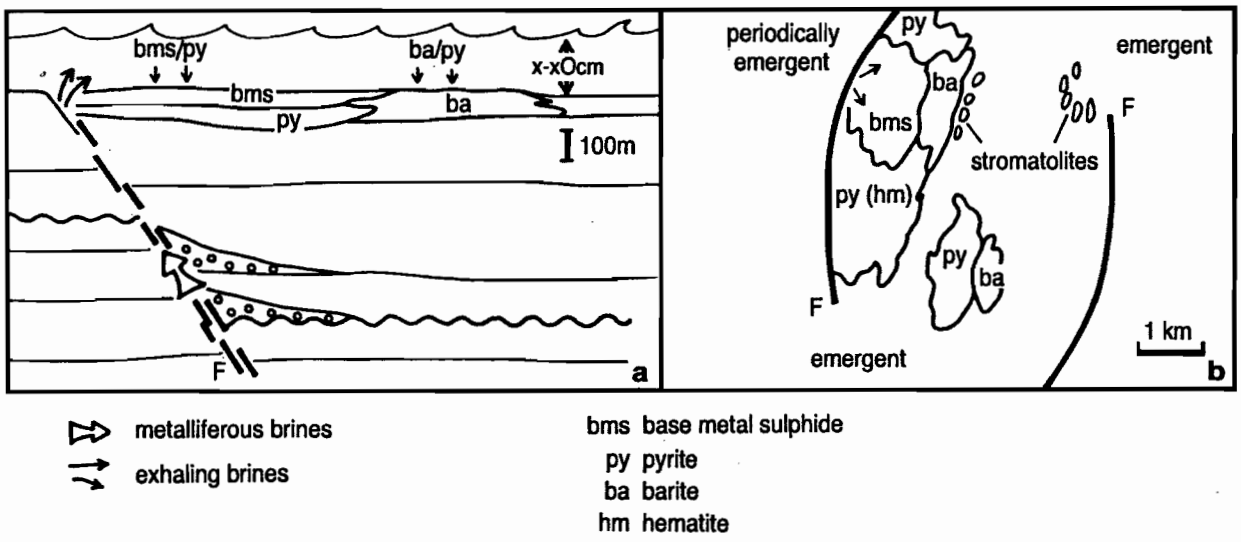

Figure 12 Schematic illustration of a syngenetic-exhalative mineralization model for the Lady Loretta deposit.

a) cross-sectional view showing hydrothermal fluids traversing syn-sedimentary faults and exhaling onto the basin floor or into the water column to deposit pyrite, base metal sulphides and barite

b) plan view of a showing the distribution of mineralization about the feeder fault and its relationship to deeper parts of the sub-basin

Eldridge et al., (1993) have speculated that a single hydrothermal system may be the ultimate metal source for both the early pyrite (cool solutions - carrying Fe only, not base metals) and later base metal sulphides (warm solutions - base metal-rich) for the HYC deposit. A waning of the system to cool fluids provided Fe for the pyritic parts of the hanging wall sequence.

A similar hydrothermal fluid evolution may have occurred at Lady Loretta, with an earlier cooler phase of hydrothermal activity promoting locally prolific biological activity ('microbial oasis'). Anaerobic decomposition of this organic matter resulted in abundant diagenetic Fe sulphides accumulating in the sediment, and sequestered large amounts of sulphate from the basin waters (hence the heavy $\partial^{34}S$ in Lady Loretta pyrite). Barite and hematite may have formed from these cool fluids where they escaped into the overlying, oxidized, water column. As the temperature of the system increased (perhaps associated with other physico-chemical changes in the fluid) the amount of base metals in solution increased. Higher temperatures may have helped promote non-biogenic production of reduced S at the site of mineralization (Dixon and Davidson, in press). The main ore lens would have built up incrementally near the peak

temperatures of hydrothermal activity, but at the same time, closer to the sediment-water interface, conditions must have been conducive to continued microbial activity and diagenetic pyrite formation. Ore grade accumulation of base metal sulphides ceased when the system cooled down again, or when increased sedimentation (e.g., hangingwall turbidites) swamped the hydrothermal system, or through some combination of these.

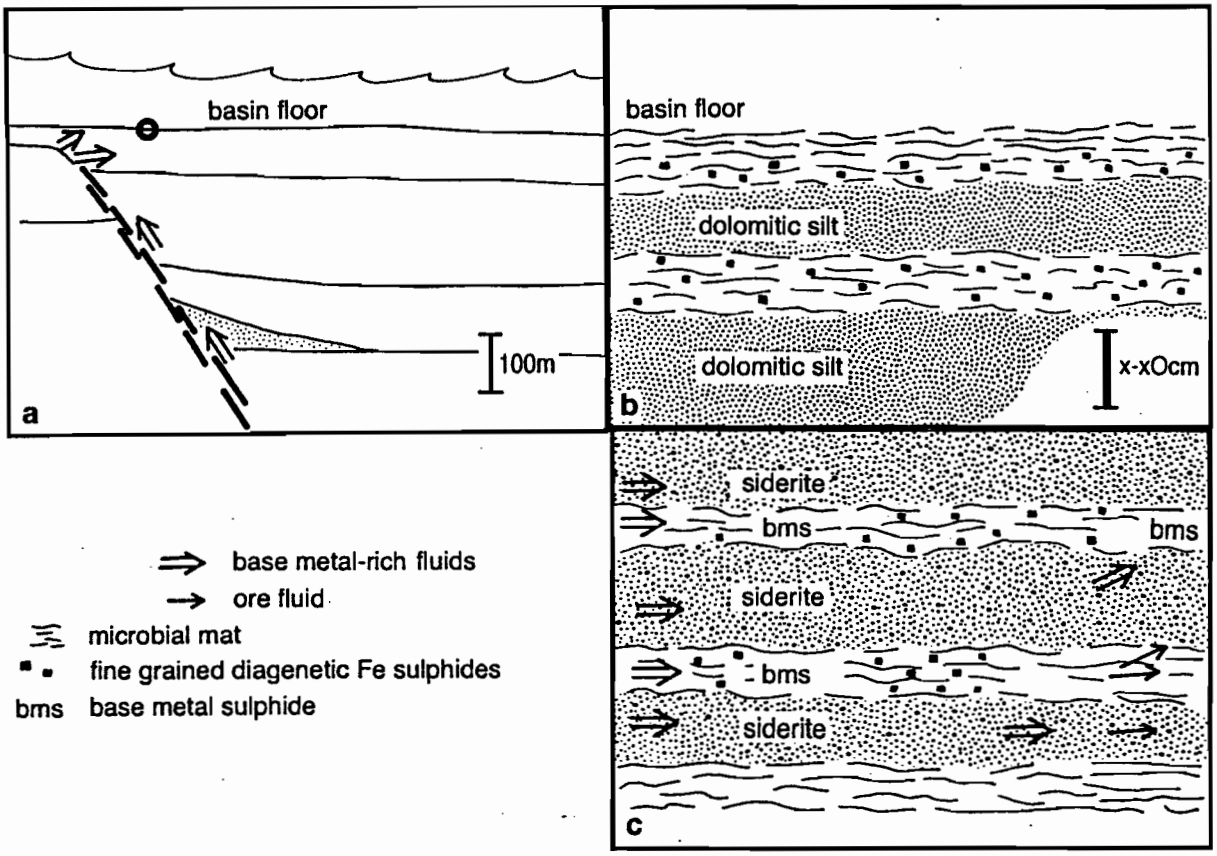

Figure 13 Schematic illustration of a syn-sedimentation - early model for the Lady Loretta deposit.

a) base metal bearing fluids travel up syn-sedimentary faults, but do not escape to the basin floor, but move along aquifers in the subsurface (circle shows the approximate location of Figs 13 b & c)

b) close-up sectional view of the upper few centimetres of soft sediment prior to the introduction of base metal rich solutions; on going microbial (?algal mat) growth at the basin floor results in thick accumulations of decaying organic matter and related sulphate reduction and precipitation of Fe sulphide and ultimately diagenetic pyrite

c) base metal rich solutions moving through the subsurface precipitate base metal sulphides in the Corg and Fe sulphide rich horizons and convert dolomite to siderite in silt/shale layers; thick base metal sulphide accumulations (and dispersion halos) are built up incrementaly

A **'syn-sedimentation - late' model** (Fig. 14) for Lady Loretta shares some similarities with the 'syn-sedimentation - early' model just described, but base metal-rich hydrothermal solutions were not introduced to the sediments until a large sediment thickness (up to several hundred metres) has built up above the ore position. Mineralization formed where transient base metal-rich hydrothermal fluids encountered a suitable chemical trap site in the subsurface (i.e., Fe sulphide and organic carbon-rich parts of the sediment pile). Ore formation was essentially a simultaneous event for the entire thickness of the Ore Horizon, with the distribution of base metal mineralization being controlled by the quantity of available reactants deposited in the unconsolidated sediments, and lateral and cross-stratal porosity/permeability variations.

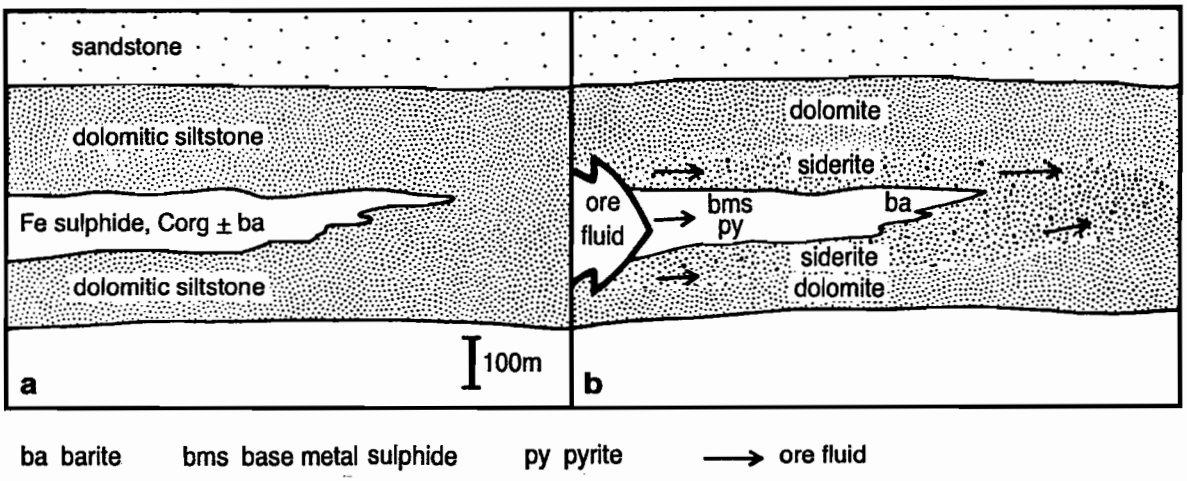

Figure 14 Schematic illustration of a late syn-sedimentation model for Lady Loretta

a) barren dolomitic, pyritic, carbonaceous siltstone sedimentary package several hundred metres thick

b) base metal rich fluids utilize primary (or secondary porosity) to infiltrate and chemically interact with Fe sulphide, Corg -rich parts of this package and precipitate base metal sulphides; mineralization and footwall and hangingwall primary dispersion halos form more ore less simultaneously

Where barite fits in this model is not clear. It may have formed at the same time as the base metal mineralization by replacement of earlier (evaporitic?) sulphate minerals, or, alternatively, it may not be directly related to the base metal mineralization, but formed much earlier at the sediment - water interface.

In both of the syn-sedimentation models much of the fluid flow would have been parallel to the sedimentary layering and controlled by local permeability and porosity variations (e.g., algal mat would make an excellent permeability barrier to cross-stratal flow).

Several other features of the syn-sedimentation models are not well constrained. These include the driving mechanism for fluid flow (e.g., gravitational, thermal, tectonic) and whether fluid flow was episodic or continuous. A better understanding of the physico-chemical character

(esp. temperature and oxidation state) of the mineralizing fluid is also required and would place constraints on the viability of various sulphide precipitation mechanisms, and is the subject of on-going work for this project.

The implications for primary geochemical halo formation of the various genetic models are considered in Part 5 of this report (Large and McGoldrick, 1993).

REFERENCES

Carr, G.R., 1981, The mineralogy, petrology and geochemistry of the zinc-lead-silver ores and host sedimentary rocks at Lady Loretta, northwest Queensland, Ph.D. thesis (unpublished), The University of Wollongong, 431 p.

Carr, G.R., 1984, Primary geochemical and mineralogical dispersion in the vicinity of the Lady Loretta Zn-Pb-Ag deposit, northwest Queensland, Jour. Geochem. Explor., V22, p217-238.

Carr, G.R., and Smith, 1977, A comparative isotopic study of the Lady Loretta zinc-lead-silver deposit, Mineralium Deposita, V12, p105-110.

Carr, G.R., Andrew, A.S. and Bryce, A.J., 1985, Sulfur isotope variations within sedimentary cycles in the Lady Loretta zinc-lead-silver deposit, CSIRO Division of Mineralogy and Geochemistry, Research Review 1985, p25-26.

Cavaney, R.J., 1975, The stratigraphy of the Mount Isa Group equivalents in the Mount Isa — Lawn Hill area, Abstracts of the First Australian Geological Convention, Adelaide, p67.

Crick, I. H., Boreham, C.J., Cook, A.C., and Powell, T.G., 1988, Petroleum geology and geochemistry of Middle Proterozoic McArthur Basin, northern Australia II: assessment of source rock potential, Am. Assoc. Petroleum Geol., v72, p1495-1514.

Derrick, G.M., 1993, Metallogeny of the Mt. Isa Inlier, Part 1: Sediment-hosted Isa-McArthur type Ag-Pb-Zn deposits - Western succession: unpublished report, G.M.Derrick & Associates, January 1993, 65p.

Dixon, G and Davidson, G.J., 1993, A possible example of thermochemical sulphate reduction in a stratabound shale hosted lead-zinc deposit: Dugald River, Australia, Chemical Geology, in press

Eldridge, C.S., Williams, N., and Walshe, J.L., 1993, Sulfur isotope variability in sediment-hosted massive sulphide deposits as determined using the ion microprobe SHRIMP:II A study of the HYC deposit at McArthur River, N.T., Australia: Econ. Geol., V88, p1-26.

Eugster, H.P. and Jones, B.F., 1979, Behavior of major solutes during closed-basin brine evolution, American Jour, Sci., V279, p609-631.

Eugster, H.P., 1969, Inorganic bedded cherts from the Magadi area, Kenya, Contrib. Min.Petr., V22, p1-31.

Forrestal, P.J., 1990, MtIsa and Hilton Ag-Pb-Zn deposits, in Geology of the Mineral Deposits of Australia and Papua New Guinea (Ed F.E. Hughes) p927 - 934 (The Australasian Institute of Mining andMetallurgy: Melbourne).

Hancock, M.C. and Purvis, A.H., 1990, Lady Loretta silver-lead-zinc deposit, in Geology of the Mineral Deposits of Australia and Papua New Guinea (Ed. F.E. Hughes), p943 - 948 (The Australasian Institute of Mining andMetallurgy: Melbourne).

Hutton, L., Cavaney, R.J. and Sweet, I.P., 1981, New and revised stratigraphic units, Lawn Hill Platform, northwest Queensland, Qld.Govt. Mining Jour., V82, p423-434.

Hutton, L. and Sweet , I.P. 1982, Geological evolution, tectonic style, and economic potential of the Lawn Hill Platform Cover, northwest Queensland, BMR Journal of Australian Geology and Geophysics, V7, p125-134.

Hutton, L. and Wilson, I.H., 1984, Mount Oxide Region, Queensland – 1:100,000 geological map commentary, Bureau of Mineral Resources, Australia.

Hutton, L. and Wilson, I.H., 1985, Mammoth Mines Region, Queensland – 1:100,000 geological map commentary, Bureau of Mineral Resources, Australia.

Jones, D.A., 1986, Stratabound zinc-lead mineralisation in the middle Proterozoic McNamara Group, NW Queensland, PhD Thesis, University of New England, Armidale, 198pp.

Large,R.R. and McGoldrick, P.J., 1993, Primary geochemical halos related to Proterozoic sediment hosted Pb-Zn deposits and applications to exploration, CODES AMIRA/ARC Project P384 — Proterozoic sediment-hosted base metal deposits Report No. 3, p63-126.

Logan, R.G., 1979, The geology and mineralogical zoning of the HYC Ag-Pb-Zn deposit, McArthur River, Northern Territory, Australia, MSc thesis (unpublished), The Australian national University.

Logan, R.G., Murray, W.J., and Williams, N., 1990, HYC silver-lead-zinc deposit, McArthur river, Northern Territory, in Geology of the Mineral Deposits of Australia and Papua New Guinea (Ed F.E. Hughes), p907-911(The Australasian Institute of Mining andMetallurgy: Melbourne).

Logan, R.G., Leung, K. and Karelse, G.J.,1993, The McArthur River project, in: Mathew, I.G. (ed) World Zinc '93 Proceedings, AusIMM Publ. 7/93, p27-39.

Mathias, B.V., and Clark, G.J., 1975, The Mount Isa Copper and Silver-Lead-Zinc orebodies - Isa and Hilton mines: *in* Knight, C.L., ed., Economic Geology of Australia and Papua New Guinea: Australasian Institute of Mining and Metallurgy Monograph 5, p. 351-371.

Mathias, B.V., Clark, G.J., Morris, D., and Russell, R.E., 1973, The Hilton deposit — stratiform silver-lead-zinc mineralization of the Mount Isa type, BMR Bulletin 141, p 33-58.

McClay, K.R., and Carlisle, D.G., 1978, Mid-Proterozoic sulphate evaporites at Mount Isa Mine, Queensland, Australia: Nature, v. 274, p. 240-241.

McGoldrick, P.J., 1986, Volatile and precious metal geochemistry of the Mount Isa ores and their host rocks: Unpub. Ph.D. thesis, University of Melbourne, 330 p.

McKirdy, D.M., and T.G. Powell, 1974, Metamorphic alteration of carbon isotopic composition in ancient sedimentary organic matter: new evidence from Australia and South Africa: Geology, v. 2, p. 591-595.

Muir, M.D., 1983. Depositional environments of host rocks to northern Australian lead-zinc deposits, with special reference to McArthur River. Min. Ass. Canada, Short CourseNotes, 9, 141-174.

Neudert, M., 1983, A depositional model for the Upper Mount Isa Group and implications for ore formation: Unpub. Ph. D. thesis, RSES, Australian National University, 324 p.
Neudert, M.K., 1987, Internal report to Lady Loretta JV.

Newbery, S.P., Carswell, J.T., Allnutt, S.L. and Mutton, A.J., 1993, The Dugald River zinc-lead-silver deposit; an example of a tectonised Proterozoic stratabound sulphide deposit, in: Mathew, I.G. (ed) World Zinc '93 Proceedings, AusIMM Publ. 7/93, p7-21.

Page, R.W., 1993, Geological constraints given by U-Pb geochronology in the Mount Isa Inlier, Symposium on recent advances in the Mount Isa Block, A.I.G. Bull. No. 13, p13-15.

Webb, M., and Rohrlach, B., 1992, The Walford Creek prospect — an exploration overview, Exploration Geophysics, V23, p407-412.

Russell, R.E., 1978, Mt Novit prospect, Mt Isa, 3rd Australian Geological Convention Abstracts, p.31.

Schieber, J., 1986, The possible role of benthic microbial mats during the formation of carbonaceous shales in shallow Mid-Proterozoic basins, Sedimentology, V33, p521-536.

Schieber, J., 1989, Pyrite mineralization in microbial mats from the mid-Proterozoic Newland Formation, Belt Supergroup, Montana, Sedimentary Geology, V64, p79-90.

Shepherd and Main, 1990, Recent developments in the evaluation of the Dugald River zinc/lead deposit, Queensland, Geol. Soc. Aust. Abstracts No. 25, 10th AGC Hobart, p 113-114.

Sweet, I.P., Mock, C.M., and Mitchell, J.E., 1981, Siegel, Northern Territory, Hedleys Creek, Queensland – 1:100,000 geological map commentary, Bureau of Mineral Resources, Australia.

Valenta, R.K., 1988, Deformation, fluid flow and mineralization in the Hilton area, Mount Isa, Australia, unpub. PhD, Monash University.

Waltho, A.E. and Andrew, S.J., 1993, The Century zinc-lead deposit, northwest Queensland, The AusIMM Centenary Conference, Melbourne, p41-61.

Waltho, A.E., Allnutt, S.L. and Radojkovic, A.M., 1993, Geology of the Century zinc deposit, northwest Queensland, n: Mathew, I.G. (ed) World Zinc '93 Proceedings, AusIMM Publ. 7/93, p111-129.

Williams, N., 1978a. Studies of the Base Metal Sulfide Deposits at McArthur River, Northern Territory. Australia: I. The Cooley and Ridge Deposits. Econ. Geol., 73, 1005-1035.

Plate 1

a Base of a coarse siltstone decorated with millimetre sized halite casts. Sample is from the Lady Loretta Formation about 40 km SSE of Century deposit (AMG 693 928 on Lawn Hill Region 1:100,000 map).

b Photomicrograph of gypsum moulds in (weathered) mudstone from the Ore Horizon equivalent in the Big Syncline, Lady Loretta.

c Hangingwall sediment samples from the Small Syncline, Lady Loretta. The left hand sample has band of laminated pyrite just above the scale, and well developed flame structures in silty lithologies. Right hand sample is a coarse silt containing minor cross bedded units; the sample is quite sideritic with well developed brown discolouration.

d Samples from the hangingwall (Cyclic Unit), Small Syncline, Lady Loretta. Pyrite bands are present in all the samples (both 'laminated' and 'fluffy' varieties. The third sample from the left has several pyrite bands separating individual siltstone/mudstone cycles. The fourth sample from the left has pyrite top and bottom with three siltstone/shale cycles in between; layering in the siltstone bases has been disturbed by compaction/dewatering effects.

e Detail of 'fluffy' pyrite bands from the hangingwall (Cyclic Unit), Small Syncline, Lady Loretta. Note the planar bases and irregular jagged tops to the pyrite bands. Internal (microbial?) laminations are well preserved in the left hand sample, but a sub-vertical layering (cleavage?) is more prominent in the pyrite band in the right hand sample.

f Sediment samples from the hangingwall (Cyclic Unit), Small Syncline, Lady Loretta. The left hand sample has a laminated pyrite band (just above the scale) and the overlying siltstone/shale cycle contains pyrite flecks in the base of the siltstone (second type of macroscopic pyrite - see text).

g Polished slab of high grade Zn-Pb mineralization from Lady Loretta. Fine scale layering and folding is well developed in pyrite-rich parts of the specimen; the base metal sulphides are not as obviously layered and appear to infil around, and be coarser than the pyrite bands.


cm
inch
a
mm
b
cm
inch
c
cm
inch
d
cm
inch
e
f
cm
inch
g

Plate 2

a Photomicrograph of fine grained pyrite from the Lady Loretta Ore Horizon (e.g., pyrite bands in Plate 1g). The sample has been etched for 30 seconds with 50% HNO_3 and pyrite overgrowths ('Py_2') are present on some grains ('Py_1').

b A selection of sulphide-rich samples from the Ore Horizon at Lady Loretta. Finely banded pyrite dominates the left hand sample, in contrast, the most base metal rich material lacks obvious fine banding and has an almost massive appearance (e.g., third sample from the left).

c Photomicrograph of base metal sulphide mineralization from the Lady Loretta Ore Horizon. A folded layer of fine grain pyrite is present in the lower half of the field of view, and the upper part of the field of view is mainly sphalerite with some coarse euhedral pyrite and minor fine grain pyrite.

d Left hand sample is a graded polymictic breccia unit from within the Ore Horizon at Lady Loretta (Small Syncline). Reverse grading near base indicates this unit was deposited from a high density mass flow; lighter clasts are mainly carbonate, while pyrite dominates the upper part of the unit. No unequivocal clasts of base metal sulphide are present in this unit. The right hand sample is high grade mineralization from Lady Loretta with layered base metal sulphides and an upwards widening discordant vein or pipe. The pipe contains fragments of pyrite and base metal sulphides in a fine sulphide matrix. This feature is interpreted as a fluid escape structure suggesting high fluid pressures and cross-stratal fluid flow syn- or post the formation of the ores.

e Chert with wavy cryptalgal laminations from the Ore Horizon, Small Syncline, Lady Loretta.

f Detail from e showing delicate digitate stromatolite within the chert horizon.

g Desiccation cracks in weathered mudstone a few metres stratigraphically above the Lady Loretta Ore Horizon, Big Syncline (see Plate 1 b for detail).

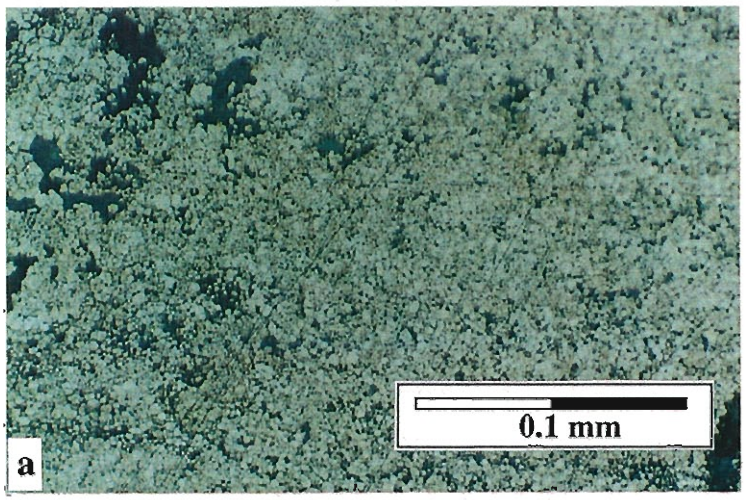
0.1 mm
a


cm
inch
b

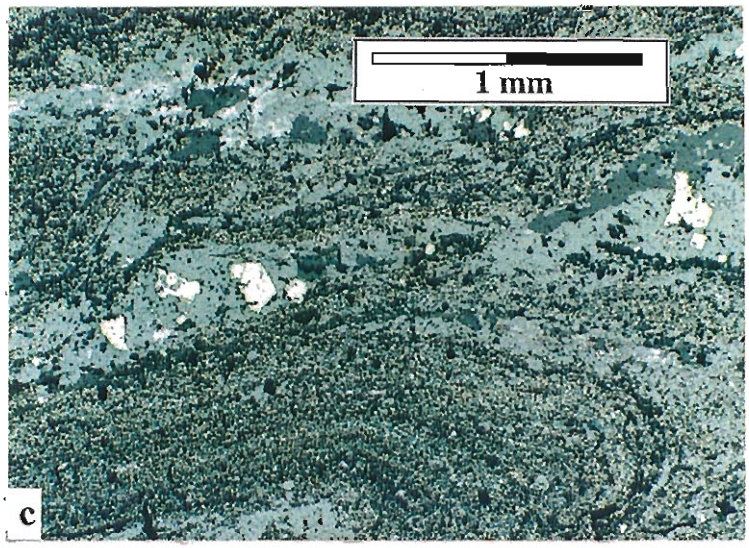
1 mm
c

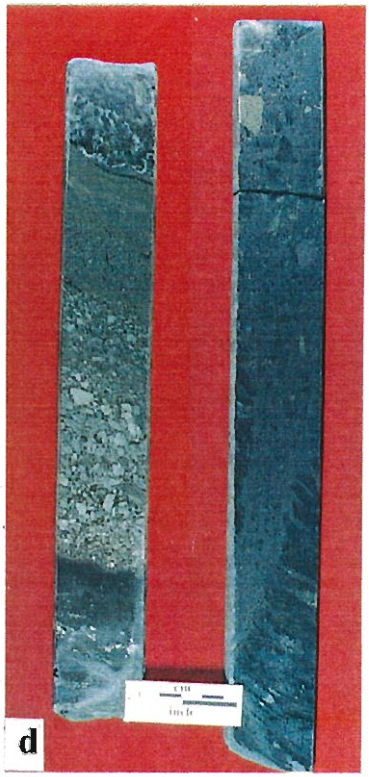
d


cm
inch
e


f

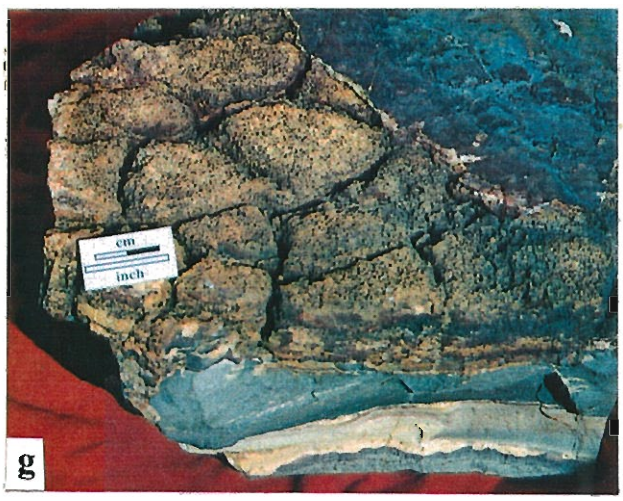
cm
inch
g

DEPOSIT HALOS

4. Sampling and whole rock analyses for the Lady Loretta deposit

Peter McGoldrick

SUMMARY

This report documents the sampling program carried out at Lady Loretta in May 1992. Complete analyses for 30 major and trace elements for 104 sediment samples are presented. All samples were analysed at the University of Tasmania, and a summary of the techniques used for geochemical analysis is provided. These analyses provide the basic data for developing the geochemical halo models presented in Large and McGoldrick, (1993). Appendix 4-I presents an assessment of commercial ICP-ES data for the same group of samples. Appendix 4-II gives a detailed description of the XRF technique developed for determining Tl.

SAMPLING

All material used for geochemical work on the Lady Loretta deposit came from surface and underground diamond drill core. Analyses of 104 sediments (siltstones, mudstones and shales) are reported here and presented on Table 1. These data can be provided to sponsors as a text file on diskette on request. Every effort was made to avoid visibly mineralized and/or pyritic samples. Results from about fourty pyrite and twenty base metal sulphide-rich samples will be presented in a later report. Most samples were found to contain less than two percent S (Fig. 1a), however, a number of samples from the Ore Horizon and the hangingwall sediments contained percent levels of Zn (Fig. 1b). Also, obviously weathered or oxidized material was avoided, but the poor condition of the older ('P' series) core, and brown discolouration on the surface of siderite-bearing core meant visual inspection was not always a good guide to core condition. Although weathered surfaces were ground off the samples prior to crushing, one sample (W3) produced a very brown powder, and several other siderite-rich samples produced

khaki to greenish powders. All the others were grey coloured and could reasonably be assumed to be unweathered.

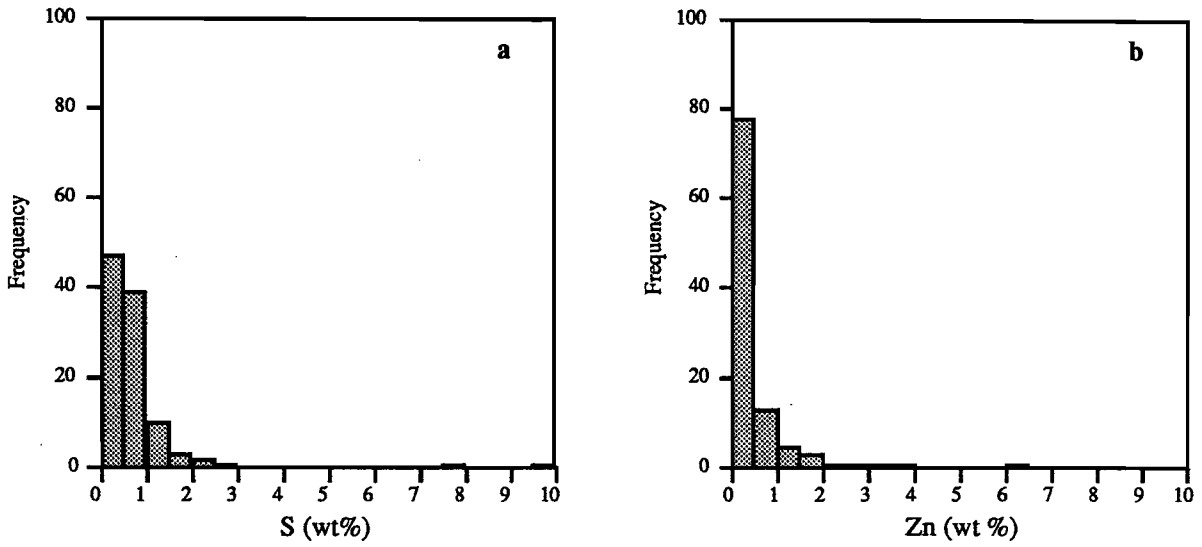

Figure 1
Histograms displaying data for S and Zn for104 sediments (siltstone and shale/mudstone) samples from Lady Loretta.

For convenience, and partly to assess the 'robustness' of our data analysis, all samples are used in the analysis and interpretation presented in part 5 of this report (Large and McGoldrick, 1993). However, in practise it is not recommended that weathered or strongly mineralized samples be used.

The material analysed comprised pieces of quarter or one third core, ten to twenty centimetre long, that were cleaned, coarse crushed in a jaw crusher, then milled to a fine powder in a WC ring mill. Wherever possible, individual samples were from a single lithology or recognisable depositional unit (e.g., complete cycles in thinner cyclic units) were analysed. Thicker units were cut to generate separate siltstone and shale/mudstone samples.

SAMPLE LOCATIONS

The original sampling program made use of available underground and surface drill-core to collect samples of the sediments enclosing the Lady Loretta orebody. Figure 2 shows the location of surface drill holes and cross-sections sampled for this study. Sampling was concentrated in the Small Syncline (80 samples) on, or near, four sections (2120, 2210, 2330, and 2450 mN - mine grid), and individual sample localities are shown on Figures 3 - 6. Footwall sampling was relatively straight forward with samples from a few metres to more than 150 metres stratigraphically below the Ore Horizon being collected. Comprehensive sampling of the hangingwall sequence proved more difficult, with the maximum stratigraphic

distance above the Ore Horizon for a sampled point being about fifty metres. A small group of samples were recently collected from Lady Loretta aimed at rectifying this deficiency and results will be presented in a subsequent report.

Twenty four samples from the Big Syncline were analysed and their localities are shown on Fig. 7. None of the sampled holes contained ore grade mineralisation, but the position of the Lady Loretta ore horizon was interpreted to be represented by an interval of strong pyrite (±barite, ±hematite) development in three of the four sampled holes. Hence, these samples provide data for stratigraphic equivalents of the Lady Loretta host sediments some distance from ore grade mineralization.

ANALYTICAL TECHNIQUES

The original sample set had previously been analysed by ICP-ES in a commercial laboratory but, unfortunately, the quality of these analyses was very mixed (McGoldrick, 1992),. Hence, all samples have been re-analysed by XRF at the University of Tasmania for major and trace elements. Thermal decomposition - infra red spectroscopy (Carlo Erber™ spectrometer) was used to measure **total** C, H, S and N in all samples. For the purpose of calculating analysis totals H was recalculated as H_2O and C as CO_2. This assumes that carbonate rather than organic matter is the important C host in all the samples, however, a few analyses yielded totals greater than 100 percent and probably contained significant organic C. It is planned to analyse a number of these samples for organic C at a later date. Ammonium enrichments have been reported from Selwyn Basin sedimentary Pb-Zn deposits (Benton, 1984), howeer, none of the Lady Loretta samples had detectable N (detection limit was about 0.05wt% N).

A detailed comparison of commercial and University XRF analyses is presented in Appendix 4-I, and several recommendations for monitoring quality control are made.

Major elements (SiO_2, Al_2O_3, FeO, MnO, MgO, CaO, Na_2O, K_2O, and P_2O_5) were determined on fused glass discs following a modified Norrish and Hutton technique (Norrish and Hutton, 1969), and trace elements (Zn, Pb, Ba, Cu, Ni, As, Sb, Tl, Rb, Sr, Cr, V, Zr, Y, U, Th and Br) were determined on pressed powder pellets.

Thallium is not normally determined by XRF and considerable effort was put in to developing a reliable and sensitive method for measuring this element on pressed powder pellets. Details of the technique are provided in Appendix 4-II.

REFERENCES

Benton, L.M., 1984, Ammonium geochemistry of Pb-Zn-Ag sedimentary exhalative ore deposits: a possible exploration tool (Abstract), Geol. Soc. America, Annual meeting Reno NV, p442-443.

Large, R.R. and McGoldrick, P.J., 1993, Deposit Halos 5. Primary geochemical halos related to Proterozoic sediment hosted Pb-Zn deposits and applications to exploration,CODES AMIRA/ARC Project P384 — Proterozoic sediment-hosted base metal deposits Report No. 3, p63-126.

Norrish, K. and Hutton, J.T., 1969, An accurate X-ray spectrographic method for the analysis of a wide range of geological samples, Geochim. Cosmochim. Acta, V33, p431-453.

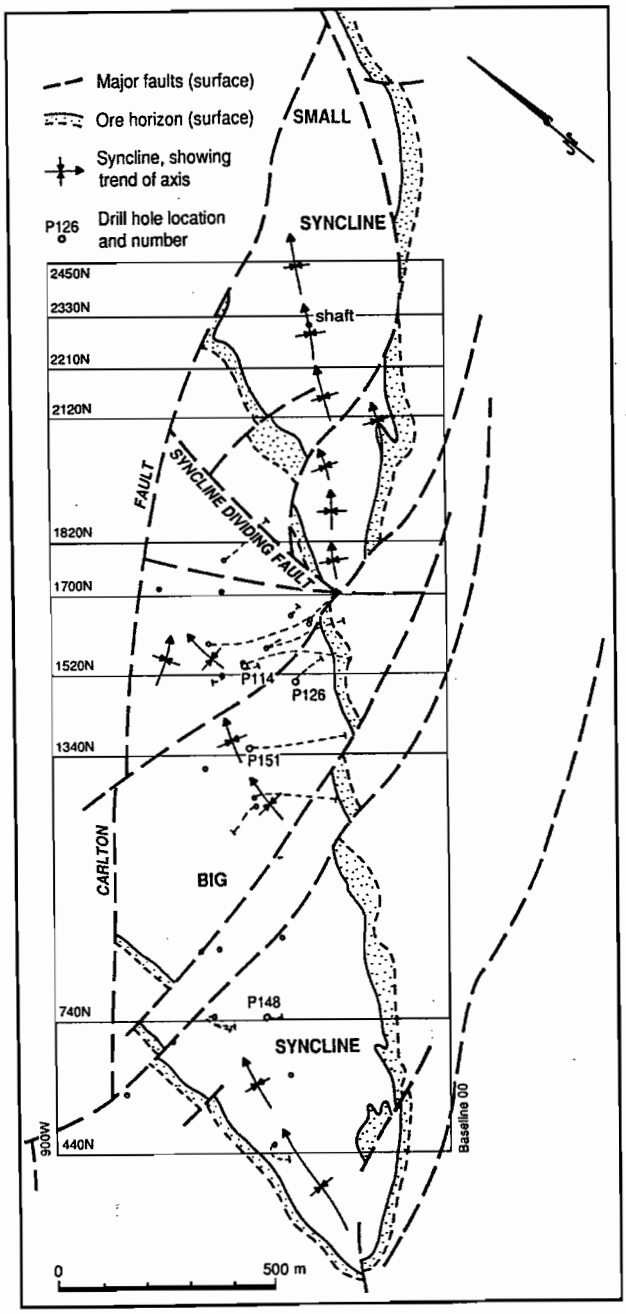

Figure 2 Surface plan showing the mine grid with the location of the sampled sections from the Small Syncline and sampled diamond drill holes from Big Syncline

Table 1 Lady Loretta sediment analyses

I.D.	Location	Depth (m)	Section	Prj. Section	Easting	RL	Drill Hole	Lithology/comment
E1	Small Syncline	0.1	2210	2210	692	1008.5	221 WD20	mst (MU)
E2i	Small Syncline	2.5	2210	2210	689.5	1007.5	221 WD20	slts base (MU)
E2ii	Small Syncline	2.5	2210	2210	689.5	1007.5	221 WD20	mdst top (MU)
H1	Small Syncline	1.0	2450	2450	668.5	1012.5	245 EI22	slts (CU)
H3	Small Syncline	7.0	2450	2450	674.5	1014.5	245 EI22	mst (CU)
H4	Small Syncline	16.5	2450	2450	682.5	1018.5	245 EI22	slts (CU)
I1	Small Syncline	8.5	2450	2450	676	1011	245 EI01	slts (CU)
I2	Small Syncline	11.1	2450	2450	678	1011	245 EI01	sh (CU)
I4	Small Syncline	21.0	2450	2450	688	1011	245 EI01	pale (?dol) slts (MU)
J1	Small Syncline	4.8	2450	2450	672	1008	245 ED25	grey mst (CU)
J2	Small Syncline	11.5	2450	2450	678	1005.5	245 ED25	grey mst (CU)
J9	Small Syncline	72.2	2450	2450	732	979.5	245 ED25	grey sh (PU)
K1	Small Syncline	3.4	2450	2450	663.5	1006.5	245 V90	slst (CU)
L2	Small Syncline	10.8	2340	2330	692	999.5	234 ED30	5cm slt/mud cycle (CU)
L4	Small Syncline	30.3	2340	2330	704.5	992.5	234 ED30	mst (CU)
L5	Small Syncline	34.8	2340	2330	708.5	990.5	234 ED30	slts (CU)
L7	Small Syncline	54.4	2340	2330	725.5	981.5	234 ED30	mst (MU)
L14	Small Syncline	104.1	2340	2330	769.5	958	234 ED30	py (PU)
L15	Small Syncline	106	2340	2330	771	957	234 ED30	sh/py (PU)
L21	Small Syncline	135.1	2340	2330	797	945	234 ED30	sltst (PU)
L25	Small Syncline	173	2340	2330	832	929	234 ED30	mst (LSU)
L27	Small Syncline	182	2340	2330	841	925	234 ED30	sltst (LSU)
L31	Small Syncline	189.1	2340	2330	847	923	234ED30	mst (LSU)
M1	Small Syncline	13.3	2330	2330	691	999	233ED30	sh (CU)
M4	Small Syncline	46.1	2330	2330	719	983	233 ED30	slts (CU)
M7	Small Syncline	61.4	2330	2330	731.5	976	233 ED30	sh (MU)
M14	Small Syncline	96	2330	2330	762	960	233 ED30	slts (PU)
N1	Small Syncline	6	2310	2330	682.5	1000	231 ED62	py & mst (CU)
N2	Small Syncline	16.8	2310	2330	688	990.5	231 ED62	mst (CU)
N4	Small Syncline	24.8	2310	2330	692	983.5	231 ED62	slts & py (CU)
N5	Small Syncline	29.4	2310	2330	694	980	231 ED62	slst/mst (CU)
N7	Small Syncline	38.2	2310	2330	698.5	972.5	231 ED62	slts (CU)
N10i	Small Syncline	69.6	2310	2330	715	945	231 ED62	slts top (CU)
N10ii	Small Syncline	69.6	2310	2330	715	945	231 ED62	sh/mst base (CU)
N14	Small Syncline	78.4	2310	2330	719.5	937.5	231 ED62	sh/mst (MU)
N22	Small Syncline	139.8	2310	2330	753	886.5	231 ED62	slts (LSU)
N23	Small Syncline	150.5	2310	2330	759	878	231 ED62	mst/slts (LSU)
O2	Small Syncline	29.8	2330	2330	668.5	977	233 WD79	slts (CU)
O3	Small Syncline	37.5	2330	2330	666.5	969.5	233 WD79	slts (CU)
O4	Small Syncline	38.5	2330	2330	666	968.5	233 WD79	grey sh (CU)
O5	Small Syncline	72.3	2330	2330	658	935.5	233 WD79	slst/sh (CU)
P2i	Small Syncline	74.1	2330	2330	641	940	233 WD64	sh (MU but prob. top of OH)
P2ii	Small Syncline	74.1	2330	2330	641	940	233 WD64	sh/slst cycle (MU but prob. top of OH)
P4i	Small Syncline	79.4	2330	2330	639	935	233 WD64	lam. slts ('Ore Sediments' = top of OH)
P4ii	Small Syncline	79.4	2330	2330	639	935	233 WD64	sulphidic sh ('Ore Sediments' = top of OH)
Q2	Big Syncline	77.5	740	740	410w	1258	P148	sh/mst (h/w above CU)
Q3	Big Syncline	81.5	740	740	408w	1251	P148	slst (h/w above CU)
Q4	Big Syncline	81.6	740	740	408w	1251	P148	sh/mst (h/w above CU)
Q6	Big Syncline	97.8	740	740	407w	1235	P148	slst/sh (h/w above CU)
Q8	Big Syncline	134.4	740	740	403w	1198	P148	mst/slst (CU)
Q9	Big Syncline	135.5	740	740	403w	1198	P148	slst (CU)
Q11i	Big Syncline	158.5	740	740	400w	1174	P148	silty base of slst/sh cycle (CU? just above OH position)
Q11ii	Big Syncline	158.5	740	740	400w	1174	P148	mst/sh top (CU? just above OH position)
Q16	Big Syncline	200.0	740	740	394w	1133	P148	grey ?mst from PU just below OH position
R1	Big Syncline	191.5	1496	1520	382w	1152	P126	grey sh (h/w of OH posn)
R3	Big Syncline	232.1	1496	1520	378w	1109	P126	slst (h/w of OH posn)
R4	Big Syncline	247.6	1496	1520	375w	1095	P126	slst/sh (h/w of OH posn)
R5i	Big Syncline	262.8	1496	1520	372w	1089	P126	fine slst base (h/w of OH posn)
R5ii	Big Syncline	262.8	1496	1520	372w	1089	P126	sh top (h/w of OH posn)
R8	Big Syncline	312.7	1496	1520	362w	1030	P126	slsts (h/w of OH posn)
S1	Big Syncline	444.0	1340	1340	246w	954	P151	slst/sh/py (f/w of OH)
S2	Big Syncline	431.2	1340	1340	249w	963	P151	slst (f/w of OH)
S7	Big Syncline	353.5	1340	1340	308w	1020	P151	slts/f.g. slst/py (in OH?)
S10	Big Syncline	294.8	1340	1340	345w	1066	P151	large slst/sh (h/w of OH)
T1	Small Syncline	202.0	2120	2120	743	1148	P138	sh with py bed @ base (h/w? up-dip on E limb)
T3	Small Syncline	210.8	2120	2120	741	1139.5	P138	slst (h/w? up-dip on E limb)
T4	Small Syncline	220.0	2120	2120	740	1130	P138	sh (OH equivalent)
T5	Small Syncline	243.5	2120	2120	738	1108	P138	slst (OH equivalent)
V9	Small Syncline	185.0	2450	2450	821	1161	P109	py/sh (OH up-dip on E limb)
W3	Small Syncline	202.0	2120	2120	811	1158	P84	brown dolostone (?OH equ. up-dip on E limb)
W4	Small Syncline	211.0	2120	2120	815	1149	P84	slst/py (?OH equ. up-dip on E limb)

Table 1 Lady Loretta sediment analyses

I.D.	SiO2 (wt%)	TiO2 (wt%)	Al2O3 (wt%)	FeO (wt%)	MnO (wt%)	MgO (wt%)	CaO (wt%)	Na2O (wt%)	K2O (wt%)	P2O5 (wt%)	Total (wt%)
det. lim.											
E1	59.91	0.43	15.27	7.03	0.22	1.83	0.05	0.04	5.45	0.09	99.04
E2i	48.88	0.38	12.27	13.96	0.43	2.11	0.21	nd	4.52	0.07	99.39
E2ii	54.63	0.40	13.61	10.89	0.33	1.81	0.12	nd	4.99	0.06	99.32
H1	55.81	0.28	8.31	14.79	0.56	1.77	0.18	nd	3.12	0.08	100.11
H3	42.83	0.41	12.85	18.02	0.58	1.92	0.18	nd	4.65	0.09	99.12
H4	79.63	0.29	9.98	1.36	<0.01	0.92	0.01	0.05	3.52	0.09	99.04
I1	74.13	0.37	10.99	4.59	<0.01	1.41	0.01	0.03	3.26	0.05	100.79
I2	70.00	0.50	15.39	1.91	<0.01	1.50	0.01	0.09	5.52	0.10	98.94
I4	65.00	0.58	19.17	2.04	<0.01	1.58	0.02	0.11	6.65	0.09	99.84
J1	67.91	0.48	14.06	4.89	0.10	1.44	0.02	0.05	4.98	0.06	99.77
J2	67.26	0.23	7.77	10.59	0.24	1.31	0.03	0.01	2.43	0.04	99.08
J9	82.34	0.12	10.34	0.50	0.00	0.32	0.01	0.01	1.25	0.05	99.52
K1	37.03	0.28	8.18	23.84	0.96	1.78	0.22	nd	2.93	0.06	98.91
L2	61.22	0.52	16.98	5.88	0.06	2.38	0.23	0.11	6.40	0.15	99.83
L4	58.37	0.54	16.03	7.54	0.24	1.64	0.11	0.07	6.42	0.16	99.77
L5	54.01	0.27	8.58	15.76	0.58	1.82	0.17	0.06	3.99	0.09	99.45
L7	67.47	0.57	21.29	0.77	<0.01	0.22	<0.01	0.06	0.38	0.06	99.77
L14	60.24	0.38	11.70	10.85	0.28	1.55	0.06	0.04	4.26	0.07	100.01
L15	62.74	0.49	13.74	6.66	0.17	1.63	0.05	0.03	5.10	0.09	101.78
L21	59.78	0.30	9.21	3.19	0.12	4.31	6.45	0.13	4.83	0.11	101.85
L25	58.41	0.27	8.05	3.19	0.11	4.47	7.52	0.16	4.48	0.10	101.65
L27	53.69	0.42	12.35	4.52	0.10	4.18	5.85	0.17	6.03	0.16	102.67
L31	56.37	0.43	12.43	3.12	0.06	3.59	5.11	0.14	7.04	0.18	105.44
M1	63.41	0.50	17.66	4.57	0.05	2.32	0.14	0.10	6.53	0.15	100.00
M4	56.12	0.44	13.81	10.51	0.31	1.81	0.16	0.04	5.04	0.12	99.56
M7	66.39	0.58	20.18	1.13	<0.01	0.76	0.02	0.08	3.65	0.04	99.37
M14	68.11	0.25	13.65	5.05	0.06	1.42	0.01	0.00	4.99	0.06	99.59
N1	58.37	0.47	16.46	7.58	0.22	2.32	0.16	0.08	6.27	0.13	99.22
N2	61.52	0.54	19.16	4.09	0.05	2.25	0.18	0.14	7.14	0.18	100.22
N4	39.95	0.29	9.57	5.15	0.33	7.38	12.60	0.17	4.06	0.12	101.09
N5	45.64	0.35	11.97	18.03	0.79	2.00	0.19	0.05	5.19	0.09	99.78
N7	64.58	0.30	9.67	11.24	0.31	1.69	0.05	nd	3.27	0.05	101.01
N10i	46.57	0.38	11.26	5.84	0.22	5.30	8.68	0.17	4.95	0.13	100.21
N10ii	56.43	0.42	13.33	3.38	0.11	3.61	5.48	0.17	5.81	0.12	100.03
N14	51.52	0.41	13.11	3.95	0.13	4.50	7.06	0.18	5.37	0.12	100.24
N22	68.12	0.26	8.07	10.36	0.22	1.34	0.03	0.04	2.29	0.04	99.13
N23	63.29	0.54	17.05	3.91	0.04	1.62	0.05	0.12	7.88	0.13	100.18
O2	32.20	0.23	8.02	5.83	0.40	8.84	15.83	0.24	3.19	0.11	101.13
O3	65.12	0.30	9.60	9.82	0.30	1.55	0.18	0.08	4.44	0.12	99.82
O4	55.31	0.47	15.05	3.46	0.09	3.93	4.80	0.16	6.44	0.13	100.56
O5	68.46	0.52	16.21	2.15	0.02	1.66	0.02	0.10	6.00	0.06	99.86
P2i	59.98	0.46	15.54	7.49	0.12	1.97	0.30	0.10	6.48	0.12	100.49
P2ii	53.76	0.41	13.46	12.53	0.23	2.27	0.42	0.11	5.58	0.11	100.16
P4i	48.46	0.23	6.58	16.48	0.35	0.94	0.07	nd	3.54	0.08	100.13
P4ii	47.62	0.47	11.76	13.74	0.14	1.23	0.08	nd	5.58	0.17	100.82
Q2	60.52	0.48	17.01	6.02	0.09	2.43	0.06	0.07	7.05	0.10	99.51
Q3	61.24	0.44	14.88	6.44	0.13	1.66	0.06	0.08	7.39	0.08	99.37
Q4	63.48	0.44	16.26	5.22	0.12	1.88	0.05	0.06	7.26	0.09	102.19
Q6	58.82	0.49	15.83	7.61	0.19	2.21	0.16	0.04	6.63	0.13	99.74
Q8	59.73	0.48	15.32	7.44	0.20	1.55	0.04	0.08	5.64	0.10	98.84
Q9	67.31	0.47	14.83	6.02	0.08	1.45	0.02	0.05	5.32	0.11	101.26
Q11i	67.91	0.45	20.06	1.89	<0.01	1.21	0.01	0.07	5.58	0.05	103.40
Q11ii	66.06	0.47	18.23	1.75	<0.01	1.32	0.02	0.06	6.22	0.05	98.64
Q16	70.28	0.44	15.57	1.51	<0.01	1.47	0.01	0.05	5.76	0.09	100.82
R1	49.46	0.40	13.73	3.71	0.14	5.12	7.50	0.18	6.01	0.13	100.86
R3	37.45	0.28	7.49	7.93	0.34	6.90	13.01	0.19	3.82	0.11	101.86
R4	56.91	0.40	12.90	4.06	0.11	3.64	4.96	0.14	6.06	0.13	100.14
R5i	53.30	0.43	12.97	4.05	0.15	3.97	6.11	0.19	6.42	0.15	101.33
R5ii	54.61	0.45	13.43	3.82	0.14	3.74	5.66	0.17	6.58	0.15	101.71
R8	58.37	0.48	14.89	3.01	0.08	3.18	3.90	0.16	6.50	0.14	100.23
S1	55.12	0.49	15.63	2.94	0.09	3.68	4.62	0.19	6.67	0.14	99.92
S2	57.57	0.22	6.98	2.77	0.15	5.30	8.52	0.16	3.58	0.09	99.91
S7	53.56	0.36	10.30	5.26	0.13	4.30	7.05	0.18	4.98	0.12	101.54
S10	62.66	0.49	16.98	2.02	0.03	2.46	1.90	0.15	6.92	0.12	99.81
T1	58.44	0.49	15.51	9.13	0.31	1.96	0.11	0.07	5.26	0.11	100.57
T3	59.41	0.41	14.45	10.23	0.33	1.60	0.10	0.10	4.87	0.15	100.98
T4	63.49	0.49	16.83	4.75	0.12	1.68	0.02	0.13	6.11	0.06	99.71
T5	63.84	0.21	19.61	2.01	0.01	1.63	0.02	0.11	8.45	0.06	99.82
V9	69.59	0.33	14.70	1.12	0.01	0.84	0.00	0.04	4.23	0.11	98.43
W3	18.23	0.09	2.84	43.89	0.98	2.89	0.58	0.04	0.96	0.02	100.80
W4	29.24	0.17	4.35	4.22	0.36	11.38	18.88	0.19	1.74	0.10	101.21

I.D.	H20 (wt%)	CO2 (wt%)	S (wt%)	Zn (wt %)	Pb (ppm)	Ba (ppm)	Cu (ppm)	Ni (ppm)	As (ppm)	Sb (ppm)	Tl (ppm)	Rb (ppm)
det. lim.					1.5	4	2	1.2	4	2	1.5	0.6
E1	2.59	4.82	0.29	0.87	19	980	<10	14	13	13	21	239
E2i	2.14	11.07	0.67	2.63	38	980	nd	25	172	15	17	195
E2ii	2.32	7.62	0.80	1.64	43	890	11	35	221	18	18	211
H1	1.61	11.58	0.42	1.45	12	1160	<10	10	11	4	7	112
H3	2.32	12.60	0.25	2.29	22	1120	nd	4	9	4	15	200
H4	1.79	0.18	0.50	0.02	216	4840	16	9	55	4	13	130
I1	2.77	2.45	0.50	0.16	34	565	6	28	11	6	7	113
I2	2.68	0.59	0.45	0.03	86	1250	9	16	55	6	16	217
I4	3.22	0.33	0.65	0.06	240	2420	16	19	101	8	17	219
J1	2.59	2.13	0.62	0.30	72	890	15	18	57	8	14	190
J2	1.97	4.73	1.60	0.76	42	734	13	18	65	8	10	87
J9	3.40	0.51	0.56	0.02	37	572	5	6	18	8	9	45
K1	1.43	18.17	0.32	3.69	30	687	nd	11	30	6	10	124
L2	3.04	2.24	0.39	0.12	11	634	2	8	11	8	24	265
L4	2.77	4.54	0.81	0.43	33	756	3	10	15	12	23	245
L5	1.16	11.54	0.30	1.01	13	690	<10	9	16	7	15	136
L7	7.69	0.62	0.52	0.03	421	569	29	26	65	9	<1.5	8
L14	2.23	7.25	0.55	0.51	83	138	<10	6	10	5	10	168
L15	2.68	6.41	1.44	0.51	33	163	<10	16	16	5	14	202
L21	1.16	11.51	0.69	0.01	23	320	6	13	15	3	8	163
L25	0.89	13.48	0.45	0.003	13	297	5	7	10	<2	3	142
L27	1.79	11.73	1.61	0.005	56	340	17	18	33	4	7	208
L31	1.43	14.00	1.46	0.01	45	378	9	19	26	4	3	214
M1	3.31	0.95	0.19	0.04	34	386	2	8	14	8	22	265
M4	2.32	7.15	0.57	0.98	16	1250	<10	20	36	8	19	210
M7	5.18	0.55	0.60	0.03	127	1160	29	24	51	9	8	96
M14	2.41	1.98	1.29	0.27	36	166	5	18	34	5	19	196
N1	2.95	3.55	0.47	0.13	22	360	6	19	37	6	20	254
N2	3.40	1.03	0.38	0.08	21	370	9	15	73	8	22	287
N4	1.43	19.57	0.41	0.01	14	334	1	4	7	6	14	157
N5	1.79	12.35	0.50	0.76	22	434	<10	14	9	6	18	193
N7	1.97	6.67	0.33	0.85	30	325	<10	13	15	9	12	130
N10i	1.52	14.51	0.42	0.02	39	1750	11	10	52	9	20	187
N10ii	1.70	8.72	0.40	0.01	44	2330	12	8	30	10	26	222
N14	1.88	11.43	0.18	0.01	10	2690	8	13	20	8	24	215
N22	2.23	5.17	0.35	0.59	10	225	<10	16	6	5	5	92
N23	2.59	1.54	1.33	0.02	16	388	5	10	19	5	15	285
O2	1.34	24.66	0.19	0.01	6	284	nd	2	<4	5	11	128
O3	1.43	6.30	0.12	0.40	21	458	7	9	10	7	14	150
O4	2.23	7.73	0.63	0.01	11	725	2	14	103	14	22	250
O5	2.95	1.10	0.38	0.11	17	718	4	8	12	12	19	236
P2i	2.41	4.73	0.46	0.03	80	2060	21	17	43	23	24	252
P2ii	2.14	8.46	0.36	0.05	137	1790	45	9	27	37	21	219
P4i	1.34	8.17	7.78	6.30	9630	56400	nd	41	246	45	86	98
P4ii	2.77	4.21	9.74	3.18	11700	28500	nd	36	418	47	66	177
Q2	3.31	1.91	0.01	0.37	7	638	6	31	4	<2	8	266
Q3	2.59	3.04	0.72	0.52	10	602	<10	25	8	<2	9	240
Q4	2.68	3.66	0.29	0.59	7	557	<10	27	10	<2	9	262
Q6	2.86	3.81	0.18	0.66	7	725	<10	27	12	<2	9	255
Q8	3.13	3.96	0.62	0.43	11	890	6	18	22	3	11	249
Q9	2.95	1.87	0.44	0.20	11	980	15	23	26	3	10	224
Q11i	4.29	0.66	0.73	0.02	39	3220	14	14	38	4	11	168
Q11ii	3.22	0.62	0.38	0.01	49	1610	14	13	27	3	11	201
Q16	2.68	2.82	0.06	0.01	199	477	3	8	8	<2	3	134
R1	2.06	11.95	0.42	0.003	7	276	3	11	11	<2	7	224
R3	1.16	20.30	2.80	0.003	38	246	16	17	55	2	13	118
R4	1.70	8.46	0.59	0.003	14	558	6	12	15	2	12	210
R5i	1.61	11.18	0.69	0.003	10	671	2	6	9	<2	13	210
R5ii	1.61	10.52	0.73	0.003	10	685	3	6	9	<2	13	217
R8	1.97	6.52	0.65	0.003	21	2600	20	21	86	4	23	235
S1	2.14	7.62	0.44	0.002	8	980	4	6	11	2	13	256
S2	0.89	13.37	0.20	0.003	6	704	3	3	7	2	6	112
S7	1.25	11.58	2.12	0.002	38	2330	51	12	42	5	16	165
S10	2.50	3.11	0.36	0.002	5	596	2	11	8	<2	10	270
T1	2.95	5.61	0.33	0.20	15	516	3	6	13	3	18	225
T3	2.86	5.72	0.48	0.18	18	597	7	16	52	5	16	198
T4	3.22	1.91	0.70	0.11	30	622	23	31	160	7	19	248
T5	2.77	0.62	0.40	0.01	15	286	3	3	15	4	42	290
V9	3.93	1.25	1.84	0.01	139	3090	4	8	10	8	15	140
W3	1.61	28.03	0.28	0.32	15	59	11	8	7	5	8	43
W4	0.80	29.46	0.27	0.003	25	114	nd	3	<4	<2	10	64

Table 1 Lady Loretta sediment analyses

I.D.	Sr (ppm)	Cr (ppm)	V (ppm)	Zr (ppm)	Y (ppm)	U (ppm)	Th (ppm)	Br (ppm)
det. lim.	1	1	1.5	1	1	1.2	1.5	1
E1	72	67	75	107	34	4	17	<1
E2i	39	53	61	107	29	4	15	<1
E2ii	52	59	68	102	29	4	15	<1
H1	41	30	46	172	22	4	12	<1
H3	295	60	70	103	25	9	17	<1
H4	423	28	35	145	49	4	12	<1
I1	120	36	68	270	37	8	15	<1
I2	453	61	73	150	45	6	19	<1
I4	316	74	139	161	35	7	22	<1
J1	176	61	65	128	25	4	17	<1
J2	126	21	26	134	21	2	10	<1
J9	66	14	19	35	9	3	6	<1
K1	172	34	39	101	23	2	11	<1
L2	13	77	88	122	26	5	19	<1
L4	195	70	87	145	28	8	20	<1
L5	36	30	33	124	19	3	11	<1
L7	226	83	70	151	18	11	24	<1
L14	154	37	43	242	36	6	16	<1
L15	211	58	74	204	36	7	18	<1
L21	32	50	41	195	22	3	10	<1
L25	40	30	38	200	25	3	11	2
L27	29	47	66	170	32	5	15	<1
L31	28	49	72	190	29	5	15	2
M1	67	75	87	118	25	6	21	<1
M4	103	57	68	126	29	3	16	<1
M7	128	79	54	164	19	6	21	<1
M14	176	12	23	119	31	10	19	<1
N1	56	70	84	116	25	7	19	<1
N2	74	88	102	125	27	10	19	<1
N4	84	50	66	80	15	4	10	2
N5	42	57	69	90	21	6	13	<1
N7	100	31	35	133	20	4	11	<1
N10i	95	49	57	144	25	3	13	2
N10ii	73	62	67	119	23	4	15	<1
N14	86	60	71	123	25	3	15	1
N22	50	33	29	191	20	4	10	<1
N23	17	62	74	167	32	6	19	<1
O2	93	44	56	67	19	6	8	2
O3	48	34	39	121	20	5	10	<1
O4	43	66	79	127	25	3	15	<1
O5	133	66	77	143	29	7	21	<1
P2i	15	66	78	117	25	4	18	<1
P2ii	10	58	71	111	25	3	16	<1
P4i	142	21	35	203	14	3	27	1
P4ii	350	46	81	154	17	7	27	<1
Q2	61	75	83	118	27	12	17	<1
Q3	91	60	73	113	29	6	17	<1
Q4	107	66	80	108	30	14	19	<1
Q6	61	75	78	128	27	3	18	<1
Q8	468	65	82	124	27	4	17	<1
Q9	458	59	69	120	23	4	16	<1
Q11i	94	51	90	151	23	6	15	<1
Q11ii	79	63	94	130	22	6	15	<1
Q16	132	58	67	134	31	5	16	<1
R1	40	64	79	108	24	5	14	<1
R3	61	38	63	87	20	3	11	3
R4	52	56	58	146	25	4	15	<1
R5i	58	62	75	133	23	5	16	1
R5ii	54	66	78	131	23	5	16	<1
R8	63	65	73	133	24	4	16	<1
S1	30	63	72	127	26	5	17	<1
S2	45	26	33	232	20	4	10	<1
S7	63	47	58	120	20	3	12	2
S10	25	77	83	123	24	5	19	<1
T1	16	69	77	132	29	5	18	<1
T3	16	47	53	155	36	3	14	<1
T4	94	70	84	123	26	5	18	<1
T5	13	7	24	145	36	8	26	<1
V9	793	39	63	95	11	6	18	1
W3	2	13	19	25	20	2	4	<1
W4	37	24	30	57	17	2	5	2

Table 1 Lady Loretta sediment analyses

I.D.	Location	Depth (m)	Section	Prj. Section	Easting	RL	Drill Hole	Lithology/comment
W5	Small Syncline	222.6	2120	2120	820	1139	P84	slst with py bands (?OH equ. up-dip on E limb)
W7	Small Syncline	227.5	2120	2120	821.5	1135	P84	mst (?OH equ. up-dip on E limb)
W8	Small Syncline	232.0	2120	2120	824	1130.5	P84	(?OH equ. up-dip on E limb)
W9	Small Syncline	232.2	2120	2120	824	1130.3	P84	mst (?OH equ. up-dip on E limb)
W12	Small Syncline	248.6	2120	2120	831	1115.5	P84	slst (?PU equ. up-dip on E limb)
W16	Small Syncline	259.7	2120	2120	835.5	1105.5	P84	mst (?PU equ. up-dip on E limb)
W19	Small Syncline	273.3	2120	2120	842	1093.5	P84	slst cycle (?PU equ. up-dip on E limb)
X1	Small Syncline	238.0	2120	2120	704.5	1111	P96	sh (CU abt 10 m into h/w of OH)
X7	Small Syncline	317.0	2120	2120	678	1036	P96	slst (f/w abt 40m below base of OH)
X8	Small Syncline	317.2	2120	2120	678	1036.2	P96	slst (f/w abt 40m below base of OH)
Y2	Small Syncline	296.6	2210	2210	692.5	1147.5	P87	slst (CU abt 40m into h/w)
Y3	Small Syncline	297.0	2210	2210	692.5	1147	P87	sh (CU abt 40m into h/w)
Y4	Small Syncline	297.3	2210	2210	692.5	1147	P87	sh (CU abt 40m into h/w)
Y5	Small Syncline	301.6	2210	2210	691.5	1143.5	P87	slst (CU abt 40m into h/w)
Y6i	Small Syncline	506	2210	2210	652	842	P87	slst base (deep f/w; abt 100m below PU/OH contact)
Y6ii	Small Syncline	506	2210	2210	652	842	P87	shale top (deep f/w; abt 100m below PU/OH contact)
Z3	Small Syncline	18	2420	2450	671.5	992.5	242 ED72	sh (MU)
Z5	Small Syncline	24.2	2420	2450	673	988	242 ED72	sh/slst (MU)
Z7i	Small Syncline	28.8	2420	2450	675	982	242 ED72	slst base(MU)
Z7ii	Small Syncline	28.8	2420	2450	675	982	242 ED72	shale top (MU)
Z12	Small Syncline	48.6	2420	2450	681.5	963	242 ED72	slts (OH-'Ore Sediments')
Z14	Small Syncline	56.8	2420	2450	684	955.5	242 ED72	slts (OH-'Ore Sediments')
Z26	Small Syncline	103.5	2420	2450	698.5	911	242 ED72	grey dolomite + carb. veins (PU)
P114-	Big Syncline	301.8	1530	1520	436w	1043	P114	shale (h/w, abt.100m above inferrred OH)
P114-	Big Syncline	321.6	1530	1520	435w	1024	P114	sltst (h/w, abt 80m above inferrred OH)
P114-	Big Syncline	321.6	1530	1520	435w	1024	P114	mst (h/w, abt 80m above inferrred OH)
P114-	Big Syncline	340	1530	1520	433w	1004	P114	shale (h/w, abt 60m above inferrred OH)
P114-	Big Syncline	350	1530	1520	432w	994	P114	shale (h/w, abt 50m above inferrred OH)
P155-	Small Syncline	302.7	2270	2210	952	1057	P155	dk grey/black sh (deep f/w - collared E of OH outcrop)
P155-	Small Syncline	338.5	2264	2210	951	1021	P155	lam carbc slst with minor mst (deep f/w)
P155-	Small Syncline	365.9	2260	2210	949	994	P155	lam carbc slst (deep f/w - collared E of OH outcrop)
P155-	Small Syncline	395.3	2252	2210	948	965	P155	part. lam. f.g. slst/mst (deep f/w)
P155-	Small Syncline	528.9	2232	2210	945	832	P155	'massive' slst (deep f/w - collared E of OH outcrop)

Table 1 Lady Loretta sediment analyses

Ident	SiO2 (wt%)	TiO2 (wt%)	Al2O3 (wt%)	FeO (wt%)	MnO (wt%)	MgO (wt%)	CaO (wt%)	Na2O (wt%)	K2O (wt%)	P2O5 (wt%)	Total (wt%)
W5	23.06	0.15	3.76	4.78	0.38	12.86	20.86	0.26	1.46	0.09	101.75
W7	54.75	0.45	13.63	3.90	0.07	3.63	4.42	0.14	6.01	0.20	102.64
W8	53.97	0.15	11.80	3.15	0.13	4.66	6.87	0.16	6.60	0.08	100.46
W9	69.27	0.18	11.04	1.68	0.05	2.28	2.62	0.10	6.06	0.09	100.84
W12	33.47	0.13	3.41	4.88	0.34	10.48	18.08	0.23	1.71	0.08	101.67
W16	61.66	0.47	15.14	7.11	0.38	1.59	0.37	0.11	5.98	0.13	100.32
W19	69.74	0.25	12.95	1.20	0.03	2.30	2.29	0.08	6.15	0.10	100.67
X1	67.01	0.49	16.91	2.56	0.01	1.95	0.04	0.05	5.72	0.11	99.53
X7	64.01	0.44	14.55	5.15	0.10	1.45	0.11	0.14	6.63	0.21	99.31
X8	69.82	0.40	11.85	3.37	0.08	1.09	0.08	0.08	5.74	0.13	100.04
Y2	54.19	0.25	7.86	15.47	0.58	1.59	0.23		3.92	0.13	99.82
Y3	55.50	0.49	16.18	7.50	0.24	1.65	0.16	0.03	6.80	0.13	98.95
Y4	63.59	0.57	18.05	2.87	0.03	1.71	0.08	0.10	7.24	0.14	100.35
Y5	60.64	0.20	7.07	13.12	0.49	1.79	0.17	nd	3.16	0.09	99.13
Y6i	31.62	0.20	5.81	4.60	0.29	10.32	17.17	0.19	2.70	0.10	101.63
Y6ii	46.21	0.41	9.19	3.44	0.17	6.59	10.45	0.16	4.79	0.13	102.48
Z3	58.36	0.44	15.03	8.72	0.21	1.66	0.08	0.06	5.44	0.04	99.27
Z5	55.57	0.43	14.21	10.68	0.33	1.71	0.10	0.03	5.18	0.08	99.42
Z7i	56.14	0.45	13.63	11.47	0.24	2.25	0.09	nd	4.29	0.11	100.15
Z7ii	56.00	0.46	14.29	11.39	0.23	2.60	0.04	0.02	4.47	0.04	99.82
Z12	65.78	0.44	15.15	4.21	0.04	1.69	0.03	0.09	5.43	0.11	100.45
Z14	72.65	0.41	11.74	1.84	0.01	1.03	0.05	0.11	3.65	0.16	100.68
Z26	66.18	0.08	21.76	0.22	<0.01	0.12	0.01	0.03	0.05	0.04	98.40
P114-1	57.71	0.50	16.63	2.23	0.06	3.14	3.19	0.17	7.13	0.14	98.72
P114-2i	50.45	0.43	12.99	4.77	0.21	4.57	7.21	0.16	5.87	0.14	101.76
P114-2ii	52.15	0.48	14.63	4.27	0.16	4.07	5.60	0.21	6.05	0.13	100.20
P114-3	50.94	0.43	13.07	4.31	0.22	4.44	7.18	0.23	5.49	0.13	100.90
P114-4	56.02	0.50	17.65	2.75	0.10	3.24	3.51	0.21	7.07	0.15	99.71
P155-1	62.82	0.55	17.27	2.42	0.01	1.93	0.78	0.13	8.63	0.17	102.90
P155-2	48.40	0.35	9.63	3.37	0.11	6.30	10.02	0.23	4.57	0.11	100.51
P155-3	58.56	0.36	9.71	2.84	0.07	4.50	6.71	0.20	4.44	0.10	100.57
P155-4	58.71	0.20	5.77	2.74	0.09	5.80	9.01	0.23	3.06	0.09	101.25
P155-5	53.87	0.41	10.03	2.54	0.06	5.92	8.03	0.20	4.02	0.13	101.02

Table 1 Lady Loretta sediment analyses

I.D.	H20 (wt%)	CO2 (wt%)	S (wt%)	Zn (wt %)	Pb (ppm)	Ba (ppm)	Cu (ppm)	Ni (ppm)	As (ppm)	Sb (ppm)	Tl (ppm)	Rb (ppm)
det. lim.					1.5	4	2	1.2	4	2	1.5	0.6
W5	0.89	32.90	0.29	0.00	22	119	nd	1	<4	<2	7	56
W7	2.59	10.44	2.35	0.00	49	255	4	14	26	4	30	212
W8	1.43	10.48	0.93	0.00	19	227	1	5	14	<2	35	194
W9	1.34	5.50	0.59	0.00	13	199	2	3	8	3	34	185
W12	0.54	28.10	0.19	0.00	20	112	1	5	8	<2	2	57
W16	2.41	4.21	0.67	0.03	18	230	1	19	11	<2	16	264
W19	1.52	3.77	0.25	0.00	13	192	4	5	9	<2	12	228
X1	2.86	0.81	0.55	0.34	116	890	21	27	130	11	22	247
X7	2.59	3.19	0.60	0.05	14	455	1	12	16	9	21	227
X8	1.88	4.84	0.57	0.04	16	408	4	16	19	9	18	189
Y2	1.25	11.21	0.93	1.99	67	1610	<10	7	33	11	20	125
Y3	2.77	5.13	0.75	1.49	42	890	<10	21	54	13	20	255
Y4	3.22	1.72	0.80	0.12	27	692	4	12	30	13	20	269
Y5	1.43	8.98	0.38	1.59	17	341	<10	6	19	7	10	93
Y6i	0.80	27.19	0.57	0.01	12	131	1	0	14	4	24	82
Y6ii	1.16	18.91	0.80	0.01	14	264	2	3	9	5	36	133
Z3	2.50	5.68	0.19	0.70	15	1070	<10	16	23	8	17	232
Z5	2.59	6.01	1.25	1.06	140	1250	49	33	478	12	18	222
Z7i	3.22	5.39	1.49	1.22	175	1250	19	28	163	9	21	192
Z7ii	3.49	4.40	1.23	0.97	85	1340	29	29	377	11	19	204
Z12	2.95	3.04	0.76	0.28	343	3050	4	16	39	11	17	181
Z14	2.23	1.47	1.43	0.45	713	23600	11	7	45	14	13	73
Z26	8.67	0.40	0.28	0.01	110	3670	5	4	7	1	2	1
P114-1	2.32	5.13	0.30	0.00	8	355	20	12	16	2	9	273
P114-2i	1.61	12.16	1.12	0.00	22	322	8	11	56	2	11	201
P114-2ii	2.23	9.23	0.92	0.00	19	291	12	12	50	3	9	224
P114-3	1.79	11.91	0.70	0.00	9	342	6	7	12	<2	9	205
P114-4	2.50	5.72	0.22	0.00	6	387	19	10	16	<2	9	279
P155-1	2.23	4.80	1.07	0.00	15	496	7	20	20	3	3	308
P155-2	1.25	15.65	0.46	0.00	31	280	9	10	11	3	2	165
P155-3	1.34	11.10	0.57	0.00	11	291	11	14	11	<2	<1.5	170
P155-4	0.80	14.29	0.41	0.00	26	256	7	14	11	<2	<1.5	95
P155-5	1.52	13.52	0.72	0.00	11	184	4	17	17	<2	<1.5	161

Table 1 Lady Loretta sediment analyses

I.D.	Sr (ppm)	Cr (ppm)	V (ppm)	Zr (ppm)	Y (ppm)	U (ppm)	Th (ppm)	Br (ppm)
det. lim.	1	1	1.5	1	1	1.2	1.5	1
W5	43	23	25	52	12	2	4	2
W7	19	55	81	156	26	5	18	1
W8	20	8	19	89	29	8	15	<1
W9	9	15	27	82	21	5	13	<1
W12	53	15	13	80	10	3	6	2
W16	12	60	65	123	25	7	17	<1
W19	15	16	26	94	20	9	15	<1
X1	171	58	72	137	31	5	19	<1
X7	18	38	61	258	41	7	19	<1
X8	16	38	63	255	33	6	16	<1
Y2	76	26	32	133	24	3	9	<1
Y3	46	70	86	127	26	5	19	<1
Y4	61	74	92	145	28	6	20	<1
Y5	33	20	24	146	21	4	9	<1
Y6i	37	32	47	75	13	2	7	2
Y6ii	25	55	56	129	15	4	12	<1
Z3	54	67	75	112	24	3	17	<1
Z5	209	62	73	111	25	5	16	<1
Z7i	199	53	65	181	29	4	17	<1
Z7ii	34	56	64	146	27	4	15	<1
Z12	547	38	65	330	55	8	19	<1
Z14	928	30	64	424	69	11	22	<1
Z26	201	24	19	38	3	2	6	<1
P114-1	27	73	85	124	23	4	18	<1
P114-2i	34	60	73	155	26	5	15	1
P114-2ii	29	73	91	134	28	11	16	1
P114-3	45	65	76	117	24	6	15	<1
P114-4	26	84	93	119	26	5	17	<1
P155-1	24	60	79	184	32	4	24	<1
P155-2	39	42	55	212	22	4	12	<1
P155-3	29	43	50	277	24	4	13	<1
P155-4	34	18	22	127	16	3	7	<1
P155-5	32	43	65	181	20	5	10	1

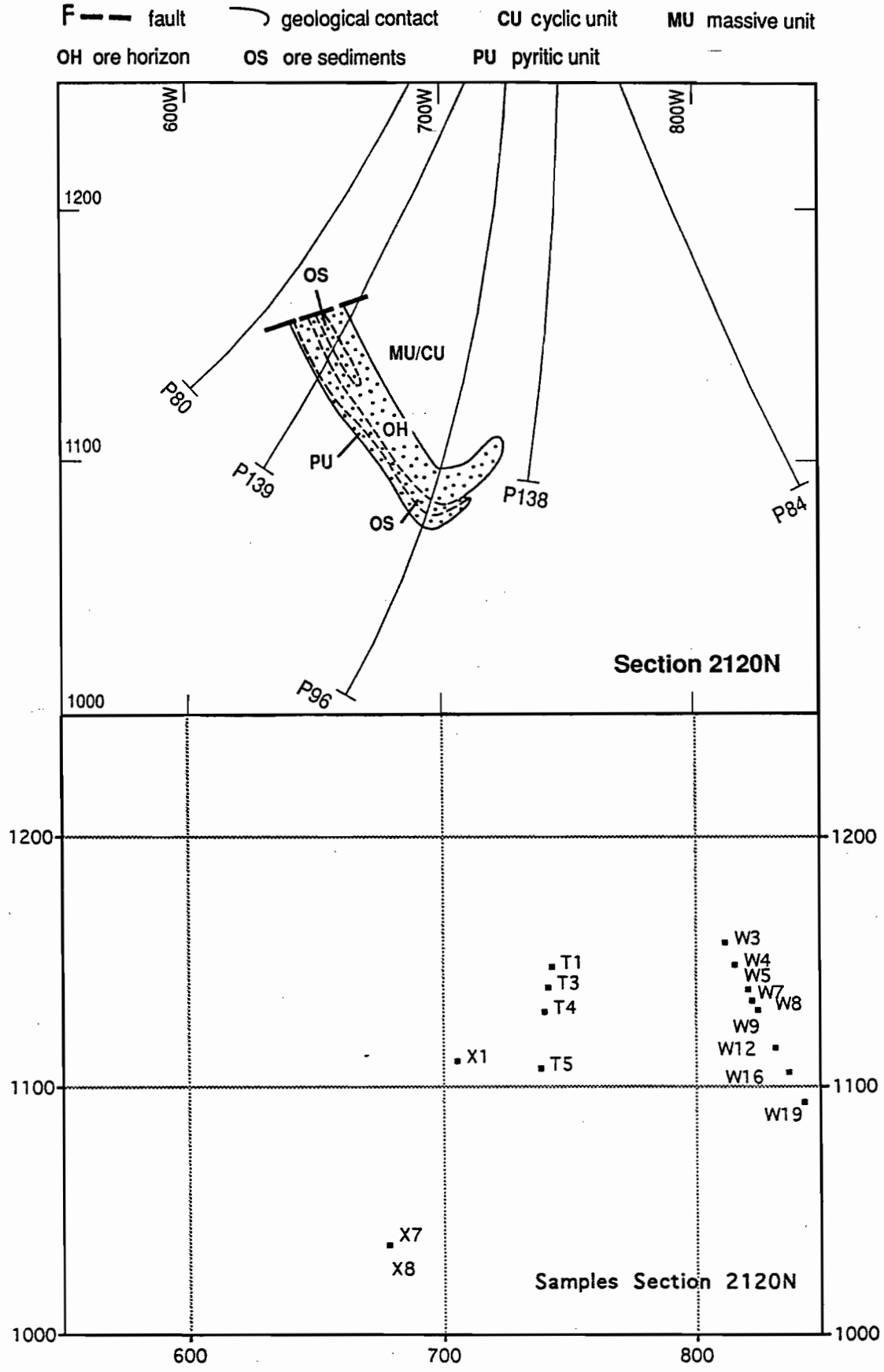

Figure 3 Cross-section from 2120 m N mine grid showing generalized geology and drill hole locations (top) and sample locations (bottom)

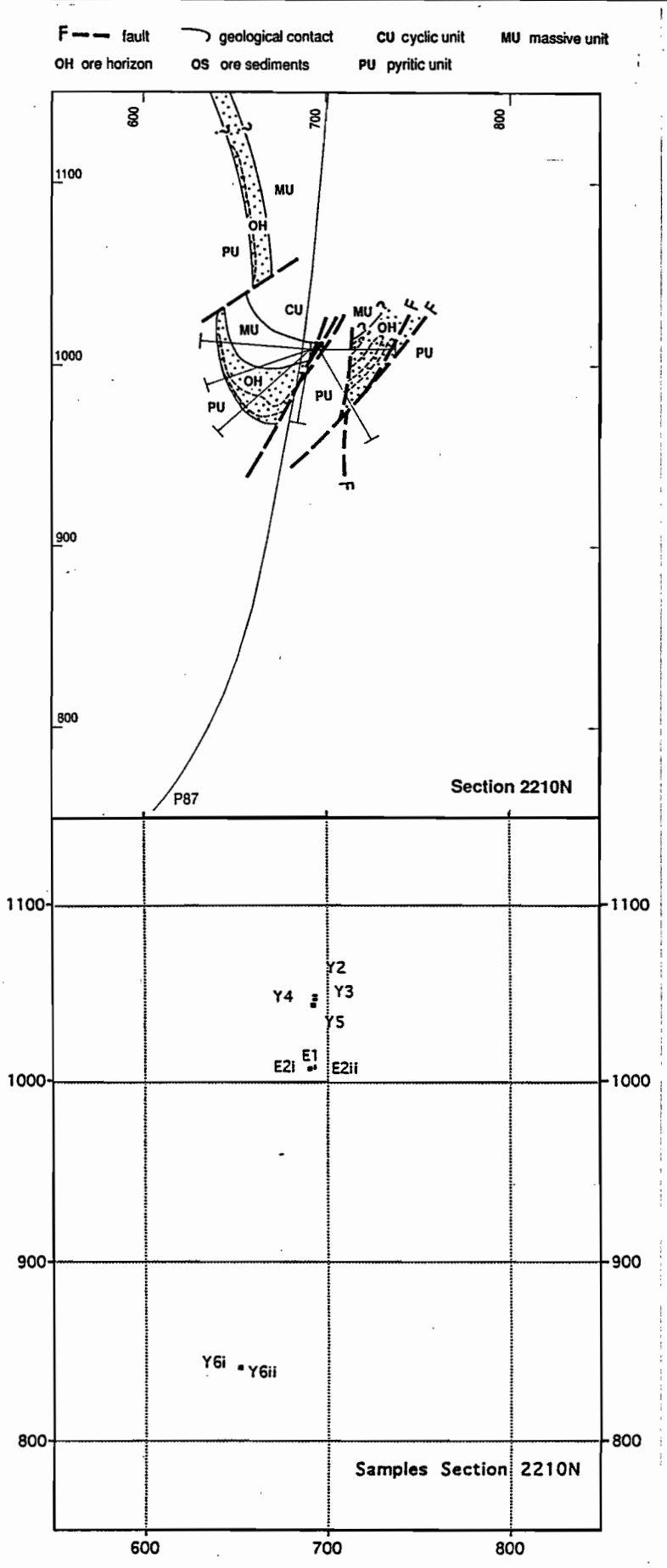

Figure 4 Cross-section from 2210 m N mine grid showing generalized geology and drill hole locations (top) and sample locations (bottom)

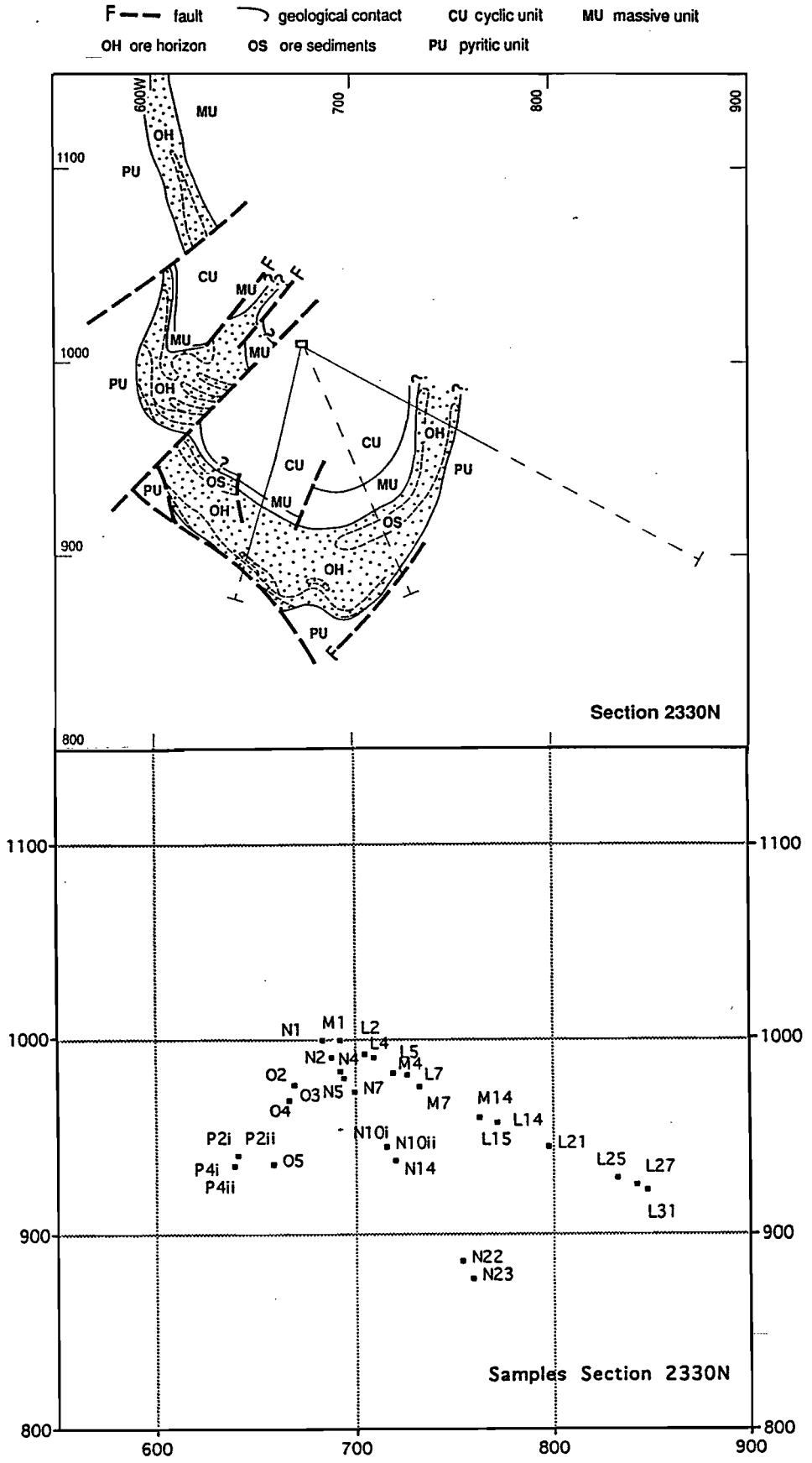

Figure 5 Cross-section from 2330 m N mine grid showing generalized geology and drill hole locations (top) and sample locations (bottom)

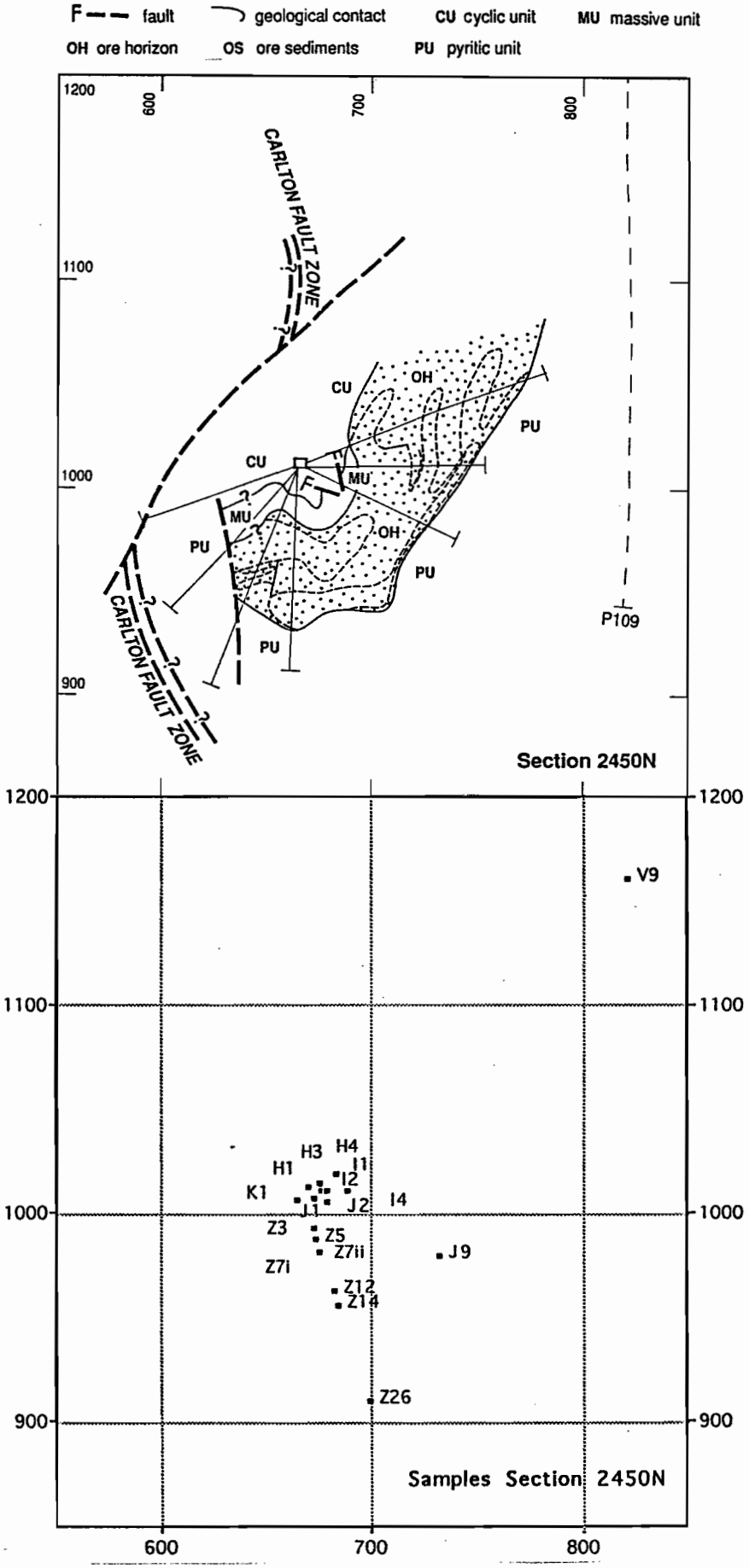

Figure 6 Cross-section from 2450 m N mine grid showing generalized geology and drill hole locations (top) and sample locations (bottom)

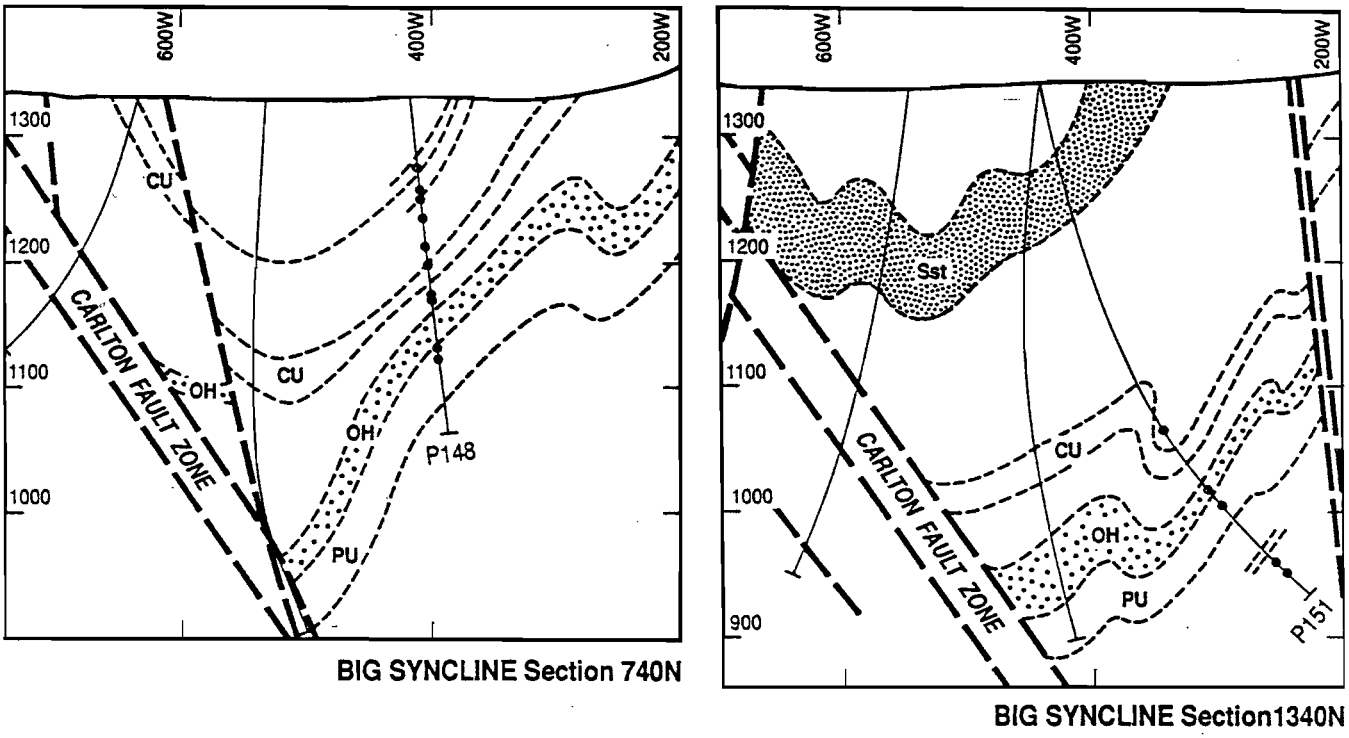

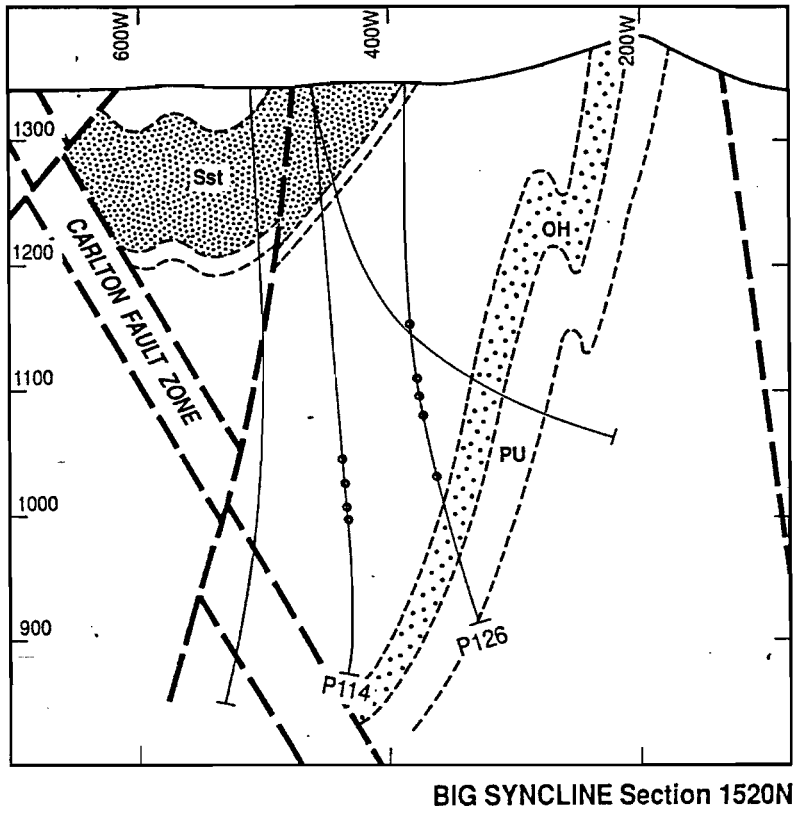

Figure 7 Sample localities displayed on three cross-section from the Big Syncline

Appendix 4-I
Comparison of commercial (ICP-ES) and University of Tasmania data

This appendix continues the attempt to estimate accuracy and precision of the commercially obtained, multi-element ICP-ES analyses originally reported in Appendix III of McGoldrick (1992). Thallium analyses (by mixed acid digest – graphite furnace AAS) are compared with XRF determinations.

The XRF data are assumed to be both accurate and precise. Quality control was monitored at the University of Tasmania by constant cross-checking of international reference rocks, Geology Department standard rocks and duplicate analyses. New equipment and an experienced, commited full time analyst also help ensure high quality analyses.

RESULTS

Twenty elements (Pb, S, Fe, Zn, Cu, V, Ca, Mg, Mn, Sr, Ti, Zr, Al, K, Ba, Cr, Ni, Sb, Na, and Tl) were common to both data sets. Figures I1 to I4 compare XRF results with the commercial analyses (complete commercial data set was presented in McGoldrick (1992)). Elements that show a good correlation and a one to one relationship are assumed to be satisfactorily determined by ICP-ES at the levels present in the Lady Loretta sediments (Figs I1 and I2).

Accurate and precise analyses for Pb, Zn, Ca, Mg, Mn, S, Fe, and Sr can be obtained for the range specified by low cost ICP-ES:

Pb	from detection limit (~ 5 ppm) to ≥ 1.5 wt%
Zn	from detection limit (~ 5 ppm) to ≥ 6 wt%
CaO	from detection limit (~ 10 ppm) to ≥ 8 wt%
MgO	from detection limit (~ 10 ppm) to ≥ 5 wt%
MnO	from detection limit (~ 10 ppm) to ≥ 0.3 wt%
S	from detection limit (~ 10 ppm) to ≥ 4 wt%
FeO	from detection limit (~ 10 ppm) to ≥ 25 wt%
Sr	from detection limit (~ 10 ppm) to ≥ 200 ppm

The plots for CaO, MgO, MnO and Sr (Fig. I2) curve away at higher concentrations, suggesting that the ICP calibration is not linear. For samples reading beyond these levels analyzing a dilution of the original solution would permit accurate determinations of these elements Strontium shows a similar curving away at levels above about 200 ppm, but with more scatter. For Cu and V (Fig. I2) the XRF and ICP data correlate quite well, but, there is quite a deal of scatter in the data. This may reflect lack of precision in these elements by either or both techniques at the relatively low levels (< 100 ppm) present in most samples. It is anticipated that both elements could be determined successfully at higher levels by ICP-ES (e.g., Jarvis and Jarvis, 1992).

A number of elements (Ti, Zr, Al, K, Ba and Cr) show a pattern where some ICP analyses match the XRF data, but many are much lower (Figs I3 and I4). Potassium suffers interference from Fe in emmission spectroscopy (Jarvis and Jarvis, 1992), and the poor results for K may be due to inadequate correction for Fe. The patterns for Ti, Zr, Ba, Cr and Al probably reflect incomplete sample dissolution or precipitation of insoluble salts or hydroxides during the mixed acid ($HF/HNO_3/HCl$) digest used to dissolve the samples.

Nickel (Fig. I4) is similar to Cu and V, but with greater scatter in the data, Sb (Fig. I4) was present at or below the detection limit of ICP in most of the samples. Meaningful assessment of the quality of ICP-ES for both these elements cannot be made without further data.

There is no systematic relation between XRF and ICP-ES determinations of Na (Fig. I4). It is inferred that the ICP results are wrong, however, some follow-up is planned to independently assess the XRF data because of the significance of Na in the primary halo at Lady Loretta (see part 5 of this report – Large and McGoldrick, 1993).

RECOMMENDATIONS

1) Because the cost per element is low, continue to use ICP-ES for Pb, Zn, Ca, Mg, Mn, S, Fe, Cu, V, and Sr.

2) Investigate alternate dissolution techniques if useful data are needed for Ti, Zr, Al, Cr and Ba (e.g., $HF/HClO_4/HNO_3$ digestion ; Na2O sinter or fusion).

3) Be prepared to pay slightly more for usable Na analyses. Sodium is important for the 'Alteration Index' discussed in part 5 of this report. It should be possible to have Na

determined for a small extra cost (using a flame photometer or AAS) on the same solution used for ICP-ES analysis.

4) Commercial analyses should be constantly checked by including well characterized standard rock powders with every batch of samples submitted for analysis. It is imperative that the standards be hidden among the unknowns. This which may neccessitate double handling of samples (i.e., get samples pulped and returned, then re-submit unknown powders with standards included).

REFERENCES

Jarvis, I. and Jarvis, K.E., 1992, Inductively coupled plasma-atomic emmission spectrometry in exploration geochemistry, Jour. Geochem. Exploration, V44, p139-200.

Large,R.R. and McGoldrick, P.J., 1993, Primary geochemical halos related to Proterozoic sediment hosted Pb-Zn deposits and applications to exploration, CODES AMIRA/ARC Project P384 — Proterozoic sediment-hosted base metal deposits Report No. 3, p63-126.

McGoldrick, P.J., 1992, Lady Loretta geochemical studies: preliminary results, AMIRA/ARC Project Report No. 1, p39-57.

Figure I-1

Comparison of ICP-ES and XRF analyses for Pb, S, FeO and Zn for 104 sediment samples from Lady Loretta

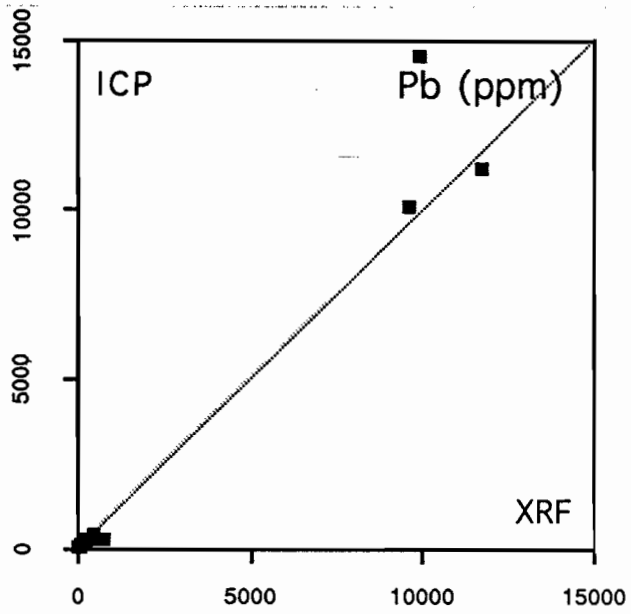
ICP
Pb (ppm)
XRF
0
5000
10000
15000

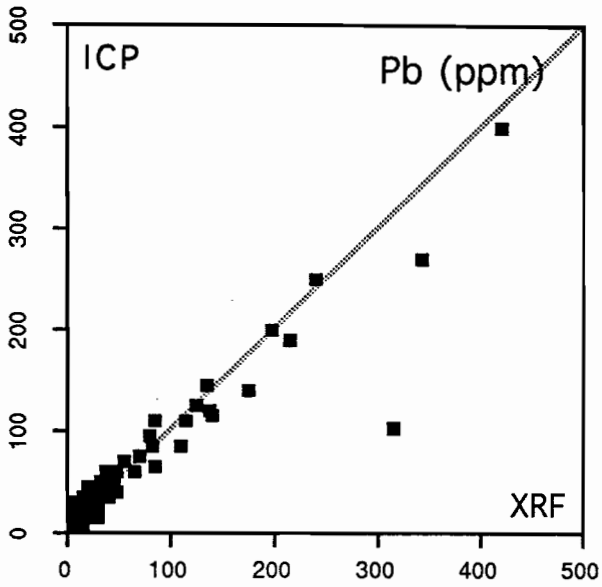
ICP
Pb (ppm)
XRF
0
100
200
300
400
500

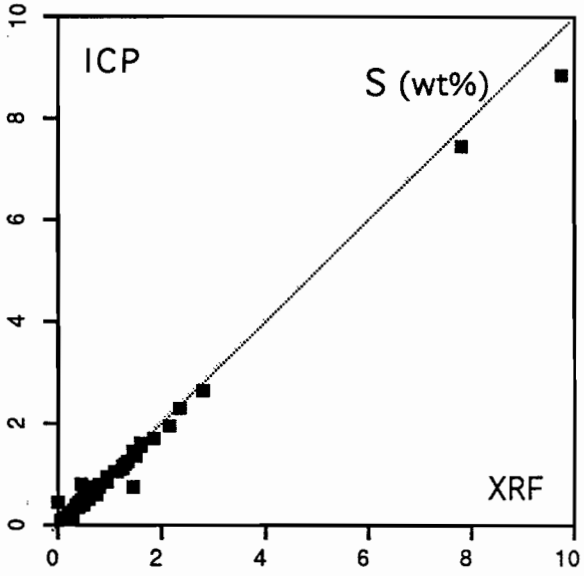
ICP
S (wt%)
XRF
0
2
4
6
8
10

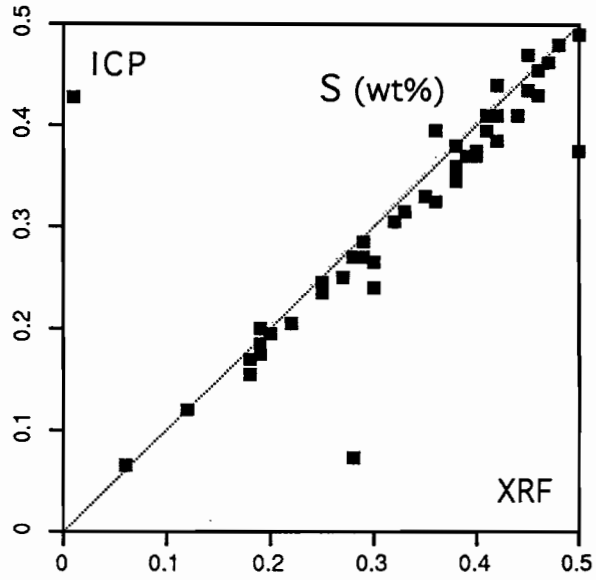
ICP
S (wt%)
XRF
0
0.1
0.2
0.3
0.4
0.5

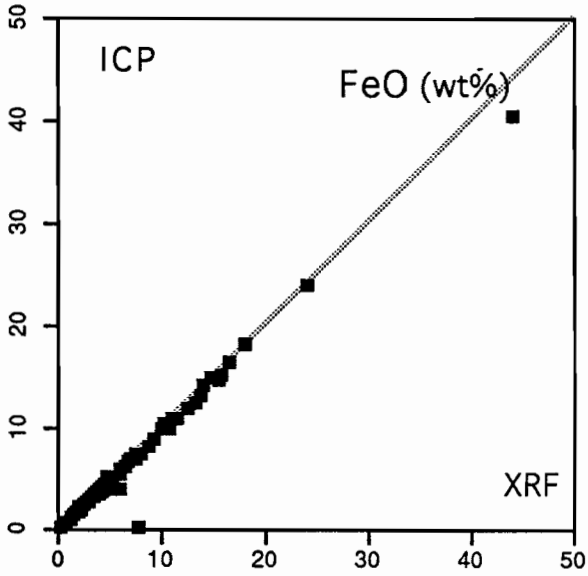
ICP
FeO (wt%)
XRF
0
10
20
30
40
50

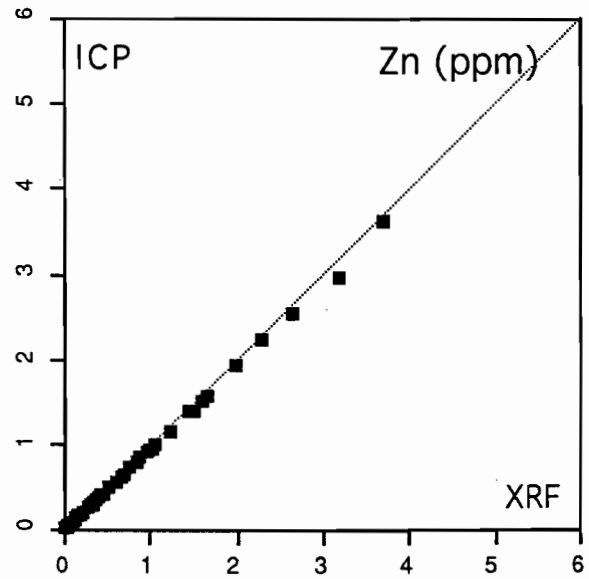
ICP
Zn (ppm)
XRF
0
1
2
3
4
5
6

Figure I-2

Comparison of ICP-ES and XRF analyses for Cu, V, CaO, MgO, MnO, and Sr for 104 sediment samples from Lady Loretta

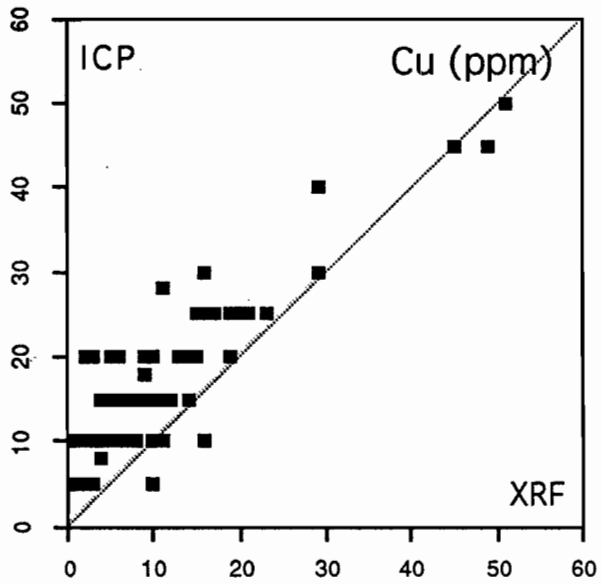
ICP
Cu (ppm)
XRF
0
10
20
30
40
50
60

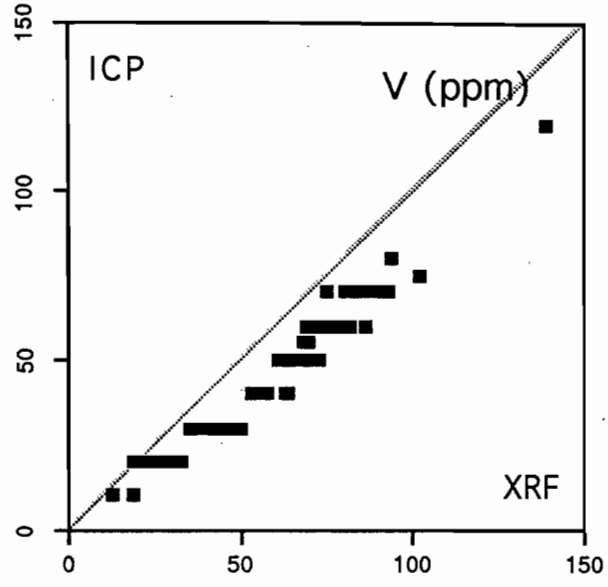
ICP
V (ppm)
XRF
0
50
100
150

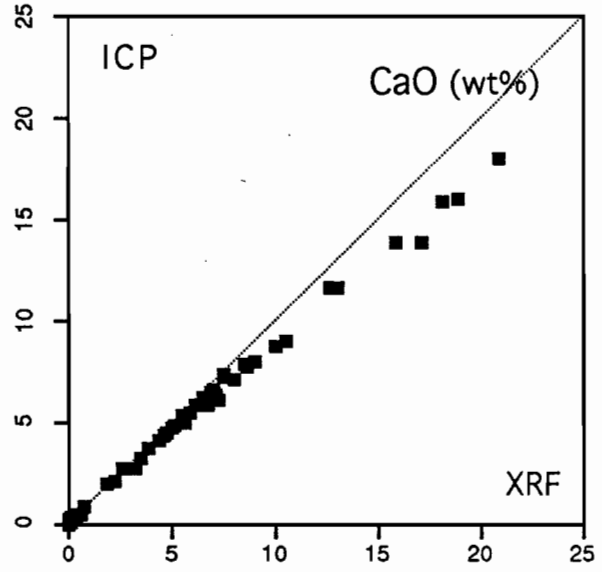
ICP
CaO (wt%)
XRF
0
5
10
15
20
25

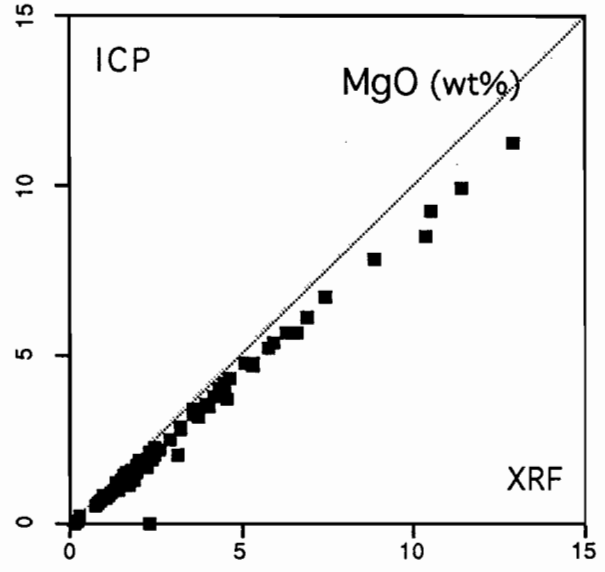
ICP
MgO (wt%)
XRF
0
5
10
15

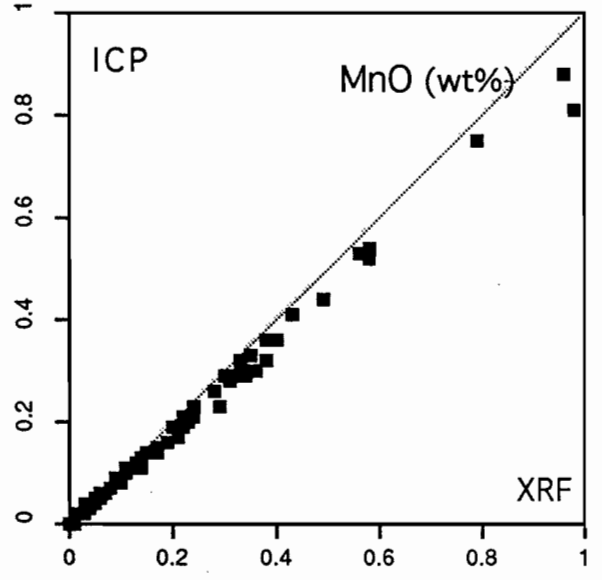
ICP
MnO (wt%)
XRF
0
0.2
0.4
0.6
0.8
1

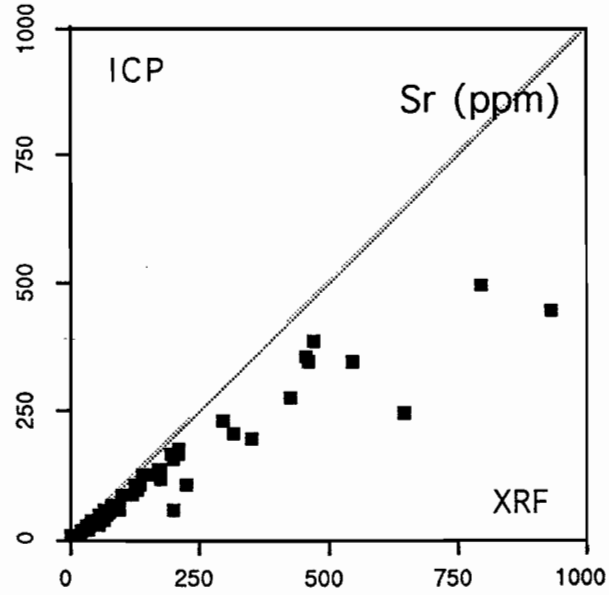
ICP
Sr (ppm)
XRF
0
250
500
750
1000

Figure I-3
Comparison of ICP-ES and XRF analyses for TiO_2, Zr, Al_2O_3, K_2O, and Ba for 104 sediment samples from Lady Loretta

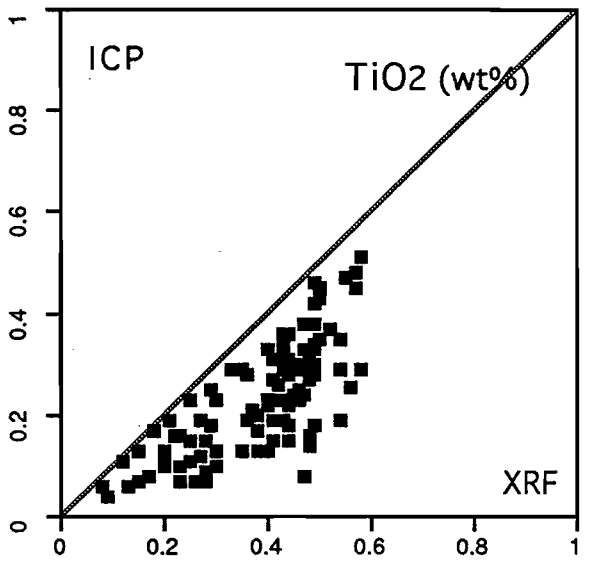
ICP
TiO2 (wt%)
XRF
0
0.2
0.4
0.6
0.8
1

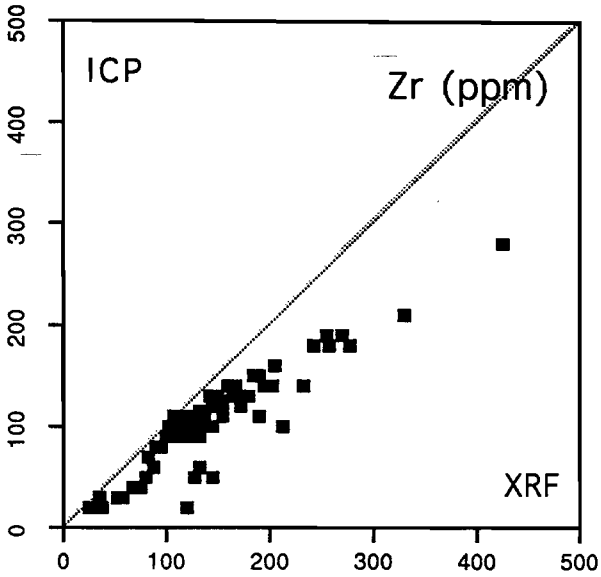
ICP
Zr (ppm)
XRF
0
100
200
300
400
500

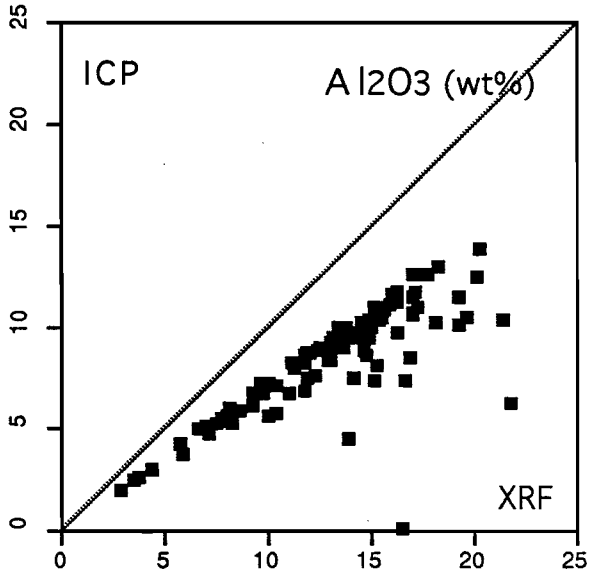
ICP
Al2O3 (wt%)
XRF
0
5
10
15
20
25

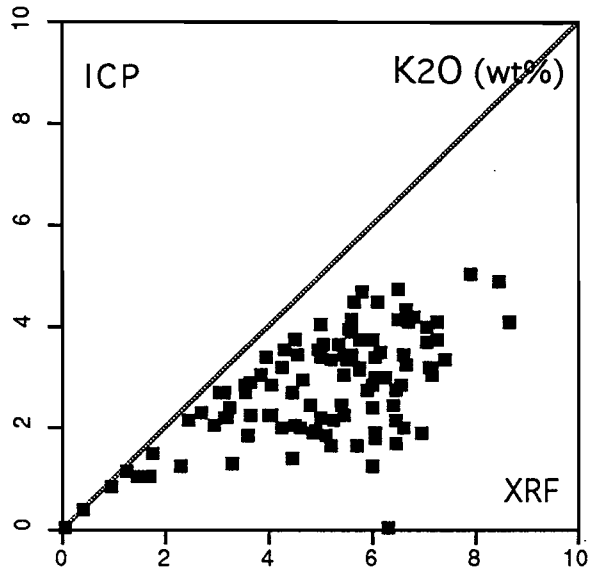
ICP
K2O (wt%)
XRF
0
2
4
6
8
10

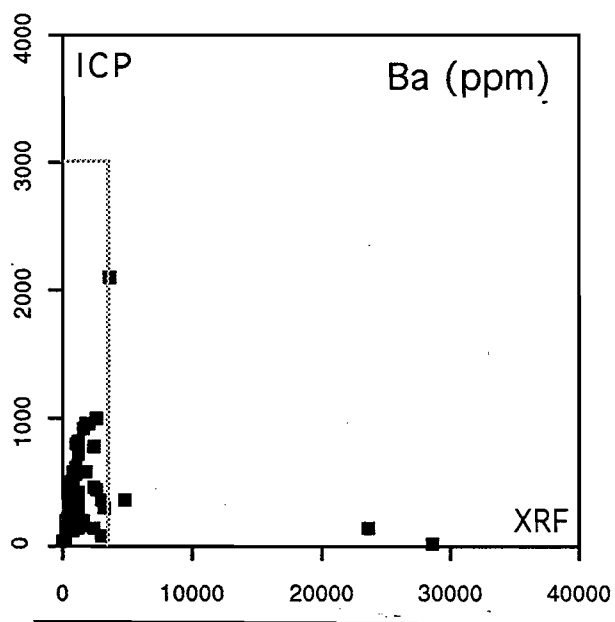
ICP
Ba (ppm)
XRF
0
1000
2000
3000
4000
0
10000
20000
30000
40000

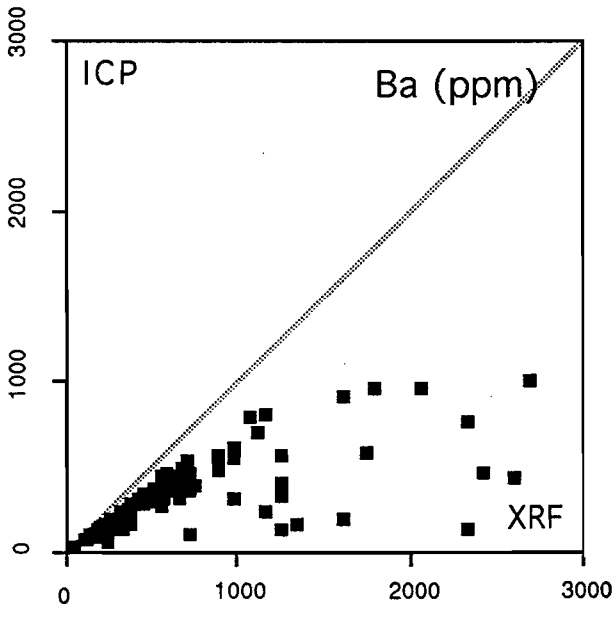
ICP
Ba (ppm)
XRF
0
1000
2000
3000
0
1000
2000
3000

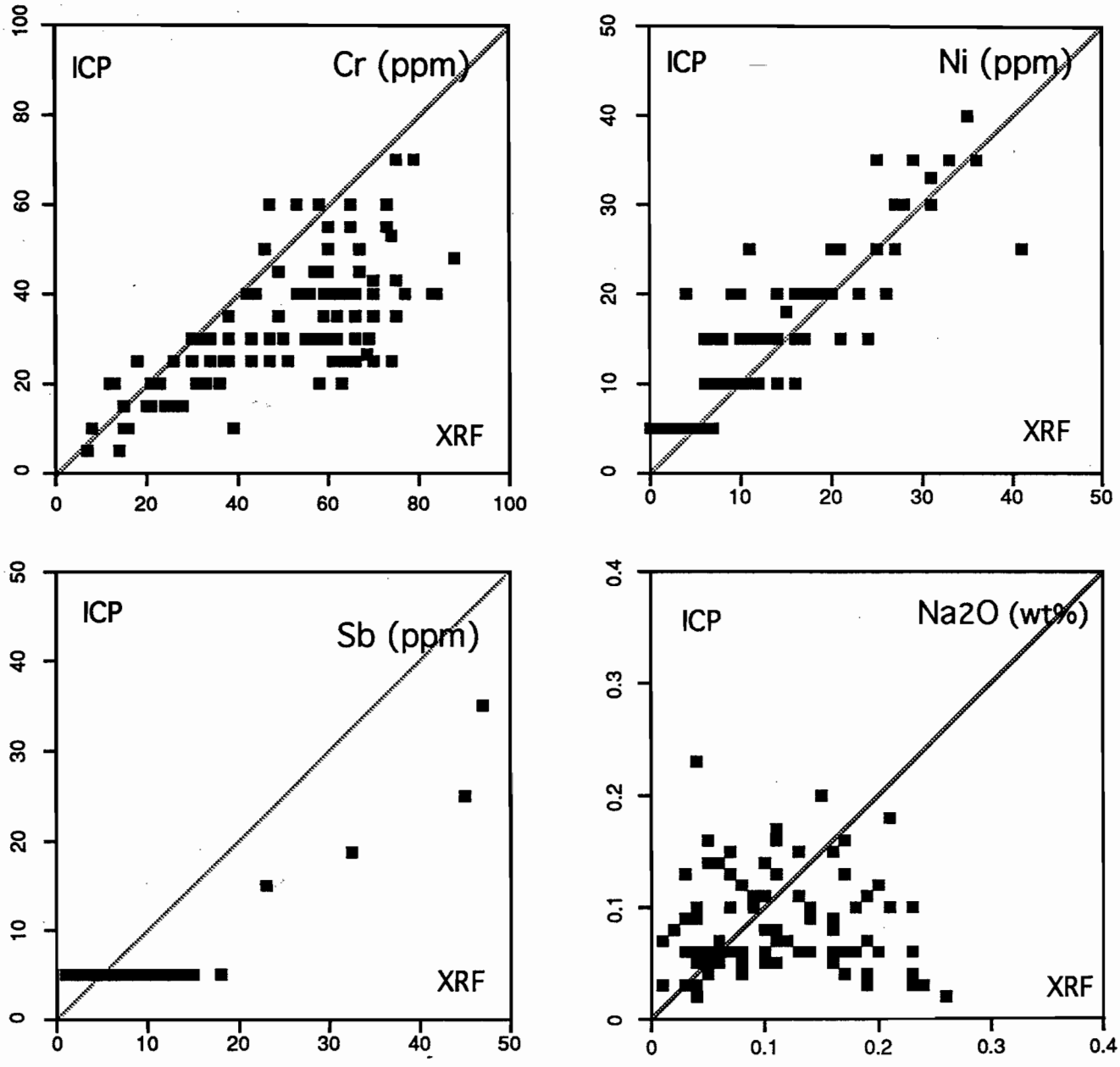

Figure I-4

Comparison of ICP-ES and XRF analyses for Cr, Ni, Sb, and Na_2O for 104 sediment samples from Lady Loretta

Appendix 4-II
Thallium determination by XRF

Thallium is an element known to form large primary dispersion halos around stratiform sedimentary lead-zinc deposits (Smith, 1973; Smith et al., 1974; McGoldrick, 1986; McGoldrick et al., in prep. - see Appendix 5-IV of this report). Because commercial Tl analyses by graphite furnace-AAS were found to be unsatisfactory (Appendix III, McGoldrick, 1992) it was decided to investigate X-ray fluorescence spectrometry (XRF) as a potentially cost-effective technique for determining Tl at ppm levels. Although XRF is subject to interelement and matrix effects, it has the advantage of non-destructive sample preparation. Hence, low analyses caused by Tl loss during acid digestion, or incomplete sample dissolution cannot occur. Pressed pellets of powdered rock are quick to prepare and quick to analyse using modern automated XRF units.

Theoretically, optimum sensitivity for the XRF determination of Tl would be achieved with the Tl Lα line (1·207 angstroms) using a Molybdenum X-ray tube at 100 kV, a LiF 200 crystal, fine collimator and both the scintillation counter and the gas flow proportional counter as detectors. However, the Tl $L\alpha_1$ line suffers high interference from Gα Lβ lines and generally cannot be used for accurate analysis.

For this work the Tl $L\beta_1$ line (wavelength 1·015 angstroms) was used. Minor interferences from Se, Ba, Pb, W and Hg occur but were minimised by using the scintillation counter with auxiliary collimator without the gas flow proportional counter. Careful choice of appropriate background angle positions is essential. Interference from Ba $K\beta_{1,2}$ (3rd order) lines was reduced with a narrow pulse height analyser window but could not be eliminated (>1000ppm Ba). Although loss in sensitivity does occur with the above conditions, a detection limit (3σ, 99% confidence) of 1ppm Tl in a quartz matrix is achievable with a background counting time of 400 seconds.

Standards containing 2000 ppm Tl were prepared by mixing fresh high purity thallium oxide with pure quartz in a laboratory ring mill and pressed powder pellets were made containing PVA as a binder. Matrix corrections were applied using the standard Compton Scattering method with the Mo X-ray tube.

Blanks of fused Spectrosil™ along with spectroscopically pure silica powder pills were also run. Accuracy was checked by analysing twelve international standard rocks. Agreement was good

with the limited amount of published data available (Table II-1). Most international standard silicate rocks also have a low Tl content (< 4ppm).

Table II-1: Comparison of published values for Tl in international standard rocks with XRF determinations at University of Tasmania

	STM1	GSP1	GH	RGM1	G2	GXR1	GXR2	GXR3	GXR4	SY-2	SY-3	MICAFE
Published value:	0.26*	1.43**	1.8*	0.93*	0.91*	0.39*	1.03*	3.6*	3.2*	1.5*	1.5*	16*
XRF determination:	<1	1.6	1.7	1.1	1.3	<1	1.1	3.4	3.4	1.8	0.9	15.4

(*suggested value; **recommended value)

Analyses of thirty sedimentary rock samples from Mount Isa, Queensland, allow a direct comparison of the XRF and RNAA techniques. Figure II-1 displays these data and demonstrates excellent agreement between the two techniques. The correlation coefficient (for ranked data) between the two techniques is 0·895.

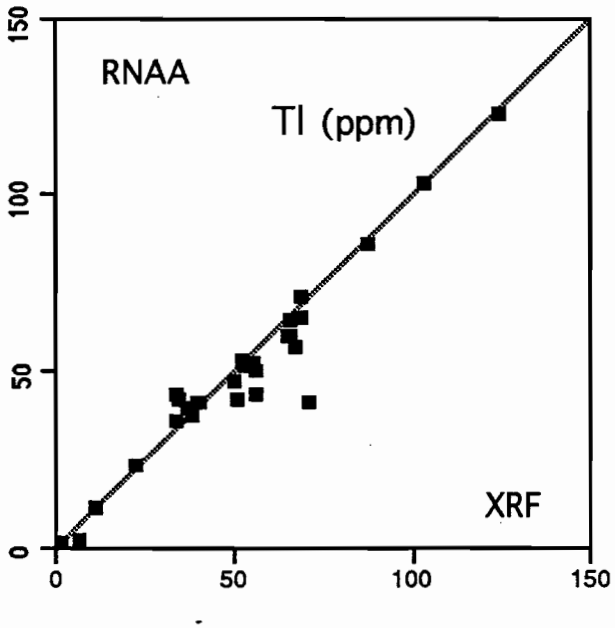

Figure II-1

Comparison of Tl analyses by XRF and RNAA for 34 sediments from Mount Isa

The commercial Tl analyses for the 104 Lady Loretta samples are compared with XRF analyses in Figure II-2, and the results confirm that all the AAS data are too low. There are two possible explanations for the much lower Tl values obtained by AAS, either

i) mixed acid digest resulted in incomplete sample dissolution, or

ii)Tl was lost at some stage of analysis (why this should happen is not well understood, but it may relate to formation of volatile Tl^+ chloride complexes)

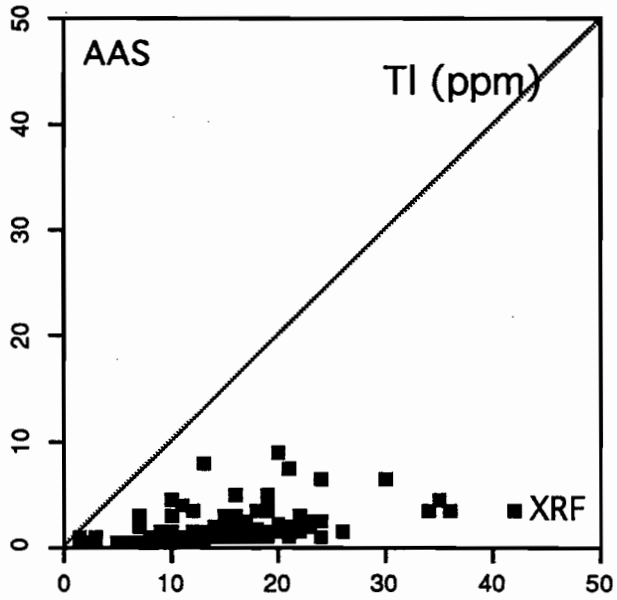

Figure II-2

Comparison of Tl analyses by XRF and ICP-ES for 104 sediments from Lady Loretta

RECOMMENDATIONS

1) XRF should be the preferred technique for measuring Tl at levels above about 1ppm (automated measurement using pressed powder pellets may be cost effective).
2) Alternatively, consideration should be given to using a Na_2O_2 sinter followed by dissolution in nitric acid and AAS finish; this would have the combined effect of ensuring complete sample dissolution and oxidizing any Tl to the trivalent oxidation state.

REFERENCES

McGoldrick, P.J., 1986, Volatile and precious metal geochemistry of the Mount Isa ores and their host rocks: Unpub. Ph.D. thesis, University of Melbourne, 330 p.

Smith, R.N., 1973, Trace element distribution within some major stratiform orebodies. Unpubl. B.Sc (Hons) thesis, part II. Univ. of Melbourne

Smith, R.N., Ewers, G.R. and Keays, R.R., 1974. Volatile metal haloes as a guide to base metal deposits. Abs. Geol. Soc.Aust. Joint Specialist Group Meeting, p. 64-67.

DEPOSIT HALOS

5. Primary geochemical halos related to Proterozoic sediment hosted Pb-Zn deposits and applications to exploration

Ross Large and Peter McGoldrick

SUMMARY

The purpose of our research in the geochemical halo module of AMIRA Project P384, is to develop a model for geochemical dispersion associated with Australian Proterozoic stratiform Pb-Zn deposits (Fig. 1) that is applicable to mineral exploration. In this report, primary halos around the Lady Loretta deposit are documented and discussed in detail, based on the sample collection and analysis programme outlined in McGoldrick (1992, 1993a&b). The halo model developed for Lady Loretta is then compared with published data on geochemical dispersion surrounding the HYC deposit (Lambert & Scott, 1973), and a derived halo model is designed for HYC. A series of criteria for determining vectors towards ore for both Lady Loretta and HYC have been developed from the halo models. The outcome of this study is the formulation of a new approach to lithogeochemistry applied to stratiform Pb-Zn mineral exploration which has outstanding potential for application in Australian Proterozoic sedimentary basins.

LADY LORETTA HALO STUDY

Previous Work

As part of his PhD research on the Lady Loretta deposit, Carr (1984) reported on primary geochemical and mineralogical dispersion around the deposit. The full paper is included as Appendix 1. A summary of his major findings is given below (Carr, 1984).

- The stratiform Pb-Zn orebody is surrounded by a halo of pyrite-rich layers within the dolomitic siltstone host rocks.

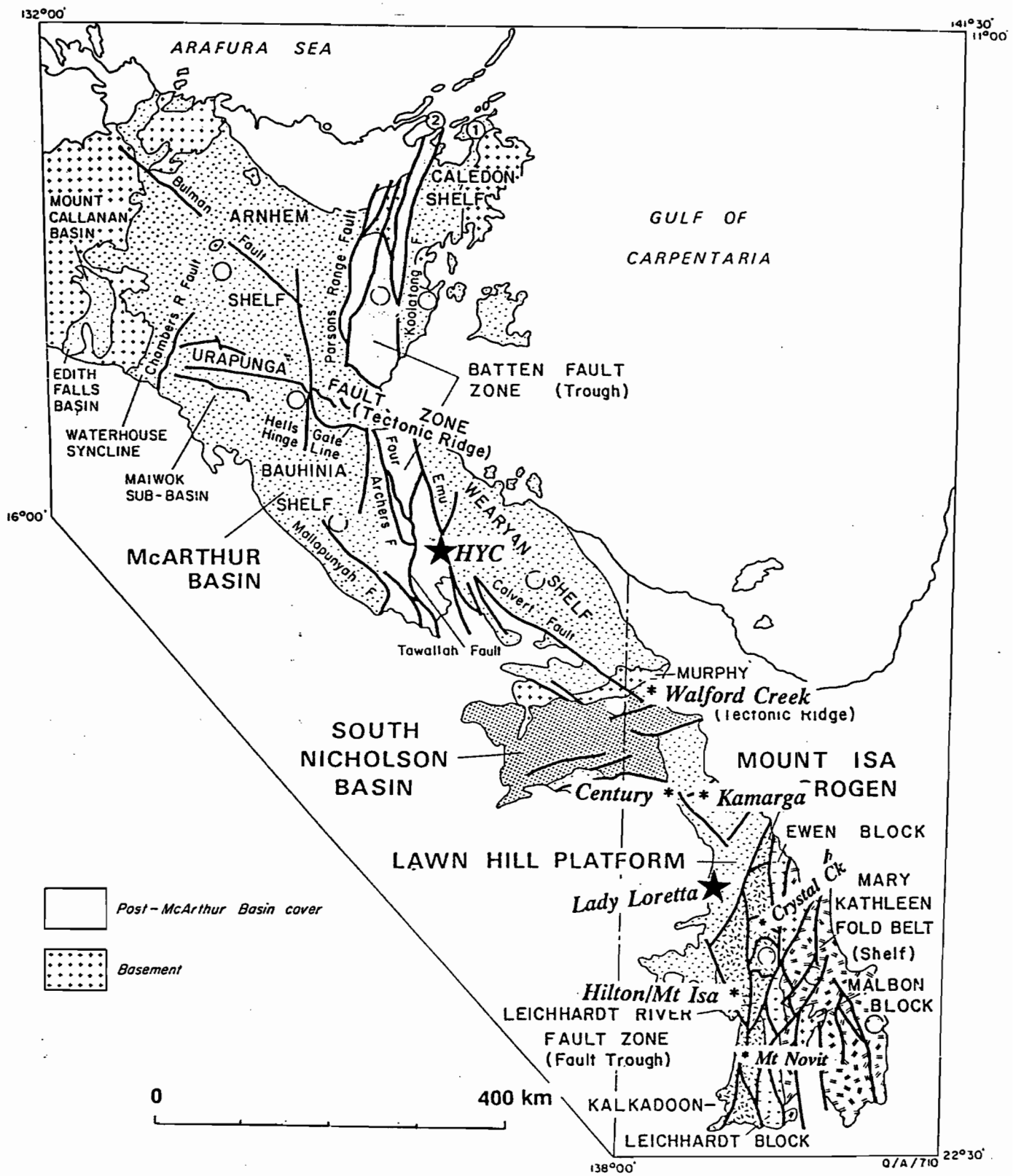

Figure 1 Locality map showing position of Lady Loretta and HYC deposits (from Derrick, 1993).

- The proportion of pyrite-rich layers increases progressively from about 2% at 150m stratigraphically below the ore to >90% in the top 10m of the footwall rocks. Hangingwall rocks contain up to 20% pyrite layers for at least 100m above the ores (Fig 2).

- A siderite halo surrounds the ore body, extending 50m above and 75m below the deposit. Sideritic siltstones give way to dolomitic siltstones beyond this halo (Fig 3).

- Zn shows the maximum primary dispersion around the deposit, extending as a halo up to 100m into the footwall and 50m into the hangingwall. Laterally the halo extends for some 1.5km along strike from the orebody.

- Hg, Pb, Ag, Cd and Ba exhibit dispersion halos which are less extensive than Zn.

Sampling data base for this study

A total of 104 rock samples have been analysed for their major and minor elements. A full listing of the data and analytical techniques is given in McGoldrick (1993b). The samples were collected from a series of drill holes in the Small Syncline (80 samples) and Big Syncline (24 samples) in order to provide a spread of lithologies including hangingwall, footwall and ore horizon. Sample locations on drill sections are given in McGoldrick (1993b). The sampling was designed to avoid sediments with obvious pyrite mineralisation. A separate set of pyrite-rich sediments was collected, but they are not part of the study reported here.

The Lady Loretta data-base has been analysed using the Excel™ and Cricket Graph™ software packages. Because of the simple mineralogy of the host rocks, it has been possible to use graphical means to study mineral chemical variations in the data set and therefore develop a halo model based on both element variation and mineral chemical variation around the deposit.

Mineralogy of the host rocks

Preliminary petrographic and XRD analysis indicates that the dolomite siltstone and shale host rocks have a simple basic mineralogy of quartz, mica (muscovite), carbonate (dolomite or siderite), and pyrite. K-feldspar, chlorite, kaolinite, barite and smectite are present in minor amounts in some samples. Within the siderite envelope (Fig 3), the carbonate is

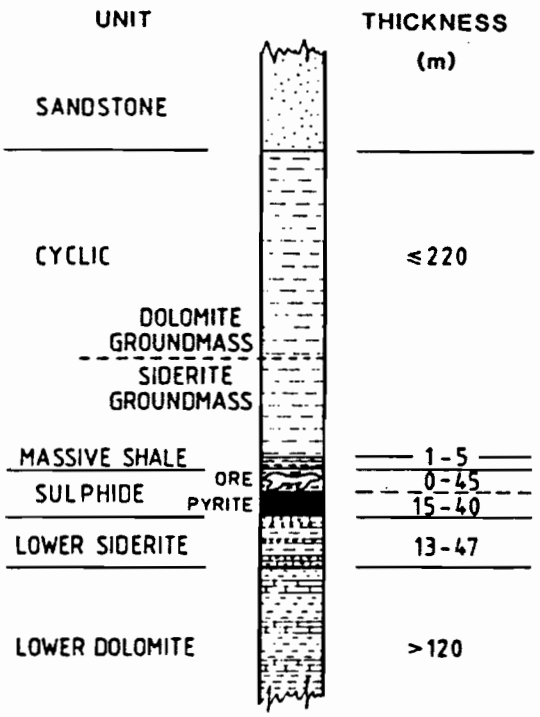

Figure 2: Generalised stratigraphic column at Lady Loretta showing rock types and pyrite, siderite distribution (from Carr, 1984).

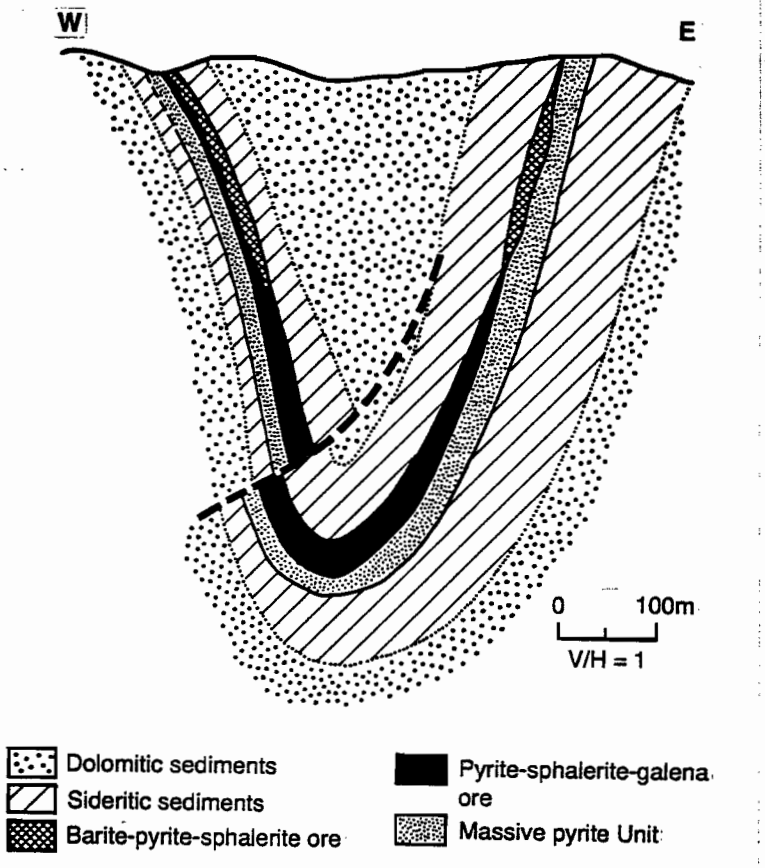

Figure 3 Generalised cross-section through Lady Loretta (after Derrick, 1992, modified rom Carr & Smith, 1977).

exclusively siderite, while outside the envelope the carbonate is exclusively dolomite. In the Small Syncline barite-rich (up to 60 wt%) parts of the Ore Horizon occur in the northerly part of the east limb of the fold, and up-dip on the western limb, and tends to be sphalerite-rich and galena-poor (Hancock and Purvis, 1990). Pyrite - barite (± hematite and chert) characterise the Ore Horizon in the Big Syncline.

The Siderite Halo (Fig 3)

The outer margin of the siderite halo against the dolomitic sediments has not been accurately defined in the present study. Within the halo, siderite occurs as a very fine grained phase varying from <2% up to 70% of the sediment, and it appears to replace, or exist as an alternative phase, to the dolomite present outside the halo. Based on our sampling and analysis, the siderite halo extends at least 50m into both the hangingwall and footwall of the ore deposit. Both our studies and those of Carr (1984) indicate that the siderite halo penetrates deeper into the footwall below the thickest concentration of Pb-Zn ore, and thins laterally towards the extremities of the ore lens.

Although the presence of siderite is visible in the drill core, due to a distinct brown colouration associated with surface oxidation, it is commonly difficult to pick the siderite/dolomite boundary at Lady Loretta, probably due to the fact that the dolomite is also Fe-rich (ferroan-dolomite) and develops a brown strain on oxidation. Our work has indicated that the simplest geochemical method of recognising siderite siltstones versus ferroan dolomite siltstones is by CaO analysis.

As shown in figure 4, the dolomitic siltstones contain greater than 1% CaO, while the sideritic siltstones contain less than 1% CaO. In fact, there are two orders of magnitude difference between the median sideritic siltstone (~0.1% CaO) and the median dolomitic siltstone (~10% CaO). Another significant factor revealed by figure 4 is that the dolomitic siltstones (outside the siderite halo) have much lower zinc contents (20 - 200ppm Zn, median 50ppm) compared with sediments within the siderite halo (70ppm to 10% Zn, median 3000ppm). In other words, the siderite halo at Lady Loretta also appears to represent a zinc halo.

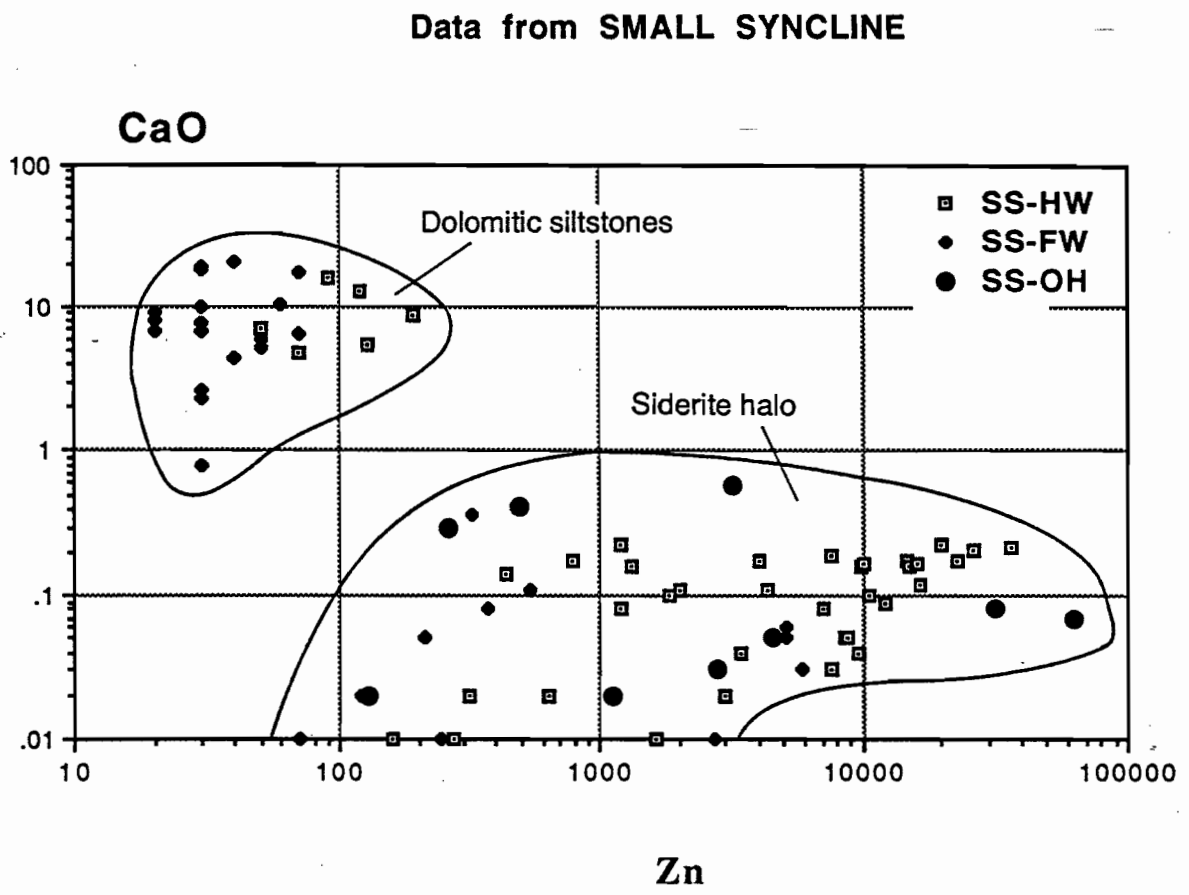

Figure 4 CaO vs Zn for Lady Loretta small syncline sediments. The two major groups ofd olomitic siltstones and sideritic siltstones (siderite halo) are clearly separated on his plot.

Composition of carbonates

Due to the simple mineralogy of the sediments at Lady Loretta and the fact that the host rocks contain either dolomite or siderite but never both carbonates together, then it is possible to gain a preliminary indication of the variability in composition of the carbonates using whole rock scatter plots such as those in figure 5. These plots show that the carbonates are not simply pure dolomite and siderite but that the dolomite contains variable and minor Fe and Mn while the siderite is enriched in Mn and Mg. Figure 5a gives a clear distinction between the siderite and dolomite sample sets due to the paucity of CaO in the former. Figure 5b shows that the siderite contains up to 2wt% MgO (however, this may be related to minor intergrown chlorite), while figure 5c indicates that the dolomite contains variable FeO contents.

From figure 5d it is apparent that the siderite contains a higher Mn content than the dolomite. By extrapolation it is possible to determine that the siderite contains a mean value of 1.9wt% MnO compared to 0.7wt% MnO for the dolomite. Based on the complete Lady Loretta Small Syncline whole rock data set, the following mean compositions of dolomite and siderite have been calculated:

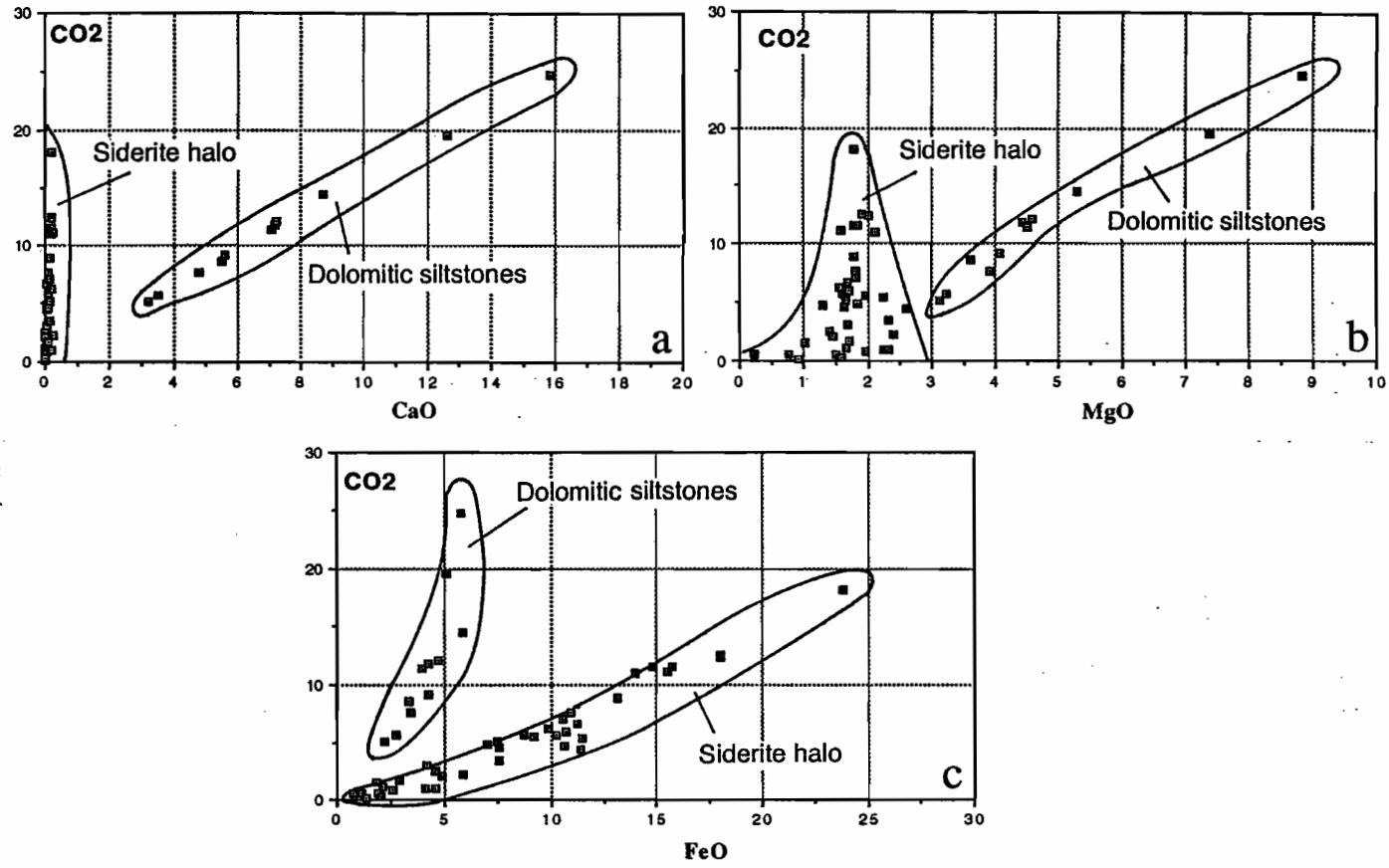

Figure 5: Scatter plots of the Lady Loretta hanging wall sediments showing the variation in carbonate type and composition: a) CO2 vs CaO b) CO2 vs MgO c) CO2 vs FeO.

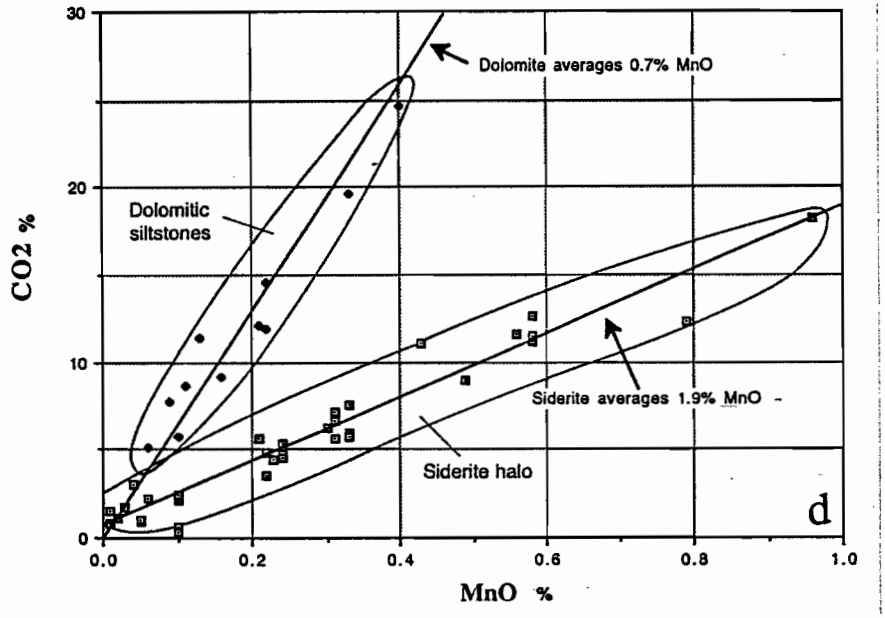

Figure 5d: Variation in wt% MnO in hanging wall sediments indicating that siderite average 9wt% MnO and dolomite average 0.7wt% MnO.

mean dolomite composition $(Ca_{0.50}Mg_{0.39}Fe_{0.10}Mn_{0.01})CO_3$

mean siderite composition $(Fe_{0.85}Mg_{0.10}Ca_{0.02}Mn_{0.03})CO_3$

Data from the hangingwall sediments (Fig 6) shows a log-log correlation between zinc and CO_2, suggesting the possibility of zinc substitution within the lattice of the siderite. This conclusion is supported by data from Carr (1984) who records zinc substitution in siderite from 0 to 14 mole % $ZnCO_3$. No such relationship is apparent for the dolomite.

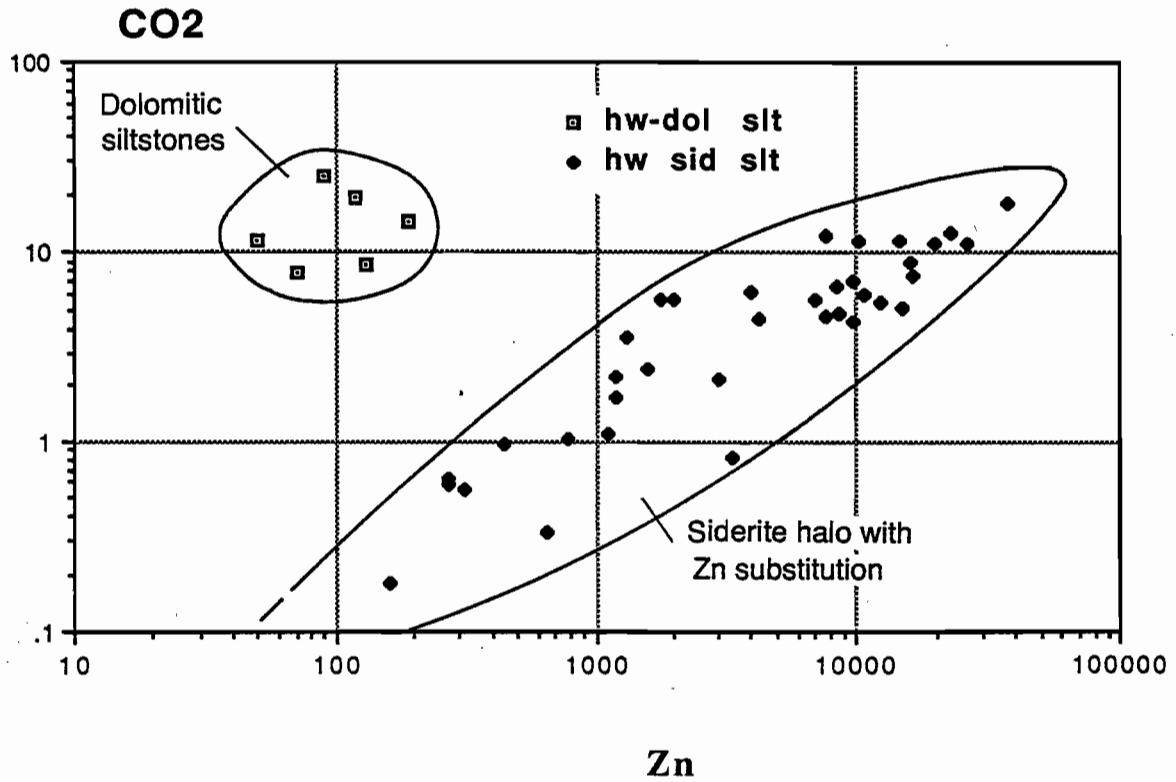

Figure 6 CO_2 vs Zn plot showing that sediments in the siderite halo exhibit increasing Zn values with increasing carbonate contact.

Element dispersion into footwall and hanging wall sediments

In order to study major and minor element dispersion about the ore position, the Small Syncline data set has been plotted in a series of graphs showing stratigraphic distance from the ore position against elemental variation. Samples have been collected up to 265m into the footwall and 60m into the hangingwall. Consequently, although our data set is adequate for the study of FW dispersion, it is limited on the HW side. Due to the tight synclinal structure at Lady Loretta, it was difficult to obtain primary core samples, lacking oxidation, greater than 50m stratigraphically above the ore position.

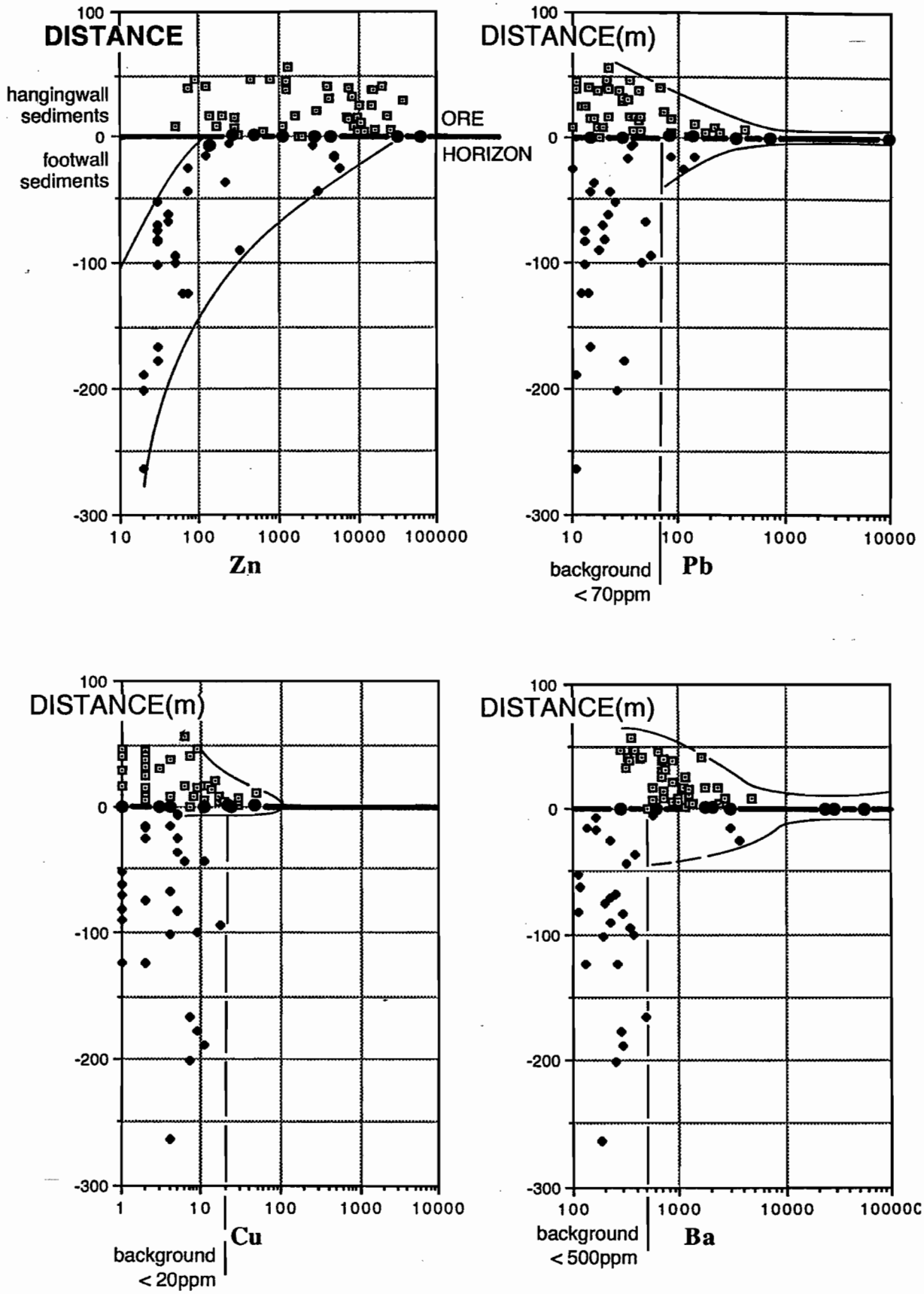

Figure 7 Stratigraphic disperion of Zn, Pb, Cu and Ba in hanging wall and footwall sediments, Lady Loretta Small Syncline.

The following elements which show significant dispersion, Zn, Pb, Cu, Ba, CaO, MgO, K_2O, Na_2O, MnO and Tl, are discussed individually below.

Zinc (fig 7a) - broad dispersion (+50m to -150m)

Footwall: Zn shows a general increase over a stratigraphic distance of 150m from 30ppm to 10,000ppm
Hangingwall: Zn is erratic from 70ppm to 3% with no general increase toward ore
Background: deep footwall (>150m); 20-30ppm Zn

Lead (fig 7b) - tight dispersion (+25m to -25m)

Footwall: obviously anomalous Pb (>70ppm) is restricted to 25m into footwall. Values from 30 to 70ppm extend to 100m
Hangingwall: values above 70ppm are restricted to 25m above ore horizon
Background: deep footwall (>150m); 10-30ppm Pb.

Copper (fig 7c) - tight dispersion (+20m to 0)

Footwall : no apparent dispersion; all <20ppm
Hangingwall: anomalous values (10-50ppm) extend up to 20m above ore position
Background: probably 1 to 10 ppm.

Barium (fig 7d) - extensive lateral ore position dispersion up to 1.5km
- broad hanging wall dispersion
- (+50m to - 25m)

Footwall: generally <500ppm except within 25m of ore when it reaches 2000ppm
Hangingwall: general increase from 300ppm to 1% over 50m towards ore
Background: less than 500ppm in deep footwall.

Calcium (fig 8a) - depletion halo (+50m to -50m) related to siderite zone

Footwall: marked depletion to <0.1wt% within 50m of ore
Hangingwall: depletion to <1.0wt% over 50m but includes some dolomite zones >1%
Background: 1-20% CaO in dolomite siltstones

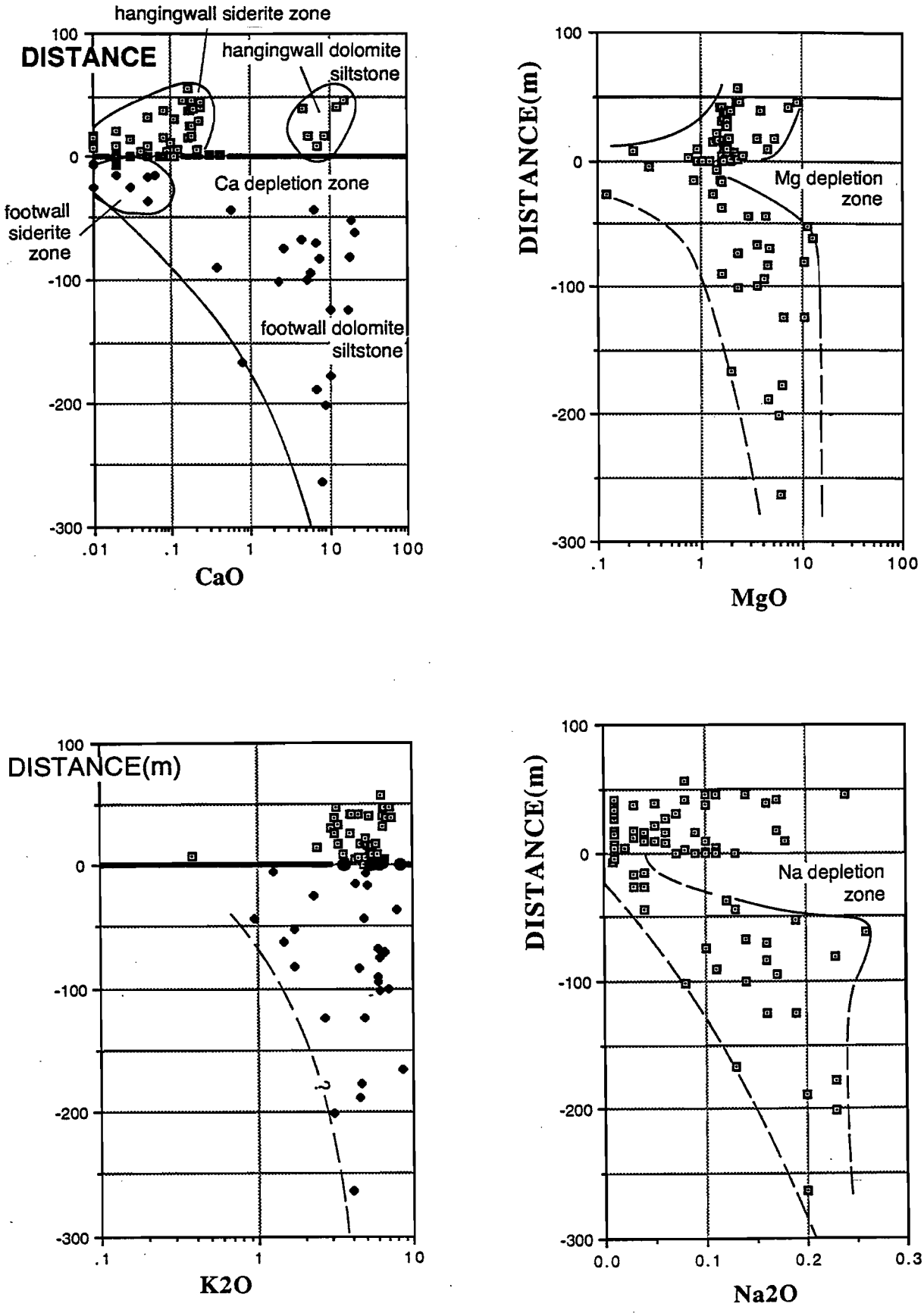

Figure 8 Stratigraphic dispersion of CaO, MgO, K_2O and Na_2O in hanging wall and footwall sediments, Lady Loretta Small Syncline.

Magnesium (fig 8b) - general depletion halo (+50m to -50m)

Footwall: complete depletion <2% MgO within 40m
Hangingwall: general depletion <2% MgO within 50m
Background: 2-16% MgO in dolomitic siltstones

Potassium (fig 8c) - no obvious halo

Footwall: erratic from 1 to 10% K_2O
Hangingwall: consistent 2 - 8% K_2O
Background: 1 to 10% K_2O

Sodium (fig 8d) - general depletion halo (+40m to - 50m)

Footwall: depletion to <0.05% within 50m of ore
Hangingwall: erratic from 0.01 to 0.25% but generally depleted compared with deep footwall
Background: 0.1 to 0.3% Na_2O in FW beyond 50m

Manganese (fig 9a) - very broad dispersion (+50m to - 150m)

Footwall: erratic variation 300 to 4000ppm MnO up to 150m from ore
Hangingwall: erratic variation 200 to 10000ppm MnO up to 50m from ore
Background: deep footwall 600-1200ppm MnO

Thallium (fig 9b) - very broad dispersion (+50m to -150m)

Footwall: erratic distribution 2ppm to 40ppm over 150m below ore
Hangingwall: tight anomalous population to to 25ppm over 50 in above ore
Background: less than 4ppm Tl

Strontium (fig 9c) - very tight dispersion (+30m to -30m)

Hangingwall: increases from 100 to 500ppm towards ore over 30m
Footwall: erratic 100-800ppm within 30m of ore
Background: 10-50ppm in FW beyond 30m

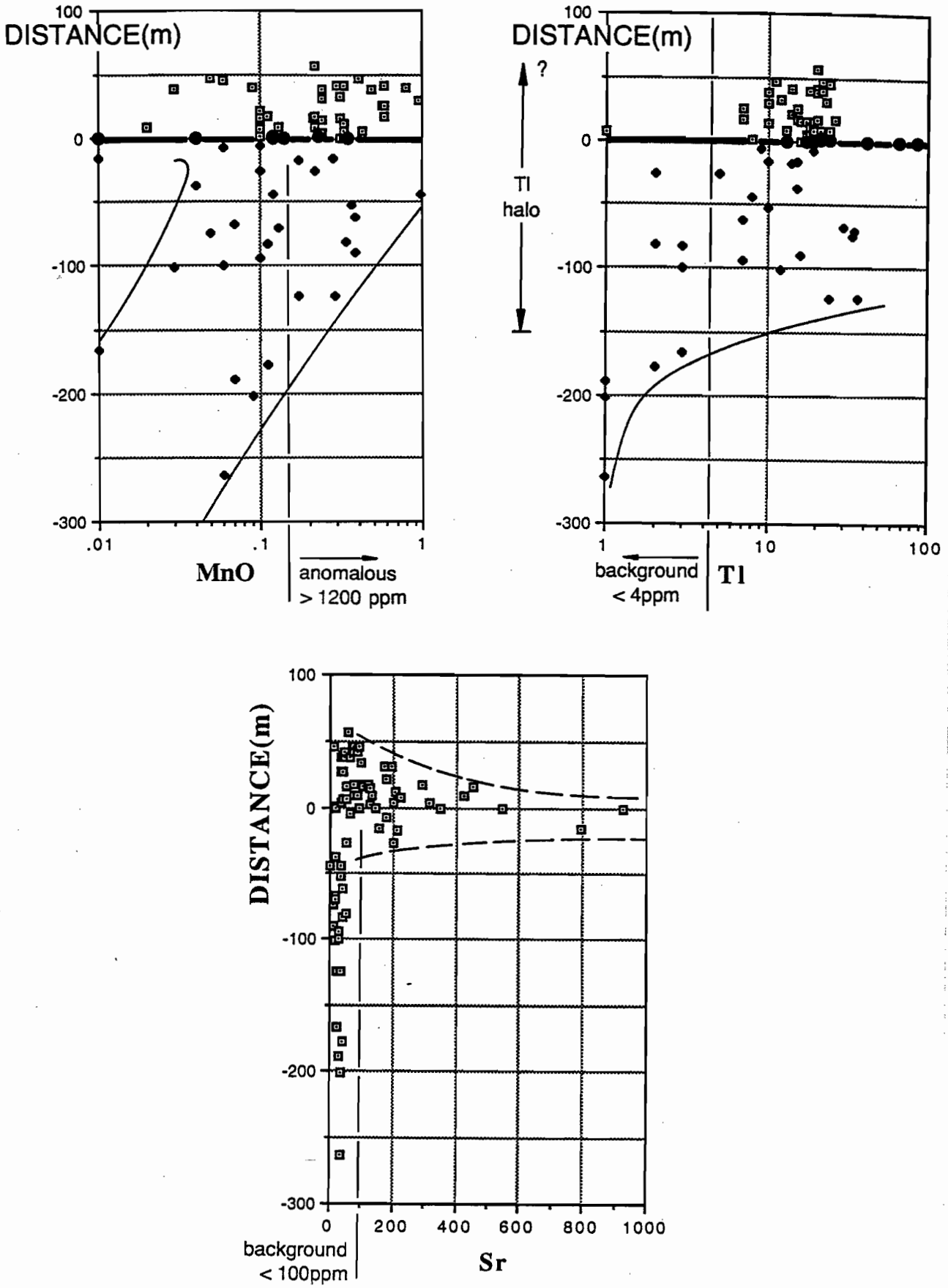

Figure 9 Stratigraphic dispersion of MnO, Tl and Sr in hanging wall and footwall sediments, Lady Loretta Small Syncline.

Discussion of element dispersion across stratigraphy

This study allows us to group the halo indicator elements into four classes, depending on their degree of dispersion and relative enrichment or depletion.

Enriched halo indicators

1.	Very broad dispersion (up to 150m)*	Tl, Mn
2.	Broad dispersion (up to 50m)	Ba, Zn, Fe
3.	Tight dispersion (less than 30m)	Pb, Cu, Sr

* metres across strata

Depleted halo indicators

4.	Broad depletion	CaO, MgO, Na_2O

The Lady Loretta Big Syncline data set indicates that the across strata dispersion applies equally to along strata dispersion, but over a greater distance (probably about an order of magnitude greater).

Along favourable horizon dispersion

Edge of orebody ⎤⎦ (Cu, Pb, Sr) ' . (Ba, Zn, Fe) ' (Tl, Mn)
(← CaO, MgO, Na_2O depletion →)

Discussion of Thallium and Manganese

Our data indicates that Tl and Mn dispersion extends beyond the siderite halo at Lady Loretta. This is clearly shown for Tl in figure 10, where it is evident that the dolomite siltstones (>1% CaO) contain Tl values from 1 to 40ppm, with about two-thirds of the data above the background threshold of 4ppm. This compares with the Zn-CaO pattern (Fig 4) where only the sideritic siltstones exhibit anomalous Zn values, and the dolomites have background values.

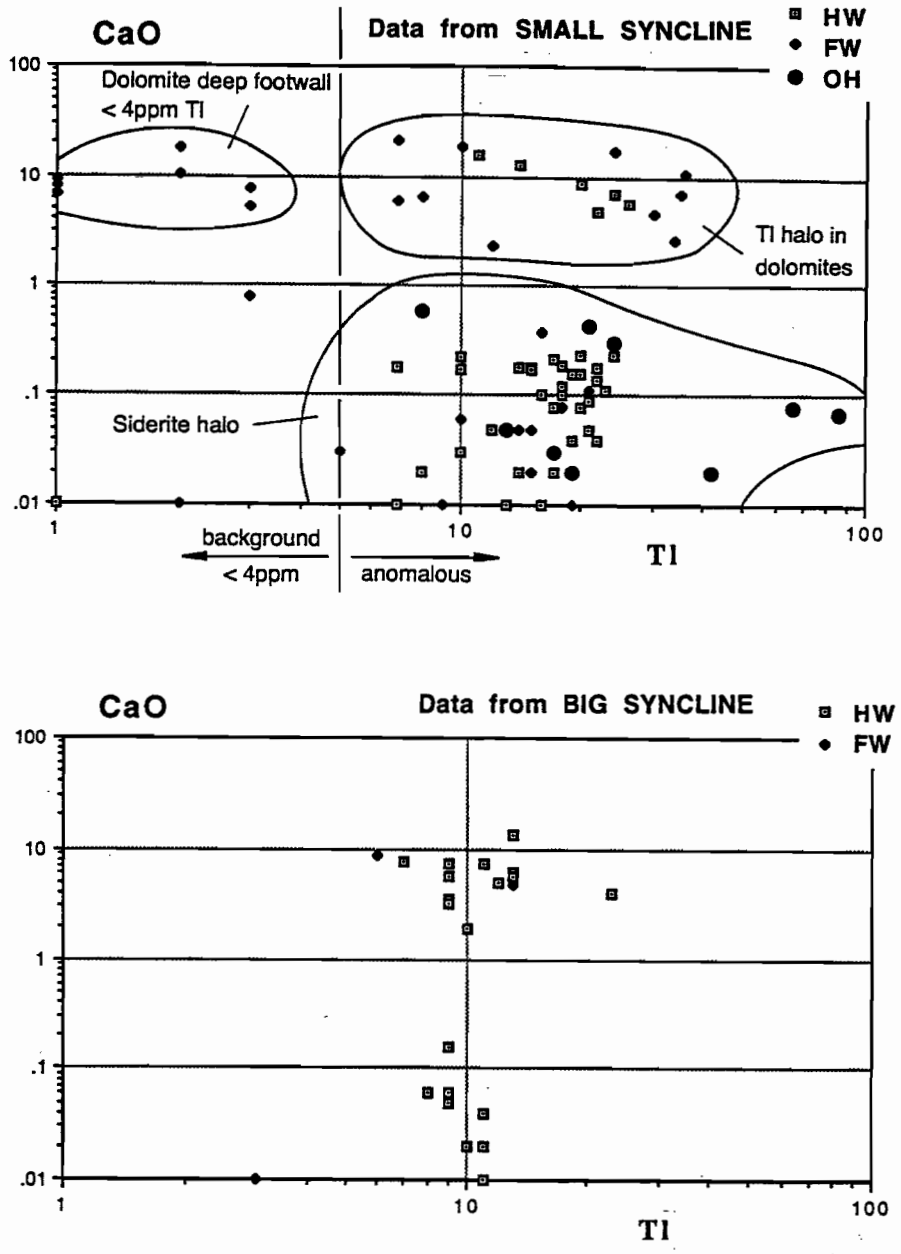

Figure 10 CaO vs Tl for Small and Big Synclines. Background values of thallium(<4ppm) occur deep in the footwall of the Small Syncline.

Broad primary dispersion halos of Tl were recognised at HYC in the early '70s (Smith, 1973; Smith et al., 1975) and similar halos exist around the Mount Isa Pb-Zn orebodies (McGoldrick, 1986; McGoldrick et al., in prep. – see Appendix 5-I). At Mount Isa Tl is hosted by sulphides in base-metal mineralized and pyritic samples, but substitutes for K in K-feldspar in low-sulphide samples. At Lady Loretta muscovite, not K-feldspar, is the main K-silicate in the host sediments and hence, is the likely Tl host in low-pyrite samples.

By contrast, Mn has been shown in this study to substitute for Fe and Mg in siderite and dolomite in carbonate facies sediments. Consequently, the two major distal halo indicates, Tl and Mn, are controlled by the facies of sedimentation around the deposit, as indicated below.

	Sediment facies	*Distal halo indicator*
1.	Carbonate only (eg Tynah)	Mn
2.	Shale only (eg Tom)	Tl
3.	Dolomitic shales (eg Lady Loretta, HYC)	Mn and Tl
4.	Sandstones, quartzites (eg Sullivan)	No indicator

Development of a metal index vector

Utilising the fact that the key metal halo indicators Pb, Zn and Tl exhibit different dispersion patterns (ie Pb-tight, Zn-broad and Tl-very broad), it should be possible to develop a metal index factor that increases systematically towards ore throughout the full extent of the deposit halo.

The metal index selected by trial and error for this purpose is:

$$\text{Metal Index} = 100Pb + 100Tl + Zn$$

with Pb, Tl and Zn in ppm.

Figure 11 shows that this metal index increases in a general fashion over a distance of 200m towards ore in the footwall of the Lady Loretta deposit. The hangingwall rocks, however, show an anomalous pattern with no systematic increase towards ore.

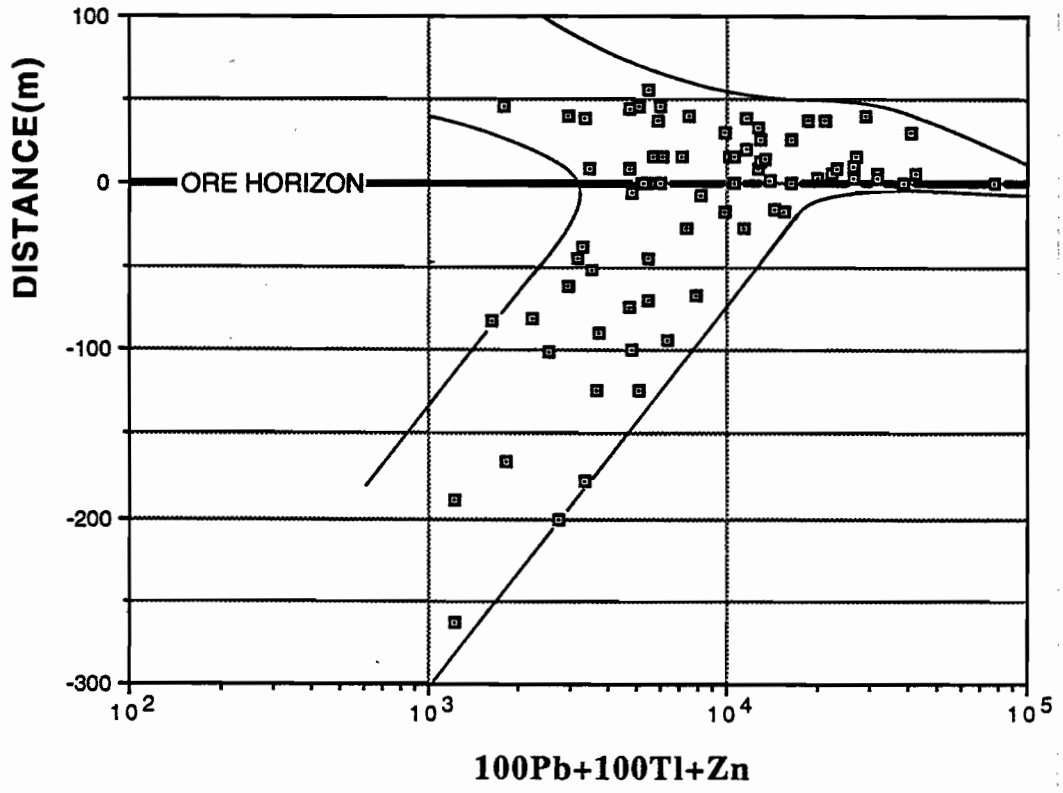

Figure 11 Variation in metal index with stratigraphic distance from ore horizon, Lady Loretta, Small Syncline.

Development of an Alteration Index

In light of the successful use of the alteration index developed by Ishikara et.al. (1976) for volcanic hosted massive sulphide deposits (VHMS), it was decided to attempt to develop a similar index for sediment hosted Pb-Zn deposits based on our Lady Loretta data set. Ishikara's alteration index has proved particularly useful in VHMS exploration, especially for drill core analyses, to provide vectors towards ore in the broad altered footwall system to a massive sulphide deposit.

The concept of an alteration index is to determine the key enrichment elements and key depletion elements and to combine them in an index that varies from 0 to 100.

$$\text{Thus, Alteration Index} = \frac{\text{(key enriched halo elements) x 100}}{\text{(enriched + depleted elements)}}$$

In the case of Lady Loretta we selected MnO and FeO as the enriched elements and MgO and Na_2O as the depleted elements. Other combinations using CaO and K_2O were tried but found less useful.

The selected index is:

$$\text{Alteration Index for Sed H Pb-Zn} = \frac{100[10MnO + FeO]}{[10MnO + FeO + MgO + Na_2O]}$$

MnO is factored by 10 to bring its values up to the level of FeO and MgO.

From a plot of alteration index against stratigraphic distance (Fig 12) it is evident that the alteration index increases fairly systematically from a background of about 30 to a maximum of 95 approaching the orebody from the footwall side. In the hangingwall sediments, the alteration index varies from 50 to 90 within 50m of the orebody.

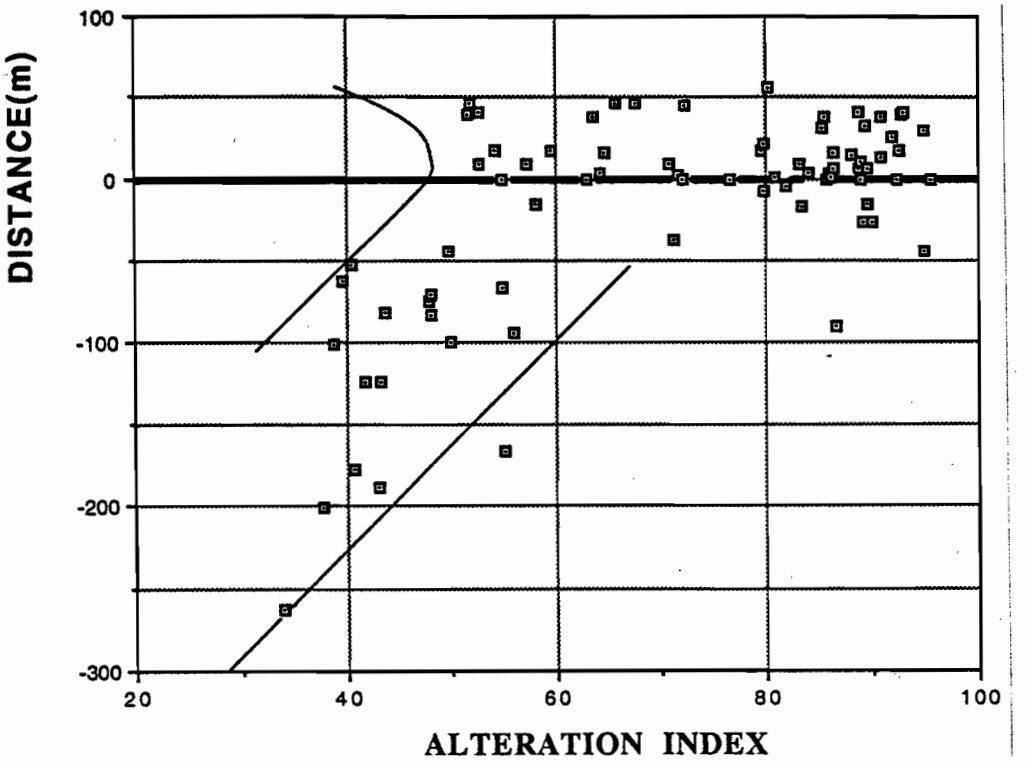

Figure 12 Variation in alteration index with stratigraphic distance form ore horizon, Lady Loretta, Small Syncline.

A surprisingly good relationship emerges from a plot of alteration index against zinc in the Lady Loretta Small Syncline data (Fig 13). This relationship indicates that zinc enrichment in the halo sediments is accompanied by a change in alteration index, thus reflecting changing chemistry in the composition of the carbonate minerals. In other words, the hydrothermal processes that have led to zinc deposition are the same processes that have caused changes in MnO, FeO, MgO and Na_2O accompanying modification of the chemistry of the carbonate minerals dolomite and siderite. This pattern of zinc and alteration index has major implications for mineral exploration, as will be outlined later.

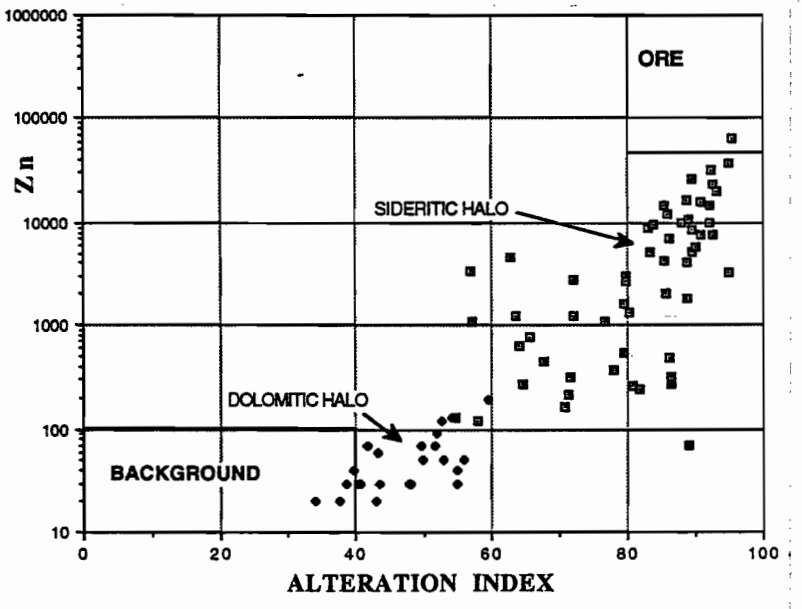

Figure 13 Linear trend between alteration index and zinc content for sediments in the Small Syncline, Lady Loretta.

Manganese content of Carbonates (MnO_D, MnO_S)

We have shown that Mn substitutes for Mg and Fe in dolomite and siderite (Fig 5) in the host sediments around Lady Loretta and that overall MnO content of the sediments increases erratically towards the orebody (Fig 9a). This erratic variation in whole rock MnO is largely due to the variation in the amount of carbonate in the various sedimentary facies in the halo. Because dolomite and siderite are the only major carbonate minerals present in the samples, and because they are virtually mutually exclusive of each other, it is possible to eliminate the effect of variable sediment carbonate content by re-calculating sample MnO (to 100% carbonate) using the following relationships:

MnO content of dolomite; $MnO_D = \frac{MnO_{WR} \times 30.41}{CaO_{WR}}$ .....(1)

MnO content of siderite; $MnO_S = \frac{MnO_{WR} \times 62.01}{FeO^*}$ .....(2)

- where FeO^* = (whole rock FeO) - (FeO present in pyrite)
- MnO_{WR} and CaO_{WR} are the whole rock values.

It is strongly recommended that the MnO_D formulae only be used for rocks with >1wt% CaO, as rocks with <1wt% CaO are virtually devoid of significant dolomite.

Using equations 1 and 2, the MnO content of carbonates from the Lady Loretta Small Syncline have been calculated and are plotted in figure 14. MnO_D shows a very systematic increase in the footwall sediments towards ore from a background value of ~0.2wt% to a maximum of 0.6wt% at the dolomite/siderite boundary.

MnOs has considerably higher values generally in the range 0.4 to 4.0wt% MnO in siderite; however, some samples close to, or within, the ore horizon contain from 4 to 30wt% MnO in siderite. The combined values MnO_D and MnO_S are plotted in figure 15, and indicate this to be an extremely useful vector towards ore.

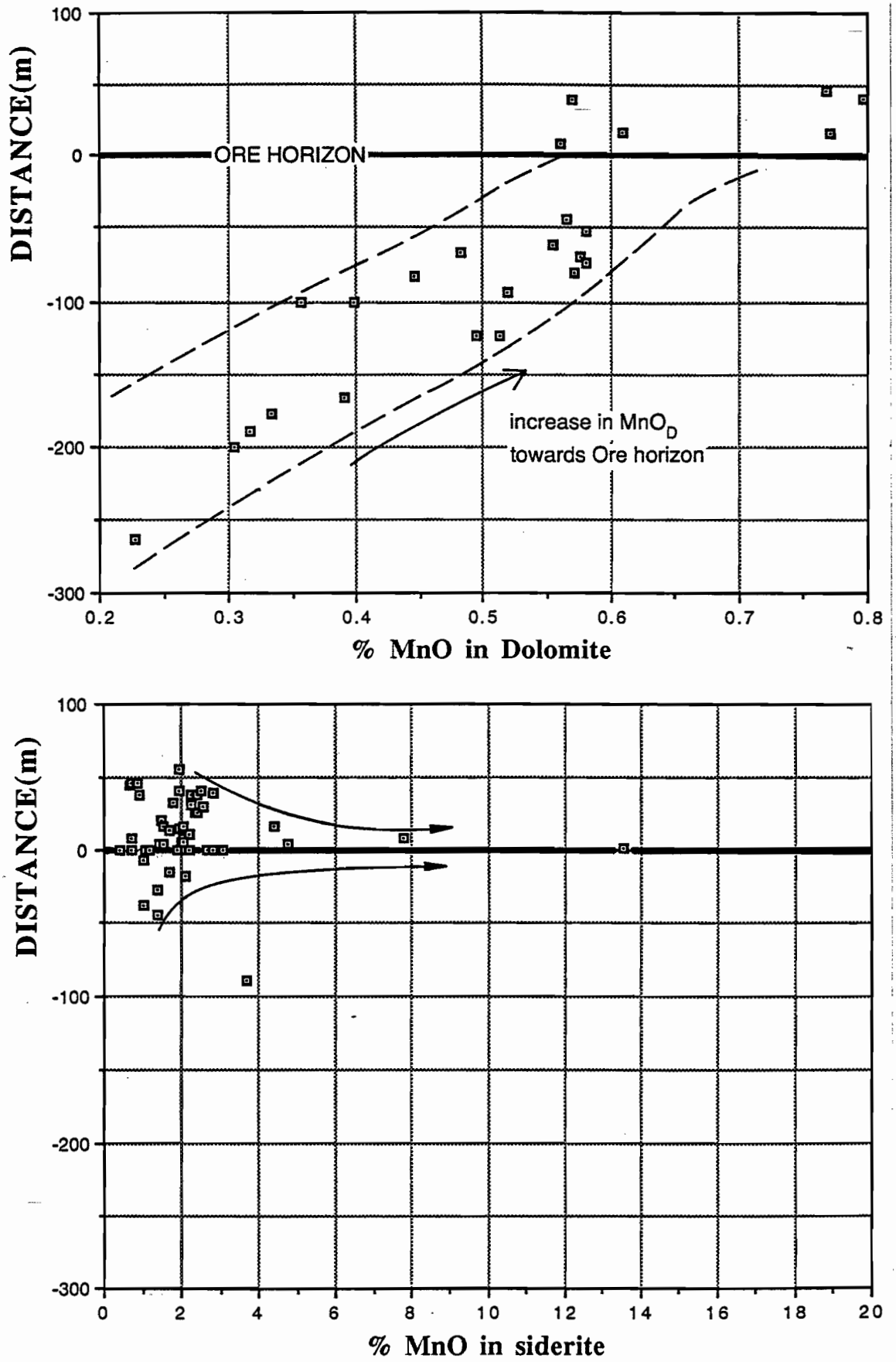

Figure 14 Variation in MnO content of carbonate calculated from whole rock data of sediments in the Small Syncline, Lady Loretta.

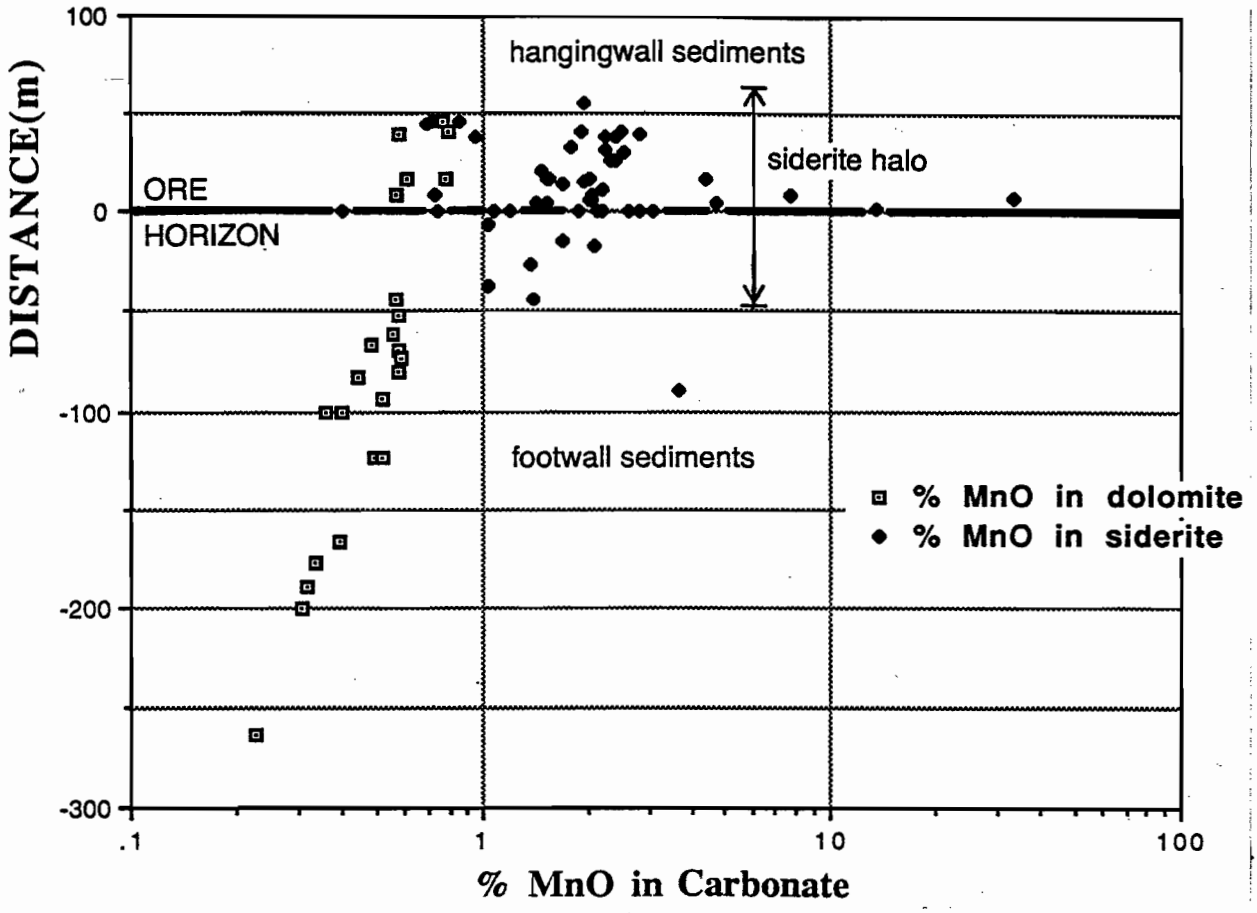

Figure 15 Composite plot showing the calculated variation in MnO content of carbonates with stratigraphic distance from the ore horizon, Lady Loretta, Small Syncline.

Halo Model for Lady Loretta

By combining the element dispersion and mineral chemistry data outlined in this report with the known geology of the deposit from Hancock and Purvis (1990) and McGoldrick (1993a), it has been possible to develop a primary halo model for Lady Loretta (fig 16). This is a pre-folding reconstruction which utilises the Small Syncline and Big Syncline geochemical data base. The major features of the halo model are:

1) An inner siderite halo which surrounds the ore body and extends several hundred metres (up to about 1km) as a narrow sheath surrounding the ore horizon.

2) An outer dolomite halo with anomalous Mn and Tl which surrounds the siderite halo and extends further along the ore horizon.

Variations in alteration index (AI) and MnO content of carbonates (MnO_D, MnO_S) related to the halo model are outlined in figure 16b.

Identification of Potential Ore Horizon in Distal Locations (>500m)

Parameters useful in the identification of a potential ore horizon in the Lady Loretta Formation are:

1) Alteration index AI > 40

where $AI = \frac{100[10MnO + FeO]}{[MgO+Na_2O + 10MnO + FeO]}$

2) MnO content of dolomite

$MnO_D > 0.2$wt% when $CaO_{WR} > 1.0$wt%

3) Thallium > 4ppm

4) Zinc > 70 ppm

Coincidence of all four factors above should be considered highly promising. High Zn values by themselves are not considered to be a good indicator.

Vectors towards ore

Based on our Lady Loretta case study, the following vectors are recommended:

- change from dolomite to siderite as major carbonate
  - within 50m of orebody across strata
  - within 500-1000m of orebody along favourable horizon
- MnO_D increases from 0.2% to 1% over 300m approaching orebody from FW side.
- AI increases from 30 to >90 over at least 300m in FW and ?HW.
- Zn content of whole rock increases erratically from 100ppm to 1% over 100m in FW and possibly >200m in HW.

- Tl content of whole rock increases erratically from < 4ppm to 100ppm over 150m in FW and possibly >200m in HW.

- Metal index (100Pb + 100Tl + Zn) increases towards ore over 100m across strata.

Application to Big Syncline Exploration

Over 20 years of exploration by various companies has failed to identify a significant mineral resource in the Big Syncline, to the south of Lady Loretta. Although the Ore Horizon crops out and has been intersected in several drill holes, only one hole returned economic grades and widths (DDH P68, 3m at 5.7% Zn and 5.2%Pb).

With the development of the Lady Loretta halo model and related vectors to ore outlined here, it will be possible to re-evaluate the previous drilling programme and possibly identify new targets for further drilling. Limited sampling of four Big Syncline drill holes has been carried out as part of this study (McGoldrick, 1992b) and the initial results are encouraging (Fig 17 and 18). Only one of the four holes sampled (DDH P148 on Section 740N) revealed the presence of the inner siderite halo (Fig 17). The other four holes intersected dolomite surrounding the ore horizon, suggesting more distal locations with respect to ore. Application of the alteration index supports this conclusion and shows that samples from Section 740mN fall into two groups:

AI = 50 to 60 and AI = 60 to 90. Samples from the latter group would be interpreted to be close to ore. All samples from sections 1340mN and 1520mN gave low alteration indices (40 - 60) and low zinc values (≤ 30ppm), supporting distal locations The only ore grade intersection in the Big Syncline is from P68 (near 1520mN section), unfortunately, this interval of core is lost. Obviously further sampling and analyses are required on the Big Syncline drill holes in order to fully test the application of our model.

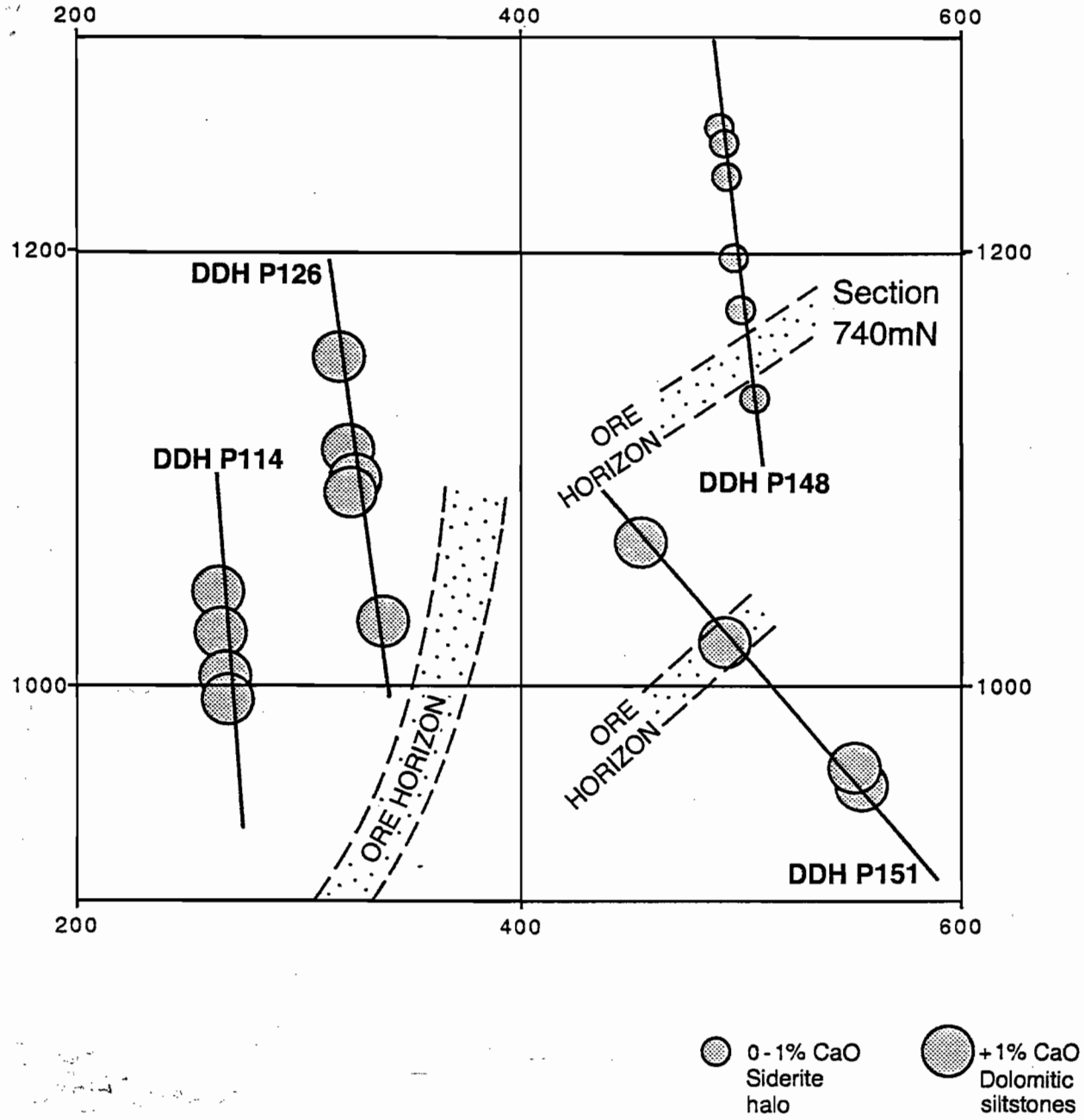

Figure 17 Drill holes sampled in the Lady Loretta Big Syncline Study, composited on the same section. Circles indicate the level of whole rock CaO. Siderite alteration (<1% CaO) is indicated in all samples from DDH P148.

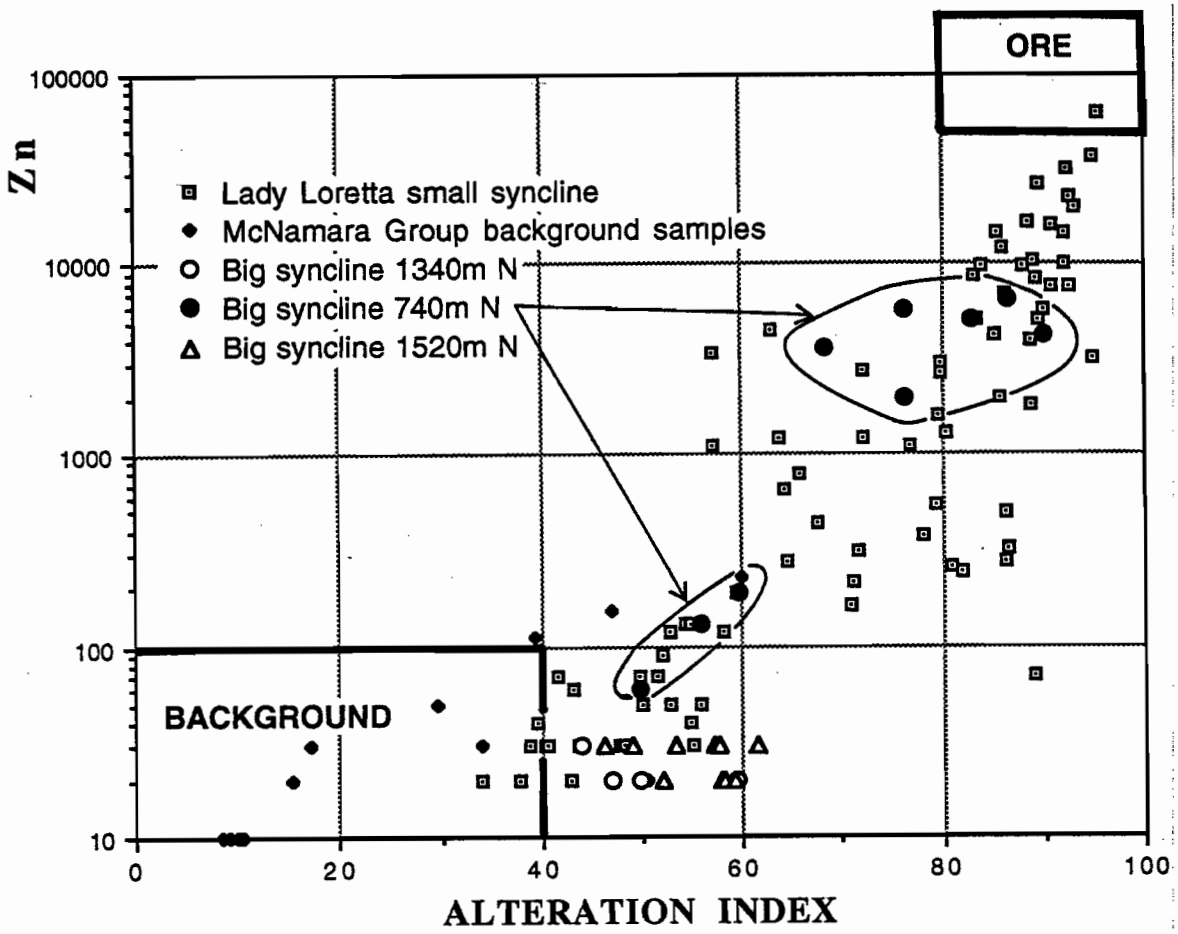

Figure 18 Big Syncline data plotted on the Small Syncline trend, Lady Loretta. Onlysamples from Section 740m N indicate likely proximity to ore grade mineralisation.

HALO FORMATION AND ORE GENESIS

The samples used for defining halos at Lady Loretta are fresh rock from drill core (McGoldrick, 1993b), hence, the halos described in this report are 'primary dispersion halos') assumed to form as an integral part of the ore genesis. Three generalised genetic models for the Lady Loretta deposit have been discussed in part 3 of this report (McGoldrick, 1993a). These were the

i) exhalative - syngenetic model
ii) syn-sedimentation - early model,
iii) syn-sedimentation - late model.

All three involve an external hydrothermal fluid as the source of base metals and this fluid would also be the cause of the primary geochemical halos.

VHMS deposits provide a useful analogue for sedimentary exhalative-syngenetic mineralization, however, a simple exhalative-syngenetic process does not easily account for the symmetrical, nested pattern exhibited by the halos at Lady Loretta. Most VHMS deposits have intense footwall alteration, with more cryptic hangingwall alteration, and primary dispersion tend to be in the form of 'exhalite' horizons at the same stratigraphic level as the orebody (e.g., Duhig et al., 1992). This pattern results from the profound physico-chemical changes experienced by the ore fluid at or near the sea floor. Hanging wall alteration is weaker because it caused by a hydrothermal system that is waning and/or being overwhelmed by lavas or volcaniclastics.

The similarity between the halos in sediments below the ore at Lady Loretta with those above implies that hanging wall alteration mimicked footwall alteration. For the deposit to be syngenetic a process must operate that permits the hanging wall rocks to interact with fluids essentially identical to those forming the mineralization and the footwall alteration. This might happen if the hydrothermal system persisted unchanged well after the ore beds were deposited, but presumably more syngenetic mineralization would be forming higher in the sequence from such fluids. Although sampling to date has not defined the upper limits of the halos at Lady Loretta, no such mineralization is recognized. Most of the pyritic beds in the hanging wall (presumably good sites for such later syngentic mineralization) contain only minor base metals. Another possibility is that syngenetic mineralization formed from hydrothermal fluids confined to a brine pool or sub-basin (lake?) in which hydrothermal fluid input dominated water chemistry. This fluid was not displaced by sediment during deposition of the hanging wall, but remained as a pore fluid capable of affecting the alteration responsible for the hangingwall halo. The final extent of the halo is determined by the size of the persistent brine pool. The chief problem with this scenario is the large fluid volumes (orders of magnitude more fluid than the volume of the brine pool) needed to form ore grade mineralization. To achieve the neccessary fluid throughput while clastic sedimentation is taking place requires extensive fluid movement within both the hangingwall and footwall sediments. There is no *a priori* reason why these fluids would only form mineralization at the sediment-water interface. Mineralization could also form in the subsurface where conditions were favourable. Hence this model is a special case of an 'exhalative – syngenetic' model that shares many features with the 'syn-sedimentation – early' model, with the most important distinction being that some ore fluid escapes to the basin floor to form mineralization.

In a 'syn-sedimentation - early' model hydrothermal fluid is continuously or episodically moving through the upper few centimetres or decimetres of the sediment pile. Halos develop in the siltstones and shales exposed to transient hydrothermal fluids.and, as with the ores, the halos form incrementally over the time needed to deposit the footwall, ore lens and the hanging wall sequence. The hydrothermal system must persist for as long as it takes to deposit these sediments. Furthermore, either the system undergoes an evolution from a barren (but still halo-

forming - e.g., Tl and siderite) to a fertile (i.e., base metal-rich) and then back to a barren system to account for halos on both sides of the ore, or, an ingredient required for fixing base metal sulphides was absent from the footwall and hanging wall sediments (e.g., large amounts of organic matter and reactable Fe sulphides?).

In a 'syn-sedimentation - late' model ore fluid movement is essentially simultaneous through several tens to hundreds of meteres of the sedimentary pile. Primary dispersion halos form from the effects of this fluid on the sediments, and base metal sulphide mineralization forms in the chemically reactive Fe sulphide- and organic matter-rich parts of the sequence. This model neatly explains the formation of similar hangingwall and footwall halos, but is not well constrained in other areas. For instance, sufficient porosity and permeability must be maintained for ore fluids to move through the sediment pile at the required depths. As with the other models, the fluid drive and sulphide precipitation processes are problematical.

Further work

Petrographic studies of both the ores and the host rocks at Lady Loretta may help resolve which of these genetic models is most applicable. For the moment, the textures and S isotope studies refered to in part 3 of this report (McGoldrick, 1993a) appear to support a syn-sedimentation timing for the mineralization. If the coarse siltstones can be used for deciphering the timing of siderite formation in relation to dolomitization and/or other diagenetic processes (e.g., porosity oclusion by later cements), then the timing of ore fluids introduction to the Lady Loretta sequence will be much better constrained.

APPLICATION TO THE HYC DEPOSIT

In order to test our halo model, and determine whether it is applicable to other Proterozoic sediment hosted Pb-Zn deposits, a previously published whole rock data set from the HYC deposit and surrounding sub-basins (Lambert and Scott, 1973 and Corbett et al., 1975 Appendix 2), has been thoroughly investigated.

Previous halo studies at HYC

Lambert and Scott (1973) undertook a detailed study of mineral dispersion within and surrounding the HYC deposit, and their geochemical data base (Corbett et al., 1975) has proved to be an invaluable resource for this investigation. In their study, Lambert and Scott analysed 160 whole rock samples taken from eight diamond drill holes - two within the HYC

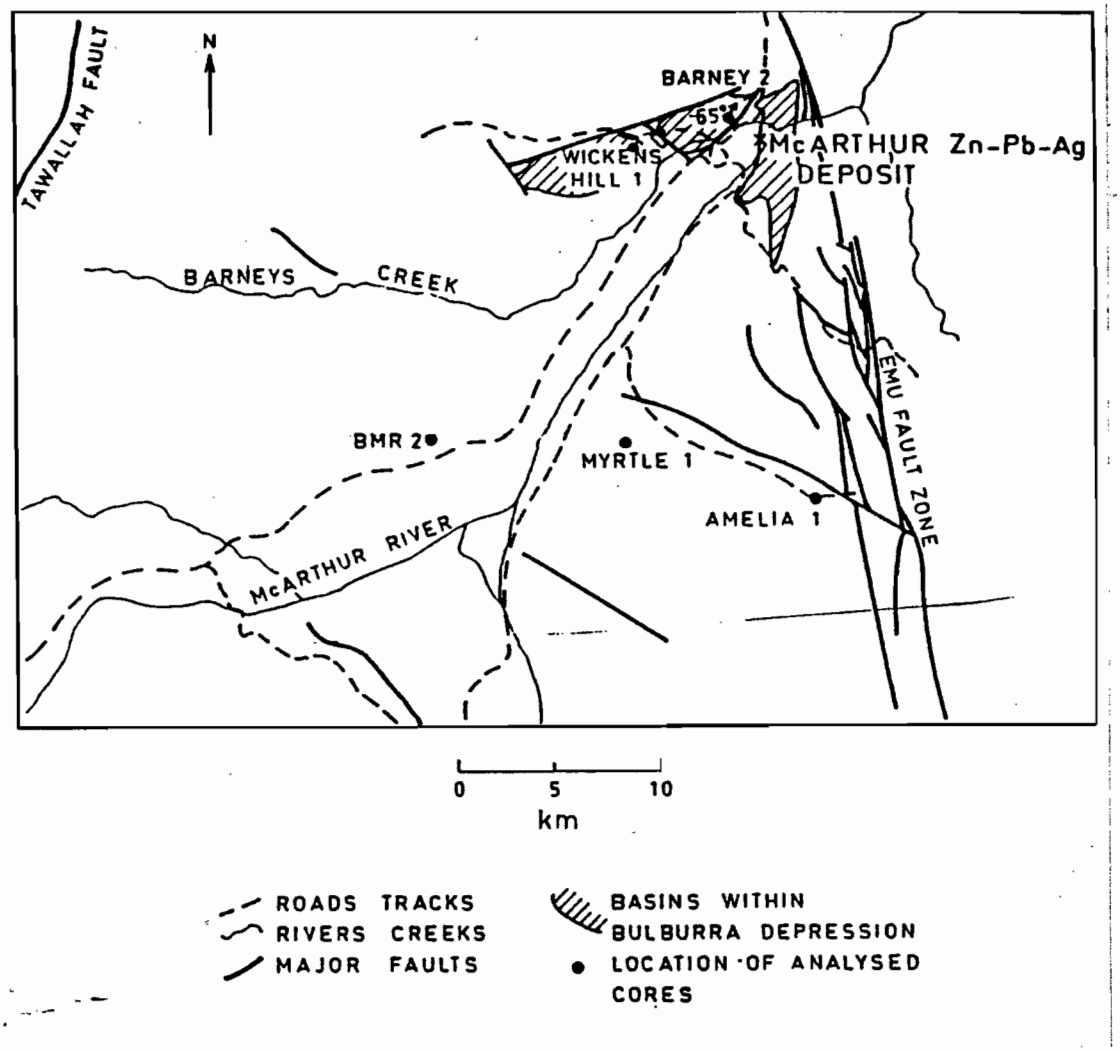

Figure 19: Location of drill holes sampled by Lambert & Scott (1973) in their HYC study.

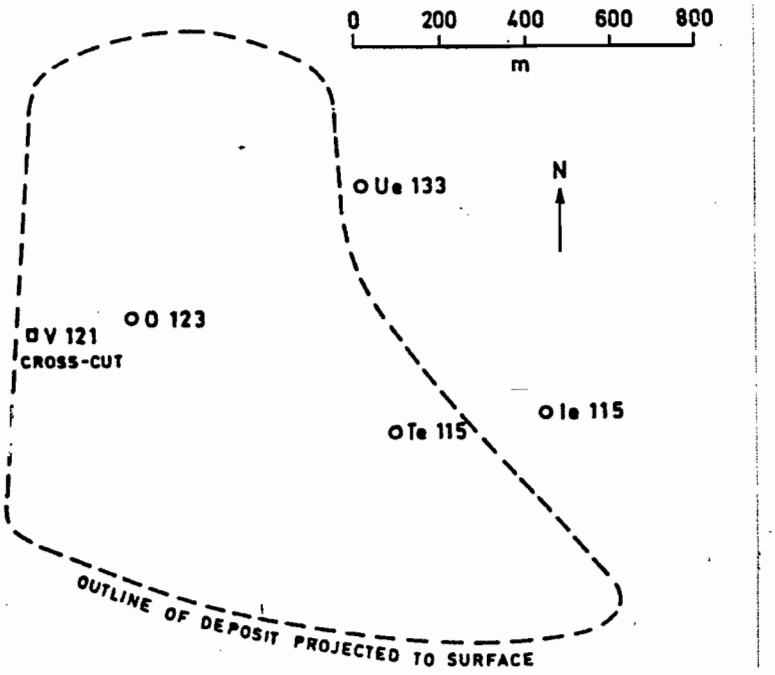

Figure 20: Drill holes sampled within and close to the HYC orebody by Lambert & Scott (1973).

deposit, two just beyond the boundaries of the deposit and four at various distances from 2.5 to 23 km away (Fig. 19). Locations of sampled drill holes intersecting the deposit are shown in plan in figure 20, and on a generalised cross-section in figure 21. Lambert and Scott (1973) concluded from their study that favourable areas for HYC type deposits should contain:

- pyritic, high-K carbonaceous shales
- anomalous Zn, Pb, Ag, Hg in shales
- dolomites with moderate to high Fe and Mn
- vitroclastic tuff bands

They also showed that the Fe content of dolomites increased towards the HYC deposit and that the Mn content of the sediments is highest in the immediate footwall of the deposit. A copy of their paper is included in Appendix 5-II.

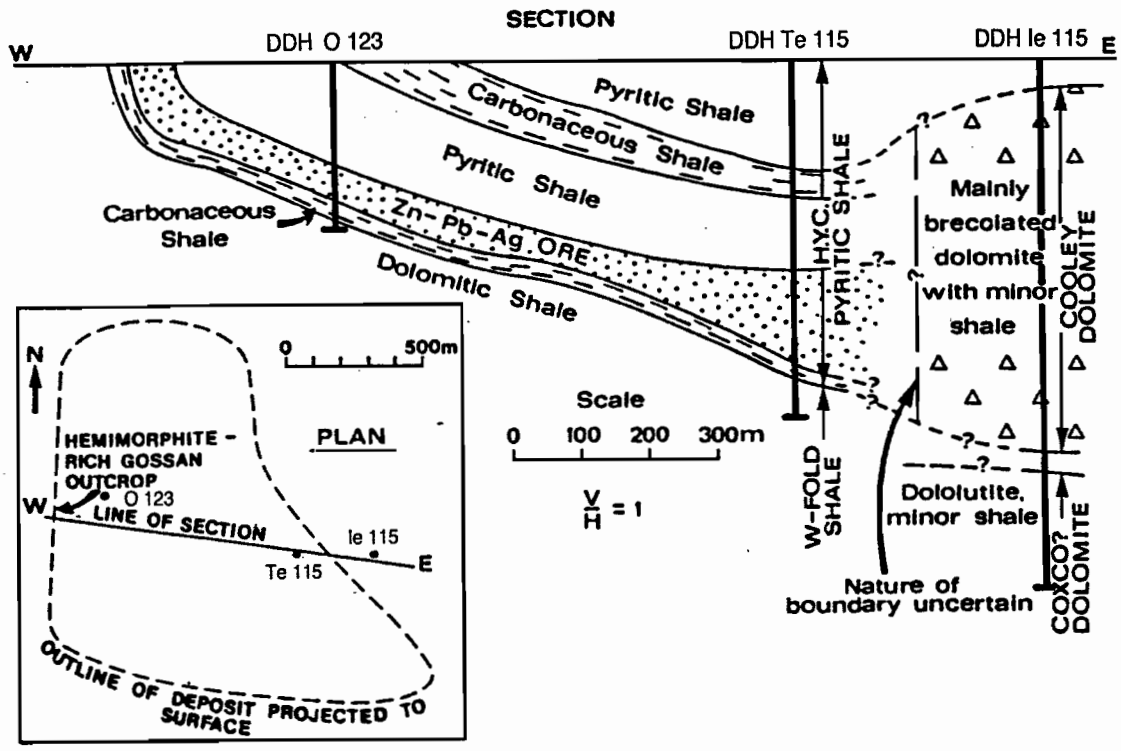

Figure 21 Cross-section and plan of HYC deposit (from Lambert, 1976, based on CEC data).The three drill holes O 123, Te 115 and Ie 115 are projected onto this section in their approximate positions.

Sampling within the HYC orebody

Two drill holes Te 115 and O 123 (Figs. 20, 21) which interset the HYC ore lenses were sampled by Lambert and Scott (1973).

HYC DDH Te115 - intersects the thickest part of the HYC ore zone. Major and minor element dispersion, down the hole, of elements relevant to this study, are plotted in figure 22.

Zinc values peak through the ore zone at greater than 10wt%. A second peak at 1% Zn occurs in the hangingwall 200m above the ore zone and suggests another potential ore horizon, which may be equivalent to the Ridge II stratiform zone (Williams, 1978).

Lead shows a similar pattern to zinc, but is generally an order of magnitude lower.

CaO shows systematic decrease (depletion?) passing up through the footwall to the orebody. The ore horizon is a mixture of a low CaO facies (shales) and high CaO facies (dolomites). The hangingwall rocks (HYC shale) are dominated by the dolomite facies.

MgO shows an identical trend to CaO.

A plot of MgO versus CaO (Fig.23) indicates that dolomite is the major carbonate present, although substitution of FeO and MnO for MgO have led to diversion of the data from the pure dolomite line.

Alteration Index (Fig.24b): AI increases form about 40-60 in the deep footwall (200m below ore) to 80-90 just below the ore. Within the ore horizon and hangingwall HYC shale the AI is variable but with a consistent upper limit of 80 to 100. Considerable scatter is present on the AI vs Zn plot for DDH Te 115 (Fig. 24a) compared to the Lady Loretta data (Fig. 13). However, there remains a distinct trend from the background field to the ore field.

MnO_D (Fig. 24c) - there is a particularly strong and systematic increase in MnO content of the footwall dolomite minerals approaching the ore deposit from 0.5wt% MnO to 11.5wt% MnO. A minor (one sample) anomaly is also present in the immediate hangingwall of the deposit. However, dolomites 50m above the ore zone exhibit close to background MnO_D values, generally <0.5wt%.

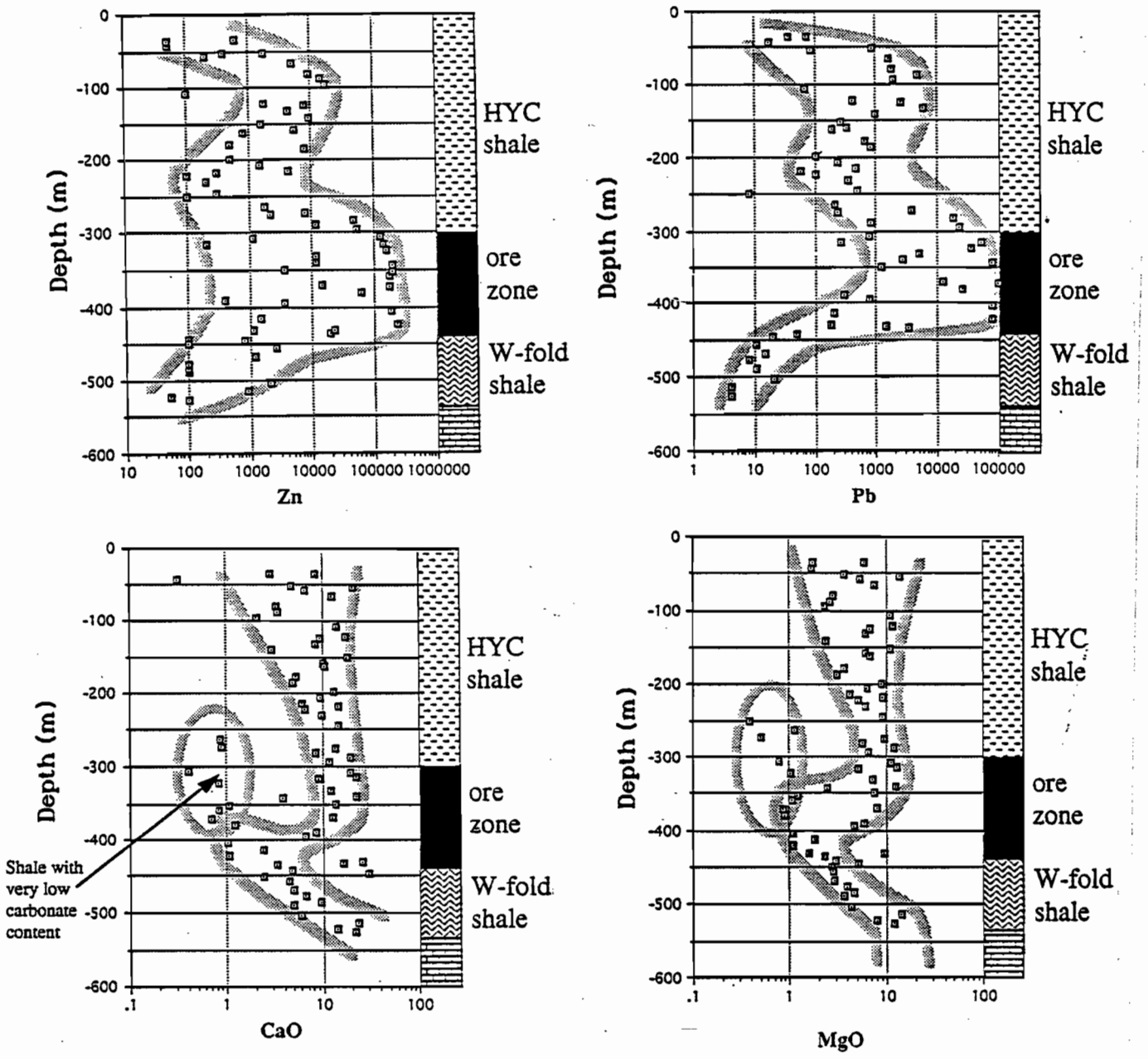

Figure 22 Variation in Zn, Pb, CaO and MgO with depth in DDH Te 115. Data from Corbett et al. (1975).
Note: All analytical data for Figures 22 to 40 are from Corbett et al. (1975).

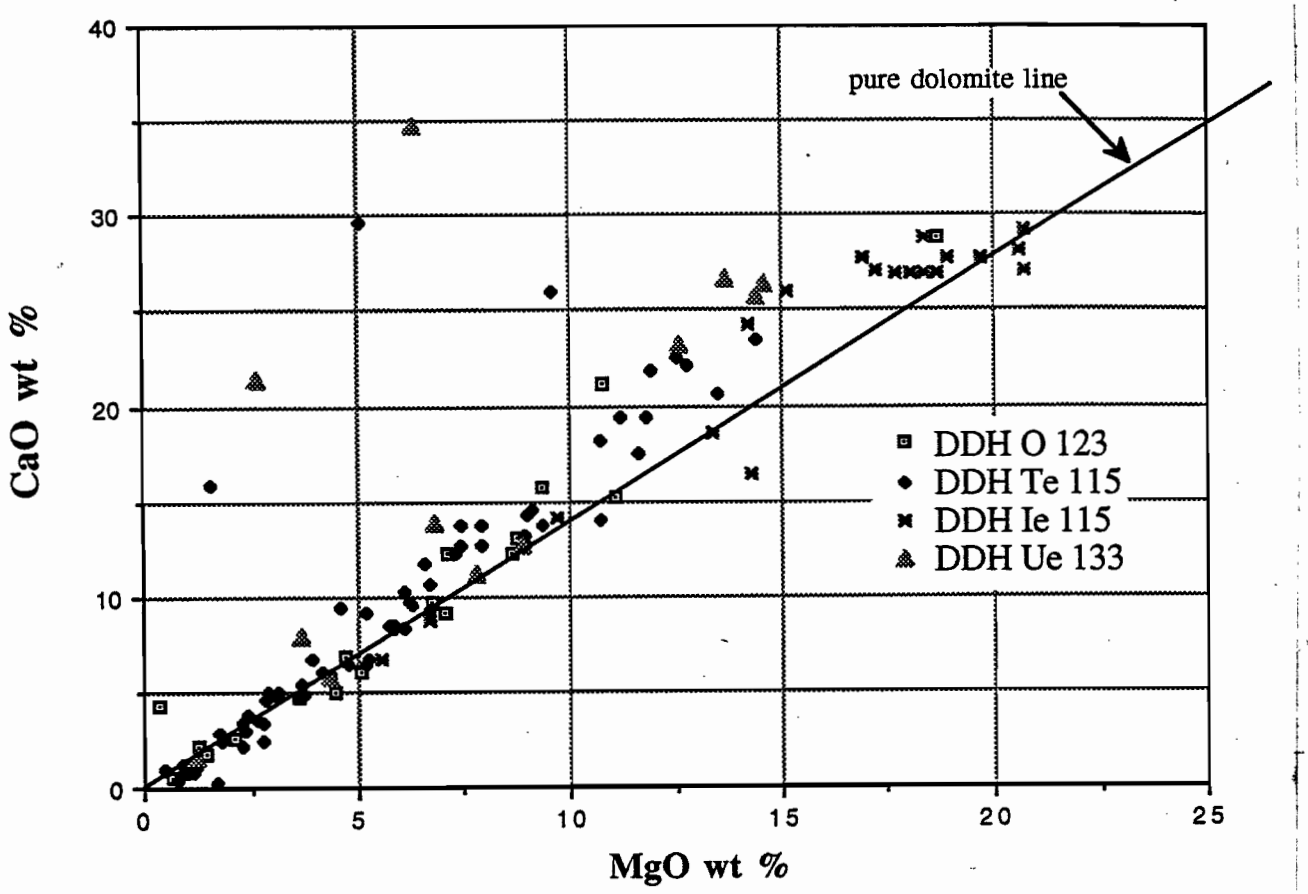

Figure 23 This correlation between CaO and MgO indicates that dolomite is the major carbonate mineral in the HYC deposit and associated host rocks. The slight departure from the pure dolomite line is probably due to Fe and Mn substitution in the dolomite. Samples which plot well above the line are probably mixtures of dolomite and calcite.

HYC DDH O 123 - intersects the western part of the HYC orebody.

Zinc (Fig. 25a): increases towards the ore zone from both the hangingwall and footwall side. Background zinc is <100ppm.

Alteration Index (Figs. 25b and 26a): increases towards the ore zone from both the hangingwall and footwall side. A spot high of 93, eighty metres above the ore zone may indicate a second potential mineralised horizon. There is a good correlation between AI and zinc (Fig. 26a).

MnO_D (Fig. 26b): increases dramatically towards the ore zone in the footwall sediments. A spot high in the hangingwall supports the interpretation of a second horizon.

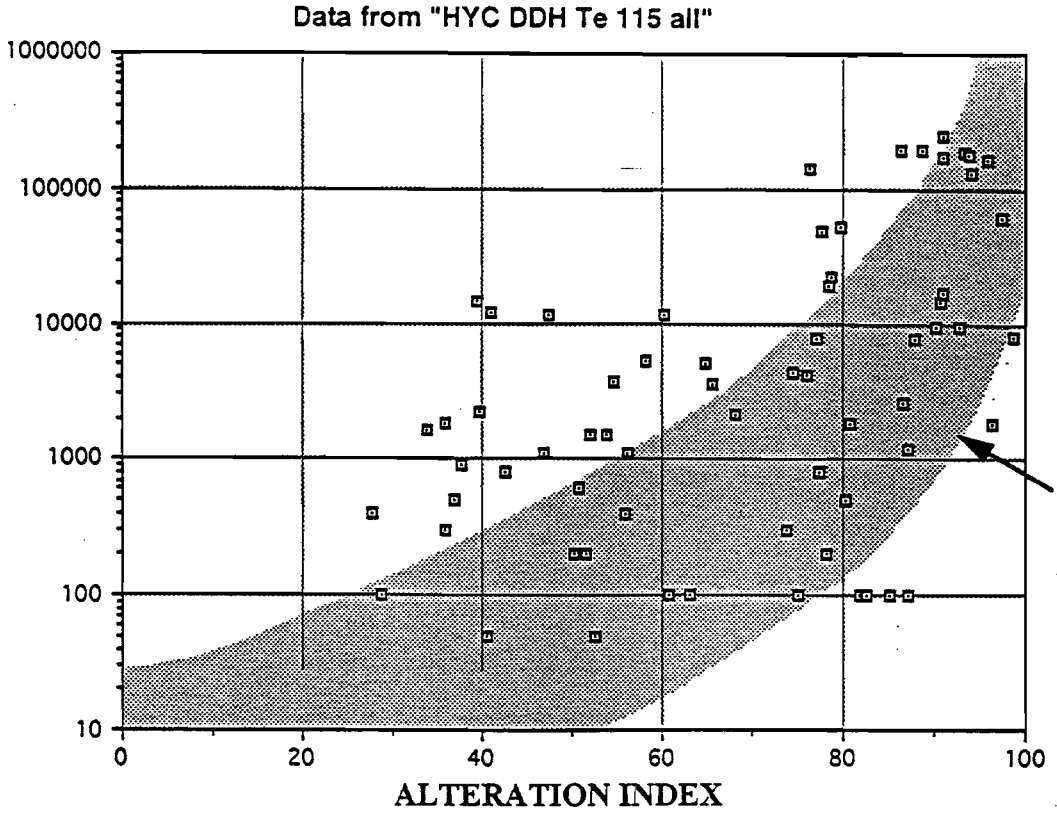

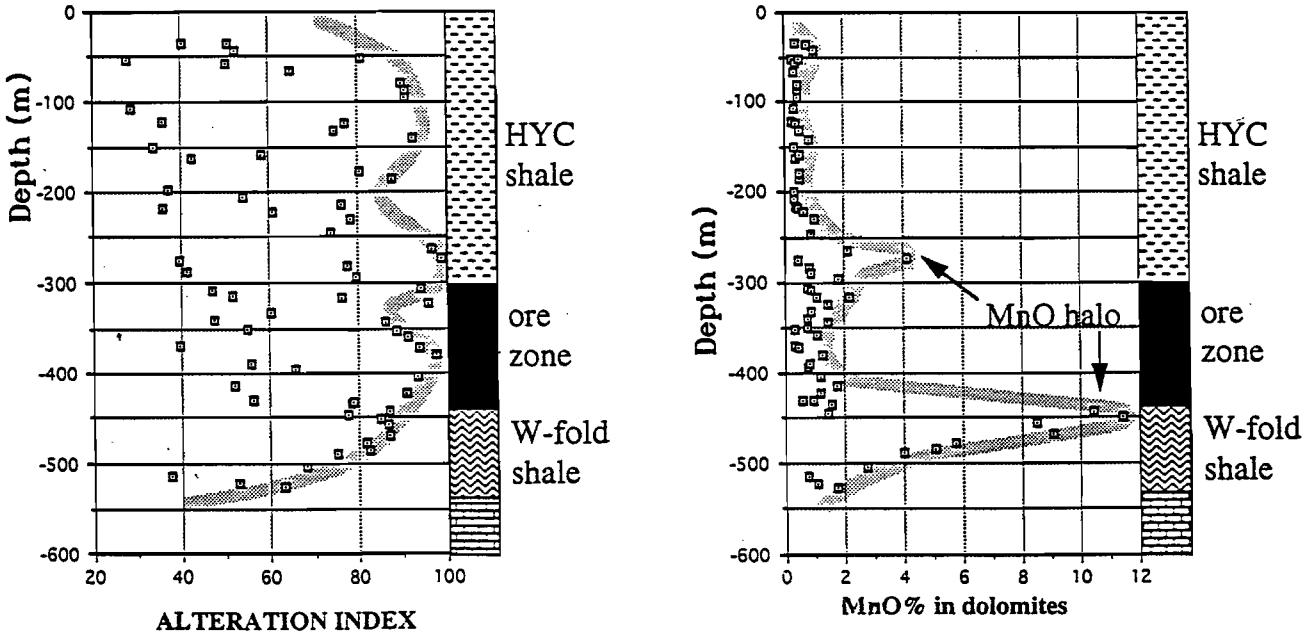

Figure 24: Data from DDH Te 115 - thickest part of HYC orebody
a) Zn vs Alteration Index
b) Variation of AI with depth
c) Variation of Calculated MnO in dolomite (MnO_D) with depth shows a systematic and strong footwall anomaly and minor hanging wall anomaly.

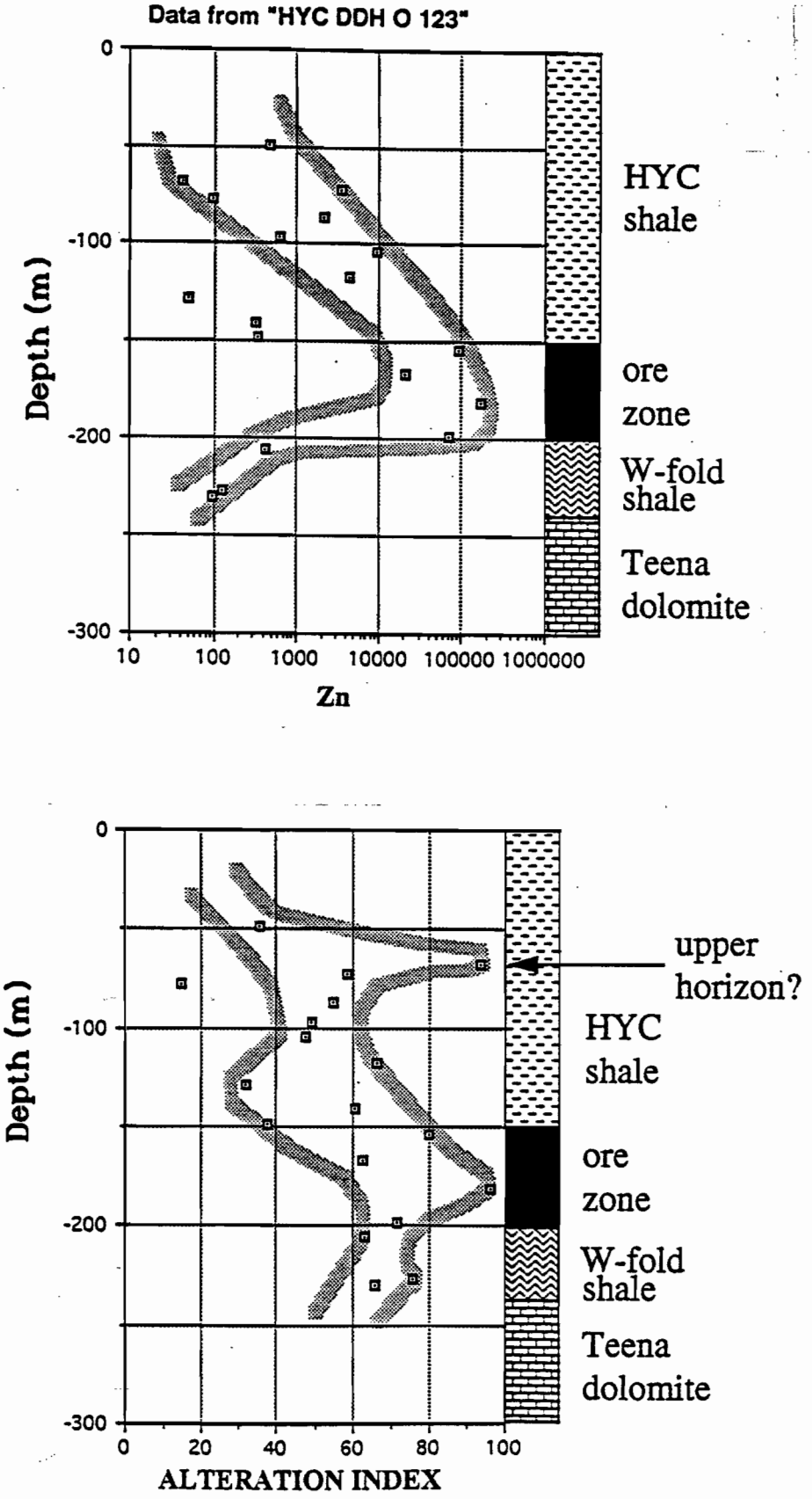

Figure 25: Data from DDH O 123 - through centre of orebody.
a) Zn vs depth
b) AI vs depth

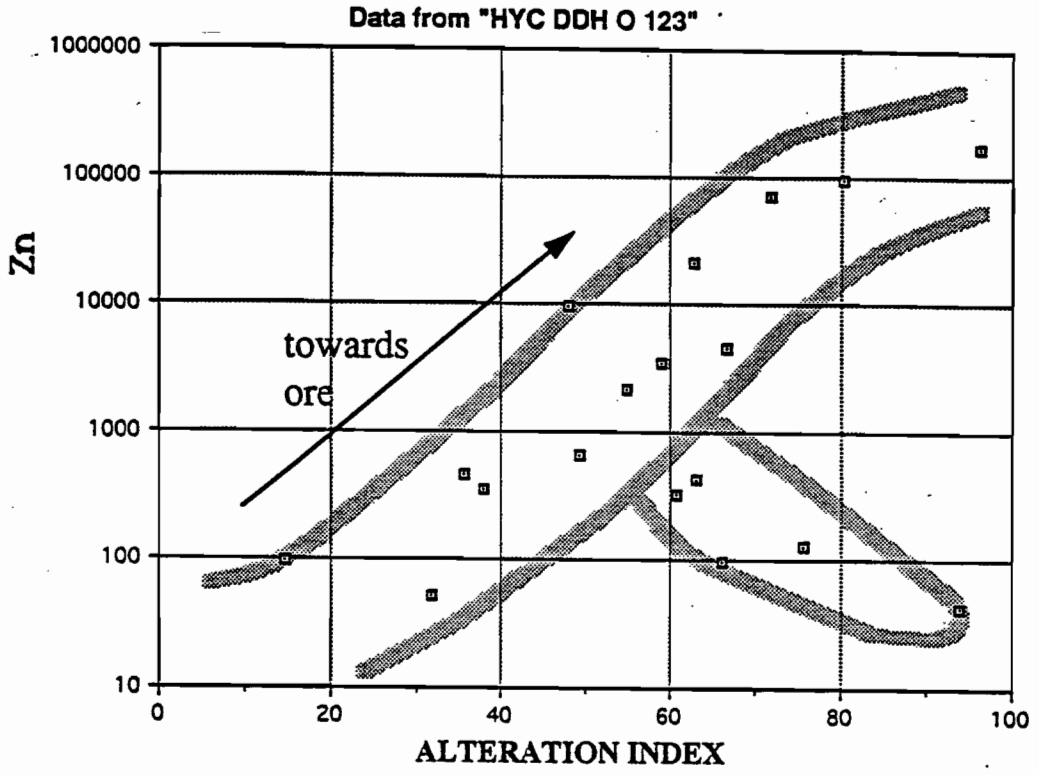

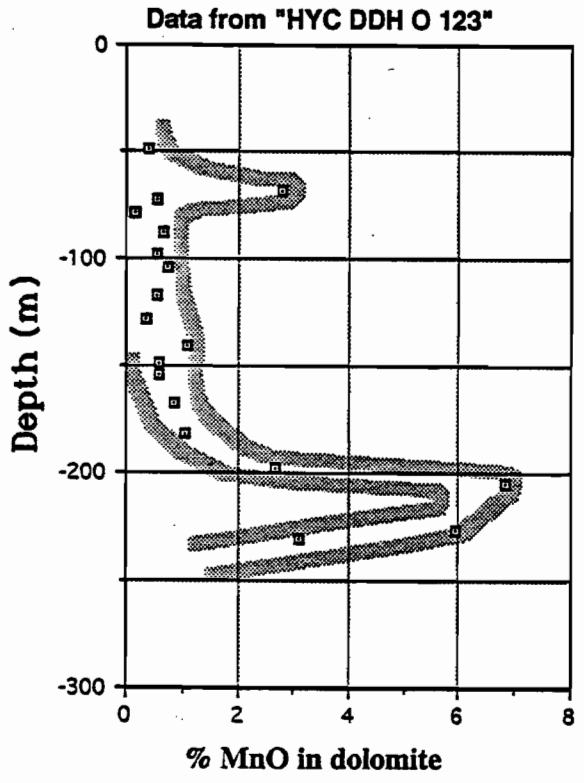

Figure 26: Data from DDH O 123 - through centre of orebody
a) Zn vs AI shows classic trend towards ore
b) MnO_D vs Depth shows strong footwall anomaly

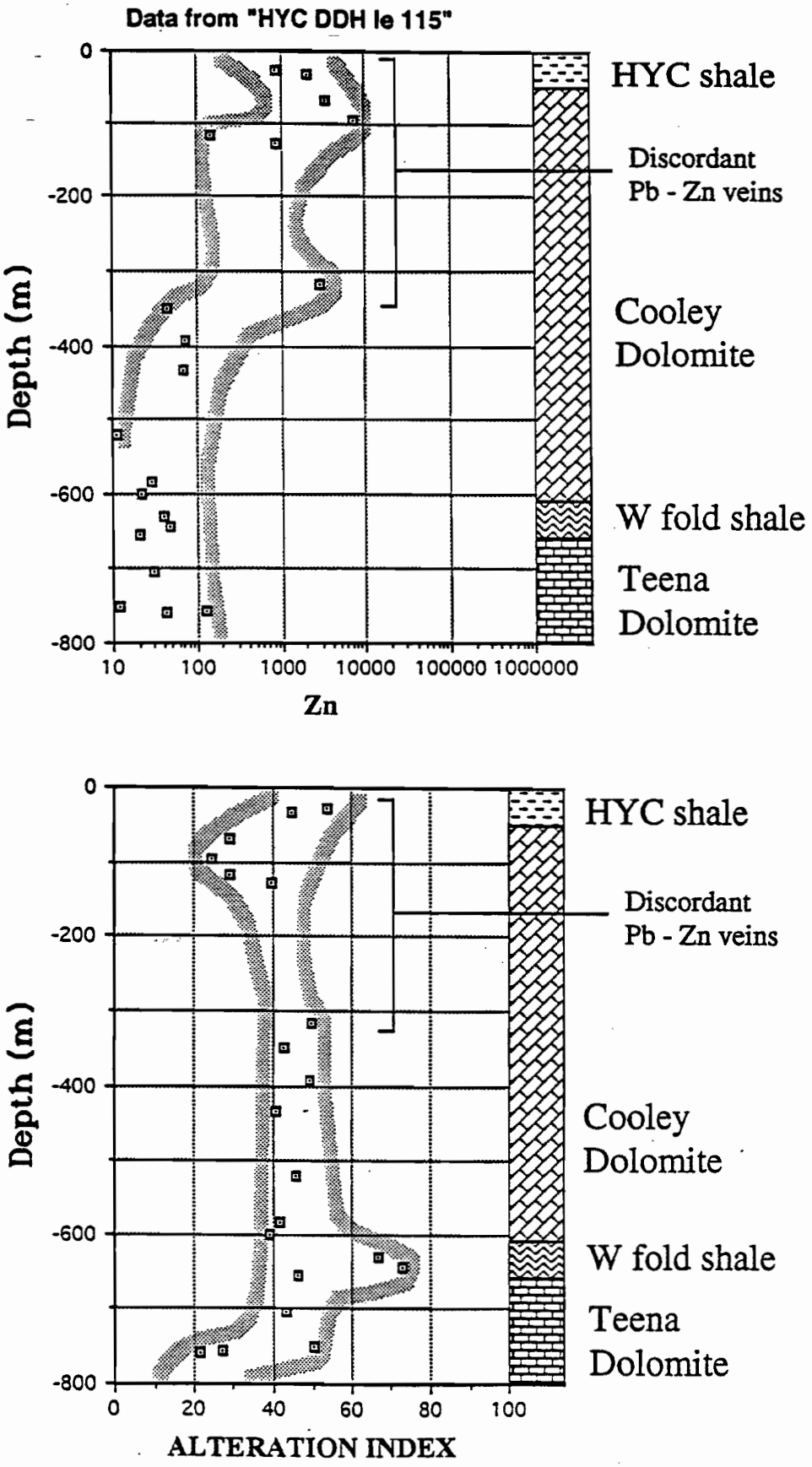

Figure 27: Data from DDH Ie 115 - outside eastern edge of orebody
a) Zn vs Depth; anomalous Zn is related to vein style mineralisation in Cooley dolomite from 0 to 320m.
b) AI vs Depth; discordant mineralisation shows no AI anomaly. Minor anomaly in W fold shales.

Drill holes outside the margin of HYC orebody

DDH Ie 115 - intersects the Cooley Dolomite breccia adjacent to the Western Fault (Fig. 21). This hole is referred to as R17/66D by Walker et.al. (1977).

Zinc (Fig. 27a) - Minor zinc (1000 - 10,000ppm) in the upper 320m of the hole is probably related to the discordant vein mineralisation in the Ridge deposit. Background zinc values (<100ppm) exist from 320 to 770m.

Alteration Index (Fig. 27b) - low values of 20 to 60 thoughout the Cooley Dolomite indicate the lack of stratiform Pb-Zn potential in this rock unit. AI values of 60 to 80 below the base of the Cooley Dolomite (600 - 650m) indicate the potential ore horizon. There is no systematic correlation between AI and ZN in this drill hole (Fig. 28a), in fact, the discordant zinc mineralisation (Ridge deposit?) shows a negative trend, unlike other stratiform zones.

MnO_D (Fig. 28b) - generally low values throughout the hole except for the W fold shale which shows distinctly anomalous values of 3-4wt% MnO in dolomite. This indicates the base of the favourable horizon.

HYC DDH Ue 133 - 30m outside the eastern boundary of the orebody (Fig. 20).

Zinc (Fig. 29a) - show marked increases from 100ppm to 1%Zn at the base of the HYC shale.

Alteration Index (Fig. 29b) - gradual increase in footwall sediments from 25 to 80 towards the favourable horizon. No clear pattern in AI vs Zn plot (Fig. 30a). However, 2 samples in the ore position have values of 90 to 100.

MnO_D (Fig. 30b) - anomalous values at base of HYC shale. Ore position clearly indicated by the MnO_D halo pattern.

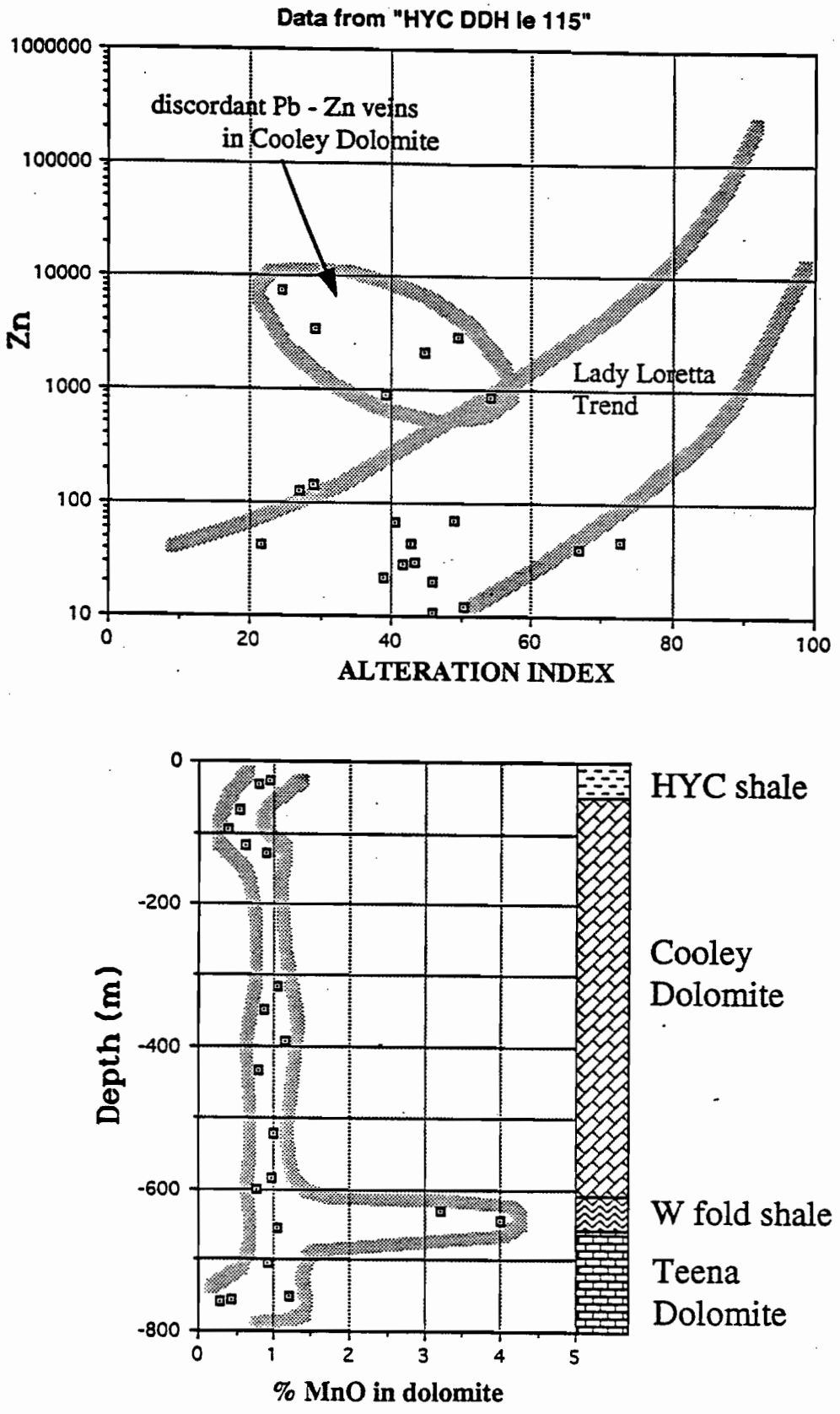

Figure 28: Data from DDH Ie 115 - outside eastern edge of anomaly.
a) Zn vs AI: no distinct trend; discordant mineralisation plots off the stratiform Lady Loretta trend.
b) MnO_D vs Depth: no anomaly associated with discordant veins.

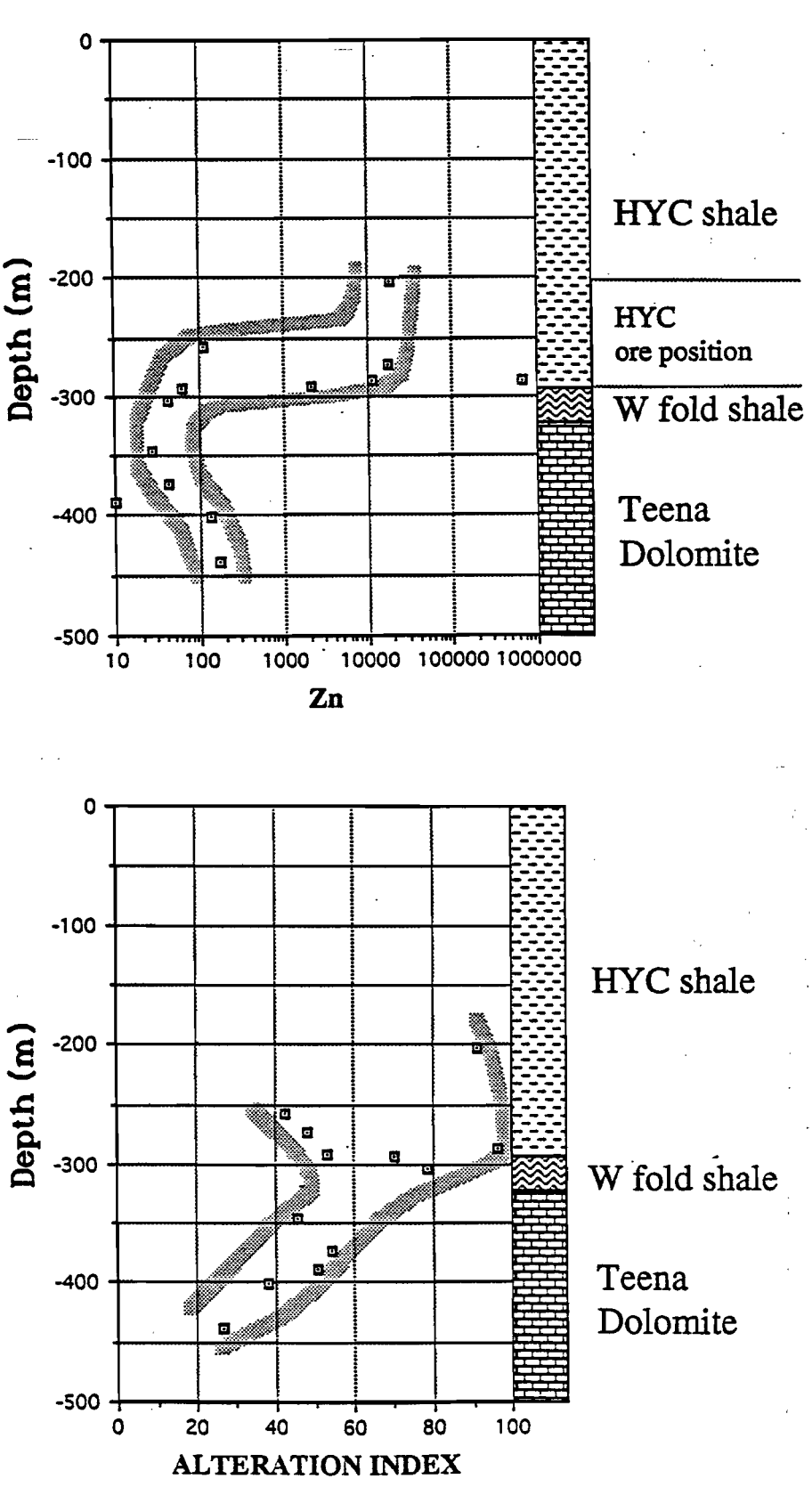

Figure 29: Data from DDH Ue 133 - outside eastern edge of orebody
a) Zn vs Depth
b) AI vs Depth

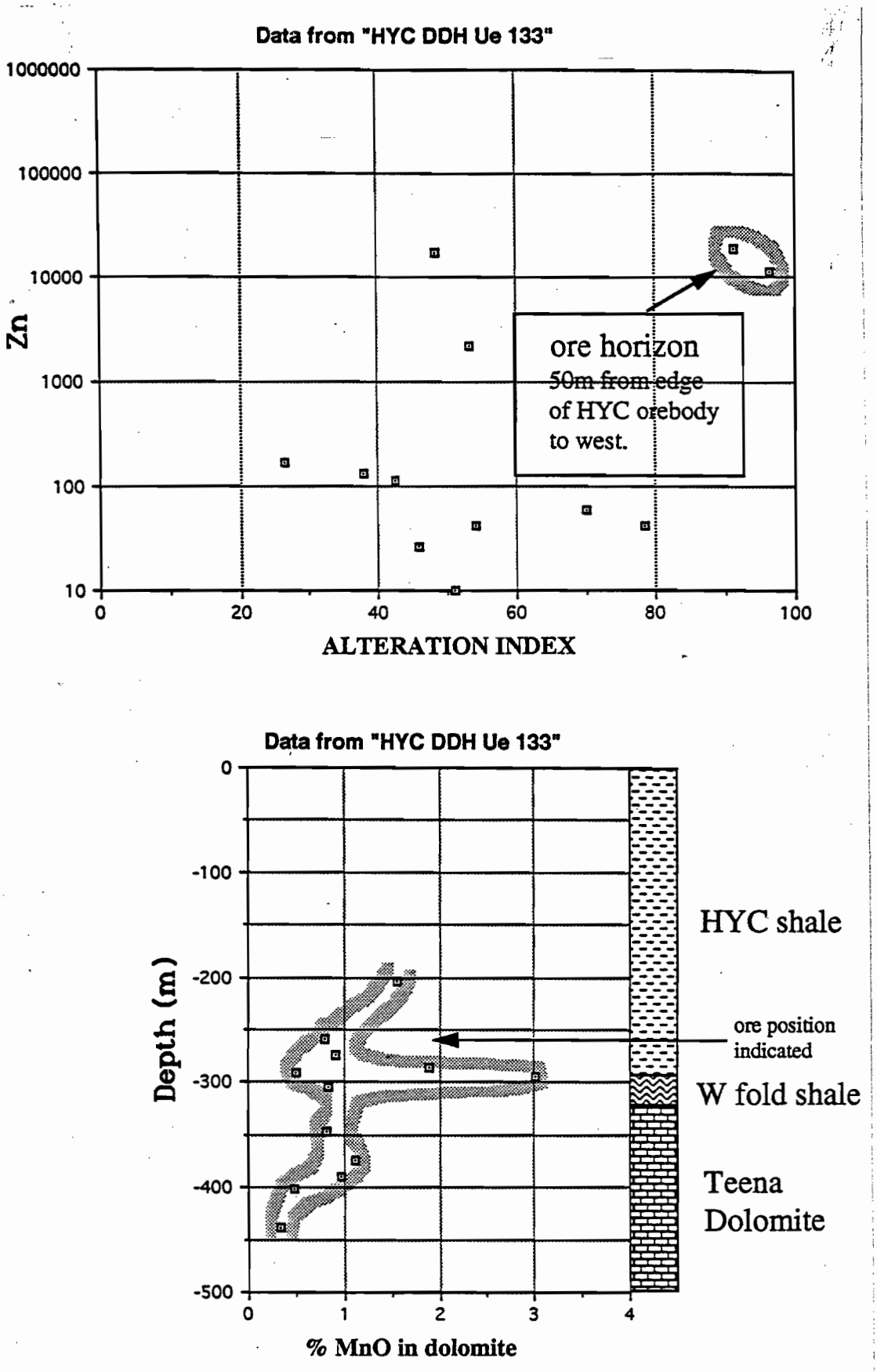

Figure 30: Data from DDH Ue 133
a) Zn vs AI - two anomalous samples at ore position 50m from edge of HYC orebody.
b) MnO_D vs Depth - ore position is bracketed by MnO_D anomalies.

Drill holes within 10km of HYC deposit (Fig. 19)

DDH Barney 2 - 2.5km to the west of HYC deposit. This hole intersected the HYC shale, W fold member and the Teena Dolomite.

Zinc (Fig. 31a): anomalous values (1,000 to 10,000ppm) occur in a 50m interval at the base of the HYC shale.

Alteration Index (Fib. 31b): Strong peak of 76 at 265m marks the potential ore position. Good correlation between AI and Zn in four anomalous samples (Fig. 32a).

MnO_D (Fig. 32b): Anomalous values between 280 - 300m in the footwall sediments below the indicated favourable horizon. The AI and MnO_D patterns in this hole provide strong support for proximity to an ore deposit.

DDH Wickens Hill - lies 6km to the west of HYC and is the site of outcropping minor Zn mineralization.

Zinc (Fig. 33a): anomalous Zn (>1000ppm) to a depth of 190m in the HYC shale. Marked drop to background below this depth.

Alteration Index (Fig. 33b): Peak of 85 at 160M depth indicates potential ore horizon. Systematic decrease in both footwall and hangingwall away from this position.

MnO_D (Fig. 34b): Anomalous values of >1% MnO in dolomite below 150m, with a spot high in the W fold shale.

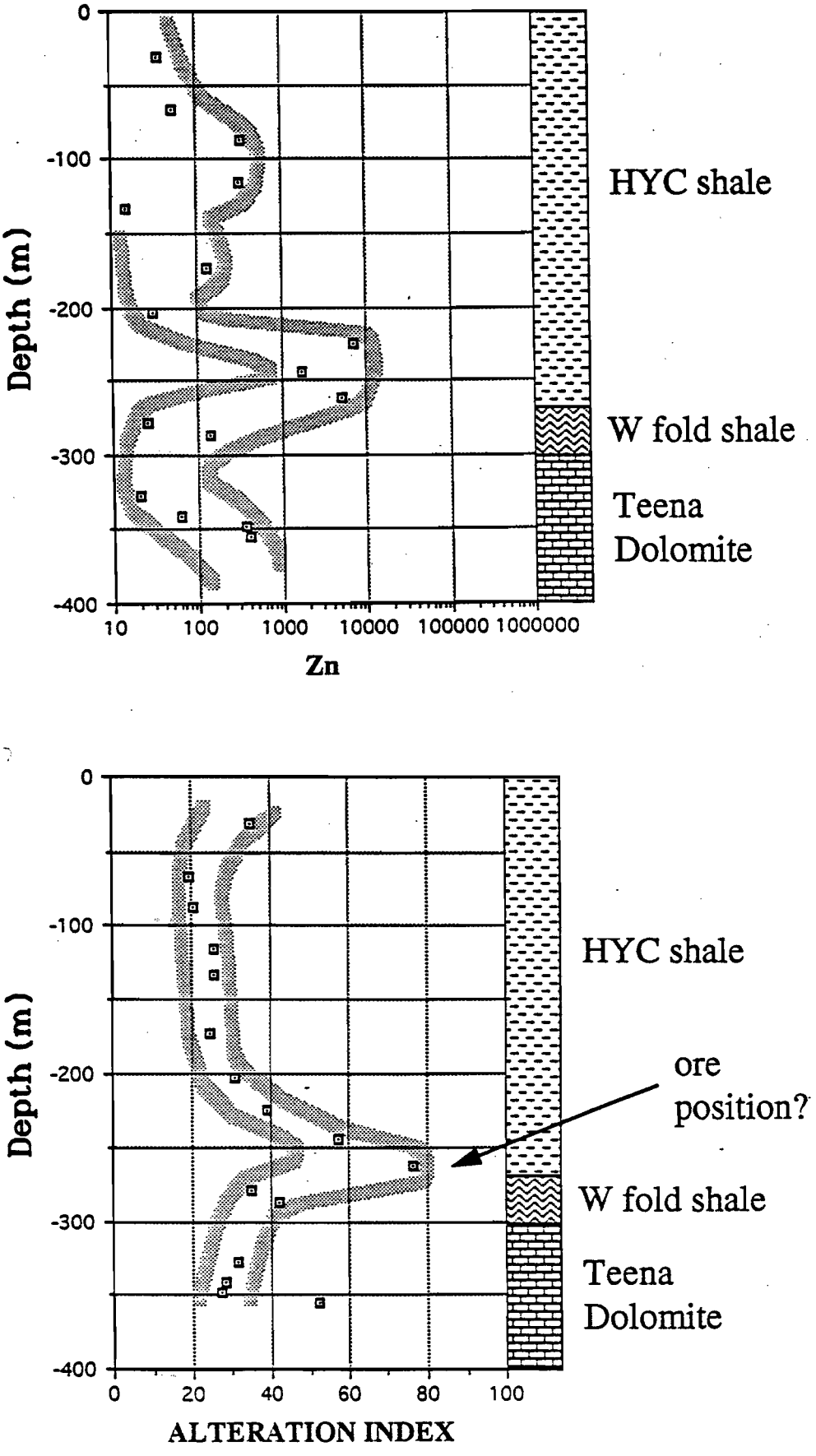

Figure 31 Data from DDH Barney 2: 2.5km west of HYC deposit
a) Zn vs Depth - ore position indicated at ≈ 250m
b) AI vs Depth - distinct anomaly at ore position.

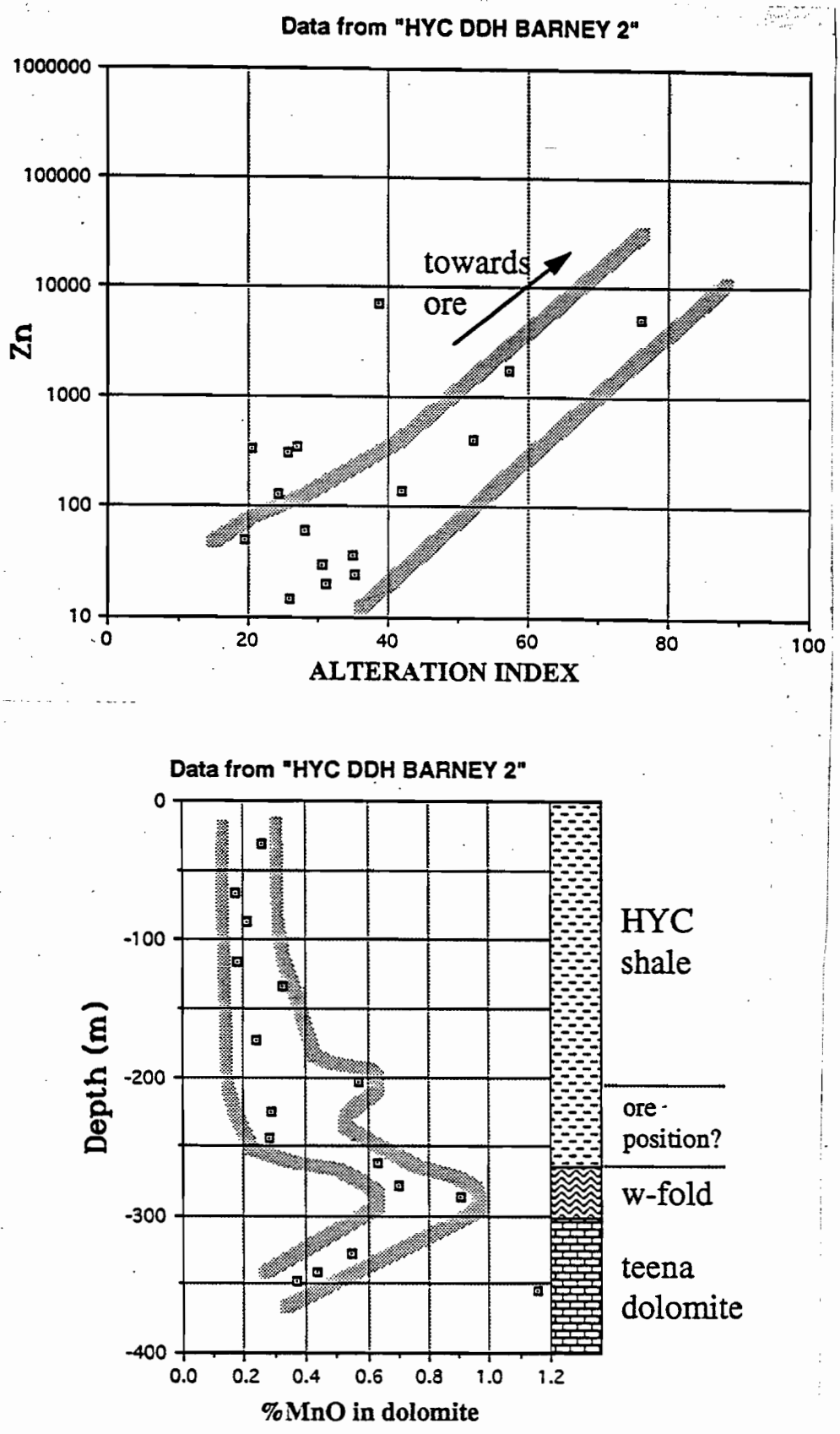

Figure 32 Data from DDH Barney 2: 2.5km west of HYC
a) Zn vs AI - positive trend indicating high potential.
b) MnO_D vs Depth - double anomaly brackets ore position.

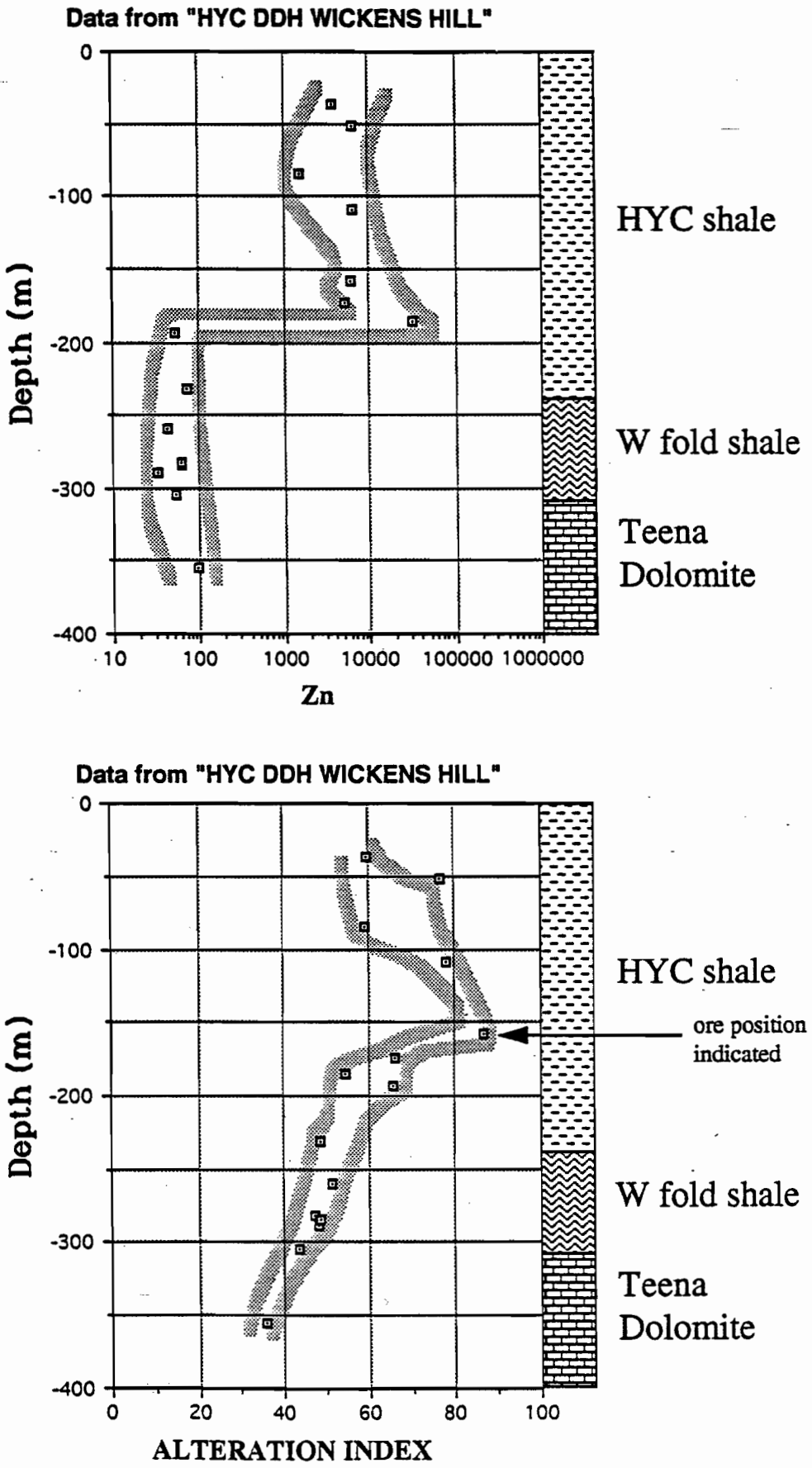

Figure 33 Data from DDH Wickens Hill - 6km west of HYC deposit.
a) Zn vs Depth - anomalous values 0 - 200m.
b) AI vs Depth - potential ore position indicated at ≈ 150m.

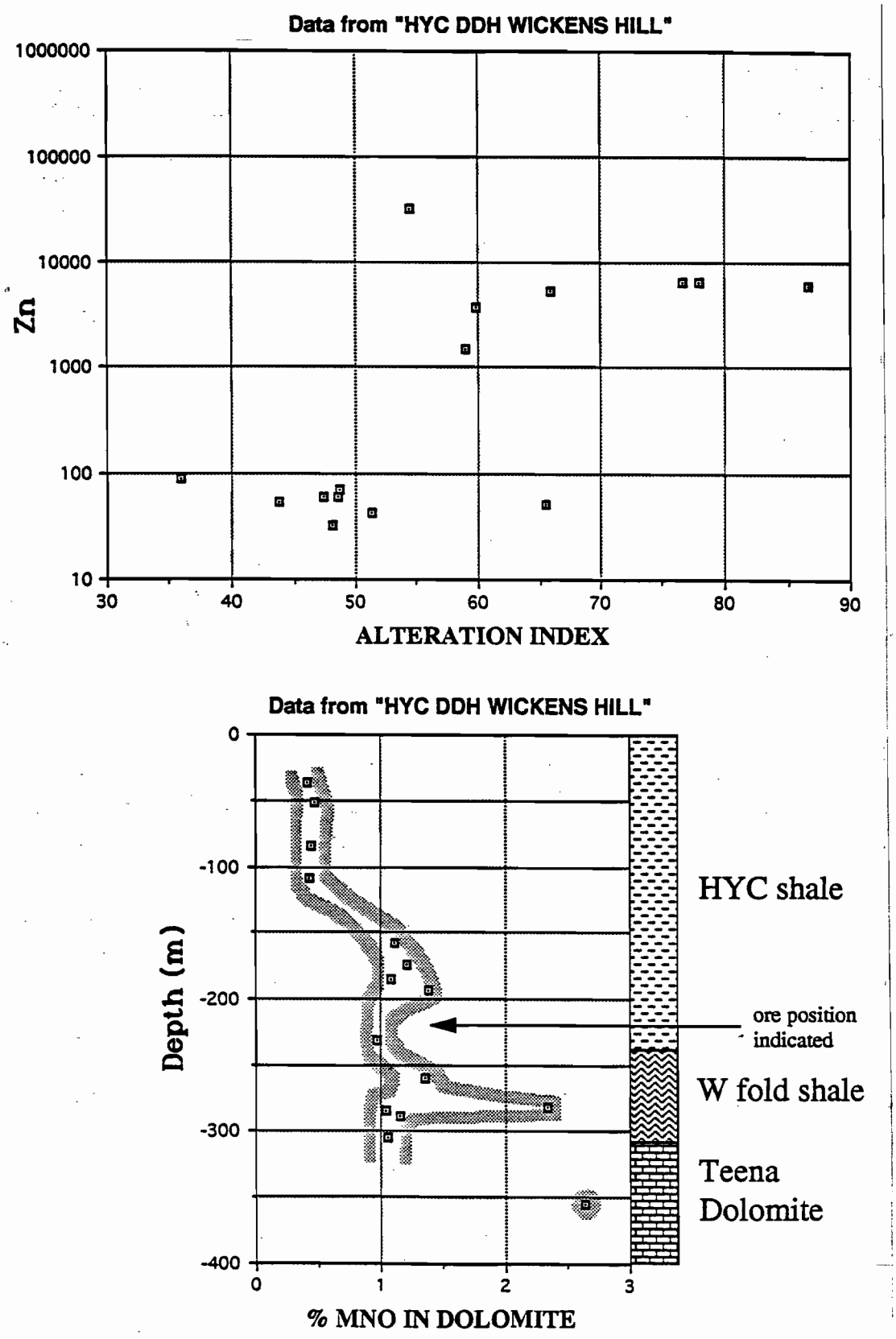

Figure 34 Data from DDH Wickens Hill - 6km west of HYC.
a) Zn vs Al: Anomalous values indicate potential.
b) MnO_D vs Depth: Ore position indicated at ≈ 230m.

Drill holes at greater than 15km from the HYC deposit

DDH BMR 2 - 23km south west of HYC (Fig. 19)
- hole intersects 120m of Barney Creek FW.

Zinc (Fig. 35a): No anomalous values, all samples less than 100ppm.

Alteration Index (Fig. 35b): Two distinct peaks with values over 80, at depths of 18m and 85m down hole indicate the possibility of two favourable horizons for stratiform Pb-Zn. AI vs Zn plot (Fig. 36a) shows a flat trend due to lack of anomalous zinc.

MnO_D (Fig. 36b): A double peak pattern in the upper **and** lower part of the hole support the interpretation of two favourable horizons.

This hole illustrates the importance of determining AI and MnO_D in addition to Zn analyses. Zn by itself would indicate no potential while the AI and MnO_D reveal two horizons worthy of follow-up.

DDH Amelia 1 - 20km south of HYC deposit.
- incomplete sampling makes interpretation difficult.

Zinc (Fig. 37a): no anomalous samples.

Alteration Index (Fig. 37b): two possible favourable horizons are indicated. However, the uppermost horizon has the best AI values and is worthy of follow-up.

MnO_D (Fig. 38a): strongly anomalous values in the upper horizon occur in samples with less than 1% CaO. This data has been excluded from the interpretaiton; however, follow-up sampling is recommended. MnO_D values in the lower horizon are well below background.

DDH Myrtle 1 - 17km south of HYC deposit.

Zinc (Fig. 39a) - erratic anomalous zinc values from 100ppm to 8,000ppm.

Alteration Index (Fig. 39b): generally unfavourable pattern with most values below 60. One spot high at 140m near contact of Teena Dolomite and Mitchell Yard Dolomite.

MnO_D (Fig. 40b): weakly anomalous values of 0.4 - 0.6wt% below 120m.

Results of the hole generally indicate low potential for proximal mineralisation.

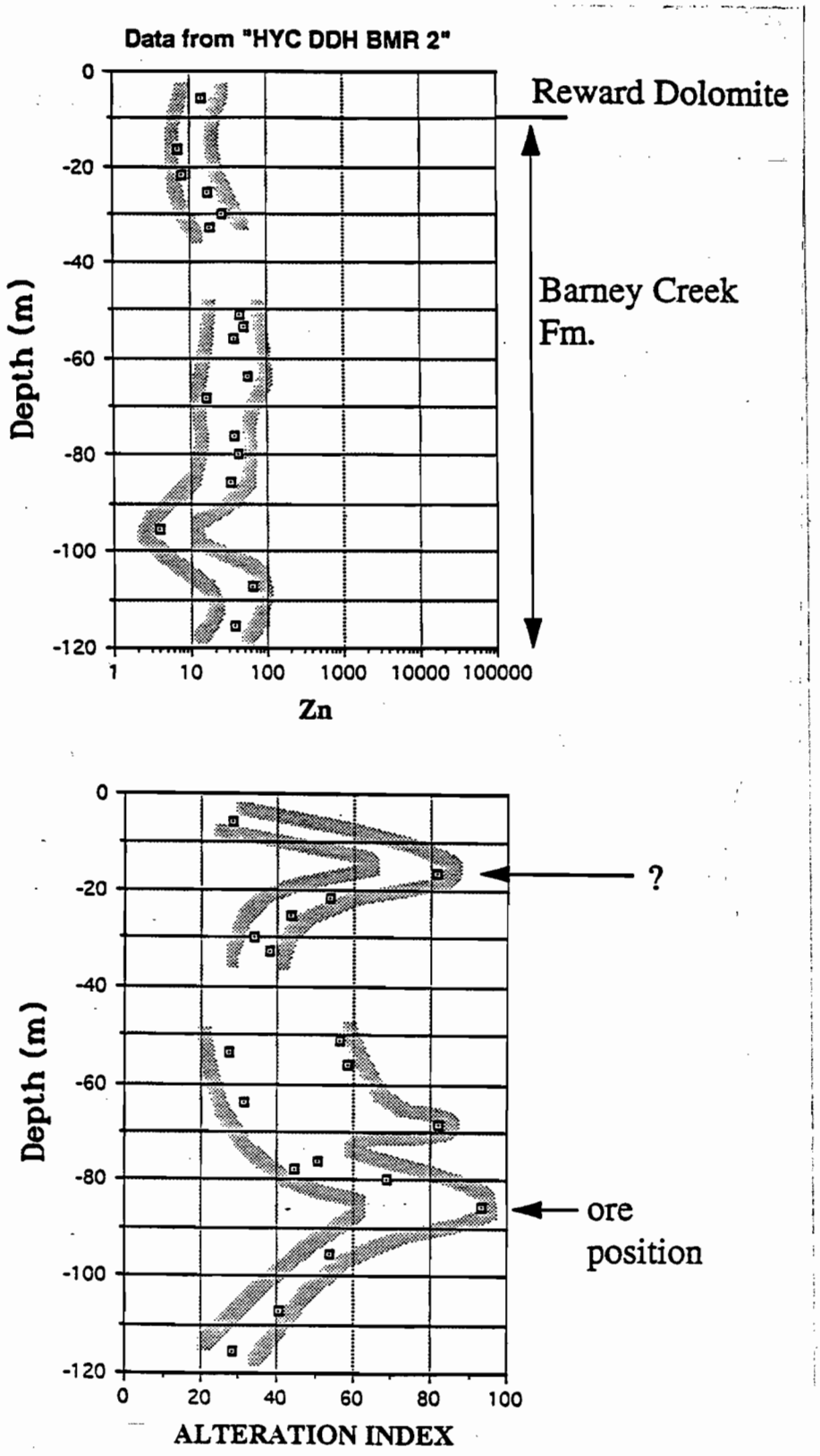

Figure 35 Data from DDH BMR 2: 23km south west of HYC.
a) Zn vs depth: No anomalous zinc values.
b) AI vs depth: Potential ore position indicated by anomaly at 85m. Second possible position at 15m.

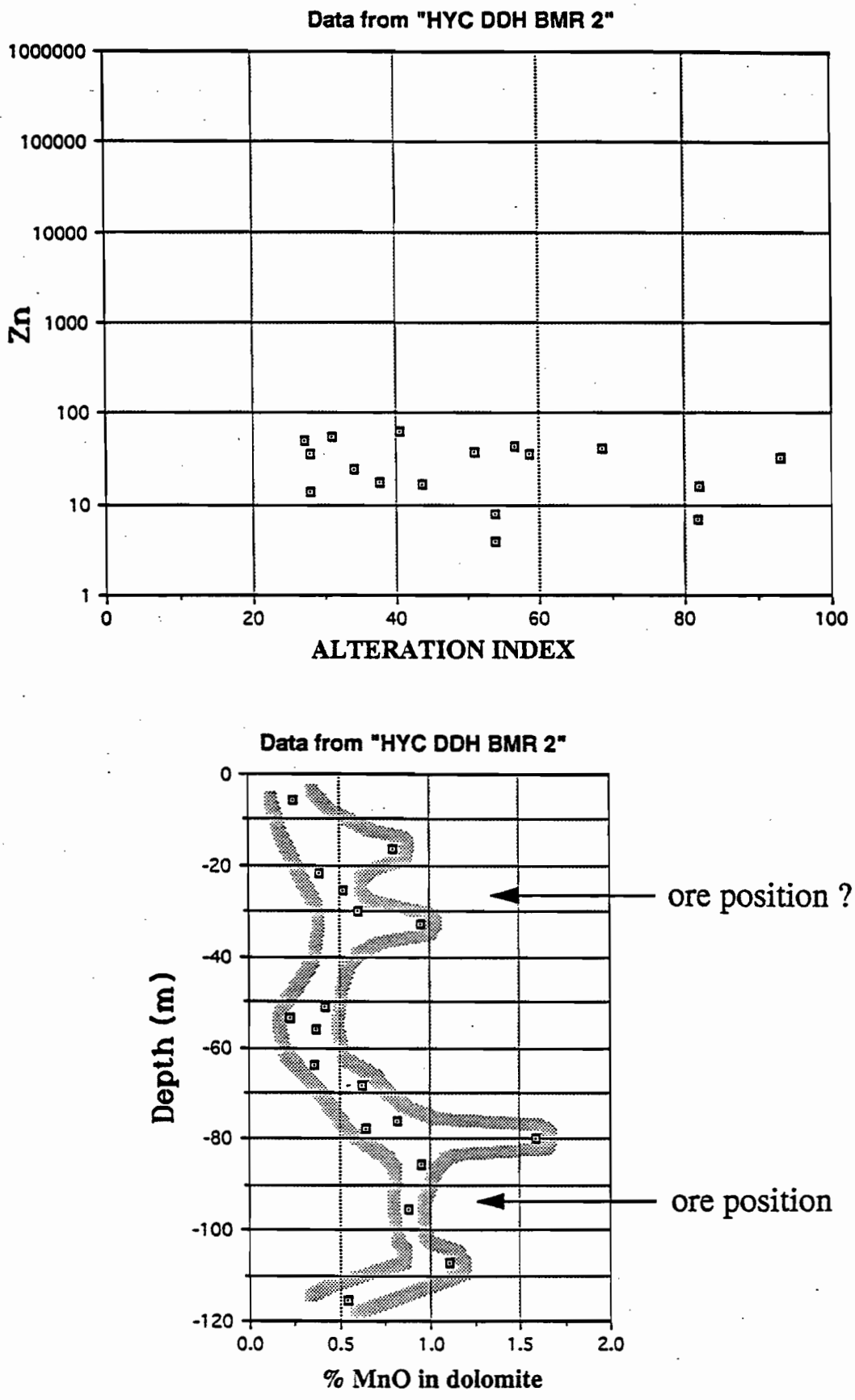

Figure 36 Data from DDH BMR 2: 23km south west of HYC.
a) Zn vs AI: Flat trend due to lack of anomalous zinc.
b) MnO_D vs Depth: two potential ore positions are indicated.

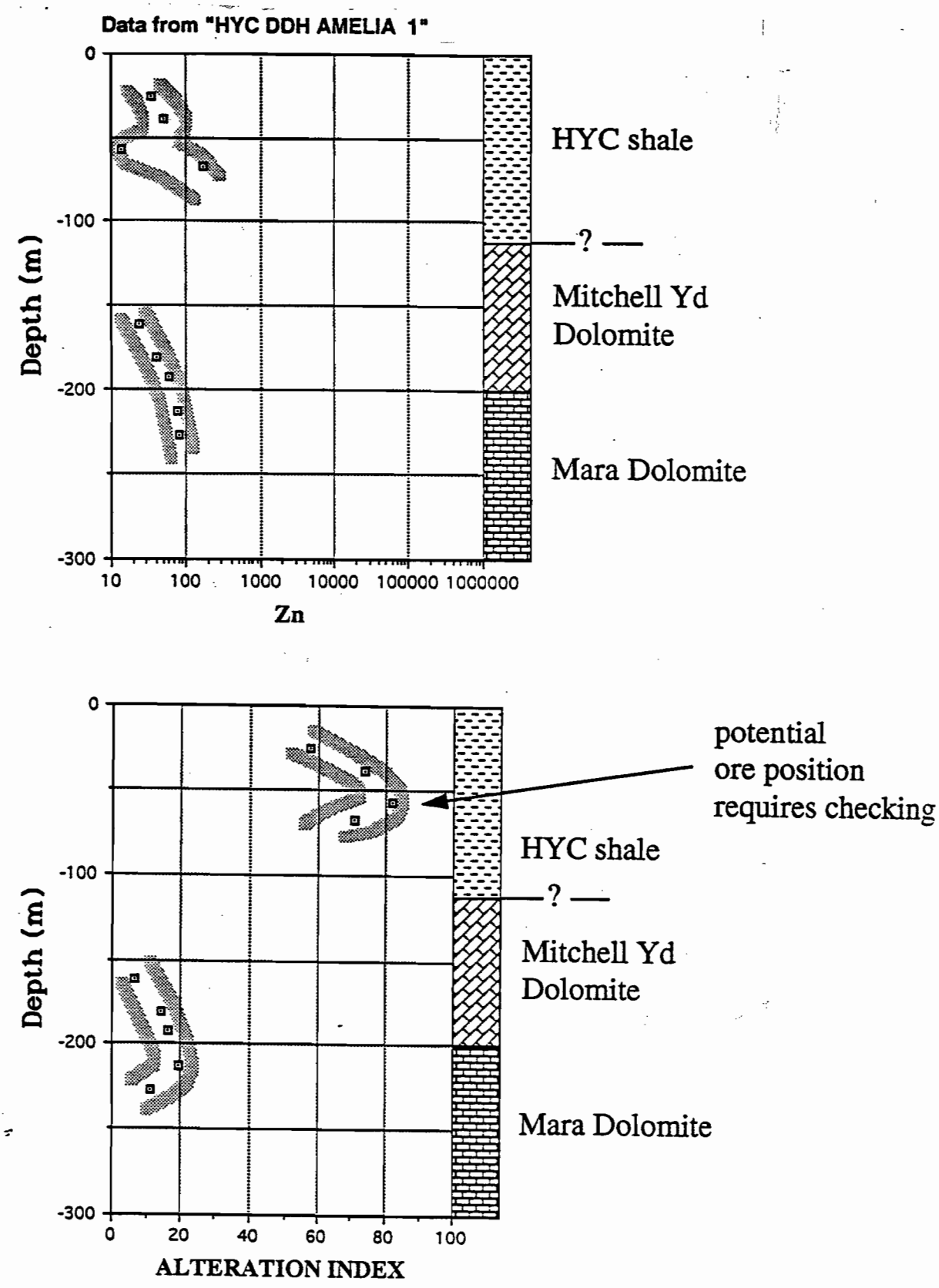

Figure 37 Data from DDH Amelia 1: 20km south of HYC.
a) Zn vs Depth: No anomalous values.
b) AI vs Depth: potential ore position at 50m.

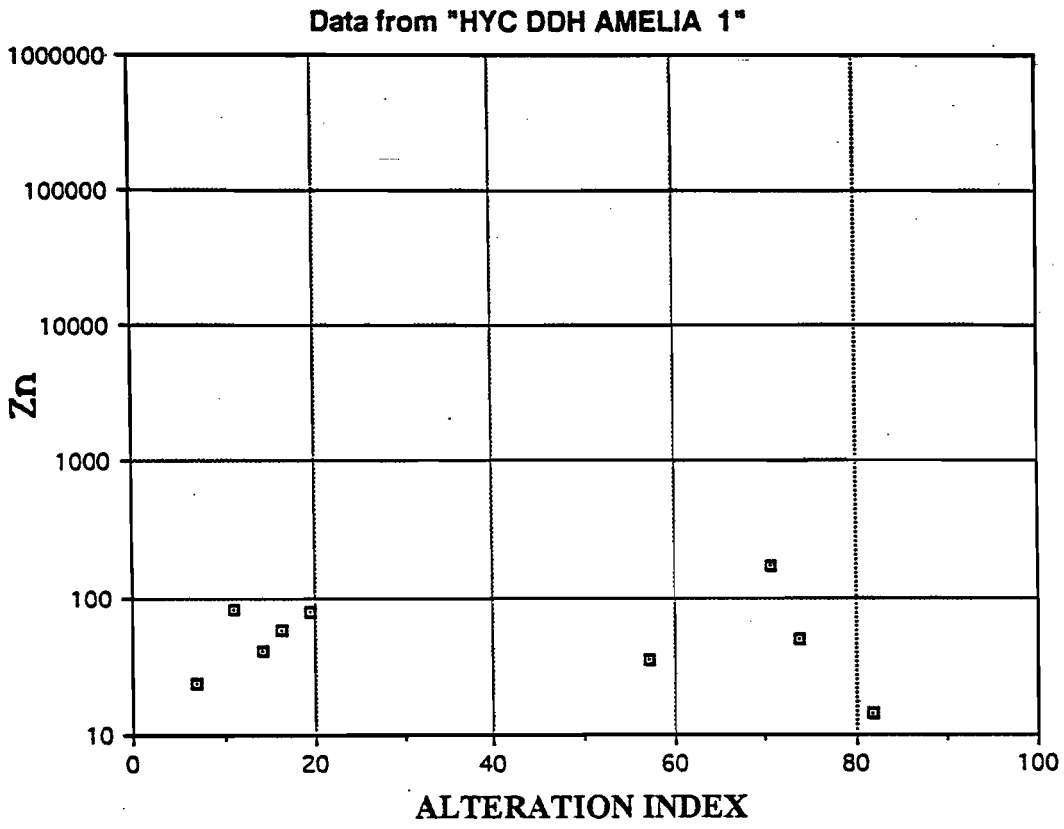

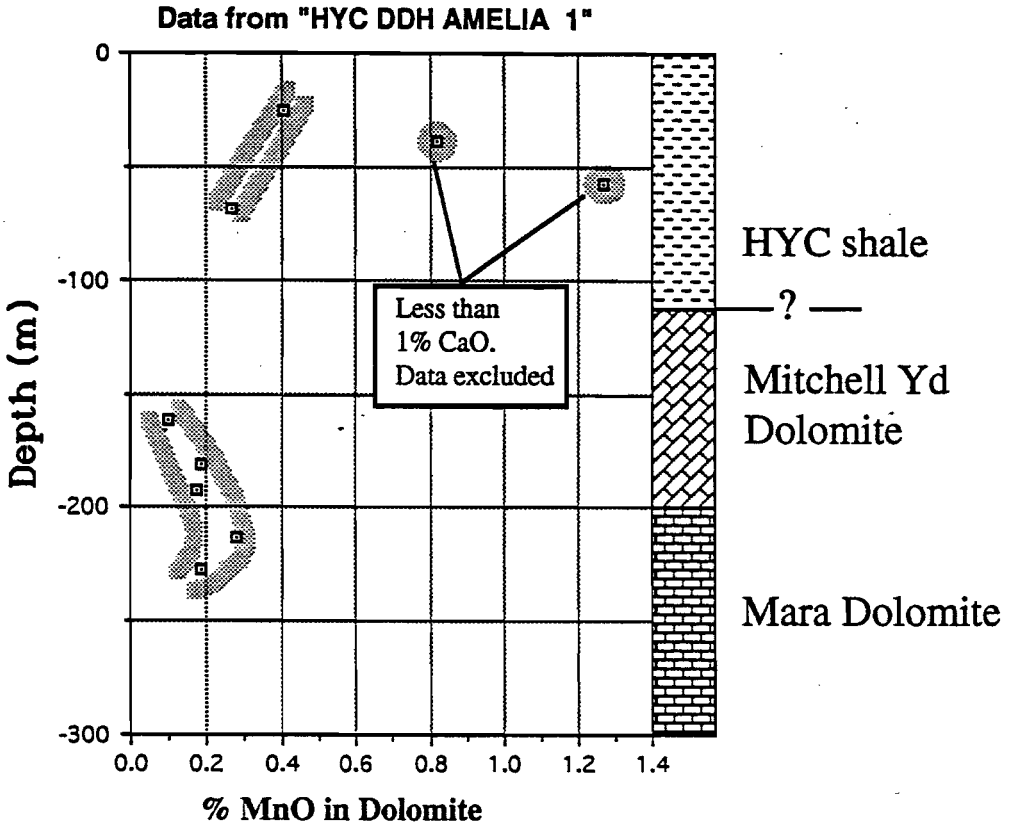

Figure 38 Data from DDH Amelia 1: 20km south of HYC.
a) Zn vs AI - flat trend indicates very distal location.
b) MnO_D vs Depth - data inconclusive due to low CaO contents.

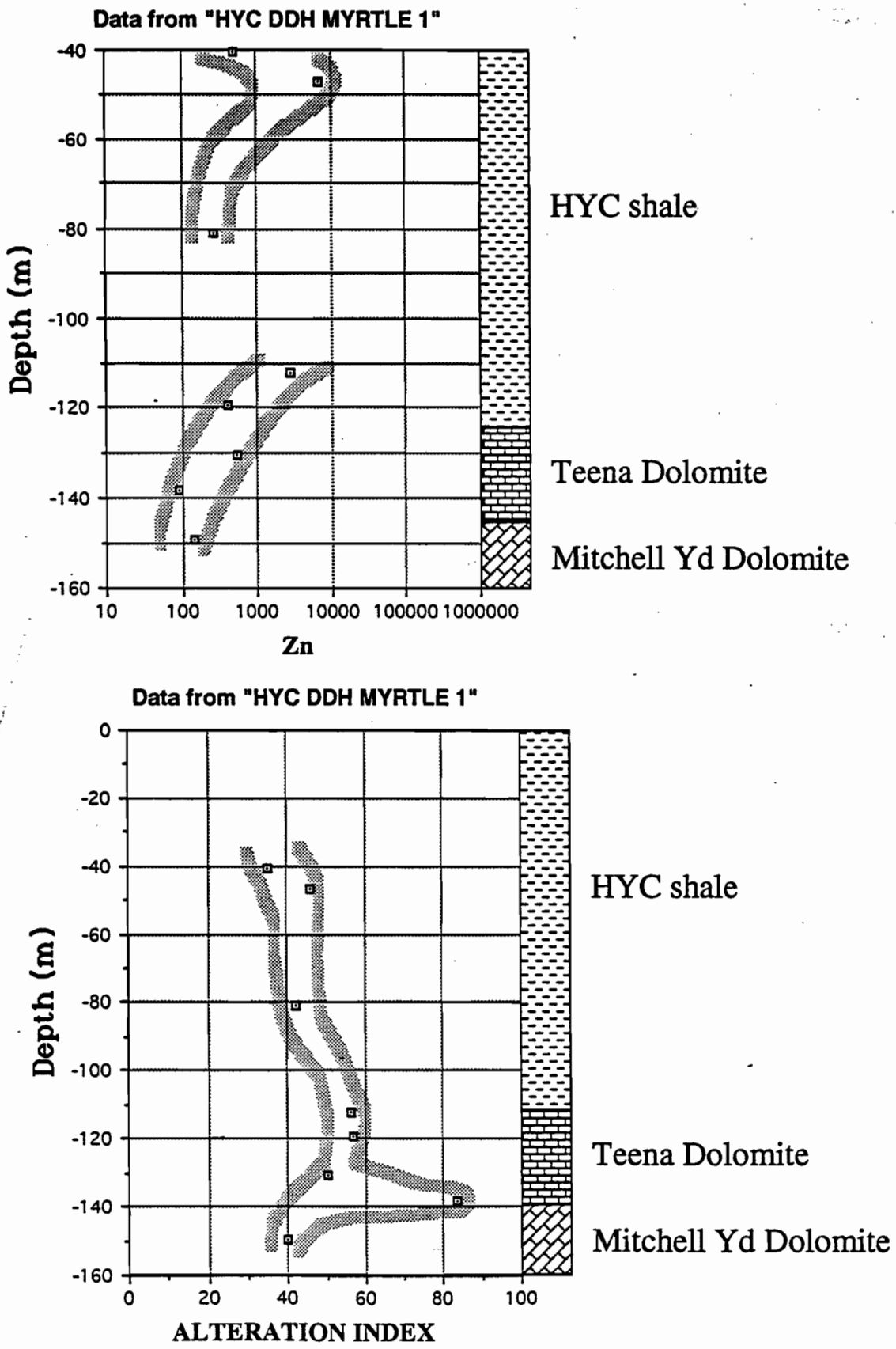

Figure 39 Data from DDH Myrtle 1: 17km south of HYC deposit.
a) Zn vs Depth - some anomalous values.
b) AI vs Depth - one sample anomaly at 140m at base of Teena dolomite.

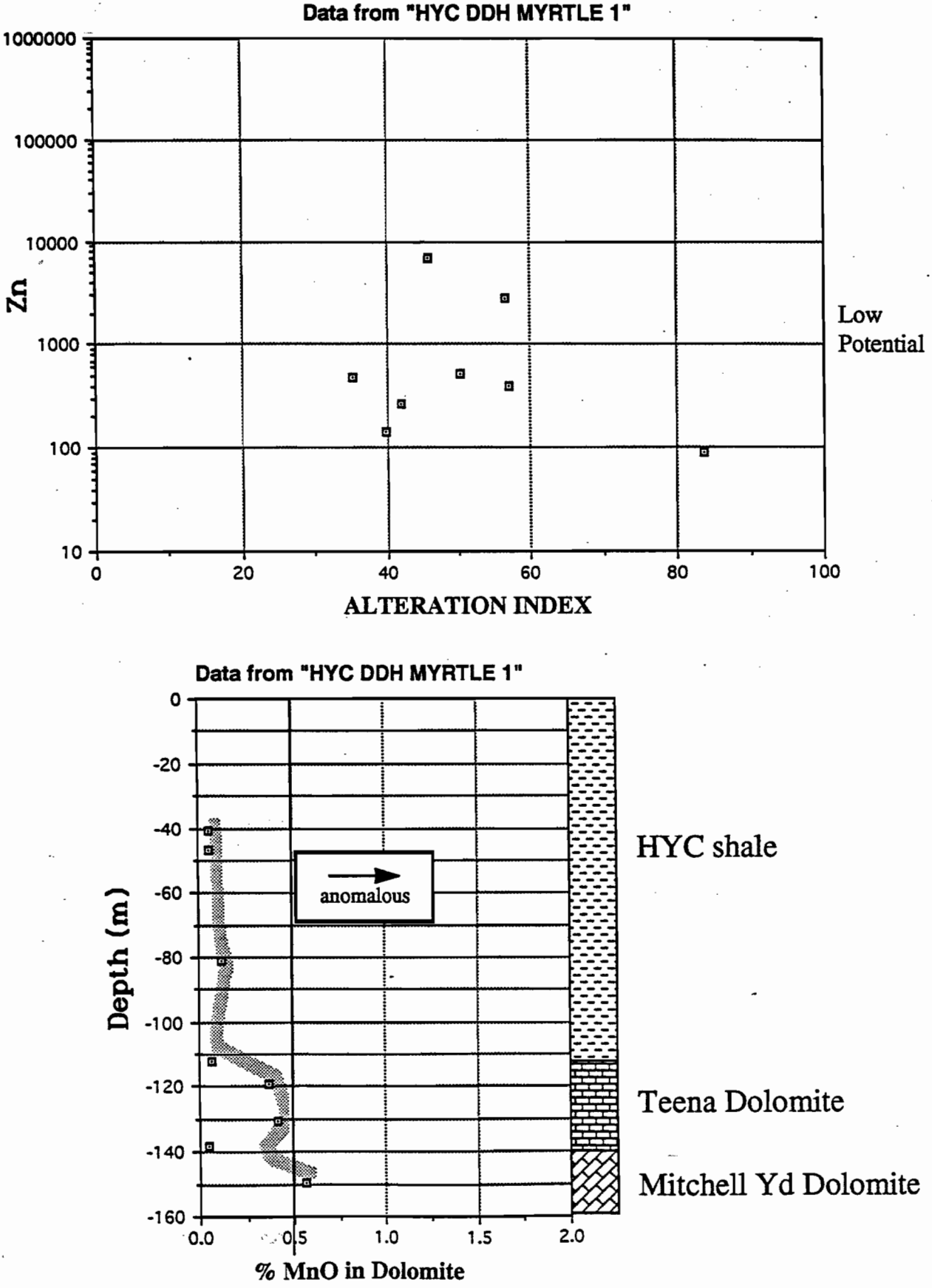

Figure 40 Data from DDH Myrtle 1: 17km south of HYC.
a) Zn vs AI - no distinct trend in data.
b) MnO_D vs Depth - no anomalous samples.

Chemistry of Carbonate Minerals

Data from the four drill holes within and close to mineralisation indicate that dolomite is the only significant carbonate phase at HYC (Fig.23). Unlike Lady Loretta, no siderite development or siderite halo is apparent at HYC. However, studies by other workers (eg Williams 1978, Lambert and Scott, 1973 and Eldridge et. al., 1993) indicate that there is a complex paragenesis of broadly dolomitic carbonate minerals at HYC, with significant variations in Fe, Mn content in both space and time. For example, Eldridge et. al. (1993) reports a relationship between dolomite composition and occurrence of Pb-Zn mineralisation based on electron microprobe analyses of selected minerals, as outline below:

non-mineralised dolomite	$(Ca_{0.50}\ Mg_{0.49})CO_3$
nodular dolomite with weak Pb-Zn	$(Ca_{0.50}\ Mg_{0.41}\ Fe_{0.07}\ Mn_{0.02})\ CO_3$
coarse dolomite with strong Pb-Zn	$(CaO_{0.50}\ Mg_{0.33}\ Fe_{0.15}\ Mn_{0.03})\ CO_3$

Eldridge et.al. (1993) emphasises that all three dolomite types can be found in the same sample, but are related to different parageneses. This indicates that the MnO_D values calculated in this study of HYC represent an average of all dolomite types that may be present in a given sample. However, more importantly the data indicates a direct relationship between the intensity of lead-zinc mineralisation and the MnO content of dolomite, and the likelihood that dolomites with anomalous MnO_D values found 23km away from HYC (eg DDH BMR 2) are related to either the HYC Pb-Zn event or another contemporaneous Pb-Zn orebody in the district.

HYC halo model

Based on the data discussed above, it has been possible to develop a cross-sectional model for element dispersion around the HYC deposit as shown in figure 41. The key features of the model are:

1. Zinc halo - erratic Zn values from 50ppm to 2%Zn, within dolomitic siltstones in a halo up to 300m thick above the central portion of the HYC deposit. Anomalous zinc also extends along the favourable horizon (base of HYC shale) up to 6km from HYC with values around 1,000ppm to 1% Zn. At distances of 17 to 25km the Zn values in the favourable horizon are commonly less than 100ppm with occasional values up to 3,000ppm.

2. MnO halo - manganese enrichment occurs in dolomites in a narrow envelope surrounding the orebody and extending along strata for at least 23km. Best Mn enrichment occurs in the footwall of the ore horizon, where MnO_D values reach a maximum of 12wt% MnO in dolomite. At 20km the MnO_D values decrease to about 1.0wt% MnO (twice background) (Table 1). The Mn halo has a constant thickness of 40-50 in the FW of the ore horizon. The hangingwall MnO_D halo is more variable and thinner.

3. Alteration Index - AI in the Zn halo varies erratically from 10 to 95. In the ore position AI is more consistent and shows anomalous values (>60) to 23km from HYC (Table 1).

TABLE 1 - Summary of halo factors at various distances from the HYC deposit (along the ore horizon)

Factor	Te 115	O 123	Ue 133	Barney 2	Wic.Hill.	Myrtle 1	Amelia 1	BMR 2
Distance from HYC	Orebody	Orebody	30m	2.5km	6km	17km	20km	23km
AI max	99	97	97	77	85	60	82	90
MnO_D Max	12%	7%	3%	0.9%	2.6%	0.7%	1.2%	1.6%
Zn Max	>10%	>10%	2%	0.8%	3%	3000ppm	200ppm	70ppm

Identification of potential ore horizons

In distal locations (>1km) from the ore deposit there is a consistent relationship between AI and MnO_D patterns in drill intersections through the potential ore horizon. These relationships are listed below and summarised in figure 42.

- Alteration Index $\dfrac{100[10MnO + FeO]}{[MgO + Na_2O + 10MnO + FeO]}$ >60

- MnO_D >0.5% may reach up to 2%

- The AI anomaly is bracketed by a double peak MnO_D anomaly (Fig.42)

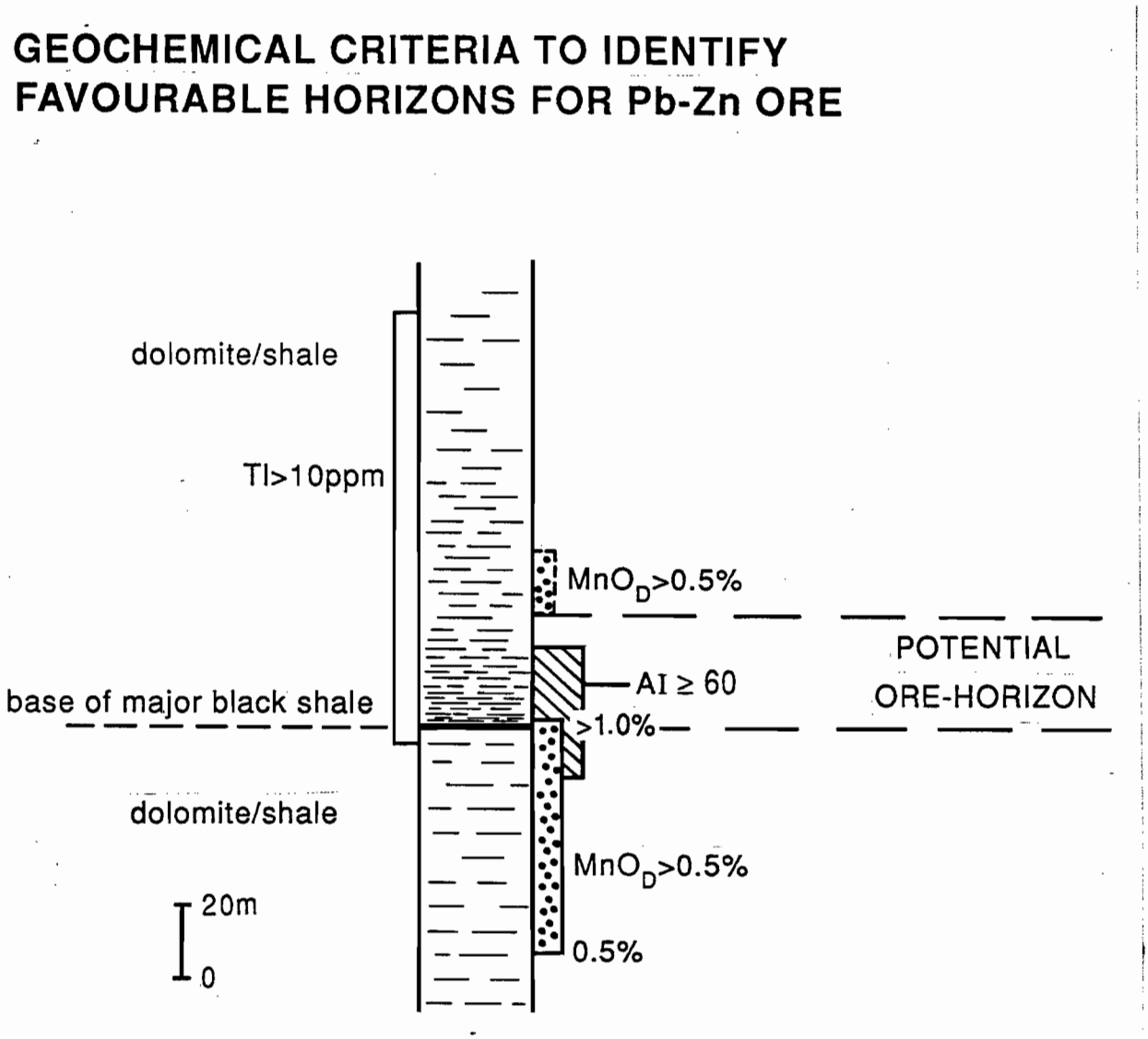

Figure 42 Key lithogeochemical criteria used to identify a potential Pb-Zn ore horizon in the McArthur Basin.

- Tl >10ppm in the ore horizon and hanging wall sediments up to 100m above the ore horizon (McGoldrick et al., in prep — see Appendix 5-I).

- Marked increase in organic carbon content (C org) passing from footwall sediments into the ore horizon. This corresponds to a change from dolomite facies sediments to carbonaceous shale/siltstone facies sediments passing upwards to the ore position.

Vectors towards ore

Based on our analysis of the HYC data set the following vectors towards ore are recommended for use:

- Alteration Index increases 60 to 100 towards ore
  - over 100m across strata
  - over several kms along the favourable horizon

- MnO_D in FW sediments increases systematically towards the favourable horizon (normal to strata) from a background of 0.5% MnO_D up to 1 to 12% MnO_D over about 50m.

- MnO_D in immediate FW halo to favourable horizon increases towards orebody (along strata) from 1.0wt% MnO to over 3wt% MnO over a distance of at least 10km.

- Thallium in hangingwall sediments increases erratically (across strata) from 1ppm to over 100ppm towards the orebody (over 300m) (McGoldrick et al., in prep — see Appendix 5-4).

A NEW APPROACH TO DRILLING FOR SEDEX DEPOSITS

The results outlined in this report indicate the potential to apply lithogeochemistry in the search for giant stratiform Pb-Zn-Ag deposits in an analogous way to the use of stratigraphic drilling and source rock studies in oil exploration. The new approach suggested here involves a two stage drilling program.

a) Lithogeochemical stratigraphic drilling (LSD) of discrete sub-basins to determine the presence or absence of potential horizons for giant Pb-Zn-Ag deposits. One drill-hole through the carbonate-shale facies stratigraphy may be sufficient to test a sub-basin of diameter up to 10km.

   If no horizons with anomalous alteration index (AI), MnO_D or thallium are identified then the sub-basin may be considered barren of giant Pb-Zn-Ag deposits.

b) Lithogeochemical Vector Drilling (LVD). If an horizon or horizons with AI and/or MnO_D and/or thallium are identified in the first LSD drill hole, follow-up drilling at 2km spacings may be used to determine the vector toward ore.

Increasing MnO_D and AI values, coupled with their relationship to sedimentary facies (Fig.42) will provide information on the placement of step-out and in-fill drilling.

Emphasis on lithogeochemistry rather than "preferred stratigraphy"

This exploration approach has the advantage that it enables an assessment of stratiform Pb-Zn mineral potential throughout all carbonate-shale facies successions and not just those successions where deposits occur. The method should be applicable to all stratigraphic levels throughout the Proterozoic that contain carbonate/shale facies sequences. In fact, there is no reason to suspect that this approach cannot be applied to sedimentary basins of all ages from Archaean to Tertiary.

CONCLUSIONS

This geochemical study of the host rocks to the Lady Loretta stratiform lead-zinc deposit indicates considerable dispersion of elements to form a series of nested halos, comprising an inner siderite halo and outer Fe-Mn dolomite halo. Key indicator halo elements are Zn, Pb, Tl, MnO, CaO, MgO and FeO. The data has been used to develop an alteration index related to hydrothermal processes responsible for the Pb-Zn ore-forming event, which provides information on proximity to mineralisation. A second vector toward ore has been developed from the MnO content of the carbonate minerals, dolomite (MnO_D) and siderite (MnO_S). By combining the element dispersion study with the alteration index and $MnO_{D/S}$ factors it has been possible to produce a simple but very powerful halo model which has immediate application to exploration on the Lawn Hill Platform.

A comprehensive set of whole rock geochemical data was available from previous research on the HYC deposit (Lambert and Scott, 1973 and Corbett et.al., 1975). Further analysis of these data has allowed the development of a refined HYC halo model which will have broad application to exploration for stratiform lead-zinc deposits in the McArthur Basin.

RECOMMENDATIONS FOR FURTHER WORK

In order to gain confidence in the application of this lithogeochemical approach to stratiform Pb-Zn exploration generally it will be necessary to answer the following questions:

a) What are the range of background values for the Alteration Index and MnO_D in barren sediments from throughout the McArthur Basin and Lawn Hill platform?

b) What is the variation in AI and MnO_D around sub-economic stratiform deposits such as the Kamarga deposit.

c) Do all stratiform Pb-Zn deposits have AI and MnO_D halos? e.g. Hilton, Walford Creek, Mt. Novit?

d) What control do primary sedimentary facies have on the halo indicator vectors?

e) Is MnO evenly distributed through dolomites in the halo zone, or is there a paragenetic sequence of carbonate deposition or recrystallisation related to diagenesis and hydrothermal alteration?

The following work programme is proposed to further refine and test the halo models.

1) Development of a lithochemical data base for sediments throughout the McArthur Basin and Lawn Hill Platform, in order to evaluate background populations for AI and MnO_D. Initially the AGSO Rockchem data base will be tested. Analysis of surface samples and drill core collected in the past field season will be added to the AGSO data base.

2) Sampling of the Kamarga Dome and Walford Creek drill holes to evaluate halos of AI MnO_D surrounding these deposits.

3) Detailed sedimentary facies analysis and geochemical sampling of McArthur River DDH BMR2 in order to evaluate the relationship between sedimentary facies and halo vectors. Further sampling and logging of other drill holes in the HYC area should be undertaken to develop a comprehensive model for this district.

4) Petrographic, microprobe and thermoluminescence studies of dolomitic siltstones exhibiting anomalous AI and MnO_D to determine the carbonate paragenesis and fluid

history related to hydrothermal alteration and mineralisation within the halo zones to Lady Loretta and HYC.

REFERENCES

Carr, G.R., 1984, Primary geochemical and mineralogical dispersion in the vicinity of the Lady Loretta Zn-Pb-Ag deposit, North Queensland: Journ. Geochem. Expl., V22, p217-238.

Carr, G.R., and Smith, J.W., 1977, A comparative isotopic study of the Lady Loretta zinc-lead-silver deposit: Mineralium Deposita, V12, p105-110.

Corbett, J.A., Lambert, I.B., and Scott, K.M., 1975, Results of analyses of rocks from the McArthur Area, Northern Territory: CSIRO Technical Communication No.57, Minerals Research Laboratories, August 1975.

Derrick, G.M., 1993, Metallogeny of the Mt. Isa Inlier, Part 1: Sediment-hosted Isa-McArthur type Ag-Pb-Zn deposits - Western succession: unpublished report, G.M.Derrick & Associates, January 1993, 65p.

Duhig, N.C., Stolz, A.J., Davidson, G.J., and Large, R.R., 1992, Canbrian microbial and silica gel textures in silica iron exhalites from the Mount Windsor volcanis belt, Australia: their petrography, chemistry, and origin. Econ. Geol., V87, p764-784.

Eldridge, C.S., Williams, N., and Walshe, J.L., 1993, Sulfur isotope variability in sediment-hosted massive sulphide deposits as determined using the ion microprobe SHRIMP:II A study of the HYC deposit at McArthur River, N.T., Australia: Econ. Geol., V88, p1-26.

Ishikawa, Y., Sawaguchi, T., Iwaya, S., and Horiuchi, M., 1976, Delineation of prospecting targets for kuroko deposits based on modes of volcanism of underlying dacite and alteration halos: Mining Geology, V.26, p.105-117 (in Japanese with English abstract).

Lambert, I.B., 1976, The McArthur zinc-lead-silver deposit: features, metallogenesis and comparisons with some other stratiform ores; in Handbook of Strata-bound and Stratiform ore deposits, K.N. Wolf (Ed.), Chapter 12, p.535-585.

Lambert, I.B., and Scott, K.M., 1973, Implications of geochemical investigations of sedimentary rocks within and around the McArthur zinc-lead-silver deposit, Northern Territory: Journ. Geochem. Expl., V2, p307-330.

McGoldrick, P.J., 1993a, Deposit Halos 3. Geology of the Lady Loretta deposit: review, new developments, and implications for ore genesis, CODES AMIRA/ARC Project P384 — Proterozoic sediment-hosted base metal deposits Report No. 3, p1-30.

McGoldrick, P.J., 1993b Deposit Halos 4. Sampling and whole rock analyses for the Lady Loretta deposit, CODES AMIRA/ARC Project P384 — Proterozoic sediment-hosted base metal deposits Report No. 3, p31-62.

McGoldrick, P.J., Smith, R.N. and Keays, R.R., In prep., Giant primary dispersion halos of thallium around northern Australian Proterozoic stratiform sedimentary zinc-lead deposits.

Walker, R.N., Logan, R.G., Binnekamp, J.G., 1977, Recent geological advances concerning the HYC and associated deposits, McArthur River, N.T.; Journ.Geol.Soc.Aust., V24, p365-380.

Williams, N., 1978, Studies of the base metal sulfide deposits at McArthur River, N.T., Australia:1. The Cooley and Ridge deposits: Econ.Geol., V73, p1005-1035.

Appendix 5-I

Primary geochemical and mineralogical dispersion in the vicinity of the Lady Loretta Zn-Pb-Ag deposit, North Queensland

Journ. Geochem. Expl., v22, p217-238.

G.R. Carr

1984

Journal of Geochemical Exploration, 22 (1984) 217—238
Elsevier Science Publishers B.V., Amsterdam — Printed in The Netherlands

PRIMARY GEOCHEMICAL AND MINERALOGICAL DISPERSION IN THE VICINITY OF THE LADY LORETTA Zn-Pb-Ag DEPOSIT, NORTHWEST QUEENSLAND

G.R. CARR*

Department of Geology, University of Wollongong, Wollongong, N.S.W. 2500 (Australia)

(Received September 28, 1983; revised and accepted February 27, 1984)

ABSTRACT

Carr, G.R., 1984. Primary geochemical and mineralogical dispersion in the vicinity of the Lady Loretta Zn-Pb-Ag deposit, northwest Queensland. J. Geochem. Explor., 22: 217—238.

Lady Loretta is a stratiform Zn-Pb-Ag deposit occurring within carbonate- and pyrite-rich argillaceous rocks of the southern part of the Lawn Hill Platform, northwestern Queensland. The deposit consists of a single massive sulphide lens within a steep-sided basinal structure and contains reserves of 8 690 000 tonnes of ore at 18.1% Zn, 6.7% Pb and 110 g t^{-1} Ag.

The proportion of pyrite-rich layers in the host rocks increases progressively from about 2% at 150 m stratigraphically below the ore to > 90% in the top 10 m of the footwall rocks. Hanging-wall rocks contain up to 20% pyrite-rich layers for at least 100 m above the ores. Siderite is the carbonate phase present within the ore and within the host rocks in an aureole that extends from 75 m beneath to 50 m above the ore. Both older and younger rocks are dolomitic. The two carbonate phases do not occur together within unmineralized host rocks although they may coexist within veins. Siderite contains up to 13 mol% $ZnCO_3$ and 32 mol% $MgCO_3$. There is an antipathetic relationship between Zn and Mg, the latter increasing with distance from the ore.

Zinc and, to a lesser extent, Hg, Pb, Ag and Ba show extensive primary dispersion within the host rocks. Within the plane of sedimentation, haloes vary in width from 50 m to 1.5 km and these dispersions are thought to be dependent on the shape of the sedimentary basin floor at the time of exhalative activity. Perpendicular to the sedimentary layering, Zn and Hg show the most extensive primary dispersion with anomalous values extending up to 100 m into the footwall and at least 50 m into the hanging wall.

INTRODUCTION

Lady Loretta is a stratiform Zn-Pb-Ag deposit of Carpentarian age occurring within a sequence of carbonate-rich argillaceous rocks of the Northwest Queensland Province, Australia. It is situated about 115 km north-northwest of Mount Isa at latitude 19°46'S, longitude 139°03'E (Fig. 1). The deposit

*Present address: CSIRO Division of Mineralogy, P.O. Box 136, North Ryde, N.S.W. 2113 (Australia)

0375-6742/84/$03.00

Appendix 5-II

Implications of geochemical investigations of sedimentary rocks within and around the McArthur zinc-lead-silver deposit, Northern Territory

Journ. Geochem. Expl., v2, p307-330.

I.B. Lambert and K.M. Scott

1973

Journal of Geochemical Exploration, 2 (1973) 307–330

IMPLICATIONS OF GEOCHEMICAL INVESTIGATIONS OF SEDIMENTARY ROCKS WITHIN AND AROUND THE McARTHUR ZINC–LEAD–SILVER DEPOSIT, NORTHERN TERRITORY

I.B. LAMBERT and K.M. SCOTT

Baas Becking Laboratory, Division of Mineralogy, C.S.I.R.O. and Bureau of Mineral Resources, Canberra, A.C.T. (Australia)
Division of Mineralogy, C.S.I.R.O., North Ryde, N.S.W. (Australia)

(Accepted for publication September 21, 1973)

ABSTRACT

Lambert, I.B. and Scott, K.M., 1973. Implications of geochemical investigations of sedimentary rocks within and around the McArthur zinc–lead–silver deposit, Northern Territory. *J. Geochem. Explor.*, 2: 307–330.

The McArthur Zn–Pb–Ag deposit occurs within a belt of Middle Proterozoic sediments which extends discontinuously from the northwest of Queensland to the north of the Northern Territory. The similar Mount Isa and Hilton deposits, as well as many smaller orebodies, occur in the same belt, and there is every reason to believe that the full mineral potential of this region is far from realized at the present time.

The McArthur deposit is effectively unmetamorphosed and has undergone a minimum of structural deformation. Therefore, it presents an ideal opportunity for investigating the genesis of this kind of stratiform ore, and establishing guidelines for prospecting for other such deposits. With these aims in mind, we analysed a large number of drill core samples of sediments from within and around the McArthur deposit, and assessed these data in the light of salient geological features.

We conclude that favourable areas for locating deposits of this type should contain all of the following features: (1) pyritic, high-potash, carbonaceous shales which have Zn contents of around 0.5% or more, and significant Pb, As and Hg anomalies; (2) dolomites with moderate to high Fe and Mn contents; (3) vitroclastic tuffite bands.

Detailed investigations in suitable areas should concentrate on the basal parts of thick carbonaceous shale sequences, proximal to major fault zones.

INTRODUCTION

The stratiform McArthur zinc–lead–silver deposit (Fig.1) (also known as the H.Y.C. deposit) is situated in the northeastern corner of the Northern Territory, at lat. 16°26′S, long. 136°5′E. It consists of thin, closely-spaced sulphide bands which are conformable within unmetamorphosed, bituminous shales of Middle Proterozoic (Carpentarian) age. It is an extremely large deposit, but its development has been hampered to date by the fine-grained nature of the ore.

The geology of the McArthur areas has been discussed by Cotton (1965), and more

Appendix 5-III

Results of analyses of rocks from the McArthur Area, Northern Territory: CSIRO Technical Communication No.57, Minerals Research Laboratories, August 1975.

J.A. Corbett, I.B. Lambert and K.M. Scott

1975

CODES: AMIRA/ARC Project P384 — Proterozoic sediment-hosted base metal deposits. October 1993

TECHNICAL COMMUNICATION 57

RESULTS OF ANALYSES OF ROCKS FROM

THE McARTHUR AREA, NORTHERN TERRITORY

J. A. CORBETT, I. B. LAMBERT and K. M. SCOTT

CSIRO Division of Mineralogy
P.O. Box 136
North Ryde, N.S.W.
Australia, 2113

AUGUST, 1975

TABLE OF CONTENTS

LIST OF TABLES

LIST OF FIGURES

1. INTRODUCTION

This report tabulates the analytical results of a geochemical investigation of rocks from within and around the McArthur zinc-lead-silver deposit. It supplements the papers by Lambert and Scott[1,2] and Scott and Lambert[3] which summarized features of these results and discussed their implications for ore genesis and exploration.

Samples were selected from the ten diamond drill holes, some of which are shown in Fig. 1 and some in Fig. 2. With the exception of BMR 1, which penetrated an up-faulted block of Tawallah Group (?) shales and intrusive dolerite, each of the drill holes penetrated the H.Y.C. Pyritic Shale Member* and the more dolomitic strata which underlie this ore-bearing unit (see Table 1).

2. ANALYTICAL METHODS

In all but the mineralized samples, Al, Ca, Fe, K, Mg, Mn, P, Si and Ti, were determined by X-ray fluorescence spectrometry (XRF) after fusion with lithium tetraborate. Samples containing greater than 10% S were analysed for the major elements (except P and Ti) and Cu, Pb, Sb and Zn by atomic absorption spectrometry (AAS) after a sodium peroxide sinter[4]; Arsenic was determined spectrophotometrically on the solution from this sinter.

Cr, Na and low levels of Cu, Pb and Zn were determined by AAS after dissolution with $HCl/HNO_3/HClO_4$, and Li and Sr from the same solution by flame emission spectrometry. Some Ag determinations were also done by AAS after HNO_3 dissolution and spraying in an ammonical solution.

Rb in samples from Barney 2 and BMR 2 was determined by XRF on pressed powders.

Gravimetric methods were used to determine S, H_2O^+ and H_2O^-. Organic carbon and inorganic CO_2 were calculated, after determining the total carbon and the carbon remaining after a dilute HCl acid treatment, using a "Leco" carbon analyser[5].

The above determinations were performed at the laboratories of the Division of Mineralogy, North Ryde.

Pressed powders of samples from diamond drill hole Te 115 were analysed by XRF at the laboratories of the Bureau of Mineral Resources,

---

* Hereafter referred to as HYC Pyritic Shale or HYC Shale.

Canberra, for U, Th, Rb and Sr. The Australian Mineral Development Laboratories, Adelaide, analysed a small number of samples for Hg using a flameless AAS technique and for Se using a spectrophotometric method.

With the exception of samples from Te 115, B, Ba, Bi, Cd, Co, Ga, Ge, La, Mo, Ni, Sc, Sn, Tl, V and Zr were determined semi-quantitatively by optical emission spectroscopy at the Division of Mineralogy. Where Tennant's technique[6] was used, values obtained with respect to the lower limit of detection are quoted. Samples from Te 115 were analysed for Ba, Co, Cr, Ni, Sc, V, Y and Zr by direct reading optical emission spectroscopy at the Bureau of Mineral Resources.

3. RESULTS

The chemical data for the major drill holes are listed in Tables 2 to 11 and miscellaneous samples are included in Table 12.

The data have been summarized in Tables 13 to 16 by presenting average compositions for the various rock types within the ore basin and outside it. The two shale members of the Barney Creek Formation, namely the HYC Pyritic Shale and W-fold Shale Members (see Table 1), have been subdivided into the following groups: mineralized samples; shales; carbonates; and siliceous samples. Samples with 4 to 20% S were considered moderately mineralized and those with greater than 20% S as highly mineralized. Samples considered as siliceous were those containing more than 60% SiO_2 and these, in general, represent the sediments with the greatest tuffaceous component. Shales have been defined as having less than 60% SiO_2 and less than 20% CO_2 and were further subdivided into three groups on the basis of their distribution about the economic mineralization. Samples with greater than 20% CO_2 were considered as carbonates.

All the analysed samples of the Cooley Dolomite Member were found to be carbonates by the above definition, but the stratigraphically lower Teena Dolomite contains a significant proportion of shales. The few samples analysed from the Myrtle Shale Member are all shales.

The arithmetic averages are presented in Tables 13 to 16 with those values quoted in parenthesis being of limited usefulness as they were calculated from relatively few analyses. Where the mean is distorted by anomalous analyses, the median value is quoted in italics.

4. ACKNOWLEDGMENTS

We are grateful to Carpentaria Exploration Company for permission to undertake this investigation and for discussions of the geology of the McArthur area. Dr M.C. Brown is also thanked for providing samples from Te 115, Ie 115 and Ue 133. The Bureau of Mineral Resources drilled holes BMR 1 and BMR 2.

5. REFERENCES

1. Lambert, I.B. and Scott, K.M. - Implications of geochemical investigations of sedimentary rocks within and around the McArthur zinc-lead-silver deposit, Northern Territory. *J. Geochem. Explor.*, 1973, 2, 307-330.

2. Lambert, I.B. and Scott, K.M. - Carbon contents of sedimentary rocks within and around the McArthur zinc-lead-silver deposit. *J. Geochem. Explor.*, 1975, 4 (3), 365-369.

3. Scott, K.M. and Lambert, I.B. - Geochemistry and mineralogy of the rocks about the McArthur deposit, Northern Territory. (In preparation).

4. Corbett, J.A., Godbeer, W.C. and Watson, N.C. - The application of sodium peroxide sintering techniques to analysis of minerals and rocks by atomic absorption spectroscopy. *Proc. Australas. Inst. Min. Metall.*, 1974, No.250, 51-54.

5. Corbett, J.A. and Mizon, K. - The determination of carbon in materials containing high concentrations of sulphur. (In preparation).

6. Tennant, W.C. - General spectrographic technique for the determination of volatile trace elements in silicates. *Appl. Spect.*, 1967, 21, 282-285.

TABLE 1. GENERALIZED STRATIGRAPHIC SUCCESSION IN THE McARTHUR AREA

System	Group	Subgroup	Formation	Member	Main rock types	
Carpentarian (Middle Proterozoic)	McArthur	Umbolooga	Reward Dolomite		Cherty dololutite, intraclast and pelletal dolarenite, dolomitic shale, coarse-graded arenites and breccia beds, tuffites	
			Barney Creek Formation	HYC Pyritic Shale (Cooley Dolomite)	Carbonaceous, dolomitic, tuffaceous shales and siltstones; pyrite, sphalerite-galena; carbonate-rich arenite and breccia interbeds, tuffites	Brecciated dolomite, minor carbonaceous shale, non-stratiform Pb-Zn(-Cu) mineralization
				W-fold Shale	Tuffaceous, dolomitic shales and siltstones	
			Teena Dolomite	Coxco Dolomite	Thin bedded dololutites with frequent thin interbeds of shales, tuffites	
					Cherty dololutites, intraclast dolarenites and flake breccias, rare halite casts	
			Emmerugga Dolomite	Mitchell Yard Dolomite	Dololutite, intraclast dolomite flake breccias, tuffites	
				Mara Dolomite	Cherty dololutite, dololutite, intraclast dolomite flake breccias and dolarenites, halite casts, tuffites	
			Tooganinie Formation	Myrtle Shale	Red dolomitic siltstone, dololutite, halite casts	
				Leila Sandstone	Dolomitic sandstones, siltstones	
			Tatoola Sandstone		Quartz and dolomitic arenites and sandstones	
			Amelia Dolomite		Dolomitic arenites and siltstones, cherts	
			Mallapunyah Formation		Dolomitic arenites and siltstones, cherts	
	Tawallah				Sandstones, siltstones, conglomerates, minor basic and felsic volcanics	

TABLES 2 - 16

Note:

–	not determined
nx	not detected at x ppm
≤ x	(for emission spectroscopic results) line seen but less than or equal to lowest standard (x ppm)

Because the matrix of the samples is variable, the limit of detection is variable and hence for one sample a value may be obtained which is lower than the limit of detection for another.

TABLE 2. ANALYSIS OF SAMPLES FROM DRILL HOLE Te 115

(Major components in wt %; minor components in ppm)

Sample No.	35149	35148	35147	35146	35145	35151	35144	35143	35142	35141
Depth (m)	34.2	35.7	43.3	51.9	53.1	57.0	66.2	80.5	87.5	95.2
SiO_2	49.5	71.6	42.6	42.3	27.2	51.1	32.1	25.0	27.4	32.1
Al_2O_3	10.2	9.32	15.8	8.86	3.53	12.3	4.86	5.18	5.25	6.99
FeO	5.06	2.16	2.56	15.4	3.63	4.75	12.5	29.8	27.4	24.7
MgO	5.84	1.75	1.69	3.70	13.5	5.25	7.43	2.77	2.64	2.31
CaO	8.40	2.88	0.31	4.77	20.6	6.67	12.6	3.36	3.48	2.11
Na_2O	0.12	2.45	0.72	0.14	0.11	0.26	0.05	0.53	0.17	0.19
K_2O	4.41	2.72	7.88	4.00	1.91	5.35	3.63	2.29	2.30	2.80
TiO_2	0.43	0.20	0.28	0.47	0.17	0.66	–	–	–	–
P_2O_5	0.14	0.06	0.05	0.12	0.09	0.19	–	–	–	–
MnO	0.11	0.07	0.01	0.08	0.16	0.08	0.13	0.05	0.05	0.03
CO_2	12.4	1.10	1.10	6.60	31.0	2.46	16.3	4.76	2.31	2.60
S	2.19	0.89	0.24	11.9	1.73	1.76	9.33	24.5	23.5	21.3
C (org)	0.64	0.20	0.06	0.30	0.28	0.43	0.25	0.26	0.46	0.48
As	65	75	50	680	225	65	430	650	870	750
Ba	500	760	1150	500	170	–	210	250	230	290
Co	17	23	19	45	19	–	35	60	80	64
Cr	70	28	n10	220	28	–	82	115	130	130
Cu	n100	<100	<100	<100	→	→	→	100	100	100
Hg(ppb)	–	50	–	–	–	–	–	–	–	–
Li	57	24	55	51	16	73	35	36	37	47
Ni	31	19	n10	50	14	–	27	50	45	42
Pb	71	38	18	860	88	–	1600	1790	4830	1940
Rb	187	66	265	167	49	–	84	78	82	121
Sb	n5	<5	→	→	→	→	→	→	→	→
Sc	13	9	7	17	9	–	10	14	12	10
Se	–	n2	–	–	–	–	–	–	–	–
Sr	41	21	14	30	33	–	28	17	15	17
Th	17	21	42	10	6	–	6	8	8	8
U	4	4	10	4	2	–	2	2	7	2
V	130	46	n10	100	41	–	58	52	73	73
Y	32	36	29	52	17	–	23	27	27	27
Zn	600	n100	n100	1800	400	200	5100	9400	14,600	16,80
Zr	190	150	370	230	n100	–	n100	100	130	150
	←	←	←	HYC	Shale	→	→	→	→	→

Table 2 cont.

Sample No.	35140	35139	35138	35137	35136	35135	35134	35133	35132	35131
Depth (m)	107.4	122.0	124.4	132.4	141.8	151.3	158.9	162.3	178.1	186.1
SiO_2	39.7	33.1	21.4	30.8	31.1	36.4	45.9	45.8	39.7	34.8
Al_2O_3	7.37	3.89	3.95	6.71	4.61	1.97	6.03	8.61	8.79	6.81
FeO	3.01	4.98	22.1	17.2	31.0	3.82	6.75	3.78	14.67	22.5
MgO	10.7	11.6	6.70	6.10	2.37	10.7	6.06	6.68	3.69	3.14
CaO	14.0	17.5	9.30	8.34	2.96	18.2	10.3	10.6	5.38	4.94
Na_2O	0.18	0.17	0.14	0.22	0.12	0.09	0.03	0.07	0.11	0.07
K_2O	3.03	1.61	1.42	2.36	1.62	0.80	2.47	3.79	3.66	3.05
TiO_2	0.32	0.10	-	-	0.21	0.08	0.23	0.35	0.36	0.31
P_2O_5	0.14	0.11	-	-	0.12	0.32	0.24	0.35	0.17	0.27
MnO	0.14	0.16	0.12	0.13	0.08	0.17	0.17	0.12	0.09	0.08
CO_2	19.9	25.8	11.8	12.3	2.67	32.8	15.8	12.0	7.70	6.30
S	0.67	2.54	18.2	13.3	25.7	1.32	4.21	1.35	11.7	18.0
C (org)	0.49	0.20	0.35	0.48	0.22	0.33	2.35	3.58	1.63	3.22
As	240	520	430	410	950	30	140	80	330	450
Ba	250	150	150	250	160	100	320	320	330	390
Co	23	25	42	27	36	25	18	110	29	21
Cr	49	18	82	92	125	18	30	47	38	185
Cu	n100	→				100	n100	→		
Hg (ppb)	80	-	-	-	-	-	80	-	350	300
Li	47	24	37	45	40	16	27	49	41	33
Ni	13	17	33	34	45	10	19	19	42	88
Pb	67	424	2580	5860	1000	265	335	192	650	835
Rb	122	53	60	108	70	32	100	135	160	124
Sb	n5	→		8	n5	→				
Sc	9	9	10	10	9	7	9	11	10	12
Se	n2	-	-	-	-	-	n2	-	n2	n2
Sr	34	32	16	32	15	39	24	38	37	29
Th	13	5	3	10	2	2	9	9	11	11
U	3	n1	n1	5	n1	2	7	9	9	12
V	73	30	46	60	39	24	44	76	58	84
Y	21	17	27	21	19	17	18	18	23	22
Zn	100	1800	7900	4400	9400	1600	5300	800	500	7700
Zr	n100	→		110	100	n100	→		100	150
	←			HYC	Shale					→

Table 2 cont.

Sample No.	35130	35129	35128	35127	35126	35125	35124	35123	35122	35121
Depth (m)	198.6	206.5	214.7	218.4	222.3	230.6	245.2	250.7	263.5	272.7
SiO_2	42.9	44.6	43.1	42.7	48.4	29.9	17.1	82.5	28.5	7.10
Al_2O_3	7.29	9.06	8.95	5.85	11.6	5.28	2.93	8.78	7.00	1.00
FeO	3.95	6.54	12.9	2.86	6.81	19.3	21.7	0.73	32.2	38.6
MgO	8.91	6.26	4.15	9.00	5.21	6.18	9.07	0.39	1.12	0.51
CaO	13.2	9.57	6.03	14.3	6.50	9.69	14.5	< 0.10	0.86	0.88
Na_2O	0.09	0.13	0.13	0.06	0.10	0.06	0.04	0.09	0.07	0.01
K_2O	3.32	3.99	4.15	3.14	5.13	2.75	1.66	6.08	4.43	0.77
TiO_2	0.30	0.38	0.38	0.21	0.43	0.21	0.10	0.30	0.34	-
P_2O_5	0.21	0.23	0.24	0.09	0.22	0.14	0.08	0.05	0.16	-
MnO	0.13	0.09	0.08	0.22	0.14	0.32	0.41	< 0.01	0.06	0.12
CO_2	20.2	11.0	8.79	21.6	9.20	12.9	22.1	0.48	2.82	< 0.01
S	1.03	3.59	9.89	0.50	3.46	14.7	16.5	0.05	25.7	34.4
C (org)	0.88	1.20	0.75	0.13	0.62	0.50	0.17	0.07	0.50	< 0.01
As	35	100	260	180	290	60	430	44	990	560
Ba	370	490	580	250	570	300	130	580	470	180
Co	19	28	40	16	20	38	24	56	54	72
Cr	62	62	130	40	130	115	56	10	232	15
Cu	n100	n100	100	100	n100	100	n100	n100	100	100
Hg (ppb)	-	-	-	-	200	-	-	-	180	410
Li	35	52	52	39	66	34	11	59	26	2
Ni	26	50	70	17	42	66	22	n10	65	36
Pb	104	242	478	59	100	347	484	8	212	3800
Rb	128	172	166	107	220	100	41	166	122	12
Sb	n5									
Sc	14	13	15	10	13	13	12	5	14	12
Se	-	-	-	-	n2	-	-	-	n2	n2
Sr	52	53	8	32	34	17	16	10	14	-
Th	10	17	10	9	1	7	6	22	8	3
U	3	5	2	4	4	3	2	4	n1	n1
V	100	110	110	52	105	66	37	16	120	28
Y	42	36	43	22	33	36	47	22	26	38
Zn	500	1500	4200	300	100	200	300	100	1800	8100
Zr	n100	130	170	n100	190	n100	n100	210	180	n100
	← HYC Shale									

Table 2 cont.

Sample No.	35120	35119	35118	35117	35116	35115	35114	35113	35112	35111
Depth (m)	274.8	282.4	288.5	294.6	305.6	307.4	314.8	316.0	323.3	331.8
SiO_2	40.2	24.2	33.6	14.6	28.0	29.8	22.6	19.4	19.5	33.4
Al_2O_3	6.14	4.35	1.75	3.68	4.91	3.92	1.46	3.68	3.72	7.56
FeO	4.18	18.1	2.74	19.2	13.3	4.27	6.06	10.5	24.7	7.57
MgO	9.34	5.75	11.8	6.58	0.78	11.2	12.8	5.21	1.03	7.26
CaO	13.7	8.42	19.4	11.7	0.41	19.4	22.1	9.15	0.84	12.3
Na_2O	0.07	0.07	0.04	0.04	0.07	0.05	0.04	0.05	0.04	0.07
K_2O	3.82	2.37	1.04	1.96	2.36	2.14	0.76	1.71	1.45	3.51
TiO_2	0.22	–	0.06	–	–	0.14	0.05	–	–	–
P_2O_5	0.10	–	0.04	–	–	0.06	0.05	–	–	–
MnO	0.20	0.23	0.55	0.70	0.01	0.57	0.76	0.65	0.04	0.35
CO_2	24.9	12.3	27.1	18.9	–	29.4	30.4	11.3	0.55	22.7
S	1.90	16.5	1.14	17.1	19.1	0.91	1.48	14.4	27.7	4.36
C (org)	0.50	0.47	0.05	0.23	–	0.36	0.23	0.27	0.33	0.28
As	140	1600	500	410	570	230	580	1200	1900	350
Ba	290	230	n100	100	230	150	n100	140	180	240
Co	27	80	20	90	52	45	12	64	140	23
Cr	42	100	14	170	150	30	10	180	66	45
Cu	n100	1500	n100	500	3300	n100	n100	1200	1800	400
Hg (ppb)	–	940	–	–	–	–	–	1240	–	–
Li	30	22	17	16	24	21	11	19	31	46
Ni	22	43	n10	40	110	13	n10	42	41	24
Pb	244	18,800	838	22,500	130,000	775	260	53,900	35,300	5050
Rb	112	73	30	42	–	70	25	–	–	144
Sb	n5	29	n5	n5	130	n5	n5	24	62	5
Sc	11	10	8	16	10	9	5	14	11	10
Se	–	n2	–	–	–	–	–	n2	–	–
Sr	32	12	28	11	–	38	30	–	–	33
Th	10	11	2	–	–	4	4	–	–	7
U	2	2	1	2	–	2	2	–	–	2
V	60	58	31	62	60	22	20	64	40	80
Y	17	28	14	62	29	13	14	43	30	16
Zn	2200	48,200	11,900	53,600	131,000	1100	200	143,000	163,000	11,500
Zr	n100 →		100	n100	→				130	n100
	←			HYC	Shale					→

Table 2 cont.

Sample No.	35110	35109	35108	35107	35106	35105	35104	35103	35152	35102
Depth (m)	340.1	343.4	350.1	352.6	358.7	370.0	372.1	380.3	389.8	395.0
SiO_2	17.8	19.2	40.6	24.8	29.5	36.1	22.9	13.4	50.0	48.5
Al_2O_3	1.55	4.25	6.81	5.08	4.38	8.71	5.44	1.68	10.4	10.1
FeO	5.60	13.8	5.70	10.2	11.2	3.78	14.3	35.1	5.18	7.63
MgO	12.5	2.42	7.40	1.23	1.05	7.89	0.86	0.88	5.82	4.73
CaO	22.5	3.81	13.7	1.05	0.84	12.7	0.70	1.22	8.48	6.49
Na_2O	0.05	0.06	0.07	0.07	0.07	0.06	0.07	0.01	0.10	0.10
K_2O	0.84	1.71	3.17	2.01	1.68	4.12	2.13	0.54	4.34	4.00
TiO_2	-	-	0.23	-	-	-	-	-	0.40	0.36
P_2O_5	-	-	0.10	-	-	-	-	-	0.15	0.18
MnO	0.57	0.18	0.33	0.01	0.03	0.14	0.01	0.05	0.23	0.16
CO_2	31.5	7.11	19.8	1.10	1.54	18.7	0.66	-	12.2	9.67
S	2.28	21.5	2.02	19.0	18.8	2.13	22.2	34.5	1.82	4.04
C (org)	0.47	0.32	0.23	0.35	0.21	0.25	0.37	-	0.43	0.47
As	500	950	120	1400	1500	420	1600	1300	400	240
Ba	n100	140	220	220	170	200	150	n100	-	430
Co	18	120	29	100	76	36	105	130	-	27
Cr	n10	145	43	94	29	32	96	105	-	55
Cu	100	2500	100	5800	5300	300	5200	1300	n100	100
Hg (ppb)	-	-	-	-	1740	-	-	-	-	-
Li	12	31	42	30	31	37	26	16	55	63
Ni	n10	58	20	220	90	19	30	29	-	42
Pb	2660	78,300	1250	114,000	105,000	12,300	102,000	26,300	300	800
Rb	25	-	123	-	-	95	-	-	-	172
Sb	n5									
Sc	5	9	9	10	10	13	8	7	-	14
Se	-	-	-	-	15	-	-	-	-	-
Sr	72	-	34	-	-	30	-	-	-	32
Th	3	-	8	-	-	11	-	-	-	10
U	1	-	1	-	-	n1	-	-	-	3
V	20	52	78	54	50	58	49	26	-	130
Y	11	19	14	33	29	23	25	18	-	28
Zn	11,600	195,000	3700	196,000	175,000	14,800	179,000	61,100	400	3600
Zr	n100								-	230

← HYC Shale →

Table 2 cont.

Sample No.	35101	35100	35099	35098	35097	35153	35096	35095	35154	35094
Depth (m)	404.4	413.9	422.1	431.0	431.9	434.6	442.6	446.2	450.5	456.3
SiO_2	21.6	71.8	27.8	26.8	41.1	52.4	57.4	27.6	55.2	58.1
Al_2O_3	4.48	10.2	5.16	2.24	9.46	12.6	10.7	3.98	13.4	10.9
FeO	16.2	2.50	11.4	4.32	5.11	7.69	6.27	3.83	8.14	6.64
MgO	1.09	1.82	1.11	9.60	1.58	2.27	3.05	5.07	2.76	2.82
CaO	1.04	2.44	1.05	26.0	15.9	3.30	4.79	29.6	2.44	4.52
Na_2O	0.10	1.79	0.06	0.07	0.56	0.31	0.25	0.12	0.24	0.14
K_2O	1.84	3.30	2.15	1.11	5.15	5.95	4.64	1.43	5.26	4.49
TiO_2	–	0.19	–	0.06	–	–	0.45	0.11	0.48	0.46
P_2O_5	–	0.05	–	0.05	–	–	0.25	0.09	0.24	0.25
MnO	0.04	0.14	0.04	0.81	0.28	0.17	1.64	1.40	0.92	1.26
CO_2	3.48	2.93	0.55	29.7	13.0	4.47	5.83	26.9	2.75	5.31
S	22.7	0.91	19.8	0.75	3.88	5.19	1.50	0.27	2.84	0.09
C (org)	0.32	0.65	0.73	0.03	0.15	0.85	0.68	0.10	0.55	0.29
As	1800	95	1550	210	190	280	55	25	140	15
Ba	210	430	180	n100	560	–	280	160	–	450
Co	72	11	92	11	8	–	26	22	–	39
Cr	110	n10	104	15	16	–	37	37	–	74
Cu	3700	100	2700	n100	100	100	n100	n100	100	100
Hg (ppb)	1180	770	–	–	–	–	–	–	–	70
Li	28	29	37	18	35	55	59	24	86	51
Ni	40	n10	47	10	11	–	22	16	–	28
Pb	81,800	205	80,000	178	1420	3400	50	20	–	11
Rb	–	81	85	39	120	–	225	51	–	223
Sb	n5	→				13	n5	→		
Sc	10	9	10	5	7	–	9	10	–	12
Se	n2	–	n2	–	–	–	–	–	–	n2
Sr	–	12	17	106	47	–	46	73	–	38
Th	–	16	16	1	16	–	13	6	–	12
U	–	2	4	2	2	–	1	2	–	3
V	60	24	72	32	45	–	33	40	–	52
Y	27	20	23	15	17	–	25	22	–	29
Zn	187,000	1500	240,000	1100	22,700	18,900	100	800	100	2600
Zr	n100	120	100	n100	n100	–	100	n100	–	150
	← HYC Shale →									W-fold ←

Table 2 cont.

Sample No.	35093	35092	35155	35091	35090	35089	35156	35088
Depth (m)	468.8	477.0	485.0	488.9	503.9	513.6	522.2	526.7
SiO_2	56.3	52.4	49.6	57.3	53.5	19.6	41.8	20.2
Al_2O_3	11.9	10.8	9.69	11.6	12.7	4.76	7.75	4.08
FeO	6.20	5.92	6.50	5.25	4.25	3.01	3.96	8.10
MgO	2.87	3.93	4.60	3.71	4.32	14.4	7.89	11.9
CaO	4.95	6.70	9.37	4.88	5.90	23.4	13.8	21.8
Na_2O	0.20	0.18	0.10	0.16	0.15	0.05	0.09	0.07
K_2O	4.98	5.09	4.47	5.56	5.88	2.78	4.47	2.47
TiO_2	0.48	0.46	0.39	0.50	0.50	0.16	0.24	0.13
P_2O_5	0.35	0.26	0.29	0.31	0.36	0.15	0.22	0.15
MnO	1.48	1.26	1.56	0.64	0.53	0.57	0.49	1.24
CO_2	5.73	7.14	13.5	5.46	10.9	31.5	19.1	32.2
S	0.05	0.01	0.01	0.03	0.08	0.15	< 0.01	0.02
C (org)	0.27	0.16	0.03	0.20	0.32	0.01	0.03	0.01
As	15	70	15	n5	→	→	25	n5
Ba	560	580	–	560	580	600	–	160
Co	62	17	–	16	20	20	–	23
Cr	82	86	–	92	110	54	–	37
Cu	n100	→	→	→	→	→	→	→
Hg (ppb)	–	–	–	–	150	–	–	140
Li	38	62	28	27	46	10	21	17
Ni	41	26	–	33	42	26	–	15
Pb	15	8	–	11	21	4	–	4
Rb	245	249	–	247	252	50	–	49
Sb	n5	→	→	→	→	→	→	→
Sc	12	12	–	14	17	12	–	9
Se	–	–	–	–	n2	–	–	n2
Sr	40	39	–	41	44	36	–	22
Th	17	14	–	15	15	4	–	7
U	2	2	–	2	1	n1	–	n1
V	54	55	–	56	64	33	–	40
Y	28	23	–	24	40	20	–	26
Zn	1200	100	100	100	2100	900	n100	1000
Zr	118	130	–	170	190	n100	–	n100
	←	←	←	W-fold Shale	→	→	→	→

TABLE 3. ANALYSIS OF SAMPLES FROM DRILL HOLE O 123

(Major components in wt %; minor components in ppm)

Sample No.	35875	35878	35879	35880	35882	35883	35884	35886	35888	35890
Depth (m)	48.8	68.2	72.6	78.1	87.4	97.6	104.3	117.4	128.7	140.9
SiO_2	42.8	53.0	51.3	10.2	50.5	44.9	37.9	46.2	51.6	76.1
Al_2O_3	8.33	12.6	12.3	0.04	11.9	6.95	7.24	9.79	10.2	8.69
FeO	3.31	5.57	5.87	1.65	5.17	4.79	5.08	8.58	2.37	1.45
MgO	8.62	4.36	4.46	18.7	5.04	7.11	8.71	4.71	7.03	1.24
CaO	12.3	4.37	5.05	28.8	6.07	12.3	13.1	6.87	9.12	2.21
Na_2O	0.23	0.26	0.27	0.11	0.29	0.10	0.19	0.20	0.17	0.21
K_2O	4.70	6.63	6.72	< 0.10	6.44	4.36	4.84	6.21	5.68	6.29
TiO_2	0.28	0.50	0.48	< 0.02	0.48	0.30	0.27	0.33	0.32	0.20
P_2O_5	0.12	0.18	0.30	< 0.02	0.25	0.12	0.18	0.23	0.07	0.05
MnO	0.16	0.10	0.09	0.16	0.13	0.22	0.31	0.12	0.10	0.08
CO_2	18.4	8.57	7.47	39.6	9.16	18.0	18.0	8.76	13.6	2.74
H_2O^+	1.45	2.45	2.32	0.38	2.08	0.77	1.27	1.71	1.50	0.98
H_2O^-	0.61	1.30	0.96	0.10	0.95	0.40	0.23	0.54	0.60	0.28
S	2.22	2.40	2.89	0.06	2.33	1.92	2.34	5.59	0.12	0.38
C (org)	0.50	0.11	0.73	0.13	0.38	0.74	1.37	0.65	0.08	0.19
Ag	–	–	1	–	19	–	3	4	–	–
As	30	58	54	n5	64	87	60	207	24	147
B	60	60	100	15	80	30	30	40	80	30
Ba	1000	400	400	n300	400	n400	→	→	400	n400
Bi	n100	→	→	→	→	→	n3	n3	n100	n100
Cd	n300	→	→	→	→	→	10	10	n300	n300
Co	n20	n20	⩽ 20	n15	n20	⩽ 20	⩽ 20	20	n20	n20
Cr	170	40	13	n10	40	n10	n10	120	n10	n10
Cu	47	54	57	11	31	86	75	200	13	53
Ga	6	8	15	n3	10	6	8	8	8	6
Ge	n30	→	→	→	→	→	4	3	n30	n30
Hg (ppb)	–	–	–	–	–	–	–	–	–	–
La	n300	→	→	→	→	→	→	→	→	→
Li	78	123	137	11	132	55	50	81	155	37
Mo	n3	n3	10	n6	3	n3	6	10	n3	⩽ 3
Ni	15	15	25	n10	15	15	15	20	⩽ 10	10
Pb	180	120	395	95	n5	164	653	2574	17	370
Rb	–	–	–	–	–	–	–	–	–	–
Sb	–	–	–	–	–	–	–	–	–	–
Sc	n10	→	→	n25	25	n25	n25	n10	→	→
Se	–	–	–	–	–	–	–	–	–	–
Sn	–	–	–	–	–	–	1	0.8	–	–
Sr	n3	15	19	58	9	19	22	11	23	20
Tl	n100	→	→	→	→	→	6	60	n100	n100
V	60	60	200	⩽ 10	80	20	80	150	40	60
Zn	470	42	3460	96	2130	650	9650	4420	51	320
Zr	80	100	80	n200	80	80	60	80	80	60
	←	←	←	← HYC Shale	→	→	→	→	→	→

Table 3 cont.

Sample No.	35891	35892	35893	35895	35897	35898	35901	35902
Depth (m)	148.7	154.3	167.1	181.2	198.3	205.3	226.9	230.3
SiO_2	37.6	36.4	27.4	21.0	6.80	70.6	58.8	46.4
Al_2O_3	5.80	8.14	2.06	3.70	0.77	12.2	11.4	9.01
FeO	3.81	9.06	11.5	19.9	8.88	1.96	5.74	6.41
MgO	11.1	2.12	9.32	0.66	10.8	1.44	3.61	6.77
CaO	15.2	2.53	15.8	0.57	21.1	1.74	4.72	9.71
Na_2O	0.09	0.23	0.13	0.13	0.09	1.98	1.17	1.55
K_2O	3.27	3.93	1.25	1.69	0.30	0.47	5.16	3.95
TiO_2	0.20	0.30	0.07	–	–	0.18	0.40	0.37
P_2O_5	0.07	0.16	0.05	–	–	0.07	0.28	0.21
MnO	0.30	0.05	0.45	0.02	1.87	0.39	0.92	0.99
CO_2	22.9	8.02	23.8	0.88	33.6	2.14	6.01	13.8
H_2O^+	1.33	–	0.49	–	0.35	0.35	2.40	1.36
H_2O^-	0.24	0.61	0.18	0.32	0.23	0.24	0.98	0.86
S	0.74	12.1	7.57	26.5	4.80	0.17	0.44	0.01
C (org)	0.22	0.20	0.15	0.45	0.12	0.03	0.05	0.03
Ag	–	75	13	108	15	1	–	–
As	365	1500	770	2300	270	33	17	5
B	40	60	20	10	20	10	100	150
Ba	n400	→	→	→	n300	n400	n400	n300
Bi	n100	n3	→	→	→	n100	→	→
Cd	n300	300	40	600	200	n300	→	→
Co	⩽ 20	30	20	60	n15	n20	80	n15
Cr	n10	→	→	40	n10	n10	50	50
Cu	48	2130	235	3480	175	69	34	44
Ga	6	8	1	4	2	8	10	6
Ge	n30	40	25	60	10	n30	→	→
Hg (ppb)	–	–	–	–	–	–	–	–
La	n300	→	→	→	→	→	→	→
Li	59	76	20	32	10	27	51	48
Mo	n3	6	n3	10	n6	n3	n3	n6
Ni	10	20	n10	15	n10	⩽ 10	30	40
Pb	405	77,000	8720	76,100	18,400	208	36	n5
Rb	–	–	–	–	–	–	–	–
Sb	–	17	n5	50	–	–	–	–
Sc	n10	→	→	→	n25	n10	n10	n15
Se	–	–	–	–	–	–	–	–
Sn	–	1	⩽ 0.8	0.8	n0.8	–	–	–
Sr	20	n3	16	n3	10	18	18	61
Tl	n100	250	200	600	40	n100	→	→
V	40	100	10	40	n10	20	40	40
Zn	350	95,000	20,600	171,000	69,900	430	127	96
Zr	60	80	n60	n60	n200	80	80	n150
	←	←	←	HYC Shale	→	→	W-Fold Shale	Teena Dolomite

TABLE 4. ANALYSIS OF SAMPLES FROM DRILL HOLE Ie 115

(Major components in wt %; minor components in ppm)

Sample No.	35332	35333	35336	35338	35340	35341	35360	35366	35371
Depth (m)	27.5	33.6	67.7	94.6	116.8	129.0	317.8	350.1	392.5
SiO_2	31.2	11.5	5.05	4.54	8.47	6.63	13.6	5.50	6.91
Al_2O_3	6.50	1.36	0.51	0.24	1.49	1.15	3.38	0.93	1.17
FeO	7.08	5.52	3.55	3.14	3.11	4.68	5.71	6.14	7.17
MgO	9.67	15.1	20.6	20.7	20.7	19.7	14.2	18.9	18.1
CaO	14.1	26.0	28.1	29.2	27.1	27.8	24.3	27.7	26.9
Na_2O	0.08	0.04	0.03	0.03	0.04	0.06	0.06	0.03	0.06
K_2O	4.22	0.90	< 0.10	< 0.10	< 0.10	< 0.10	2.11	< 0.10	< 0.10
TiO_2	0.28	0.07	< 0.02	< 0.02	0.05	0.03	0.12	0.02	0.03
P_2O_5	0.12	0.05	< 0.02	< 0.02	0.02	0.05	0.07	0.05	0.02
MnO	0.44	0.68	0.50	0.36	0.54	0.81	0.83	0.81	1.03
CO_2	20.0	39.5	44.6	44.7	39.7	41.0	35.9	42.4	41.3
H_2O^+	1.30	0.55	0.41	0.41	1.60	1.13	0.85	0.85	1.19
H_2O^-	0.35	0.10	0.22	0.17	0.70	0.60	0.27	0.25	0.60
S	3.25	1.76	0.63	0.99	0.19	0.18	0.84	1.37	0.22
C (org)	0.51	0.11	0.08	0.08	< 0.02	< 0.02	0.37	0.54	0.13
Ag	n2	→					3	n2	n2
As	170	121	30	28	17	10	60	322	11
B	25	15	n15	n15	⩽ 15	⩽ 15	40	15	15
Ba	n300	→							
Bi	n100	→							
Cd	n300	→							
Co	20	n20	30	20	⩽ 15	n15	→		
Cr	35	40	20	8	17	23	18	25	30
Cu	13	11	69	9	5	8	16	12	14
Ga	4	n3	→						
Ge	n30	→							
Hg (ppb)	30	–	–	–	–	–	–	–	–
La	n200	n200	n300	→					
Li	38	45	14	7	23	41	38	25	37
Mo	n3	⩽ 6	n6	→					
Ni	25	30	30	10	n10	→			
Pb	81	106	34	250	30	25	140	44	128
Rb	–	–	–	–	–	–	–	–	–
Sb	n5	→							
Sc	n10	n10	n30	→					
Se	n2	–	–	–	–	–	–	–	–
Sn	–	–	–	–	–	–	–	–	–
Sr	7	7	19	18	25	13	13	11	14
Tl	100	n100	→						
V	30	10	n15	→			15	15	15
Zn	850	2110	3350	7300	145	890	2880	44	72
Zr	n60	n60	n150	→					
	HYC Shale →		←				Cooley Dolomite	→	

Table 4 cont.

Sample No.	35375	35382	35390	35391	35393	35395	35397	35400	35403	35404	35405
Depth (m)	434.6	520.3	584.4	600.9	615.5	630.7	655.8	705.8	750.3	755.8	760.1
SiO_2	5.16	7.74	25.5	9.20	51.8	47.9	6.74	6.44	6.12	55.2	34.9
Al_2O_3	0.55	0.94	8.71	1.47	10.7	10.3	1.17	1.42	1.25	1.98	2.87
FeO	5.15	5.33	4.95	4.26	6.00	4.32	6.27	6.38	7.26	1.54	1.98
MgO	18.4	16.9	14.3	17.2	5.55	6.67	18.4	18.7	17.7	8.94	13.4
CaO	28.8	27.7	16.4	27.1	6.76	8.70	26.9	27.0	26.9	12.8	18.6
Na_2O	0.06	0.02	0.04	0.06	0.08	0.04	0.04	0.26	0.03	0.02	0.07
K_2O	<0.10	0.43	4.33	0.90	5.06	4.95	<0.10	<0.10	<0.10	1.07	1.24
TiO_2	<0.02	0.02	0.30	0.05	0.43	0.38	0.05	0.03	0.03	0.08	0.08
P_2O_5	0.02	0.05	0.23	0.05	0.23	0.25	0.05	0.05	0.05	0.05	0.05
MnO	0.75	0.90	0.53	0.68	0.89	0.92	0.94	0.81	1.06	0.18	0.17
CO_2	44.4	42.7	25.7	42.3	9.82	12.6	41.0	41.2	41.9	19.0	28.2
H_2O^+	0.91	0.41	0.52	0.44	2.86	2.63	0.28	1.95	1.29	0.59	0.89
H_2O^-	0.30	0.15	0.22	0.15	0.62	0.86	0.39	0.33	0.29	0.17	0.28
S	0.09	0.11	0.03	0.09	0.03	0.02	0.10	0.10	0.11	0.03	0.05
C (org)	0.07	0.08	0.10	0.37	0.13	0.20	0.06	0.03	0.07	0.08	0.19
Ag	4	4	n2	→							
As	5	13	9	n5	→			6	n5	→	
B	⩽ 15	15	40	20	150	200	15	15	n15	20	40
Ba	n300	n300	300	n300	n300	300	n300	→			
Bi	n100	→									
Cd	n300	→									
Co	n15	20	n15	15	30	15	⩽ 15	n15	→		
Cr	20	18	28	5	22	45	35	25	28	158	40
Cu	156	255	4	17	4	3	3	4	7	9	5
Ga	n3	n3	10	n3	15	15	n3	→			
Ge	n30	→									
Hg (ppb)	–	140	–	40	–	–	–	–	–	–	–
La	n300	→									
Li	9	10	86	15	65	94	21	48	44	22	74
Mo	n6	→									
Ni	n10	n10	10	n10	40	30	n10	→		15	20
Pb	23	51	11	385	13	14	16	19	9	14	34
Rb	–	–	–	–	–	–	–	–	–	–	–
Sb	n5	→									
Sc	n30	→									
Se	–	n2	–	n2	–	–	–	–	–	–	–
Sn	–	–	–	–	–	–	–	–	–	–	–
Sr	20	n5	10	20	12	13	14	10	n5	8	21
Tl	n100	→									
V	n15	n15	20	n15	25	30	n15	→		15	15
Zn	68	11	29	22	46	39	20	30	12	127	42
Zr	n150	→			150	150	n150	→		150	n150
	Cooley Dolomite →				W-Fold Shale →			Teena Dolomite →			

TABLE 5. ANALYSIS OF SAMPLES FROM DRILL HOLE Ue 133

(Major components in wt %; minor components in ppm)

Sample No.	35406	35411	35413	35414	35416	35417	35419	35423
Depth (m)	203.3	258.3	273.6	286.1	291.6	293.4	303.8	346.8
SiO_2	14.7	14.7	14.2	29.3	21.8	56.0	43.0	46.2
Al_2O_3	2.40	2.17	0.74	6.03	1.91	12.3	7.67	9.50
FeO	34.7	4.05	4.88	33.7	1.60	4.79	4.10	3.67
MgO	3.70	14.4	13.7	1.21	6.33	4.31	2.67	7.79
CaO	7.97	25.7	26.7	1.60	34.8	5.85	21.4	11.2
Na_2O	0.03	0.06	0.03	0.06	0.05	0.19	0.10	0.10
K_2O	1.83	1.64	0.47	3.98	1.46	6.01	4.23	6.24
TiO_2	0.12	0.05	< 0.02	0.23	0.03	0.50	0.28	0.35
P_2O_5	0.09	0.05	0.02	0.09	0.05	0.23	0.23	0.34
MnO	0.41	0.67	0.80	0.10	0.57	0.58	0.59	0.30
CO_2	12.9	38.7	38.4	1.17	34.1	7.59	18.1	16.2
H_2O^+	-	0.46	0.22	1.71	0.39	2.60	1.11	1.26
H_2O^-	0.65	0.20	0.19	0.41	0.18	1.04	0.41	0.27
S	28.6	0.30	1.51	27.1	0.21	0.01	0.13	< 0.01
C (org)	0.32	0.07	0.37	0.52	0.25	0.06	0.04	0.09
Ag	n2	→		5	3	3	3	12
As	1280	40	30	850	31	n5	→	
B	n10	100	20	25	30	200	100	100
Ba	n400	n300	n300	n400	n300	300	300	600
Bi	n3	n100	n100	n3	n100	→		
Cd	6	n300	n300	10	n300	→		
Co	25	n15	⩽ 15	25	⩽ 15	15	15	n15
Cr	25	33	23	32	18	45	70	70
Cu	15	6	18	144	9	3	39	3
Ga	4	n3	n3	6	n3	8	6	6
Ge	6	n30	n30	6	n30	→		
Hg (ppb)	340	-	-	-	-	-	450	-
La	n200	n300	n300	n200	n300	→		
Li	12	16	13	39	12	95	36	39
Mo	15	n6	n6	15	n6	→		
Ni	10	15	⩽ 15	25	15	60	40	20
Pb	2320	42	25	3280	1190	15	33	12
Rb	-	-	-	-	-	-	-	-
Sb	n5	→		5	n5	→		
Sc	n10	n30	n30	n10	n30	→		
Se	n2	-	-	-	-	-	n2	-
Sn	n0.8	-	-	⩽ 0.8	-	-	-	-
Sr	21	12	26	26	49	29	35	20
Tl	200	n100	n100	200	n100	→		
V	15	15	n15	40	20	40	30	30
Zn	18,850	115	17,400	11,380	2185	62	43	27
Zr	n60	n150	n150	n60	n150	150	150	150
	← HYC Shale →				← W-fold Shale →			

Table 5 (cont.)

Sample No.	35425	35427	35429	35434
Depth (m)	373.8	389.5	401.7	439.2
SiO_2	12.4	21.4	52.6	47.7
Al_2O_3	1.63	2.29	2.25	6.12
FeO	7.65	5.78	1.96	1.84
MgO	14.6	12.6	6.78	8.87
CaO	26.4	23.1	13.9	12.7
Na_2O	0.04	0.07	0.02	0.06
K_2O	1.07	2.05	1.83	3.89
TiO_2	0.05	0.10	0.08	0.30
P_2O_5	0.05	0.05	0.02	0.09
MnO	0.97	0.74	0.22	0.14
CO_2	39.8	34.6	20.8	18.9
H_2O^+	0.50	0.47	0.51	0.96
H_2O^-	0.20	0.18	0.01	0.52
S	0.10	0.12	0.02	0.04
C (org)	0.04	0.06	0.18	0.11
Ag	5	5	3	3
As	9	13	n5	n5
B	15	15	30	200
Ba	n300	→	→	→
Bi	n100	→	→	→
Cd	n300	→	→	→
Co	n15	15	n15	n15
Cr	33	18	163	86
Cu	10	182	3	3
Ga	n3	→	→	4
Ge	n30	→	→	→
Hg (ppb)	–	–	–	–
La	n300	→	→	→
Li	21	14	15	230
Mo	n6	→	→	→
Ni	n15	15	⩽ 15	200
Pb	14	14	28	68
Rb	–	–	–	–
Sb	n5	→	→	→
Sc	n30	→	→	→
Se	–	–	–	–
Sn	–	–	–	–
Sr	12	10	12	19
Tl	n100	→	→	→
V	n15	n15	15	20
Zn	43	10	136	171
Zr	n150	n150	150	150
	← Teena Dolomite →			

TABLE 6. ANALYSIS OF SAMPLES FROM DRILL HOLE BARNEY 2

(Major components in wt %; minor components in ppm)

Sample No.	35835	35837	35838	35839	35840	35842	35844	35845	35846	35847
Depth (m)	31.6	67.1	87.2	115.5	133.3	173.9	203.6	224.9	243.8	262.3
SiO_2	37.6	32.5	37.8	42.3	34.9	39.1	40.3	39.7	40.3	43.9
Al_2O_3	6.50	4.29	5.08	7.43	5.40	6.65	7.22	5.50	7.12	9.35
FeO	3.98	2.08	1.99	2.73	2.64	2.50	2.29	5.38	10.1	13.5
MgO	9.34	12.4	12.2	9.92	12.9	10.8	11.2	10.6	8.14	3.57
CaO	14.0	17.6	17.4	13.6	17.8	15.1	14.8	14.6	10.8	4.80
Na_2O	0.31	0.41	0.24	0.36	0.13	0.63	0.35	0.12	0.16	0.93
K_2O	2.80	1.86	2.14	3.17	2.14	2.74	3.36	2.34	3.54	4.37
TiO_2	0.25	0.17	0.22	0.25	0.22	0.25	0.27	0.17	0.27	0.38
P_2O_5	0.28	0.14	0.27	0.27	0.18	0.25	0.18	0.11	0.11	0.30
MnO	0.12	0.10	0.12	0.08	0.19	0.12	0.28	0.14	0.10	0.10
CO_2	20.5	20.0	27.4	20.8	28.7	21.5	22.6	22.1	16.8	6.86
H_2O^+	1.91	4.10	1.38	< 0.01	1.93	–	2.11	1.80	2.09	–
H_2O^-	0.92	0.61	0.47	< 0.01	0.60	1.28	0.37	0.36	0.53	1.28
S	2.48	1.07	1.11	1.41	1.32	1.02	0.91	3.44	7.41	10.2
C (org)	0.85	3.05	0.74	1.45	0.32	0.59	0.36	< 0.05	0.42	0.03
Ag	–	–	n1	→		–	n1	→		3
As	31	23	10	20	20	25	100	110	180	275
B	60	60	60	150	40	60	60	25	60	60
Ba	n400	n400	n300	→		n400	n300	→		n400
Bi	n100	n100	n1	→		n100	n1	→		n100
Cd	n300	n300	n10	→		n300	n10	10	n10	n300
Co	20	n20	n10	→		n20	n10	→		20
Cr	170	90	45	105	80	120	85	135	230	325
Cu	29	25	10	10	10	27	10	20	15	50
Ga	6	4	3	8	4	4	6	4	6	8
Ge	n30	n30	0.8	n0.6	n0.6	n30	n0.6	1	0.6	n30
Hg(ppb)	90	–	–	–	–	–	–	–	–	700
La	n300	n300	n200	→		n300	n200	→		n300
Li	78	60	30	35	25	86	45	30	40	93
Mo	6	n3	4	n3	⩽ 3	n3	n3	3	4	15
Ni	20	10	n10	→		15	n10	→		30
Pb	n5	25	55	50	70	44	70	3000	160	765
Rb	110	80	90	130	100	140	150	70	110	150
Sb	–	–	–	–	–	–	–	–	–	n5
Sc	n10	→								
Se	n2	–	–	–	–	–	–	–	–	n2
Sn	–	–	n0.4	1	n0.4	–	0.4	0.4	0.8	–
Sr	30	35	20	30	20	36	25	25	25	n3
Tl	n100	n100	⩽ 1	1	n1	n100	1	20	20	100?
V	30	20	25	60	25	30	40	20	40	80
Zn	36	51	335	310	15	128	30	7100	1700	5100
Zr	n60	n60	80	80?	n80	n60	n80	→		n60
	←			HYC	Shale					→

Table 6 cont.

Sample No.	35848	35849	35852	35854	35855	35856
Depth (m)	278.3	286.7	327.0	341.3	348.6	355.0
SiO_2	29.1	42.8	17.0	48.3	56.0	8.62
Al_2O_3	5.93	9.67	1.95	7.69	1.87	0.36
FeO	3.43	3.16	3.31	1.80	1.53	7.74
MgO	14.4	8.87	17.1	8.52	8.36	16.7
CaO	19.1	11.4	24.9	11.1	13.2	27.8
Na_2O	0.07	0.23	0.11	0.17	0.12	0.03
K_2O	2.82	5.30	1.81	4.88	1.27	< 0.10
TiO_2	0.22	0.38	0.07	0.25	0.05	< 0.02
P_2O_5	0.23	0.23	0.05	0.07	< 0.02	< 0.02
MnO	0.44	0.34	0.45	0.16	0.16	1.06
CO_2	27.6	16.7	37.2	16.1	19.8	39.4
H_2O^+	0.45	1.06	2.74	1.07	0.45	2.24
H_2O^-	0.43	1.07	0.43	1.36	0.39	0.32
S	0.02	0.03	0.02	0.04	0.12	0.06
C (org)	0.40	0.03	0.06	0.05	0.03	0.03
Ag	n1	–	–	–	–	–
As	n10	n5	n5	5	10	10
B	20	60	15	60	15	n15
Ba	n300	n400	n300	n400	600	n300
Bi	n1	n100	→			
Cd	n10	n300	→			
Co	n10	20	n15	n20	n20	n15
Cr	130	145	100	105	60	140
Cu	n5	19	15	22	19	19
Ga	3	6	⩽ 3	8	⩽ 3	n3
Ge	⩽ 0.6	n30	→			
Hg (ppb)	–	–	–	–	–	–
La	n200	n300	→			
Li	20	55	3	240	41	15
Mo	4	n3	n6	n3	n3	n6
Ni	n10	20	n10	⩽ 10	⩽ 10	n10
Pb	30	149	15	29	74	74
Rb	90	160	25	–	30	–
Sb	–	–	–	–	–	–
Sc	n10	n10	n25	n10	n10	n25
Se	–	–	–	–	–	–
Sn	n0.4	–	–	–	–	–
Sr	20	30	16	14	53	16
Tl	1	n100	→			
V	15	40	10	30	10	⩽ 10
Zn	25	140	20	61	350	400
Zr	n80	60?	n200	n60	n60	n200
	← W-fold Shale →		← Teena Dolomite →			

TABLE 7. ANALYSIS OF SAMPLES FROM DRILL HOLE WICKENS HILL 1

(Major components in wt %: minor components in ppm)

Sample No.	35803	35804	35806	35807	35810	35812	35813	35814	35817	35818	35819
Depth (m)	36.3	51.2	84.2	109.1	157.9	173.9	185.0	193.4	231.9	259.4	282.1
SiO_2	56.9	41.7	43.8	53.2	56.7	56.9	43.1	69.9	32.3	69.7	61.8
Al_2O_3	12.0	9.24	10.4	11.0	11.7	12.7	3.68	11.4	4.70	9.35	19.3
FeO	5.60	12.5	6.87	9.49	8.63	4.30	4.85	2.05	5.72	0.94	1.31
MgO	3.83	3.50	5.02	2.59	1.33	2.84	7.88	1.34	12.2	2.34	1.59
CaO	3.61	5.14	6.97	2.83	1.36	3.99	12.9	1.76	18.5	3.82	0.39
Na_2O	0.27	0.54	0.45	0.20	0.08	0.20	0.03	0.16	0.03	0.16	0.20
K_2O	4.58	3.30	4.29	4.65	5.84	6.97	1.83	7.66	2.16	7.54	11.6
TiO_2	0.52	0.40	0.43	0.48	0.43	0.50	0.13	0.32	0.15	0.12	0.25
P_2O_5	0.21	0.27	0.46	0.34	0.18	0.23	0.23	0.07	0.21	0.05	0.05
MnO	0.05	0.08	0.10	0.04	0.05	0.16	0.46	0.08	0.59	0.17	0.03
CO_2	1.06	16.7	8.65	9.15	5.03	1.83	20.4	2.49	27.4	6.22	0.61
H_2O^+	2.84	3.12	-	3.34	2.92	2.36	0.96	0.45	1.54	0.73	2.07
H_2O^-	1.41	1.39	1.11	0.97	0.78	0.94	0.22	0.56	0.17	0.22	1.52
S	2.79	10.5	4.20	7.09	6.29	1.86	2.79	0.19	0.07	0.02	0.02
C (org)	1.59	2.40	1.54	1.26	0.72	1.65	< 0.05	0.20	0.28	0.03	0.01
Ag	5	1?	n0.5	1?	1?	-	n1	-	n1	-	-
As	286	300	206	30	220	97	120	41	70	6	11
B	100	150	80	200	200	80	20	40	n20	10	150
Ba	n400	n300	n400	300	300	n400	n300	n400	n300	n400	n400
Bi	n100	n1	n100	n1	3?	n100	n1	n100	n1	n100	n100
Cd	n300	10	n300	n10	n10	n300	100	n300	n10	n300	n300
Co	40	15	25	20	15	15	n10	n20	n10	n20	n20
Cr	210	710	137	240	240	215	135	152	150	105	100
Cu	66	40	39	110	156	85	20	25	n5	25	25
Ga	10	15	10	10	10	10	6	10	n3	4	15
Ge	n30	0.8	n30	1	0.8	n30	6	n30	0.8	n30	n30
Hg(ppb)	330	-	200	-	-	-	-	-	-	-	-
La	n300	n200	n300	n200	n200	n300	n200	n300	n200	n300	n300
Li	105	30	80	40	30	68	15	47	15	6	33
Mo	6	25	15	6	3	6	n3				
Ni	30	30	30	30	40	30	n10	⩽ 10	n10	n10	n10
Pb	640	1400	280	1800	1900	46	5300	8	60	n5	20
Rb	-	-	-	-	-	-	-	-	-	-	-
Sb	-	-	-	-	-	-	-	-	-	-	-
Sc	n10	10	n10	10	10	n10					
Se	n2	-	n2	-	-	-	-	-	-	-	-
Sn	-	0.4	-	0.6	0.4	-	n0.4	-	0.4	-	-
Sr	5	20	8	15	25	12	n5	15	10	18	16
Tl	n100	60	n100	100	15	n100	6	n100	n1	n100	n100
V	250	150	200	150	200	250	20	60	15	10	10
Zn	3740	6500	1530	6500	5900	5250	32,000	52	70	42	60
Zr	⩽ 60	n80	⩽ 60	80	80	⩽ 60	n80	60?	n80	60?	60?
	← HYC Shale →									←	W-fold Shale

Table 7 cont.

Sample No.	35824	35825	35826	35831
Depth (m)	284.0	289.0	305.0	355.6
SiO_2	61.6	55.0	48.6	41.9
Al_2O_3	19.5	12.7	13.8	13.1
FeO	2.03	1.93	1.47	11.2
MgO	2.39	4.43	4.96	20.7
CaO	0.88	6.04	7.22	0.46
Na_2O	0.08	0.12	0.15	0.03
K_2O	9.98	10.1	11.4	< 0.10
TiO_2	0.45	0.35	0.25	0.42
P_2O_5	0.14	0.09	0.05	0.28
MnO	0.03	0.23	0.25	0.04
CO_2	0.06	9.23	11.4	0.19
H_2O^+	3.42	0.55	0.46	2.03
H_2O^-	0.58	0.34	0.25	2.04
S	0.03	< 0.01	0.13	0.19
C (org)	0.01	0.01	0.03	0.01
Ag	–	–	–	–
As	n10	13	13	22
B	60	n10	n10	10?
Ba	n400	400	400	n400
Bi	n100 →			
Cd	n300 →			
Co	n20 →			
Cr	20	70	60	340
Cu	90	24	32	25
Ga	10	6	6	15
Ge	n30 →			
Hg (ppb)	–	–	–	–
La	⩽ 100	n300 →		
Li	34	12	9	450
Mo	n3 →			
Ni	⩽ 10	⩽ 10	n10	15
Pb	460	14	136	n5
Rb	–	–	–	–
Sb	n5	–	–	–
Sc	⩽ 10	n10 →		
Se	–	–	–	–
Sn	–	–	–	–
Sr	18	12	16	4
Tl	n100 →			
V	20	10	10	40
Zn	60	32	53	91
Zr	60?	60?	60?	60?
	← W-fold Shale →			Teena Dolomite

TABLE 8. ANALYSIS OF SAMPLES FROM DRILL HOLE MYRTLE 1

(Major components in wt %; minor components in ppm)

Sample No.	35859	35860	35863	35866	35867	35870	35871	35872
Depth (m)	40.6	46.8	81.0	112.2	119.3	130.7	138.2	149.5
SiO_2	47.5	52.0	52.8	42.6	68.2	68.0	53.3	65.5
Al_2O_3	10.4	10.8	10.8	5.33	11.7	9.96	9.63	10.1
FeO	3.22	4.36	3.67	7.22	1.74	1.49	11.6	1.07
MgO	6.50	5.44	5.99	6.70	1.41	2.02	2.17	2.97
CaO	8.34	6.21	6.27	11.6	1.92	3.48	3.01	5.06
Na_2O	0.30	0.27	0.29	0.18	0.21	0.15	0.21	0.16
K_2O	6.03	5.52	5.17	4.17	8.35	8.06	6.64	8.21
TiO_2	0.42	0.53	0.47	0.17	0.20	0.13	0.33	0.33
P_2O_5	0.14	0.21	0.18	0.18	0.09	0.07	0.28	0.09
MnO	0.05	0.05	0.09	0.17	0.04	0.07	0.05	0.10
CO_2	10.5	9.16	10.4	19.0	2.19	5.54	3.66	7.70
H_2O^+	2.58	2.41	2.22	0.86	1.05	0.57	1.26	0.46
H_2O^-	1.09	1.08	1.04	0.30	0.66	0.25	0.53	0.20
S	1.20	2.20	0.87	4.65	0.98	0.68	9.09	0.32
C (org)	1.52	0.74	0.87	0.51	0.30	0.28	0.72	0.12
Ag	–	n0.5	–	3	–	–	–	–
As	130	52	30	223	77	28	226	33
B	60	60	40	n10	25	10	10	n10
Ba	n300	n300	n400	400	n400	→		
Bi	n3	→				n100	→	
Cd	n6	8	n6	⩽ 6	n6	n300	→	
Co	20	⩽ 20	n20	20	n20	n20	20	n20
Cr	150	122	122	180	106	15	259	60
Cu	45	100	30	66	40	32	110	31
Ga	10	10	8	6	8	4	6	8
Ge	⩽ 1	1.5	1	⩽ 1	⩽ 1	n30	→	
Hg (ppb)	–	740	230	400	150	–	–	–
La	n300	→						
Li	110	95	100	11	30	13	31	10
Mo	10	4	n3	6	6	6	10	8
Ni	25	25	20	30	15	10	30	10
Pb	100	770	160	190	100	214	212	30
Rb	–	–	–	–	–	–	–	–
Sb	–	–	–	–	–	–	n5	–
Sc	n10	→						
Se	–	2	n2	n2	n2	–	–	–
Sn	2	2	0.8	⩽ 0.8	0.8	–	–	–
Sr	33	23	21	19	22	16	n3	7
Tl	4	6	0.6	25	2	n100	100	n100
V	80	200	200	80	80	40	150	40
Zn	490	6890	270	2780	400	527	90	142
Zr	n60	60	60	n60	60	60	60	80
	← HYC Shale →					Teena Dolomite		Mitchell Yard Dol.

TABLE 9. ANALYSIS OF SAMPLES FROM DRILL HOLE AMELIA 1

(Major components in wt %; minor components in ppm)

Sample No.	35772	35774	35776	35777	35786	35790	35793	35796	35799
Depth (m)	26.1	38.7	57.3	67.7	161.8	181.6	192.0	212.9	226.9
SiO_2	59.7	63.5	57.8	71.4	8.04	8.21	33.2	8.30	7.53
Al_2O_3	13.7	12.3	12.1	12.4	< 0.02	0.08	6.05	0.43	0.43
FeO	4.00	3.87	5.31	2.64	0.55	1.66	1.43	1.97	0.80
MgO	2.92	1.23	1.11	0.85	20.9	21.6	12.3	19.9	21.6
CaO	2.25	1.11	0.24	0.55	31.2	31.1	17.3	30.4	30.8
Na_2O	0.30	0.25	0.09	0.29	0.04	0.03	0.12	0.03	0.03
K_2O	7.09	7.25	6.94	7.31	< 0.10	< 0.10	4.95	< 0.10	< 0.10
TiO_2	0.55	0.07	0.50	0.05	< 0.02	< 0.02	0.22	< 0.02	< 0.02
P_2O_5	0.21	0.80	0.14	0.39	0.46	0.02	0.05	< 0.02	< 0.02
MnO	0.03	0.03	0.01	< 0.01	0.10	0.19	0.10	0.28	0.19
CO_2	3.15	0.33	< 0.01	0.22	45.2	44.9	26.5	44.4	44.1
H_2O^+	3.06	2.93	7.04	1.96	0.34	0.54	0.64	0.45	0.61
H_2O^-	1.56	1.84	2.15	1.39	0.24	0.26	0.23	0.30	0.29
S	1.66	2.10	3.14	0.01	< 0.01	< 0.01	0.59	< 0.01	0.02
C (org)	0.59	2.62	4.88	0.03	< 0.01	0.06	0.24	0.01	< 0.01
Ag	–	3	n2	–	–	–	–	–	–
As	50	30	54	12	n5	n5	16	n5	n5
B	100	40	40	30	n15	n15	n10	n15	20
Ba	400	n400	400	n400	n300	n300	n400	n300	n300
Bi	n100	→							
Cd	n300	→							
Co	20	30	25	15	n15	n15	20	n15	n15
Cr	165	210	34	212	n10	75	115	107	30
Cu	40	43	13	52	26	22	41	16	14
Ga	15	10	10	10	n3	n3	6	n3	n3
Ge	n30	→							
Hg(ppb)	–	–	–	–	–	–	–	–	–
La	n300	n300	n200	n300	→				
Li	100	66	89	56	n3	5	15	24	25
Mo	6	15	20	n3	→				
Ni	60	40	40	n10	n10	10	10	n10	n10
Pb	100	1080	46	17	33	n5	33	40	8
Rb	–	–	–	–	–	–	–	–	–
Sb	–	n5	–	–	–	–	–	–	–
Sc	⩽ 25	n10	→		n25	n25	n10	n25	n25
Se	–	–	–	–	–	–	–	–	–
Sn	–	–	–	–	–	–	–	–	–
Sr	n3	13	11	19	14	11	20	18	30
Tl	n100	→							
V	200	200	100	200	⩽ 10	⩽ 10	20	⩽ 10	⩽ 10
Zn	35	50	14	173	24	41	59	79	83
Zr	60	60	⩽ 60	60	n60	n60	⩽ 60	n200	n200
	← Wea-thered	HYC Shale Wea-thered →		← Wea-thered	← Mitchell Yard Dolomite →			Mara Dolomite	

TABLE 10. ANALYSIS OF SAMPLES FROM DRILL HOLE BMR 2

(Major components in wt %; minor components in ppm)

Sample No.	37799	37800	37801	37802	37020	37021	37022	37023	38775	37024	37025
Depth (m)	5.9	16.2	21.8	25.5	30.1	32.9	51.3	53.7	56.3	63.8	68.5
SiO_2	43.8	72.5	64.2	70.6	47.1	37.4	53.3	40.9	53.7	42.4	39.2
Al_2O_3	7.08	8.56	6.99	5.35	5.61	5.63	11.2	7.95	11.6	4.99	7.10
FeO	2.38	4.55	3.46	2.11	1.89	1.94	5.11	2.86	4.46	3.07	18.3
MgO	9.09	1.04	3.65	4.21	9.00	12.0	4.43	10.2	3.52	10.7	4.24
CaO	15.1	1.89	7.09	6.97	14.1	17.2	5.74	13.5	4.94	15.3	5.82
Na_2O	0.08	0.09	0.09	0.07	0.07	0.05	0.09	0.08	0.07	0.07	0.07
K_2O	6.06	6.34	5.65	4.49	5.01	5.11	7.66	6.93	8.31	4.14	5.84
TiO_2	0.25	0.37	0.27	0.18	0.22	0.20	0.40	0.25	0.43	0.18	0.27
P_2O_5	0.23	0.11	0.53	0.09	0.55	0.07	0.50	0.14	0.82	0.23	0.23
MnO	0.12	0.05	0.09	0.12	0.28	0.54	0.08	0.10	0.06	0.18	0.12
CO_2	13.7	3.85	9.49	8.92	16.4	24.9	7.99	18.8	9.42	21.1	6.93
H_2O^+	0.74	0.69	0.53	0.30	0.74	0.51	1.41	0.69	1.23	0.69	–
H_2O^-	0.25	0.28	0.26	0.23	0.08	0.11	0.21	0.09	0.18	0.14	0.43
S	0.01	2.42	1.58	0.43	0.64	0.49	3.90	1.90	3.55	1.64	13.9
C (org)	0.10	1.23	0.59	0.18	0.96	0.23	2.50	0.99	2.06	1.08	1.76
Ag	–	–	–	–	–	–	–	–	–	–	–
As	40	30	68	11	35	20	90	80	50	35	160
B	40	60	40	60	n10	n10	25	n10	10	⩽ 10	n10
Ba	n300	→	→	→	n400	n400	400	n400	400	400	400
Bi	n100	→	→	→	→	→	→	→	→	n3	n3
Cd	n300	→	→	→	→	→	→	→	→	n6	n6
Co	n15	→	→	→	n20	n20	20	⩽ 20	20	n20	20
Cr	40	80	80	50	85	100	215	115	230	120	415
Cu	25	25	25	20	5	5	50	20	30	30	94
Ga	10	6	6	3	4	4	15	4	10	6	8
Ge	n30	→	→	→	→	→	→	→	→	n1	n1
Hg(ppb)	–	–	–	–	–	–	–	–	–	–	410
La	n300	n200	→	→	n100	→	→	→	→	→	→
Li	3	13	10	4	6	5	17	2	13	4	7
Mo	6	6	8	n6	10	30	6	15	25	8	20
Ni	150	250	400	400	n10	n10	15	15	25	15	25
Pb	200	70	20	3340	n5	45	73	85	450	25	490
Rb	80	120	100	80	80	70	160	110	170	90	100
Sb	n5	–	–	–	–	–	–	–	–	–	–
Sc	n25	→	→	→	n10	n10	⩽ 10	n10	⩽ 10	n10	n10
Se	–	–	–	–	–	–	–	–	–	–	5
Sn	–	–	–	–	–	–	–	–	–	0.8	1
Sr	30	19	58	32	100	68	28	28	29	30	23
Tl	n100	→	→	→	→	→	→	→	→	n0.6	0.6
V	20	20	20	20	15	15	250	20	60	20	30
Zn	14	7	8	17	25	18	43	50	36	54	16
Zr	150	400	150	150	n60	→	→	→	60	60	n60
	Reward Dol. Weathered	←	←	←	Barney Creek Formation						

Table 10 cont.

Sample No.	37026	37027	38776	37028	37803	37029	37804
Depth (m)	76.3	77.9	80.0	85.6	95.5	107.5	115.3
SiO_2	50.3	68.2	55.2	45.8	49.2	24.4	10.7
Al_2O_3	8.26	12.7	10.0	8.96	8.90	2.61	0.91
FeO	3.96	1.20	4.94	19.4	3.90	2.59	2.28
MgO	6.17	1.89	3.43	1.38	5.94	16.2	20.2
CaO	9.22	1.89	5.18	1.92	10.7	23.4	31.2
Na_2O	0.08	0.09	0.08	0.09	0.11	0.03	0.11
K_2O	6.85	8.50	7.06	7.00	7.43	2.53	0.92
TiO_2	0.28	0.23	0.35	0.32	0.32	0.08	< 0.02
P_2O_5	0.48	0.09	0.55	0.71	0.23	0.11	0.05
MnO	0.25	0.04	0.27	0.06	0.31	0.85	0.56
CO_2	11.9	2.49	6.49	< 0.01	13.5	33.0	41.9
H_2O^+	1.04	0.79	1.36	-	0.75	0.69	0.46
H_2O^-	0.14	0.12	0.24	0.12	0.24	0.08	0.21
S	2.63	0.60	3.40	15.6	1.86	0.44	0.12
C (org)	2.37	0.92	3.49	2.63	1.83	0.63	0.09
Ag	-	-	⩽ 0.3	n0.3	-	-	-
As	70	15	85	270	27	15	11
B	n10	n10	15	n10	40	n10	n15
Ba	400	600	600	400	n300	n400	n300
Bi	n3	n3	n1	1	n100	→	→
Cd	n6	n6	n6	n6	n300	→	→
Co	⩽ 20	n20	20	20	n15	n20	n15
Cr	165	35	170	435	80	100	30
Cu	30	5	30	65	21	n1	10
Ga	8	6	10	6	4	3	n3
Ge	n1	⩽ 1	⩽ 1	n1	n30	→	→
Hg (ppb)	330	240	-	-	-	-	-
La	n100	150	n100	n100	n300	n100	n300
Li	10	6	30	22	9	2	n2
Mo	20	40	15	15	8	8	6
Ni	15	⩽ 10	25	20	100	⩽ 10	25
Pb	75	950	60	275	70	450	30
Rb	110	180	160	110	120	40	20
Sb	-	-	-	-	n5	-	n5
Sc	n10	n10	⩽ 10	n10	n25	n10	n25
Se	n2	n2	-	-	-	-	-
Sn	2	1	2	2	-	-	-
Sr	27	13	28	19	40	23	32
Tl	2	n0.6	3	1	-	-	-
V	40	40	80	80	80	25	⩽ 15
Zn	37	n5	42	32	4	62	36
Zr	n60	60	60	n60	n150	n60	n150
	← Barney Creek Formation →						

TABLE 11. ANALYSIS OF SAMPLES FROM DRILL HOLE BMR 1

(Major components in wt %; minor components in ppm)

Sample No.	37798	35910	35911	37018	37019	35912
Depth (m)	1.2	16.6	18.8	22.1	23.3	25.2
SiO_2	52.2	51.9	61.2	51.8	51.1	50.1
Al_2O_3	11.1	15.2	8.48	13.1	11.9	12.8
FeO	7.42	10.2	8.97	12.2	11.6	12.6
MgO	8.94	7.01	7.53	8.26	7.51	6.14
CaO	5.67	0.20	2.49	1.23	2.73	1.40
Na_2O	0.08	0.12	0.03	0.20	0.30	0.19
K_2O	3.31	7.08	1.91	6.25	5.85	6.23
TiO_2	0.40	0.56	0.34	2.20	1.75	2.19
P_2O_5	0.09	0.15	0.09	0.48	0.34	0.43
MnO	0.12	0.03	0.14	0.14	0.21	0.16
CO_2	6.96	0.10	3.90	1.14	2.58	1.68
H_2O^+	3.50	3.45	4.40	4.92	3.81	4.73
H_2O^-	1.40	0.68	0.35	0.71	0.67	0.41
S	0.01	0.01	0.16	0.06	0.26	0.09
C (org)	0.04	0.13	0.04	0.04	0.05	0.04
Ag	–	n1	n1	–	–	n1
As	n10	9	11	n5	5	5
B	40	40	80	20	15	40
Ba	400	600	1000	600	1000	3000
Bi	n100	→	→	→	n3	n3
Cd	n300	→	→	→	n6	n6
Co	⩽ 20	20	20	25	40	25
Cr	60	40	60	320	310	60
Cu	16	6	10	28	25	15
Ga	8	10	6	10	10	10
Ge	n30	→	→	→	⩽ 1	⩽ 1
Hg (ppb)	–	–	–	–	–	90
La	n100	n200	⩽ 200	n100	n100	n200
Li	78	–	–	140	100	–
Mo	n3	→	→	4	⩽ 3	n3
Ni	30	40	200	15	15	250
Pb	410	n20	n20	n5	n5	n20
Rb	–	–	–	–	–	–
Sb	n5	–	–	–	–	–
Sc	⩽ 10	⩽ 10	⩽ 10	20	20	10
Se	–	–	–	–	–	n2
Sn	–	–	–	–	n0.8	n0.8
Sr	32	–	–	35	75	–
Tl	n100	→	→	→	n0.6	n0.6
V	40	25	25	250	200	150
Zn	20	–	–	58	48	–
Zr	n60	→	→	→	60	80
	(Tawallah Group?) Weathered	Shale →		Dolerite →		

TABLE 12. ANALYSIS OF MISCELLANEOUS SAMPLES

(Major components in wt %; minor components in ppm)

Drill Hole			Ee 108	Barney Ck 1	Ce 131	Ye ' 117	Ye ' 117
Sample No.	35235	35754	35903	35904	35907	35908	35909
Depth (m)	0	0	13.4	80.5	50.3	32.0	44.2
SiO_2	11.3	60.9	62.5	40.1	53.4	38.7	51.1
Al_2O_3	1.10	14.8	15.6	8.29	11.9	5.21	11.1
FeO	1.81	6.96	3.10	4.03	3.77	1.87	3.86
MgO	18.1	0.43	1.03	10.0	5.86	11.0	6.29
CaO	27.8	0.39	0.62	12.4	6.81	16.2	7.71
Na_2O	0.05	0.10	0.21	0.06	0.11	0.04	0.05
K_2O	0.74	11.5	11.0	4.53	5.97	3.37	6.26
TiO_2	0.05	2.19	2.45	0.30	0.39	0.20	0.39
P_2O_5	0.05	0.38	0.50	0.09	0.09	0.06	0.09
MnO	0.23	< 0.01	< 0.01	0.12	0.07	0.15	0.10
CO_2	38.6	0.08	1.42	18.7	10.5	24.4	12.0
H_2O^+	0.05	1.29	2.24	2.08	2.35	1.01	2.33
H_2O^-	0.29	0.21	0.92	0.37	0.52	0.19	0.29
S	0.13	0.01	0.01	0.01	0.02	0.04	0.02
C (org)	0.08	< 0.01	0.03	< 0.01	0.02	0.15	0.02
Ag	–	n1	–	n1	→		
As	19	n5	31	n5	5	n5	n5
B	15	40	200	40	80	60	60
Ba	6000	2000	2000	400	400	400	400
Bi	n100	→					
Cd	n300	→					
Co	n15	⩽ 20	40	n20	→		
Cr	75	60	20	40	40	40	60
Cu	42	10	63	8	10	10	6
Ga	n3	8	15	4	4	n3	4
Ge	n30	→					
Hg (ppb)	–	–	–	–	–	–	–
La	n300	n200	n300	n200	n300	→	
Li	12	–	68	–	–	–	–
Mo	n6	4	n6	n3	→		15
Ni	10	25	60	100	80	150	80
Pb	15	n20	60	n20	→		
Rb	–	–	–	–	–	–	–
Sb	–	–	–	–	–	–	–
Sc	n10	15	40	n10	⩽ 10	n10	⩽ 10
Se	–	–	–	–	–	–	–
Sn	–	–	–	–	–	–	–
Sr	8	–	65	–	–	–	–
Tl	n100	→					
V	15	250	400	15	25	15	20
Zn	42	–	48	–	–	–	–
Zr	n60	80	200	n60	60	n60	n60
	Stromatolite Emmerugga Dolomite	← Weathered → Dolerite		←	Myrtle Shale		→

TABLE 13. MEAN VALUES OF MINERALIZED SHALES FROM THE HYC SHALE MEMBER

	Moderately Mineralized S = 4 - 20%				Highly Mineralized S > 20%	
	McArthur Ore Basin Te 115, O 123, Ie 115, Ue 133		Other Areas Barney 2, Wickens Hill 1, Myrtle 1, Amelia 1, BMR 2		McArthur Ore Basin Te 115, O 123, Ie 115, Ue 133	
No. of Samples	18		9		13	
SiO_2	32.9		45.2		23.0	
Al_2O_3	6.37		8.91		4.62	
FeO	13.8		11.8		26.2	
MgO	4.42		4.05		1.75	
CaO	6.64		5.69		2.32	
Na_2O	0.10		0.30	*0.18*	0.12	*0.07*
K_2O	2.97		4.78		2.22	
TiO_2	0.33		0.35		(0.23)	
P_2O_5	0.19		0.31		(0.12)	
MnO	0.18	*0.12*	0.09		0.09	*0.05*
CO_2	9.48		9.90		3.22	
H_2O^+	(1.71)		2.47		(1.71)	
H_2O^-	(0.58)		0.77		(0.46)	
S	13.3		8.87		25.5	
C (org)	0.74	*0.47*	1.25		0.35	
Ag	(4)		1		(> 4)	
As	710	*430*	210		1200	
B	(50)		85	*60*	(13)	
Ba	290		280		220	
Co	49		18		70	
Cr	100		320	*240*	100	
Cu	1100	*200*	71		1300	*100*
Ga	(8)		9		(4)	
Hg (ppb)	(770)		(430)		(530)	
Li	41		39	*30*	30	
Mo	(8)		12	*15*	13	
Ni	55	*42*	27		39	
Pb	27,000	*2600*	810	*490*	30,000	*3800*
Rb	110		(120)		81	
Sc	11		n10		11	
Sr	20		18		16	
Th	10		-		(6)	
Tl	(160)		40	*22*	(330)	
V	96		110	*80*	52	
Y	32		(26)		27	
Zn	53,000	*7700*	3300	*2800*	76,000	*17,000*
Zr	99		n60		n100	

Note: Italics indicate median values.

( ) value calculated from relatively few analyses.

TABLE 14. MEAN VALUES OF SHALES (S<4%, CO_2<20%, SiO_2<60%) FROM THE HYC PYRITIC SHALE AND W-FOLD SHALE MEMBERS, TEENA DOLOMITE AND MYRTLE SHALE

	HYC Pyritic Shale Member						W-fold Shale Member				Teena Dolomite		Myrtle Shale	
	McArthur Ore Basin		Other Areas (excluding BMR 2 Area)		BMR 2 Area (Barney Ck Fm)		McArthur Ore Basin		Other Areas		All Areas Shaly Samples		Outside McArthur Ore Basin	
No of Samples	17		6		7		16		3		7		4	
SiO_2	45.9		54.0		50.0		51.7		48.8		49.8		45.8	
Al_2O_3	10.1		9.65		9.07		10.7		12.1		7.06		9.13	
FeO	4.67		4.41		3.87		5.43		2.19		5.13	*1.84*	3.38	
MgO	6.34		4.29		6.10		4.26		6.09		9.19		8.29	
CaO	9.01		4.78		9.05		8.24	*6.30*	8.22		9.00	*12.7*	10.8	
Na_2O	0.19		0.24	*0.27*	0.08		0.23	*0.16*	0.17		0.31	*0.12*	0.07	
K_2O	4.93		5.87		7.03		5.10		8.93		3.10	*3.89*	5.03	
TiO_2	0.38		0.49		0.32		0.42		0.33		0.26	*0.33*	0.32	
P_2O_5	0.17		0.19		0.47		0.27		0.12		0.14	*0.09*	0.08	
MnO	0.15		0.07	*0.05*	0.19	*0.25*	0.89		0.27		0.25	*0.16*	0.11	
CO_2	12.5		5.49		11.7		9.94		12.4		13.1	*16.1*	16.4	
H_2O^+	(1.69)		3.24	*2.50*	1.03		(2.14)		0.69		1.10		1.94	
H_2O^-	(0.72)		1.29	*1.09*	0.18		(0.70)		0.55		0.84	*0.53*	0.34	
S	1.97		2.01		2.55		0.57	*0.04*	0.05		1.36	*0.04*	0.02	
C (org)	0.70	*0.49*	1.88	*1.56*	2.03		0.20	*0.16*	0.02		0.15	*0.05*	0.05	*0.02*
Ag	8		(2)		–		(4)		–		(2)		nl	
As	130	*65*	110	*75*	62	*70*	35	*15*	9	*13*	39	*5*	n5	
B	(63)		62		15	*10*	(140)		23	*n10*	66	*20*	60	
Ba	450	*400*	n400		340	*400*	420		330	*400*	n400		400	
Co	25	*20*	22		17		27	*17*	13	*n20*	n20		n20	
Cr	48	*40*	140		150		61		92		150	*110*	45	
Cu	68	*52*	57		27		(14)		25		33	*22*	9	
Ga	8		10		8		(10)		6		6		4	
Hg (ppb)	(140)		(440)		(330)		(220)		–		–		–	
Li	74	*55*	95		12	*10*	52		25	*12*	150	*48*	–	
Mo	(4)		8	*6*	14		n6		n3		n6		5	*n3*
Ni	21	*15*	28		17		33		12		19	*15*	100	
Pb	740	*170*	290	*130*	120	*73*	130	*15*	100		57	*29*	n20	
Rb	160		–		130		(220)		(160)		(30)		–	
Sc	11		n10		n10		10	*14*	n10		n10		n10	
Sr	26		18		40	*28*	32		19		23	*14*	–	
Th	15	*12*	–		–		15		–		–		–	
V	78		180		78	*60*	43		20	*10*	44	*30*	19	
Y	26		–		–		(27)		–		–		–	
Zn	2300	*540*	2800	*2100*	33		1800	*100*	75	*53*	140	*96*	–	
Zr	110	*80*	55		n60		130		60		79		n60	

Note: Italics indicate median values ( ) value calculated from relatively few analyses

TABLE 15. MEAN VALUES OF CARBONATES (CO_2>20%) FROM THE HYC PYRITIC SHALE, W-FOLD SHALE AND COOLEY DOLOMITE MEMBERS AND TEENA DOLOMITE

	HYC Pyritic Shale Member						W-fold Shale Member		Cooley Dolomite Member		Teena Dolomite	
	McArthur Ore Basin		Other Areas (excluding BMR 2 area)		BMR 2 Area (Barney Ck Fm)		McArthur Ore Basin		McArthur Ore Basin		All areas	
No of Samples	20		10		4		5		11		9	
SiO_2	26.5		38.0		28.7		23.2		8.94	*6.91*	18.5	*12.4*
Al_2O_3	3.36		5.62		3.54		3.39		1.87	*1.15*	1.69	
FeO	5.94	*4.58*	3.42		2.47		4.17		4.84		5.37	
MgO	11.0		10.9		14.8		9.46		18.2		15.1	
CaO	19.6		15.6		21.8		27.1		26.5		23.9	
Na_2O	0.08		0.26		0.07		0.07		0.04		0.07	*0.04*
K_2O	1.83		2.45		3.18		1.85		0.71	*<0.10*	0.91	*1.07*
TiO_2	0.12	*0.10*	0.21		0.12		0.10		0.05	*0.03*	0.06	
P_2O_5	0.09	*0.07*	0.21		0.12		0.10		0.05		0.04	
MnO	0.48	*0.44*	0.22	*0.13*	0.53		0.92	*0.81*	0.70		0.71	*0.81*
CO_2	28.0		23.1		30.2		30.9		40.4		36.0	
H_2O^+	0.64		1.75		0.59		(0.39)		0.79		1.21	*0.89*
H_2O^-	0.20		0.50	*0.42*	0.14		(0.18)		0.33		0.28	
S	2.78	*1.75*	1.56	*1.22*	0.67		0.28	*0.21*	0.43	*0.19*	0.08	*0.10*
C (org)	0.28	*0.23*	0.77	*0.46*	0.51		0.08	*0.03*	0.17	*0.08*	0.08	*0.05*
Ag	(5)		n1		n1		(3)		(1)		2	
As	270	*230*	53	*31*	20		54	*25*	46	*13*	6	*n5*
B	(32)		55		n10		(30)		19		18	*15*
Ba	170		n300		n400		220	*160*	n300		n300	
Co	19		n10		n20		18		13	*n15*	n15	
Cr	26		110		88		32		19		65	*35*
Cu	81	*16*	16		11	*8*	(9)		51	*14*	28	*7*
Ga	(3)		5		3		n3		n3		n3	
Hg (ppb)	(30)		(90)		-		(140)		(90)		-	
Li	25	*19*	42	*33*	3		16		27	*23*	28	*21*
Mo	n6		n3		13	*8*	n6		n6		n6	
Ni	15		n10		14		16		n10		n10	
Pb	2000	*260*	870	*57*	140	*38*	280	*20*	100	*44*	25	*16*
Rb	68	*51*	110		55		47		-		(25)	
Sc	9		n10		n10		9		n30		n25	
Sr	30		23		38		57	*49*	15		12	
Th	6		-		-		5		-		-	
V	32	*27*	29	*25*	19		33		n15		n15	
Y	21	*17*	24		-		21		-		-	
Zn	7600	*980*	4000	*99*	43		1200	*1000*	1300	*72*	79	*30*
Zr	n100		n60		n60		n100		n150		n150	

Note: Italics indicate median values ( ) value calculated from relatively few analyses

TABLE 16. MEAN VALUES OF SILICEOUS SAMPLES

(SiO_2 > 60%)

	Mainly Tuffaceous		Na-rich	
No. of Samples	13		13	
SiO_2	69.1		71.3	
Al_2O_3	11.0		10.6	
FeO	1.86	*1.49*	2.20	
MgO	2.04		1.67	
CaO	2.87	*1.92*	2.35	
Na_2O	0.14		2.07	
K_2O	7.60		2.16	*2.72*
TiO_2	0.26		0.19	
P_2O_5	0.11	*0.09*	0.06	
MnO	0.07		0.20	*0.14*
CO_2	4.06		2.06	
H_2O^+	1.00	*0.71*	(0.35)	
H_2O^-	0.43	*0.27*	(0.24)	
S	0.59	*0.43*	0.66	
C (org)	0.32	*0.19*	0.29	*0.20*
Ag	–		(1)	
As	40	*30*	68	
B	41		(10)	
Ba	n400		460	
Co	n20		18	*n20*
Cr	63		13	*n10*
Cu	33	*25*	73	
Ga	8		(8)	
Hg (ppb)	(200)		(50)	
Li	23	*13*	27	
Mo	7	*5*	n3	
Ni	9		11	
Pb	430	*70*	150	*210*
Rb	(130)		74	
Sc	n10		8	
Sr	20		17	
Th	(22)		19	
V	34	*20*	30	*24*
Y	(22)		28	
Zn	130	*60*	660	*430*
Zr	110	*60*	120	

Note: Italics indicate median values.

( ) value calculated from relatively few analyses.

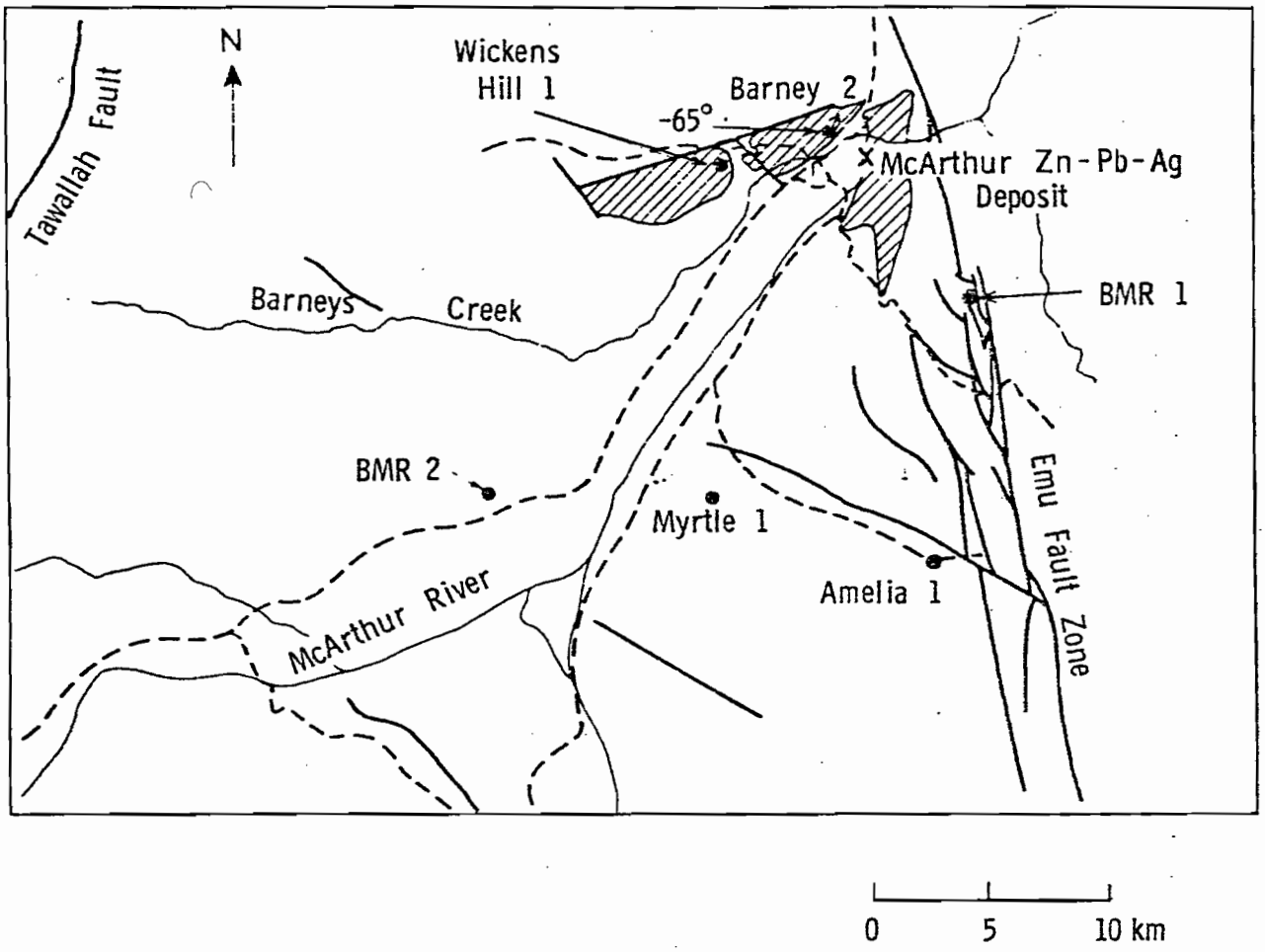

FIG. 1. McARTHUR ZINC-LEAD-SILVER DEPOSIT AND SURROUNDING AREA SHOWING LOCATION OF CORES ANALYSED

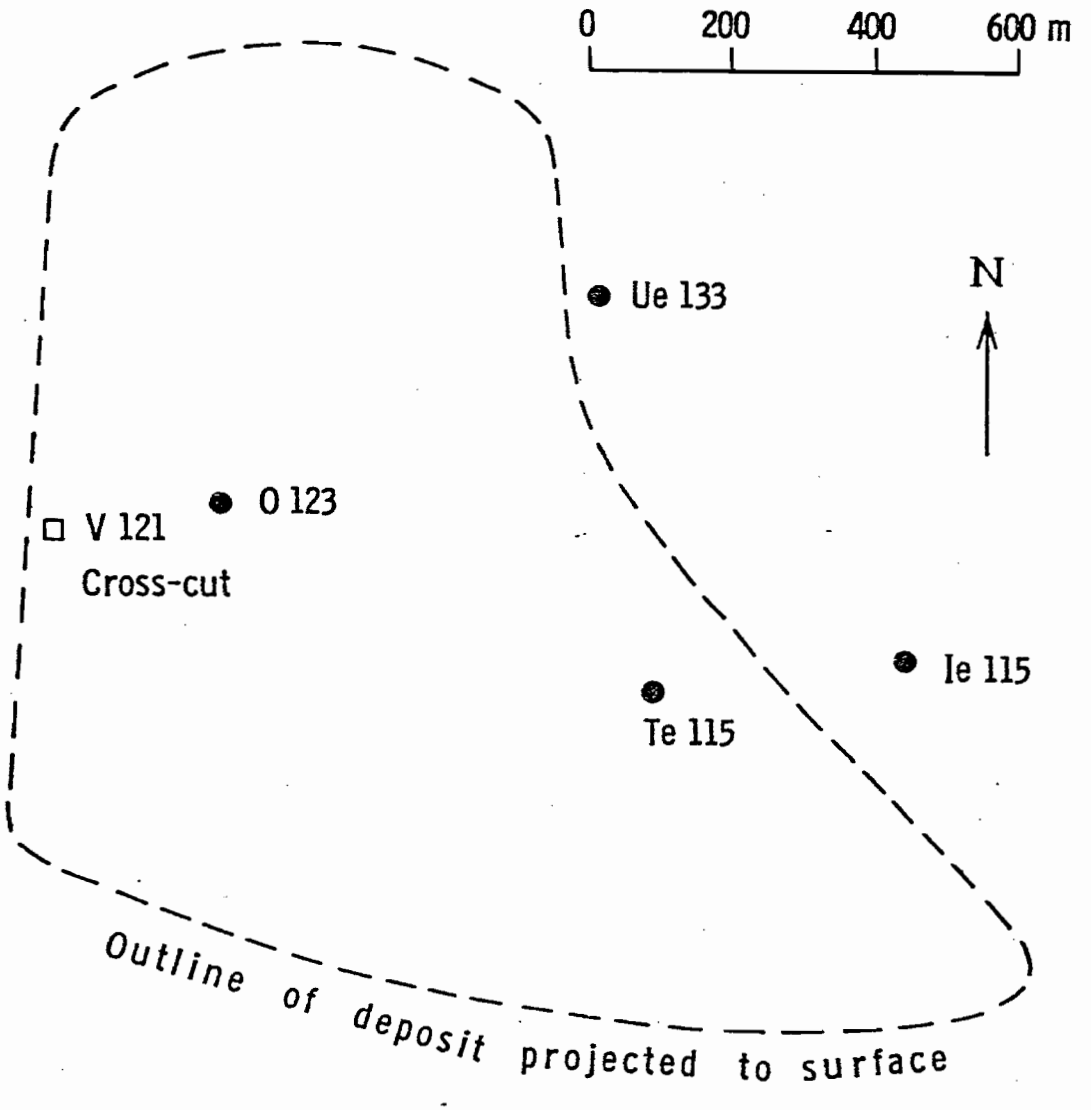

FIG. 2. PLAN SHOWING EXTENT OF McARTHUR DEPOSIT PROJECTED TO SURFACE

Hemimorphite-rich gossan crops out near V 121 shaft. The ore dips gently to the east, and is thickest in vicinity of drill hole Te 115. Ie 115 penetrates a thick sequence of Cooley Dolomite Member.

Appendix 5-IV

Giant primary dispersion halos of thallium around northern Australian Proterozoic stratiform sedimentary lead-zinc deposits

P.J. McGoldrick, R.N. Smith and R.R. Keays

to be submitted to Geology

Giant primary dispersion halos of thallium around north Australian Proterozoic stratiform sedimentary lead-zinc deposits

P.J. McGoldrick, R.N. Smith and R.R. Keays

Abstract

Introduction

The Pb-Zn-Ag orebodies at Mount Isa (Isamine) and McArthur River (HYC) in northern Australia (Fig. 1) are two of the world's largest accumulations of lead and zinc sulphides. They are hosted by Middle Proterozoic shallow water sedimentary rocks (Muir, 1983) of essentially the same age (1631±12 Ma and 1653±7 Ma - Page, 1990 and 1993). In both deposits much of the mineralisation is stratiform on all scales.

The stratiform mineralisation is believed to have formed either, syngenetically at the sediment - water interface from fluids exhaled into the ambient water column (e.g., Lambert, 1976), or during diagenesis from fluids infiltrating the sediment pile (e.g., Williams and Rye, 1974; Eldridge et al., 1993).

In this paper we describe of anomalous Tl levels in the unmineralised stratigraphic equivalents of the ore horizon at both deposits, and in the case of HYC these are up to seven kilometres along strike. Similar enrichment persists up to a hundred metres into the hanging wall of the HYC mineralisation. We discuss the origin of these giant primary geochemical halos and their implications for ore genetic models for stratiform sediment-hosted (SSH) Zn-Pb deposits.

HYC

The giant HYC deposit was discovered by Mount Isa Mines Ltd lin 1955. It contains a global resource of 227 million tonnes at 9.2 wt% Zn and 4.1 wt% Pb (Logan et al., 1990 and 1993). An underground mine to exploit higher grade parts of the mineralization with a resource of 104 Mt at 14.1 wt% Zn, 6.1 wt% Pb and 160 g/t Ag is presently under development (Logan et al., 1993).

The mineralization occurs in the lower 70 metres of the HYC Pyritic Shale Member of the Barney Creek Formation (Jackson et al., 1988). Seven individual orebodies have been distinguished, separated by lower grade siltstone and sedimentary breccia interbeds. The ores are fine grained with a simple mineralogy dominated by pyrite, sphalerite and galena and have been described in detail by Croxford, (1968), Croxford and Jephcott, (1972) and more recently by Eldridge et al., (1993).

Forty six samples from fresh drill core through the HYC deposit (DDH TE 115, UE 133, and O123) and from two distant holes WH#1 and BMR #2) were analysed for Tl by radiochemical neutron activation analysis (Smith, 1973; Smith et al., 1974). Whole rock major and trace elements had previously been determined on these samples as part of a larger geochemical

survey reported in Corbett et al., (1974) and Lambert and Scott, (1973). Drill hole WH#1 is in the W-Fold sub-basin six kilometres west of the HYC deposit. This area is the site of minor Zn mineralisation in the stratigraphic equivalent of the immediate footwall of the HYC mineralised interval (Murray, 1975; Walker et al., 1978). Drill hole BMR#2 is approximately 15 kilometres southwest of the HYC deposit in an area with no known Zn mineralisation.

Samples from HYC mineralisation contain between hundred and eight hundred parts per million (ppm) of Tl. The lowest Tl values are in barren siltstones and dolomites from WH#1 and BMR#2 and these samples indicate that background Tl is less than 2 ppm. Anomalous levels of Tl are observed in two of eight samples from BMR#2 and from four of five samples from WH#1, and in the 16 of 18 samples from the hanging wall of the HYC mineralisation and four of six samples from the W-Fold Shale Member the immediate footwall (Fig. 2).

Mount Isa

The Mount Isa mineralization (Mathias and Clark, 1975; Forrestal, 1990) comprises about thirty *en echelon* lenses within the one kilometre thick Urquhart Shale Member of the Mount Isa Group (most orebodies occur in the upper 650 metres). Urquhart Shale lithologies comprise mainly dolomitic siltstones containing locally important pyritic, carbonaceous, tuffaceous (prominent K-feldspar rich beds in the mineralised sequence are known locally as TMBs (Croxford, 1964-5)) and base metal sulfide components. The depositional setting for the Urquhart Shale was interpreted to have been a non-marine, hypersaline perennial lake (van den Heuval, 1969; Neudert; 1983) The samples analysed for Tl from Isamine comprise siltstones and pyritic siltstones, base metal sulphide ore, and TMBs collected from underground (mainly 12 orebody) and from stratigraphically equivalent drill core (Fig. 3). The Tl data from Mount Isa are summarised on Table 1. Base metal sulphide-rich and pyritic samples contain tens to hundreds of ppm Tl. Two bulk composite samples (from DDH UW 886 and WW 593 located about ten kilometres north of Isamine) and grab samples from the equivalent of 12 orebody stratigraphy in DDH G157 (located about five kilometres south of 12 orebody) indicate that background Tl in unmineralised Mount Isa Group sediments is only only one or two ppm. In contrast, 14 siltstones and 7 TMB samples from within 12 orebody, and two barren inter-orebody siltstones contain between 10 and 80 ppm Tl. Furthermore, drill-core samples of 12 orebody equivalent from up to a kilometre along strike contain anomalous Tl (Fig. 3 and Table 1)

	UW886 1m comp.	WW593 1m comp.	G157 n=2	12 orebody TMBs n=7	12 orebody siltstones n=11	12 orebody Zn-rich samples n=8	12 orebody Pb-rich samples n=4	12 orebody Pyrite-rich samples n=5
Tl (ppm)	1.1	1.0	2.73, 1.3	43-69	23-86	71-116	22-38	40-230

Table 1: Thallium in samples from Mount Isa

Formation of thallium halos

Thallium is a common minor constituent of many polymetallic base metal sulphide deposits (de Albuquerque and Shaw, 1974), reflecting the chalcophile behaviour of this element under high fS_2 conditions. However, in the absence of sulphides, univalent Tl will show lithophile behaviour and substitute for K and Rb in silicates(Shaw, 1952).

At Isamine there is a close relationship between Tl and K in unmineralised (<2wt% S) siltstone samples (Fig. 4), suggesting that K-silicates, rather than sulphides host the Tl in these rocks. The Tl in the ores must have been an original component (along with the base metals, Cd, Sb, Ag, etc - McGoldrick, 1986) of the mineralising fluids. Furthermore, because both sulphide ores and low-S sediments contain large amounts of Tl there is an implied link between the mineralising fluid and the Tl enrichment in the sediments.

Models for SSH lead-zinc deposits

Genetic models for these deposits fall into two contrasting groups: i) exhalative-syngenetic and ii) diagenetic/epigentic. The former ascribe base metal sulphide formation to precipitation from hydrothermal fluids that escape from the subsurface and into the water column. The mineralization is chemical sediment that will form ore grade accumulations if clastic sedimentation rates are low. Precipitation of metal sulphides is probably in response to sudden temperature changes in the ore fluid, or mixing with sea-water, or both. Dense exhaled fluid may pond to form brine pools (Sato, 1972, e.g., the Red Sea - Zierenberg and Schanks, 1983), but a considerable flux of fluid is required to form ore grade accumulations from a brine pool (i.e., many times the volume of the pool).

In the latter case mineralizaton forms from hydrothermal fluids moving through the unconsolidated sediment at some depth in the subsurface (this could be at depths from centimetres to hundreds of metres as long as sufficient permeability is maintained in the sediments). Sulphide precipitation is less likely to be in direct response to fluid cooling, and chemical reactions between the ore fluid and constituents of the host rocks may be important in ore formation (McGoldrick, 1986).

Halo formation

In a simple exhalative - syngenetic scenario base metal sulphides accumulate to ore grade during times of low clastic sediment input, and barren intervals represent times of accelerated sedimentation . This process would be able to produce primary dispersion halos that where low grade equivalents of the mineralisation (i.e., clastic sediment dilutes the total amount of sulphide in the rock), but this process does not explain the Tl enrichment seen in the low-S samples from Isamine and HYC.

In the special case of exhalative - syngenetic mineralisation involving sulphide precipitation from a brine pool, the persistence of the pool during clastic sediment input may allow detrital grains and hydrothermal fluid to interact and cause some enrichment of Tl in the barren sediments. However this explanation suffers from two major problems:

i) to produce laterally extensive Tl halos the brine pools would have needed to be much larger than the actual orebodies, and

ii) at Isamine and HYC the barren sediments are mainly current deposits (Neudert, 1983; Logan, 1979) and deposition of each bed is a rapid event; hence, in a strictly syngenetic model the sediments can only interact with the volume of brine trapped as connate fluid as they are deposited. Just as with ore grade accumulation of sulphide in a brine pool, mass balance calculations require many times the volume of fluid trapped in the sediment to generate the observed Tl enrichments.

On the other hand, if mineralisation formed during the passage of mineralising fluid through permeable sediments in the sub-surface ('diagenetic/epigentic' scenario) then the Tl enrichments in unmineralised sediments can be readily explained. Ore fluids moving through the unconsolidated sediment will interact with reactive clastic mineral grains and Tl will be incorporated into K-bearing minerals. The Tl halos form in the conduits or volumes of sediment through which mineralising fluids have flowed. Mineralisation forms in a smaller volume of sediment where physico-chemical conditions favour metal sulphide precipitation.

Conclusions

Giant dispersion halos of Tl are present around two world class sediment-hosted Pb-Zn-Ag deposits at Mount Isa and McArthur River. Thallium enrichment occurs for kilometres along barren equivalents of the ore horizon, and for tens of metres into the hanging wall of the ores. Thallium is hosted by K silicate minerals in low-S samples. These halos are not compatible with simple syngenetic-exhalative explanations for these deposits, but, indicate a post-sedimentation timing for the formation of the ores.

References

Corbett, J.A., Lambert, I.B., and Scott, K.M., 1975, Results of analyses of rocks from the McArthur Area, Northern Territory: CSIRO Technical Communication No.57, Minerals Research Laboratories, August 1975.

Croxford, N.J.W., 1968, A mineralogical examination of the McArthur lead-zinc-silver deposit, Proc. Austral. Inst. Min. Metal., No 226, 9p7-108.

Croxford, N.J.W., 1964-65. Origin and significance of volcanic potash-rich rocks from Mt Isa. Trans. Instn. Min. Metall., v74, p34-43.

Croxford, N.J.W., and Jephcott, s., 1972, The McArthur lead-zinc-silver deposit, N.T., Proc. Austral. Inst. Min. Metal., No 243, p1-26.

de Albuquerque, C.A.R. and Shaw, D.M., 1974. Thallium. Chapter 81 C-H. In Handbook of Geochemistry, K.H. Wedepohl (ed.), Springer-Verlag.

Eldridge, C.S., Williams, N., and Walshe, J.L., 1993, Sulfur isotope variability in sediment-hosted massive sulphide deposits as determined using the ion microprobe SHRIMP:II A study of the HYC deposit at McArthur River, N.T., Australia: Econ. Geol., V88, p1-26.

Forrestal, P.J., 1990, Mt Isa and Hilton Ag-Pb-Zn deposits, in Geology of the Mineral Deposits of Australia and Papua New Guinea (Ed F.E. Hughes) p927 - 934 (The Australasian Institute of Mining andMetallurgy: Melbourne).

Jackson, M.J., Muir, M.D., and Plumb, K.A., 1988, Geology of the southern McArthur Basin, Northern Territory, BMR Bulletin 220, 173pp.

Lambert, I.B., 1976, The McArthur zinc-lead-silver deposit: features, metallogenesis and comparisons with some other stratiform ores., in: Handbook of strata-bound and stratiform ore deposits, K.H. Wolf (ed), 6, 535-585.

Lambert, I.B., and Scott, K.M., 1973, Implications of geochemical investigations of sedimentary rocks within and around the McArthur zinc-lead-silver deposit, Northern Territory: Journ. Geochem. Expl., V2, p307-330.

Logan, R.G., 1979, The geology and mineralogical zoning of the HYC Ag-Pb-Zn deposit, McArthur River, Northern Territory, Australia, MSc thesis (unpublished), The Australian national University.

Logan, R.G., Murray, W.J., and Williams, N., 1990, HYC silver-lead-zinc deposit, McArthur river, Northern Territory, in Geology of the Mineral Deposits of Australia and Papua New Guinea (Ed F.E. Hughes), p907-911(The Australasian Institute of Mining andMetallurgy: Melbourne).

Logan, R.G., Leung, K. and Karelse, G.J.,1993, The McArthur River project, in: Mathew, I.G. (ed) World Zinc '93 Proceedings, AusIMM Publ. 7/93, p27-39.

Mathias, B.V., and Clark, G.J., 1975, The Mount Isa Copper and Silver-Lead-Zinc orebodies - Isa and Hilton mines: *in* Knight, C.L., ed., Economic Geology of Australia and Papua New Guinea: Australasian Institute of Mining and Metallurgy Monograph 5, p. 351-371.

McGoldrick, P.J., 1986, Volatile and precious metal geochemistry of the Mount Isa ores and their host rocks: Unpub. Ph.D. thesis, University of Melbourne, 330 p.

Muir, M.D., 1983. Depositional environments of host rocks to northern Australian lead-zinc deposits, with special reference to McArthur River. Min. Ass. Canada, Short CourseNotes, 9, 141-174.

Murray, W.J., 1975, McArthur River H.Y.C. lead-zinc and related deposits, N.T., *in* Knight, C.L., ed., Economic Geology of Australia and Papua New Guinea: Australasian Institute of Mining and Metallurgy Monograph 5, p329-339.

Neudert, M., 1983, A depositional model for the Upper Mount Isa Group and implications for ore formation: Unpub. Ph. D. thesis, RSES, Australian National University, 324 p.

Page, R.W., 1993, Geological constraints given by U-Pb geochronology in the Mount Isa Inlier, Symposium on recent advances in the Mount Isa Block, A.I.G. Bull. No. 13, p13-15.

Sato, T., 1972, Behaviours of ore-forming solutions in seawater, Mining Geology, v22, p31-42.

Shaw, D.M., 1952. The geochemistry of thallium. Geochim. Cosmochim. Acta, 2, 118-128.

Smith, R.N., 1973. Trace element distribution within some major stratiform orebodies. Unpubl. B.Sc (Hons) thesis, part II. Univ. of Melbourne

Smith, R.N., Ewers, G.R. and Keays, R.R., 1974. Volatile metal haloes as a guide to base metal deposits. Abs. Geol. Soc.Aust. Joint Specialist Group Meeting, p. 64-67.
Van den Heuval, H.B., 1969. Sedimentation, stratigraphy and post-depositional changes in the sediments of the upper formations of the Mount Isa Group, north-west Queensland.Unpubl. Ph.D. thesis, Univ. of Queensland, 195 pp.

Walker, R.N., Logan, R.G. and Binnekamp, J.G., 1977, Recent geological advances concerning the H.Y.C. and associated deposits, McArthur River, N.T. Jour. Geol. Soc. Aust., 24, 365-380.

Williams, N., and Rye, D.M., 1974, Alternative interpretation of sulphur isotope ratios in the McArthur lead-zinc-silver deposits, Nature, v247, p535-537.

Williams, N., 1978, Studies of the Base Metal Sulfide Deposits at McArthur River, Northern Territory. Australia: I. The Cooley and Ridge Deposits. Econ. Geol., 73, 1005-1035.
Williams, N., and Rye, D., 1974,

Zierenberg, R.A., and W.C. Shanks III, 1983, Mineralogy and geochemistry of epigenetic features in metalliferous sediment, Atlantis II Deep, Red Sea: Econ. Geol., 78, 57-72.

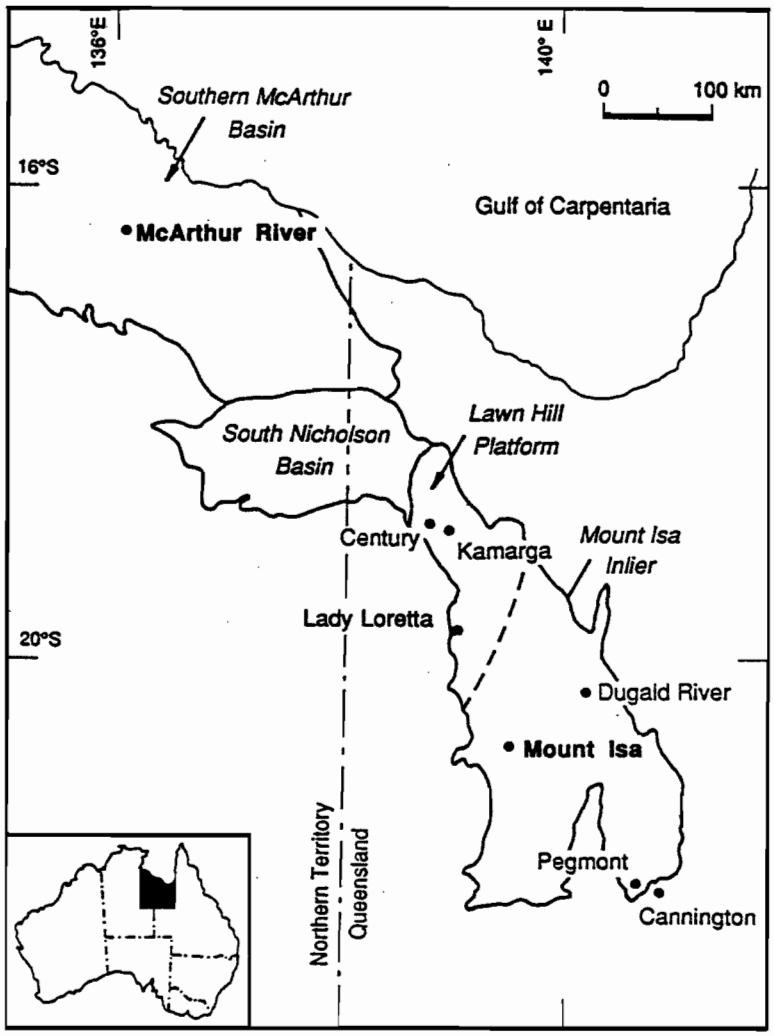

Fig.1 Locality map showing the important geological elements and the major zinc-lead deposits of northern Australia.

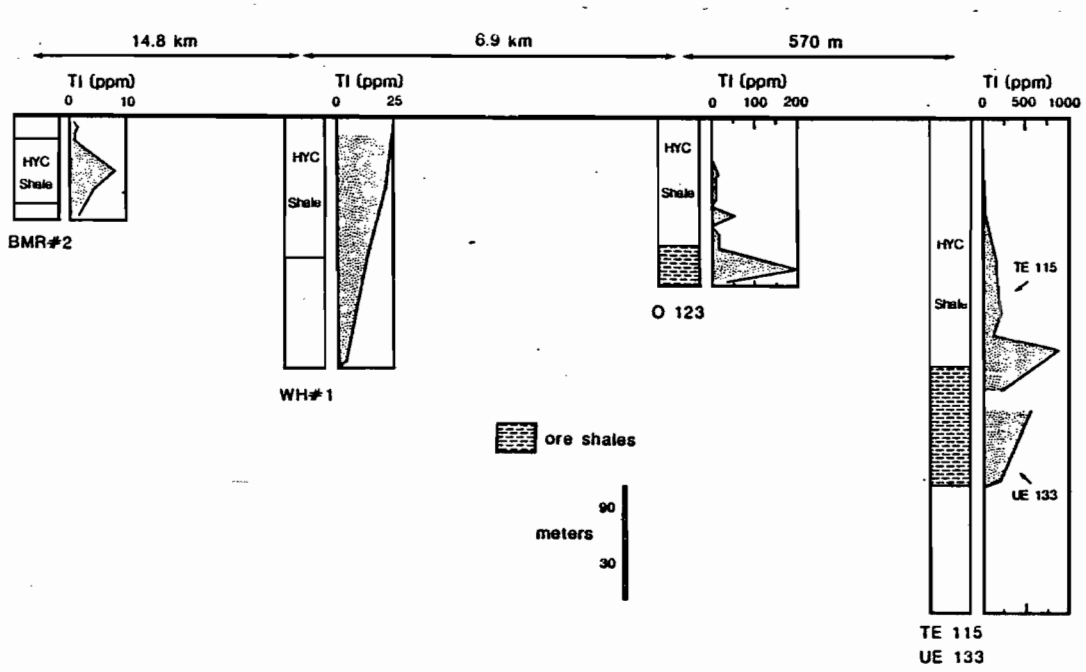

Fig. 2 Down-hole Tl distributionin five diamond drill holes from within and near the HYC deposit.

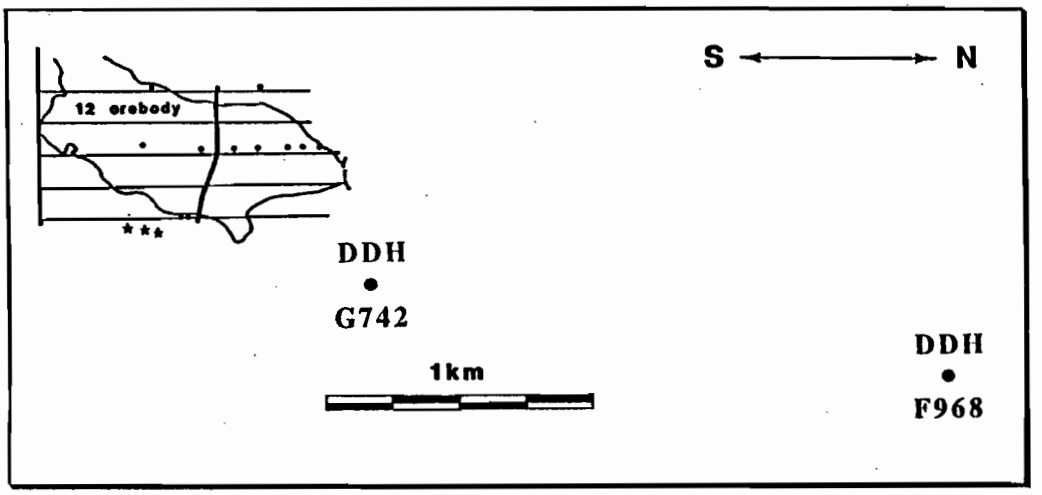

Fig. 3 Projected long section from Isamine showing the location of samples from 12 orebody and two diamond drill holes to the north (F968 and G742).

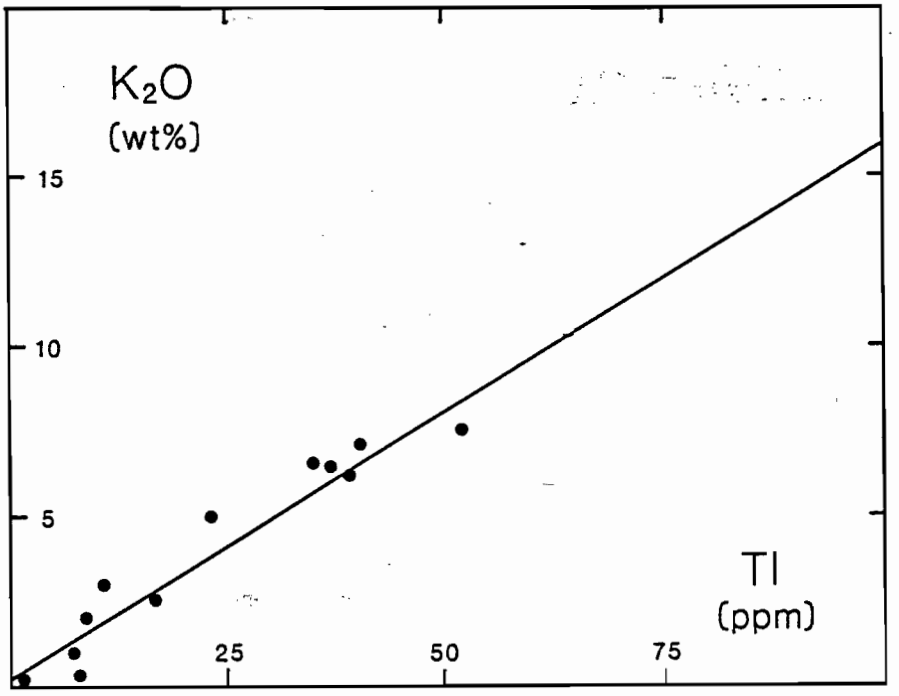

Fig. 4 Thallium vs K_2O in sediments from the mine sequence, Isamine.